Characterizing the role of protein arginine methyltransferase 7 (PRMT7) in breast cancer

Nasim Haghandish

Thesis submitted to the Faculty of Graduate and Postdoctoral Studies

in partial fulfillment of the requirements for the Doctorate in Philosophy degree

in Cellular and Molecular Medicine

Department of Cellular and Molecular Medicine

Faculty of Medicine

University of Ottawa

AUTHORIZATION

Citation for published manuscript used throughout this thesis (material and methods, results, and discussion):

Baldwin, R. M., Haghandish, N., Daneshmand, M., Amin, S., Paris, G., Falls, T. J., Bell, J. C., Islam, S., Côté, J. (2015). Protein arginine methyltransferase 7 promotes breast cancer cell invasion through the induction of MMP9 expression. *Oncotarget*, 6, 3013–3032. https://doi.org/10.18632/oncotarget.3072

EDITORIAL POLICIES

COPYRIGHT AND LICENSE POLICIES

Open-Access License
No Permission Required

Oncotarget applies the **Creative Commons Attribution 3.0 License** (CC BY 3.0) to all works we publish (read the **human-readable summary** or the **full license legal code**). Under the CC BY, authors retain ownership of the copyright for their article, but authors allow anyone to download, reuse, reprint, modify, distribute, and/or copy articles in *Oncotarget*, so long as the original authors and source are cited.

No permission is required from the authors or the publishers.

DESCRIPTION AND STATEMENT OF CONTRIBUTIONS OF COLLABORATORS AND CO-AUTHORS (PUBLICATIONS)

I. Baldwin, R. M., **Haghandish, N**., Daneshmand, M., Amin, S., Paris, G., Falls, T. J., Bell, J. C., Islam, S., Côté, J. (2015). Protein arginine methyltransferase 7 promotes breast cancer cell invasion through the induction of MMP9 expression. *Oncotarget*, 6, 3013–3032. https://doi.org/10.18632/oncotarget.3072

- I contributed towards Figures 3, 4, 6 (except for 6H), 7 and Supplemental Figures 1C, 2, 3, 4. There are a total of 7 main Figures and 4 Supplementals.
- R.M. Baldwin contributed towards Figures 1, 2, 3, 5, 6 (A, B, C), 7 (A, B) and Supplemental Figures 1 (A, B), 2, 4 (A, B, C).
- M. Daneshmand, S. Amin, and S. Islam scored tumour tissue microarrays.
- R.M. Baldwin, G. Paris, T.J. Falls, and J. C. Bell were involved in *in vivo* work.
- I was involved in the writing and editing of the manuscript alongside R.M. Baldwin and J. Côté.

II. **Haghandish, N**., Baldwin, R.M., Morettin, A., Dawit, H.T., Adhikary, H., Masson, J.Y., Mazroui, R., Trinkle-Mulcahy, L., and Côté, J. PRMT7 methylates eukaryotic translation initiation factor 2α and regulates its role in stress granule formation. Under review at *Molecular Biology of the Cell.*

- I performed all of the experiments except for data analysis of the mass spectrometry experiments (Collaboration with L. Trinkle-Mulcahy and R.M. Baldwin) and purification of human PRMT7 (H. Adhikary and J.Y. Masson).
- I wrote 100% of the manuscript and made all the figures.
- J. Côté, L. Trinkle-Mulcahy, R.M. Baldwin, and R. Mazroui contributed in editing of the manuscript.

III. **Nasim Haghandish** and Jocelyn Côté (2016). The Role of Histone Mark Writers in Chromatin Signaling: Protein Arginine Methyltransferases. Chapter 3 in *Chromatin Signaling and Diseases* (pp. 55-74). Oxford: Elsevier. *ISBN*-9780128026090. http://store.elsevier.com/Chromatin-Signaling-and-Diseases/isbn-9780128023891/ https://www.sciencedirect.com/science/article/pii/B9780128023891000034

- I wrote 100% of the book chapter and designed the figures.
- J. Côté contributed in editing of the chapter.
- Title page and abstract in the Appendix.

DESCRIPTION AND STATEMENT OF CONTRIBUTIONS OF COLLABORATORS (THESIS)

This work was a success due to the help from our collaborators. The following is a short description of those involved and the figures they had contributed towards. R. M. Baldwin contributed towards antibody validation (Figure 3A, B), tissue microarray experimentation (Figure 4A), immunocytochemical staining of cell lines (Figure 5A, B), motility and invasion assays of BT549 cells (Figures 6 and 7), *in vivo* imaging and staining of lung tumours (Figure 12), and the gelatin zymography experiment (Figure 14B). Pathologists M. Daneshmand, S. Amin, and S. Islam scored the tumour tissue microarrays (Figure 4B, C). G. Paris contributed towards Figure 12 by performing the *in vivo* imagining and staining of lung tumours. Additionally, T. J. Falls performed the injections within the tail veins of mice (Figure 12). Data analysis of the mass spectrometry experiments was performed by L. Trinkle-Mulcahy (Figures 20 and 21) and R.M. Baldwin (Appendix). Finally, human PRMT7 that was used for Figure 25 was purified from insect cells by H. Adhikary.

ABSTRACT

The development of more efficient therapeutic strategies in the treatment of breast cancer relies on understanding the biological events that promote its progression. Protein arginine methyltransferases (PRMTs) are enzymes that catalyze the methylation of arginine residues within proteins resulting in changes in several biological processes. PRMTs have been shown to be aberrantly expressed in many cancers and promote tumourigenesis and cancer progression. Specifically, PRMT7 mRNA expression correlates with breast cancer aggressiveness and invasiveness. Thus, we sought to determine whether PRMT7 promotes breast cancer progression/tumourigenesis and to further identify the functional mechanisms through which this is possible. We have shown that PRMT7 is upregulated in both breast cancer tissues and cell lines. Moreover, we have shown both *in vitro* and *in vivo* that PRMT7 enhances breast cancer cell invasion and metastasis. Using biochemical experimentation, we demonstrated that PRMT7 induces the expression of matrix metalloproteinase 9 to promote invasion and subsequent metastasis. Furthermore, using proteomic experiments, we discovered many novel PRMT7-interacting proteins. Further biochemical experimentation identified eukaryotic translation initiation factor eIF2α as an interacting protein and substrate of PRMT7. We demonstrated a regulatory interplay between eIF2α methylation and phosphorylation upon cellular stress: methylation is required for S^{51} phosphorylation. Accordingly, we have shown that stress granule formation, in the face of cellular stresses, was significantly diminished in PRMT7-knockdown cells. We additionally found that PRMT7 plays a regulatory role in protein translation. Overall, these findings suggest that PRMT7 plays a critical role in promoting breast cancer cell invasion, metastasis, stress regulation, and protein translation.

TABLE OF CONTENTS

LIST OF FIGURES

LIST OF TABLES

LIST OF ABBREVIATIONS

4E-BP	Eukaryotic translation initiation factor 4E binding protein
5'UTR	5' untranslated region
ACTG1	Gamma actin
ACTN4	Alpha actinin 4
ADMA	ω-N^G, N^G-asymmetric dimethylarginine
APEX2	Apurinic/apyrimidinic endonuclease 2
AsNAO2	Sodium arsenite
ATF4	Activating transcription factor 4
cDNA	Complementary deoxyribonucleic acid
CRISPR	Clustered regularly interspaced short palindromic repeats
CTCFL	CCCTC-Binding Factor Like
DAPI	4′,6-diamidino-2-phenylindole
DMEM	Dulbecco's modified Eagle's medium
DNA	Deoxyribonucleic acid
DNMT3b	DNA methyltransferase 3b
DTT	Dithiothreitol
ECM	Extracellular matrix
EDTA	Ethylenediaminetetraacetic acid
eEF	Eukaryotic translation elongation factor
EGTA	Ethylene glycol-bis(β-aminoethyl ether)-N,N,N',N'-tetraacetic acid
eIF	Eukaryotic translation initiation factor

EMT	Epithelial-to-mesenchymal transition
ER	Estrogen receptor
FMRP	Fragile X mental retardation protein
FOXP1	Forkhead box protein P1
FUS	Fused in sarcoma
G3BP1	Ras GTPase-activating protein-binding protein 1
GAPDH	Glyceraldehyde 3-phosphate dehydrogenase
GAR	Glycine/arginine-rich motifs
GCN2	General control nonderepressible 2
GDP	Guanosine diphosphate
GFP	Green fluorescence protein
GST	Glutathione S-transferase
GTP	Guanosine triphosphate
HDAC3	Histone deacetylase
HER2	Human epidermal growth factor receptor 2
hnRNP	Heterogeneous nuclear ribonucleoprotein
HRI	Heme-regulated initiation factor
HRP	Horseradish peroxidase
IAA	Iodoacetamide
IPTG	Isopropyl-β-D-thiogalactopyranoside
IRES	Internal ribosomal entry site
ITAF	IRES-transactivating factors
IVIS	*In vivo* imaging system

JMJ	Jumonji domain-containing protein
kDa	Kilo Daltons
LC-MS/MS	Liquid chromatography–mass spectrometry
MAPK	Mitogen-activated protein kinase
mGFP	Monomeric green fluorescent protein
MEF	Mouse embryonic fibroblast
MLL	Mixed lineage leukemia
MMA	ω-N^G-monomethylarginine
MMP	Matrix metalloproteinase
mRNA	Messenger ribonucleic acid
MTA	5'-deoxy-5'-methylthioadenosine
MTT	3-(4,5-Dimethylthiazol-2-yl)-2,5-diphenyltetrazolium bromide
NaDOC	Sodium deoxycholate
PAD4	Peptidylarginine deiminase 4
PBS	Phosphate-buffered saline
PCR	Polymerase chain reaction
PEI	Polyethylenimine
P-eIF2α	Phosphorylated eukaryotic translation initiation factor 2α
PERK	PKR-like endoplasmic reticulum kinase
PGM	Proline/glycine/methionine-rich motifs
PI3K	Phosphatidylinositol 3-kinase
PKR	Protein kinase RNA-activated
PMA	Phorbol 12-myristate 12-acetate

POLD1	DNA polymerase delta catalytic subunit
PR	Progesteron receptor
pRB	Retinoblastoma protein
PRMT	Protein arginine methyltransferase
PTM	Post-translational modification
PVDF	Polyvinylidene difluoride
R0K0	$^{12}C_6$-Arginine/$^{12}C_6$-Lysine
R6K4	$^{13}C_6$-Arginine/4,4,5,5-D4-Lysine
RNA	Ribonucleic acid
rpS2	Ribosomal protein S2
RXR	Arginine residues (R) flanked by basic residues (X) –rich motifs
SA-β-gal	Senescence-associated β-galactosidase
SAM	S-adenosyl methionine
SCID	Severe combined immunodeficiency
SDMA	ω-N^G, $N^{G'}$-symmetric dimethylarginine
SDS	Sodium dodecyl sulphate
SDS-PAGE	Sodium dodecyl sulphate polyacrylamide gel electrophoresis
sE-cadherin	Soluble extracellular E-cadherin fragment
sgRNA	Synthetic single guide RNA
shRNA	Short hairpin ribonucleic acid
SILAC	Stable isotope labelling of amino acids in cell culture
SmD3	Small nuclear ribonucleoprotein core protein D3
SWI/SNF	Switch/sucrose non-fermentable

TBST	Tris-hydrochloric acid-buffered saline and 0.05% tween 20
TDRD3	Tudor domain-containing protein 3
TIMP	Tissue inhibitor of matrix metalloproteinase
TMA	Tissue microarray
TNBC	Triple negative breast cancer
tRNA	Transfer RNA
uORF	Upstream open reading frame
UV	Ultraviolet
YY1	Ying Yang 1
ZEB1	Zinc finger E-box-binding homeobox 1

ACKNOWLEDGEMENTS

First and foremost, for giving me the opportunity to work in his laboratory and to acquire the many skills and techniques in molecular biology, I would like to thank my supervisor Dr. Jocelyn Côté. I am genuinely grateful for his invaluable guidance and support throughout the years of my studies. Having gone through this wonderful experience, I feel confident in my work and truly appreciate all the effort researchers put into scientific advancement.

I would also like to thank the members of my thesis advisory committee: Dr. Martin Holcik, Dr. Barbara Vanderhyden, and Dr. David Lohnes. They have been instrumental in the success of my research by providing me with great feedback and advice.

Additionally, I thank all members of the Côté laboratory, past and present, for sharing their expertise and making work in the laboratory enjoyable. I would especially like to express my gratitude towards Dr. Robert Mitchell Baldwin who was my mentor and collaborator as I ventured into the world of research. Furthermore, I would like to thank our collaborators whose support facilitated publication of our results.

Finally, I thank my family and friends who have continuously supported me throughout my journey. Without them, I would not have been able to accomplish my goals.

CHAPTER 1: INTRODUCTION

1.1 Cancer Hallmarks

Cancer is an extremely complex, heterogenetic disease which can be generally termed as a disease of genome instability, of altered cellular behaviour, and of altered tissue behaviour (Klausner, 2002). The dynamic gene abnormalities/alterations potentially lead to uncontrolled cell proliferation and tumour growth. Ultimately, the primary tumours may begin to spread, leading to the formation of secondary tumours through the process of metastasis. However, not all genetic alterations or abnormalities result in cancer formation. Fundamentally, cancers form when the genetic alterations occur in oncogenes (cancer-promoting) and/or tumour suppressor genes (Iurlaro, Leon-Annicchiarico, & Munoz-Pinedo, 2014). Generally, mutations of oncogenes are dominant gain-of-function, whereas mutations of tumour suppressor genes are recessive loss-of-function (Hanahan & Weinberg, 2000). Together, gain of oncogenes and loss of tumour suppressors ease the transition of a 'normal' cell state into a neoplastic state leading to defects in tissue function; in other words, cells 'evolve' into a neoplastic state. This transition is reflected via the acquisition of cancer hallmarks (Hanahan & Weinberg, 2011).

It is widely accepted that there are six main hallmarks of cancer: (1) sustaining proliferative signalling, (2) evading growth suppressors, (3) activating invasion and metastasis, (4) enabling replicative immortality, (5) inducing angiogenesis, and (6) resisting cell death (Hanahan & Weinberg, 2000). The six biological capabilities are acquired by tumour cells via a multistep process of genetic mutations, resulting in the growth, development, and spread of cancer tumours. Additionally, there are emerging hallmarks that support the six hallmark functions: dysregulation of cellular energetics and

avoiding immune destruction. These emerging hallmarks allow cells to better reprogram cellular metabolism to support neoplastic growth while also avoiding destruction via the immune system specifically by macrophages, T and B lymphocytes, and natural killer cells. Furthermore, two enabling characteristics, genome instability and tumour-promoting inflammation, further aid and accelerate the acquisition of the cancer hallmarks. Genome instability allows cells to obtain successive genomic alterations that support neoplastic growth. Finally, inflammation, although generally beneficial in fighting infections, can be misused to support tumour growth by supplying growth factors and proangiogenic factors to the tumour microenvironment (Hanahan & Weinberg, 2011) [Figure 1].

Although the hallmarks of cancer are exhibited in regular cell function, it is the excessive and abnormal usage of the hallmarks that differentiate normal from tumourigenic cells. Cancer cells, depending on the type of tissue they arise from, harbor different mutations and altered morphology and function; moreover, there is the possibility of heterogeneity within a given tissue itself. Thus, there is no single treatment option available for all the cancer sub-types. Hence, the field of cancer is ever-expanding, leading to the development of more specialized treatment options and potentially patient-specific treatment therapies. By identifying and targeting the dysregulated proteins that lead to the development of these cancer hallmarks, more effective treatments may be uncovered. Specifically in this thesis, work regarding the role a dysregulated protein plays in breast cancer cell invasion and metastasis will be presented.

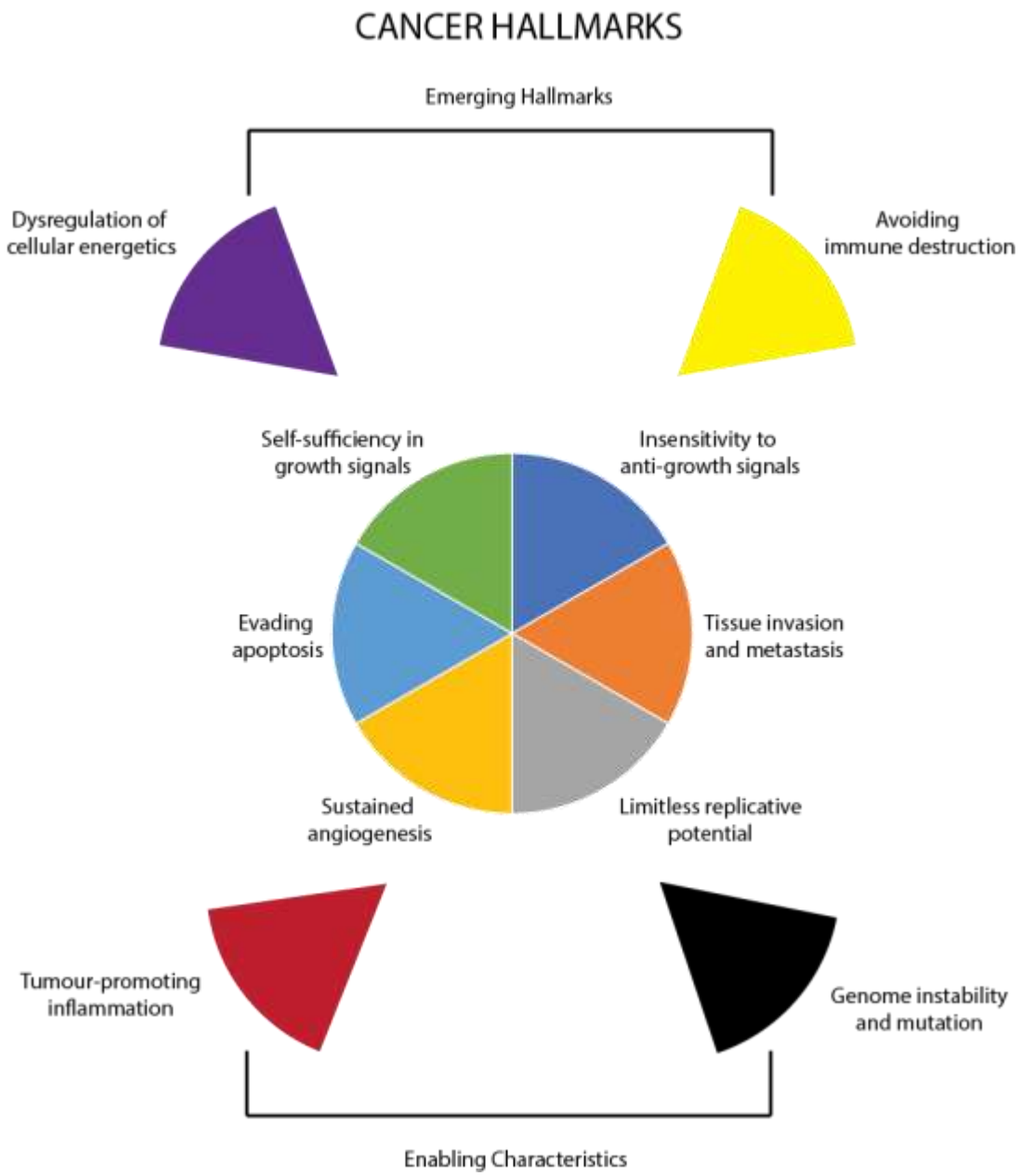

Figure 1: Cancer hallmarks schematic

The six main cellular characteristics that are termed as cancer hallmarks are self-sufficiency in growth signals, insensitivity to anti-growth signals, tissue invasion and metastasis, limitless replicative potential, sustained angiogenesis, and evading apoptosis. These are characteristics obtained by cancer cells to promote tumourigenesis. In addition to these six, there are also enabling characteristics, tumour-promoting inflammation and genome instability & mutation, as well as emerging characteristics, dysregulation of cellular energetics and avoiding immune destruction. Both enabling and emerging characteristics help support the six main hallmarks.

1.2 Invasion and Metastasis

Metastasis is the process whereby cancer cells spread from their primary site of origin and migrate to adjacent or distant sites (Comen, 2012). It is a complex process whereby cells degrade and cross the extracellular matrix (ECM). Cells then enter blood or lymphatic vessels – termed intravasation – allowing for the cancer cells to travel through the vessels to distant sites. Next, cells exit the vessel via extravasation to form secondary tumours at the distant sites. Finally, the cells at the secondary site undergo cell proliferation to form micrometastases which eventually develop into macroscopic secondary tumours (Hanahan & Weinberg, 2011; Nguyen, Bos, & Massagué, 2009). The whole process is very dynamic, involving both protein synthesis and degradation (Kohn, Alessandro, Spoonster, Wersto, & Liotta, 1995).

The process of events is aided by several mechanisms such as the following: angiogenesis surrounding the primary and secondary tumour to facilitate cell migration; downregulation of cell-adhesion proteins such as E-cadherin; expression of matrix-degrading enzymes such as matrix metalloproteinases; epithelial-to-mesenchymal transition of cells (EMT) which causes cells to lose their polarity/organization and become more motile via biochemical changes ultimately aiding cell invasion; activation of pathways that enhance evasion of apoptosis; and activation of pathways involved in enhancing cell migration and cell cycle progression such as phosphatidylinositol 3-kinase (PI3K) and mitogen-activated protein kinase (MAPK) pathways (Hanahan & Weinberg, 2011; Kalluri & Weinberg, 2009; Machesky, 2008; Roskoski, 2012; Vivanco & Sawyers, 2002). For successful treatment of breast cancer, the aggressiveness and/or invasiveness of

the cancer cells should be stopped or slowed. In terms of cell invasion, degradation of the extracellular matrix is a key step in the process.

Molecularly, to better develop motility and eventually invade the ECM surrounding cells and tissues, cancer cells undergo morphological changes. These changes in morphology include becoming more spindle-like in shape compared to normal cells and the development of sheet-like projections such as lamellipodia and long projections such as filopodia or invadopodia. These projections are formed as a result of dynamic changes in the adhesion protein and actin cytoskeleton due to the rapid assembly and breakdown of actin filaments, ultimately driving cell migration (Machesky, 2008). Invadopodia, which are vertical extensions from the ventral cell membrane into the ECM, can penetrate the basement membrane of blood vessels allowing for intravasation to occur. A key component of these invadopodia is the presence of matrix metalloproteinases (MMPs) (H. Yamaguchi, Wyckoff, & Condeelis, 2005).

MMPs are a family of endopeptidases that have proteolytic activity towards the ECM, specifically in the degradation of collagen fibers. MMPs, in the human body, are involved in many normal biological processes such as embryonic development, nerve growth, organ morphogenesis, and bone remodelling; however, cancer cells are able to use the enzymes to remove ECM during the progression of the disease (Nagase & Woessner, 1999). In ECM degradation, there are specific MMPs or MMP groups that are responsible for the removal of each ECM component (Figueira et al., 2009). When excreted from the cell, the enzyme is an inactive zymogen and requires activation through cleavage (Giannelli et al., 2004). Activation is done by membrane-bound proteinases and by non-proteolytic agents like SH-reactive agents, mercurial compounds, reactive oxygen species, and

denaturants (Nagase & Woessner, 1999). The activity of MMPs is regulated through an inhibitory interaction with tissue inhibitors of metalloproteinases (TIMPs). These inhibitors, when bound to the MMP, cause a conformational change in the protein structure, resulting in loss of enzymatic activity (Nagase & Woessner, 1999). In a 2009 study, it was observed that MMP-2, 9, and 14 are over-expressed in highly invasive and metastatic breast cancer cell lines such as MDA-MB-231 and Hs578T (Figueira et al., 2009). Not only are they expressed and secreted by cancerous cells, but MMPs and TIMPs are also expressed in the tumour stromal cells such as mast cells, fibroblasts, macrophages, lymphocytes, neutrophils, endothelial cells, dendritic cells, and hematopoietic progenitor cells, all supporting metastasis (Kessenbrock, Plaks, & Werb, 2010). The balance between MMPs and TIMPs determine whether matrix degradation or matrix stabilization/formation occurs. In fact, an increase in endogenous MMP levels could lead to the development of more invasive cancers (Levy et al., 1991). Conversely, benign tumours or non-metastatic cancers tend to have low/normal expression of MMPs (Monteagudo, Merino, San-Juan, Liotta, & Stetler-Stevenson, 1990). Thus, metastatic cancer could arise when there is an imbalance between MMPs and TIMPs – specifically either an increase in MMP expression and subsequent activation or a decrease in TIMP expression. Therefore, it is crucial to determine factors that cause alterations to this balance. By identifying and specifically targeting dysregulated proteins involved in molecular interactions that promote the development of cancer, more effective and targeted treatments may be uncovered and ultimately lead to a permanent cure.

1.3 Breast Cancer

Breast cancer is the most common type of cancer affecting women; yet, there is no definite cause for the development of the disease. The Canadian Cancer Society states that one in nine women are at risk of developing breast cancer in their lifetime (Cazzaniga & Bonanni, 2012). It is also important to note that breast cancer also affects a small number of men worldwide; thus, although it mostly affects women, it is not a gender-specific disease. Like most cancers, breast cancer patients die from metastatic breast cancer rather than the primary tumour (Figueira et al., 2009). In fact, 80% of deaths from carcinoma are a result of metastasis. One reason why death is more eminent in metastatic disease is that organ function is compromised, such as the lung or brain tissue, which could lead to death. Additionally, localized breast cancer tumours, as opposed to metastasized tumours, have a better prognosis and a five-year survival rate of 85%. This percentage drops to 23% in women with metastasized breast cancer (Iorns et al., 2012). Even with aggressive treatment options available such as surgery, chemotherapy, and radiation therapy, the incidence and mortality rates remain high worldwide (Cazzaniga & Bonanni, 2012). Moreover, tumours can recur after treatment and these new tumours are often more resistant to treatment, and more likely to metastasize to other organs in the body, resulting in poor prognosis.

The most common types of breast tumours are found in the lobules, glands that produce breast-milk, and ducts, thin tubes that drain breast-milk from the lobules to the nipple; these are called lobular and ductal carcinomas, respectively. The ducts and lobules are surrounded by connective and adipose tissue for support. Each breast contains blood and lymphatic vessels for nourishment and absorption of lymph, respectively. This is an optimal environment for tumour growth and spread – specifically, through sustained

angiogenesis and metastasis; hence, secondary tumours can spread and form. Once the cancer spreads, treatment becomes difficult as tumour resection is no longer effective and the patient prognosis becomes very poor.

Although there are different methods in classifying breast cancers based on grade, stage, gene expression, and receptor expression, the most commonly researched breast cancer subtypes are (1) estrogen (ER) and progesterone receptor (PR) positive breast cancer; (2) HER2 positive (human epidermal growth factor receptor 2) breast cancer; and (3) triple negative breast cancer (TNBC). Of the three subtypes, TNBC is the hardest to treat as its growth is not dependent on estrogen, progesterone, or HER2 receptors. Thus, hormonal therapy or therapies that target HER2 receptors are futile in the treatment of TNBC (Avery, 2018). Furthermore, the fact that breast cancers are heterogeneous makes treatment even more difficult (Bianchini, Balko, Mayer, Sanders, & Gianni, 2016). Accordingly, attempting to identify certain cellular pathways that are over-active in TNBC could lead to the development of more efficient treatment therapies rather than a more generalized therapy such as chemotherapy and radiation therapy. Interestingly, many post-translational modifications are altered resulting in the dysregulation of cellular pathways either through altered molecular signaling or altered gene expression due to histone modifications (Jin & Zangar, 2009). Thus, the aim is to develop alternative options in the treatment of TNBC using inhibitors against enzymes that promote the altered post-translational modifications or simply use these modified proteins as biomarkers to determine an effective therapy depending on which cellular pathways are affected (Jin & Zangar, 2009; Khan, Reddy, & Gupta, 2015).

1.4 Post-Translational Modifications: Arginine Methylation

To fully understand the mechanisms underlying cellular function and disease, it is important to take into consideration the intertwined web of protein interactions. These interactions are not static and are constantly undergoing changes. Looking specifically at protein interactions, alterations can occur via post-translational modifications which include proteolytic cleavage; addition of functional groups to protein residues such as phosphorylation, acetylation, and methylation; and protein degradation. These alterations are catalyzed by enzymes, allowing for functional diversity within the protein network depending on environmental contexts (Mann & Jensen, 2003). The post-translational modifications can result in either the formation or destruction of interactions between proteins, protein and deoxyribonucleic acids (DNA), as well as between protein and ribonucleic acids (RNA). Moreover, post-translational modifications can either positively or negatively influence the intrinsic activity of proteins due to conformational alterations and also affect protein localization (Duan & Walther, 2015). Our primary focus is on methylation which occurs on arginine, lysine, histidine, aspartate, and glutamate amino acids residues as well as the N or C terminus of proteins (Cha & Jho, 2012; Deribe, Pawson, & Dikic, 2010). This thesis focuses specifically on the methylation of arginine residues.

Arginine methylation is a post-translational modification that is involved in the regulation of several cellular processes such as transcription, pre-messenger ribonucleic acid (mRNA) splicing, signal transduction, protein-protein interactions, and chromatin remodelling (Leiper & Nandi, 2011; Verbiest et al., 2008). Arginine is a positively charged amino acid that mediates interactions between proteins and between proteins and nucleic acids as it contains guanidino nitrogen atoms within its side chain that are capable of

forming multiple hydrogen bonds (Gary & Clarke, 1998). The change in chemistry of arginine residues upon methylation of its nitrogen atoms can alter the protein's interactions with DNA, RNA, and proteins. For example, in protein-DNA complexes, the most frequent hydrogen bond donor to the backbone phosphate groups of DNA is an arginine residue, and with its methylation this potential hydrogen bond donor is removed (Bedford & Clarke, 2009).

The post-translational methylation of arginine residues in proteins is catalyzed by a group of enzymes termed protein arginine methyltransferases (PRMTs). These enzymes catalyze the transfer of a methyl group from S-adenosyl methionine (SAM; a methyl donor) to a guanidino nitrogen atom of arginine residues. To date, there are nine well characterized PRMTs which are classified as type I (PRMT 1, 2, 3, 4, 6, 8), II (PRMT5, 9), or III (PRMT7) [Figure 2]. Type I PRMTs catalyze the formation of ω-N^G-monomethylarginine (MMA; as an intermediate) and ω-N^G, N^G-asymmetric dimethylarginine (ADMA), type II catalyzes the formation of MMA (as an intermediate) and ω-N^G, $N^{G'}$-symmetric dimethylarginine (SDMA), and type III only catalyzes the formation of MMA (Bedford & Richard, 2005) (Figure 1). Methylation does not change the positive charge of the arginine residue; however, it does increase its bulkiness and hydrophobicity, altering its ability to interact with proteins, DNA, or RNA species (Gary & Clarke, 1998).

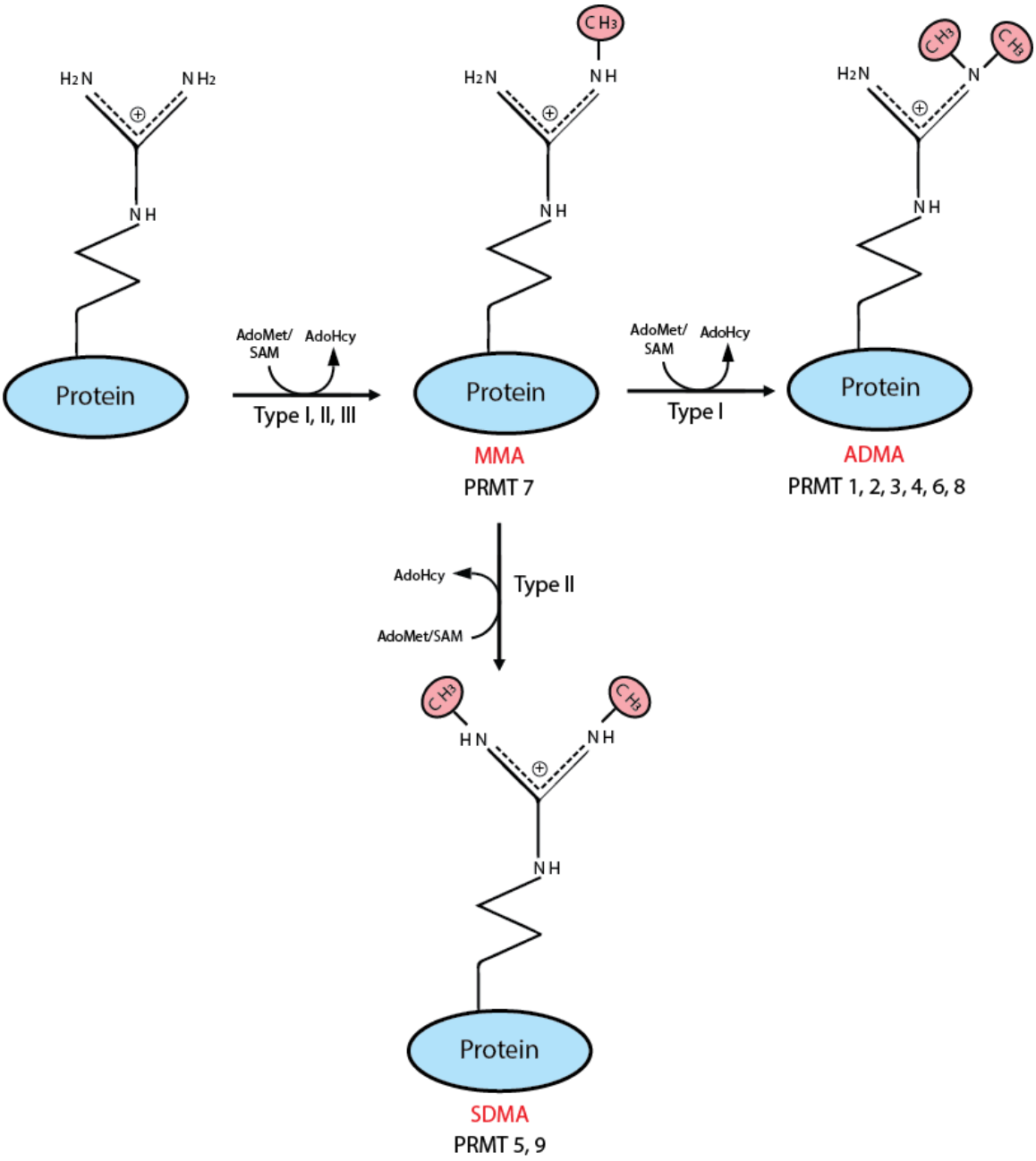

Figure 2: Schematic of protein arginine methyltransferase classification
There are three different types of PRMTs which all produce MMAs via the addition of a methyl group, donated by SAM/AdoMet, to a guanidino nitrogen atom of an arginine residue. Type I PRMTs (PRMT 1, 2, 3, 4, 6, 8) catalyze the formation of ADMA via the addition of a second methyl group to the previously methylated guanidino nitrogen atom. Type II PRMTs (PRMT 5, 9) add a second methyl group to the adjacent un-methylated guanidino nitrogen atom of the arginine residue, producing SDMA. Type III PRMTs (PRMT 7) are solely capable of mono-methylating arginine residues. Adapted from (Haghandish & Côté, 2016).

Arginine methylation had been thought to be an irreversible post-translational modification that can only be removed by protein turnover (Leiper & Nandi, 2011). However, three enzymes have been identified that prevent or reverse the methylation of arginine residues by PRMTs, proving methylation to be a more dynamic modification. Peptidylarginine deiminase 4 (PAD4) prevents arginine methylation by converting arginine residues in proteins to citrulline residues via a deimination reaction. This deimination reaction blocks methylation activity by PRMTs as they are incapable of methylating citrulline residues. PAD4 is capable of deiminating MMA (less efficiently) but not ADMA or SDMA products (Bedford, 2007; Thompson & Fast, 2006). The enzymes capable of arginine demethylation are the Jumonji domain-containing proteins, JMJD6 and JMJC. JMJD6 can demethylate both the asymmetric and symmetric forms of arginine dimethylation in histone proteins specifically at histone 3 arginine 2 (H3R2me2) and H4R3me2 (Chang, Chen, Zhao, & Bruick, 2007). Recently, it was identified that JMJD6 is also capable of demethylating the non-histone protein G3BP1 (Ras GTPase-activating protein-binding protein 1), an important process for stress granule formation in cells (Tsai, Reineke, Jain, Jung, & Lloyd, 2017). Likewise, JMJC enzymes have been shown to exhibit arginine demethylase activity towards both histone and non-histone proteins in addition to its role as a histone lysine demethylase (Walport, Hopkinson, & Chowdhury, 2016). This suggests that the demethylation process of methyl-lysine and methyl-arginine are very similar and thus the two processes share demethylases. However, these findings are still very controversial as there have been many conflicting studies (Böttger et. al., 2015).

As previously mentioned, methylation of proteins regulates many biological functions in the cell such as transcription, signal transduction, and pre-mRNA splicing

(Bedford & Clarke, 2009). Thus, if this post-translational modification is dysregulated, an imbalance in cell homeostasis can lead to altered molecular mechanisms. It is inevitable that arginine methylation can have either a positive or negative impact on cancer development. In fact, many PRMTs have been shown to be mechanistically involved in the development and progression of cancer hallmarks by affecting protein interactions in various cellular pathways. For instance, in breast cancer, PRMT1v2, one of seven splice isoforms of PRMT1, is upregulated in breast cancer cell lines compared to normal cells and promotes breast cancer cell invasion by disrupting cell-cell adhesion via a reduction in β-catenin protein levels (Baldwin, Morettin, Paris, Goulet, & Cote, 2012; Isabelle Goulet, Gauvin, Boisvenue, & Côté, 2007). PRMT1 additionally methylates the estrogen receptor α in breast cancer cells, mediating the receptor's cytoplasmic localization and recruitment of factors required for cytoplasmic signalling cascades to ultimately promote cell proliferation, survival, and migration (Le Romancer et al., 2008). PRMT4 displays oncogenic effects by negatively regulating retinoblastoma tumour suppressor protein pRB via methylation at R^{787}, leading to disruption of the pRB-E2F1 complex, allowing for the activation of S-phase regulatory genes to promote cell growth (Kim et al., 2015). Similarly, in osteosarcoma cells, PRMT5 has been shown to control cell cycle progression, specifically evasion of apoptosis, via the symmetric dimethylation of R^{111} and R^{113} of the E2F1 transcription factor (Zheng et al., 2013). PRMT6 methylates cyclin-dependent kinase inhibitor, p21, to increase the inhibitor's cytoplasmic localization which makes cancer cells more resistant to cytotoxic agents (Nakakido et al., 2015). In addition, aberrant PRMT expression is also involved in human diseases such as cardiovascular disease and spinal muscular atrophy (Bedford & Clarke, 2009).

PRMTs are also capable of changing the genomic expression of cells by either activating or repressing genes via the methylation of histone proteins which can promote tumourigenesis. For instance, PRMT1 and 4 co-operate in the positive or negative regulation of gene expression patterns within cancer cells (Kleinschmidt, Streubel, Samans, Krause, & Bauer, 2008). Specifically, PRMT1 plays a dual regulatory role in promoting breast cancer cell migration and growth through epigenetic regulation of the ZEB1 (zinc finger E-box-binding homeobox 1) transcription factor via asymmetric methylation of H4R3 within its promoter (Y. Gao et al., 2016). PRMT5 regulates breast cancer stem cell proliferation and renewal by enhancing gene expression of the transcription factor FOXP1 (forkhead box protein P1). Notably, PRMT5 symmetrically dimethylates H3R2 within FOXP1's promoter region leading to an increase in the activating gene expression mark, H3K4 tri-methylation (Chiang et al., 2017). Similarly, through dimethylation of H3R2 within the promoter of p53 (via asymmetric dimethylation rather than symmetric as with PRMT5), PRMT6 allows cells to ultimately bypass cellular senescence (Neault, Mallette, Vogel, Michaud-Levesque, & Richard, 2012). Thus, it is evident that PRMTs can epigenetically regulate cancer cells to promote tumourigenesis. In addition to their roles in regulating transcription via post-translational modification of histones and/or the regulation of transcription factors, PRMTs also regulate protein translation.

1.5 Translation Initiation and Stress Granules

Protein translation is a tightly controlled event involving many regulatory proteins. Increased cancer cell proliferation requires amplified protein synthesis to maintain cell growth and eventual cell proliferation. Thus, dysregulation of protein translation could be considered as an enabling cancer hallmark as it has been shown to be linked with cell survival, aberrant proliferation, angiogenesis, immune response alterations, and cancer energetics (Colina et al., 2008; Kevil et al., 1996; Larsson et al., 2007; Polunovsky et al., 1996). Accordingly, cancerous cells harbor a more 'selective translation' mechanism through the eIF4F complex. Specifically, elevated eIF4F activity in cancer cells result in enhanced protein translation of a subset of mRNAs that enhance cell growth and tumourigenesis (Pelletier, Graff, Ruggero, & Sonenberg, 2015). Hence, it is important that a cell precisely regulates protein translation to prevent aberrant protein expression which could eventually lead to cancer promoting hallmarks.

The process of translation entails four main steps: translation initiation, elongation, termination, and ribosome recycling. Translation initiation is the rate limiting step of protein synthesis which involves the assembly of an 80S ribosome complex from 40S and 60S subunits (Silvera, Formenti, & Schneider, 2010). First, the 43S pre-initiation complex is formed which consists of the 40S ribosomal subunit and eukaryotic translation initiation factors (eIFs) of which the ternary complex is of great importance. The ternary complex consists of eIF2α, eIF2β, and eIF2γ along with initiator methionyl tRNA ($tRNA^{Met}$) and GTP: eIF2-GTP-Met-$tRNA^{Met}$. This complex, along with the eIF4F complex (eIF4A, eIF4G, eIF4E) and eIF3, mediates the recruitment of the 43S complex to mRNAs for translation initiation, forming the 48S pre-initiation complex (Jackson, Hellen, & Pestova,

2010). Subsequently, mRNA scanning occurs and once the initiation codon is recognized, the 60S subunit joins, releasing the ternary complex and forming an elongation-competent 80S complex for translation elongation – marking the end of translation initiation (Silvera et al., 2010). This aforementioned mechanism is termed as cap-dependent translation.

To date, some PRMTs have been implicated in translational control. PRMT1 mediates global translation by methylating eIF4G to promote its stability while also maintaining the integrity of the initiation complex, to promote tumour initiation and maintenance (Hsu et al., 2017). PRMT1 additionally methylates Aven to regulate the translation of mixed lineage leukemia protooncogenes by binding mRNAs harboring G-quadruplexes along with RNA helicase DHX36 (Thandapani et al., 2015). Both PRMT5 and 7 were shown to methylate elongation factor 2 (eEF2) to potentially regulate protein synthesis (Jung et al., 2011). Finally, PRMT3 regulates the biosynthesis of ribosomes via methylation of ribosomal protein S2 (rpS2) in yeast. Mechanistically, it was proposed that methylation of rpS2 by PRMT3 could potentially regulate translation of specific mRNAs (Bachand & Silver, 2004).

Importantly, translation initiation is a rate limiting step as it requires energy from GTP (guanosine triphosphate) and is dependent on the secondary structure of the 5' untranslated region of the mRNA. Furthermore, in order for ribosome recycling to occur, the ternary complex requires that GDP (guanosine diphosphate) is re-converted back to GTP via the guanine exchange factor eIF2B. The activity of the 43S pre-initiation complex is strictly regulated by the phosphorylation state of the ternary complex, specifically phosphorylation at S^{51} of eIF2α. When a cell is under environmental stress such as oxidative stress, heat shock, osmotic stress, UV radiation, and/or viral infection, translation

initiation is blocked resulting in the disassembly of polysomes (Buchan & Parker, 2009). The phosphorylation of translation initiation factor eIF2α at S^{51} is catalyzed by the following kinases: PKR, HRI, PERK, or GCN2 (Baird & Wek, 2012; Fournier, Gareau, & Mazroui, 2010; Harding, Zhang, Bertolotti, Zeng, & Ron, 2000; Holcik & Sonenberg, 2005; Jackson et al., 2010; McEwen et al., 2005; Ruggero, 2013; Srivastava, Kumar, & Kaufman, 1998; Wek, Zhu, & Wek, 1995).

PKR (protein kinase RNA-activated) phosphorylates eIF2α when cells are infected by viral double-stranded RNA, heat shock, and UV irradiation (Srivastava et al., 1998). HRI (heme-regulated initiation factor) is activated upon oxidative stress (McEwen et al., 2005). PERK (PKR-like endoplasmic reticulum kinase) is responsible for regulating protein homeostasis and is activated when there is an increase in unfolded proteins (Harding et al., 2000). CGN2 (general control nonderepressible 2) phosphorylates eIF2α when cells are deprived of amino acids (Wek et al., 1995). When eIF2α is phosphorylated (P-eIF2α) by one of its kinases, a conformational shift occurs, resulting in the tight binding of eIF2B to the ternary complex, ultimately preventing the GDP to GTP exchange (Bogorad, Lin, & Marintchev, 2017; Kashiwagi, Ito, & Yokoyama, 2017). This tight eIF2-eIF2B complex reduces the availability, but not fully depleting, the ternary complex for further translation and ultimately results in the disassembly of polysomes (Holcik & Sonenberg, 2005; Jackson et al., 2010).

When cap-dependent translation is compromised, limiting the ternary complex, such as in the case of cellular stress, the translation of P-eIF2α-dependent transcripts is observed. Specifically, transcripts with several upstream open reading frames (uORFs) take advantage of the limited ternary complex to promote the translation of proteins such

as activating transcription factor 4 (ATF4). In the case of ATF4, uORF2 inhibits its translation. Thus, when the pool of active ternary complex is reduced, ribosome scanning through the inhibitory uORF2 occurs until a competent initiating ribosome is formed at the later uORFs, allowing for translation of AFT4 to ensue (Vattem & Wek, 2004). Furthermore, cap-independent translation is activated to promote the translation of cell survival proteins (Holcik & Sonenberg, 2005; Komar & Hatzoglou, 2011; Pestova, de Breyne, Pisarev, Abaeva, & Hellen, 2008; Robert et al., 2006). Cap-independent translation consists of the translation of mRNA transcripts with highly structured internal ribosomal entry sites (IRES) within the 5' untranslated region (5'UTR) via the recruitment of translation initiation factors (except for eIF4F complex) as well as IRES-transactivating factors (ITAFs) such as heterogeneous nuclear ribonucleoproteins (hnRNPs). Generally, the activation of IRES-dependent translation allows for the synthesis of proteins required to either promote cell survival or in some cases induce cell death; thus this mechanism is critical in regulating the cellular response towards environmental stress (Gerlitz, Jagus, & Elroy-Stein, 2002; Graber & Holcik, 2007; Komar & Hatzoglou, 2011).

Upon disassembly of polysomes, non-membranous cytoplasmic ribonucleoprotein structures are assembled which consist of non-translating mRNAs complexed with translation initiation factors, the 40S ribosomal subunit, and poly-A binding proteins (Balagopal & Parker, 2009). These structures are termed stress granules. Stress granules are formed as a coordinated response to reprogram cell metabolism by drastically reducing translation initiation upon stress to protect the cell against stress-induced damage and ultimately repair the damage (Yamasaki & Anderson, 2008). The translation of non-essential "housekeeping" proteins are stalled from polysomes and re-localized to stress

granules. Selective translation of proteins required to repair stress-induced damage is then stimulated (Yamasaki & Anderson, 2008). Additionally, cell survival is also promoted by inhibiting apoptosis through sequestration of pro-apoptotic factors within stress granules as well as sequestration of anti-apoptotic transcripts to prevent their degradation (Fournier et al., 2010). Cells that cannot phosphorylate eIF2α cannot form eIF2α-dependent stress granules; thus, these cells are hypersensitive to the toxic effects of stress and eventually apoptose (Yamasaki & Anderson, 2008). It is important to note that the components of stress granules can differ according to the nature of the cellular stress and the organism (Buchan & Parker, 2009; Buchan, Yoon, & Parker, 2011). Furthermore, stress granules can form upon eIF2α-dependent phosphorylation or via eIF2α-independent pathways such as the disruption of the eIF4F complex (Panas, Ivanov, & Anderson, 2016). It is now apparent that stress granules are essential for proper cell reprogramming upon exposure to environmental stresses to promote cell survival.

Interestingly, several chemotherapeutic drugs (bortezomib, 5-fluorouracil, 6-thioguanine, 5-azacytidine, and sorafenib) have been shown to induce stress granule formation thereby resulting in the cells resisting drug-induced apoptosis (Adjibade et al., 2015; Anderson, Kedersha, & Ivanov, 2015; Fournier et al., 2010; Kaehler, Isensee, Hucho, Lehrach, & Krobitsch, 2014). As stress granules have been shown to exist in breast tumour cells at the hypoxic core to promote cell survival, it is possible that resistance against chemotherapeutic drugs could be due to this stress granule formation (Baguet et al., 2007). Moreover, other drugs may also induce formation of stress granules, resulting in cell survival and potentially tumour recurrence after treatment. P-eIF2α can also positively regulate the Akt survival pathway to promote cell survival under stressed conditions

(Rajesh et al., 2015; Tenkerian et al., 2015). Specifically, two groups observed that P-eIF2α downregulates mTORC1 activity, ultimately alleviating its negative regulatory role in the PI3K-Akt survival pathway. Thus, absence of P-eIF2α could potentially lead to cell death via Akt activation. In essence, P-eIF2α plays a regulatory switch in Akt-related cell death or survival. Hence, P-eIF2α could potentially promote cell survival and thus further exploration in this avenue is advantageous.

As stress granules are composed of many proteins, it is inevitable that post-translational modifications are important for their assembly and/or disassembly. PRMTs have been shown to be either directly or indirectly involved in the regulation and/or assembly of stress granules. For example, upon methylation by PRMT1, FUS (Fused in sarcoma) is shuttled from the nucleus to the cytoplasm where it is localized to stress granules (Tradewell et al., 2012; Yamaguchi & Kitajo, 2012). Moreover, methylation of FUS by PRMT1 promotes phase separation and proper granule function (Hofweber et al., 2018; Qamar et al., 2018). Methylation of arginine residues within heterogeneous ribonucleoproteins and FMRP (fragile X mental retardation protein) have been linked with stress granule assembly (Ohn & Anderson, 2010; Xie & Denman, 2011). Furthermore, methylation was shown to be important for stress granule disassembly and/or stability as the use of an inhibitor of methylation (5'-deoxy-5'-methylthioadenosine; MTA) affected stress granule kinetics while altering the composition of the granules (Goulet, Boisvenue, Mokas, Mazroui, & Cote, 2008). Conversely, demethylation of certain proteins is also important for stress granule formation. Demethylation of G3BP1 promotes stress granule formation – thus, there is a critical balance that needs to be maintained between arginine methylation and demethylation of G3BP1 in order to regulate stress granule formation (W.-

C. Tsai et al., 2016; W. C. Tsai et al., 2017). Furthermore, it is apparent that both methylation and demethylation are critical for stress granule formation suggesting that methylation is a precisely regulated post-translational modification and that protein interactions are highly regulated.

Hence, it is evident that PRMTs regulate several important cellular processes including translation and stress granule formation. Although many of these findings are focused on type I or II PRMTs, not much research has been performed on type III PRMTs. Thus, this work focuses on PRMT7, the sole type III PRMT.

1.6 Protein Arginine Methyltransferase 7 (PRMT7)

Protein arginine methyltransferase 7 (PRMT7) is a type III PRMT which adds a single methyl group on a terminal guanidino nitrogen atom (Fisk et al., 2009; Zurita-Lopez, Sandberg, Kelly, & Clarke, 2012). However, it was mistakenly classified as a type II PRMT due to contamination with PRMT5 when using FLAG M2 agarose beads (Lee et al., 2005; Zurita-Lopez et al., 2012). In fact, in *C. elegans,* the PRMT7 crystal structure demonstrates that the entrance to the substrate pocket of PRMT7 is narrower than other PRMTs due to the presence of bulky residues (Hasegawa, Toma-Fukai, Kim, Fukamizu, & Shimizu, 2014). Additionally, in trypanosomal PRMT7, the bulky residues are suboptimal in forming hydrogen bonds required for appropriate S_N2 geometry to produce dimethylation (Cáceres et al., 2018). The sequence of these bulky residues within the substrate pocket are similar in mammals, implying a similar narrow pocket and substrate binding geometry. Thus, steric constraints and geometric orientation/binding of its substrates makes it unlikely that a monomethylated arginine substrate enters the substrate binding pocket of PRMT7 for a subsequent dimethylation reaction (Cáceres et al., 2018; Hasegawa et al., 2014).

PRMT7 has its own unique substrate recognition motif: an RXR motif – highly basic residues (X) flanked by arginine residues (R) (Feng et al., 2013) that differs from other PRMT recognition motifs such as glycine/arginine-rich (GAR) motifs and proline/glycine/methionine-rich motifs (PGM) (Yang & Bedford, 2013). Although PRMT7 is unable to dimethylate arginine residues, it does positively regulate dimethylation by PRMT5. Specifically, PRMT7 monomethylates arginine residues on certain proteins leading to dimethylation by PRMT5 to occur at another site through allosteric regulation

(Jain, Jin, & Clarke, 2017). This could also explain why both PRMT5 and 7 share certain substrates: histone 4 (H4), histone 3 (H3), eukaryotic elongation factor 2 (eEF2), and Sm proteins (S. S. Dhar et al., 2012; Gonsalvez et al., 2007; Jain et al., 2017; Jung et al., 2011; Majumder et al., 2010; Migliori et al., 2012). Methylation by both PRMT5 and 7 at distinct sites within the same protein also confirms that the RXR motif is unique to PRMT7.

Most PRMTs are active as either homodimers, heterodimers, or part of a larger complex such as PRMT5 and its methylosome complex (Antonysamy et al., 2012; Herrmann, Pably, Eckerich, Bedford, & Fackelmayer, 2009). Each monomer harbors a single SAM-binding domain (domain that binds the cofactor/methyl-donor). According to its crystal structure, PRMT7 exhibits pseudo-homodimerization due to its repeated PRMT core domains and two SAM-binding domains, which are thought to be a result of gene duplication (Hasegawa et al., 2014; Miranda, Miranda, Frankel, & Clarke, 2004). Thus, PRMT7 is active as a monomer (pseudo-homodimer) – a unique occurrence amongst PRMTs. As mentioned, PRMT7 is unique in that it contains two SAM-binding motifs, one at the C-terminus and one at the N-terminus. Both motifs have been shown to be required for enzymatic activity (Miranda et al., 2004). Alone, the N-terminal motif is catalytically active whereas the C-terminal motif is inactive. Nevertheless, the C-terminal motif is required for proper structural conformation and full enzymatic activity (Cura, Troffer-Charlier, Lambert, Bonnefond, & Cavarelli, 2014; Cura, Troffer-Charlier, Wurtz, Bonnefond, & Cavarelli, 2014; Miranda et al., 2004). PRMT9 is the only other PRMT known to possess two SAM-binding domains; however, it is still unclear whether PRMT9 functions as a dimer or monomer and whether both methyltransferase motifs are required for enzymatic function (Yang, Hadjikyriacou, & Xia, 2015).

Interestingly, in DC-3F hamster cells, there are two isoforms of PRMT7: alpha and beta with molecular weights of 78 and 82 kilo Daltons (kDa), respectively. PRMT7α has an exclusively cytoplasmic localization whereas PRMT7β can be found in the cytoplasm and nucleus; thus, the two isoforms may have both similar and distinct substrates (Gros et al., 2006). For instance, PRMT7α has also been implicated in the cell cycle in 10T1/2 mouse fibroblast cells as there is high expression of PRMT7α in the G1 stage and G2/mitosis stage while undetectable levels were observed in the DNA synthesis stage. Interestingly, in human cell lines, only one isoform of PRMT7 has been observed. This isoform is homologous to the PRMT7α found in hamster cells (Gros et al., 2006; Zurita-Lopez et al., 2012).

PRMT7 was originally discovered in a screen of genetic suppressor elements to identify genes that confer chemotherapeutic drug susceptibility (Gros et al., 2003). The enzyme has been shown to promote both sensitivity and resistance towards drugs, depending on the type of drug used. It was shown that PRMT7 is negatively correlated with resistance against 9-OH-ellipticine, etoposide, and cisplatin (Karkhanis et al., 2012; Verbiest et al., 2008) but positively correlated with resistance against camptothecin, bleomycin, and UV radiation (Gros et al., 2003; Verbiest et al., 2008). Over-expression of PRMT7 has been shown to either confer increased resistance or sensitivity against chemotherapeutic drugs. For instance, over-expression of PRMT7 is positively correlated with increased resistance against a topoisomerase I inhibitor, camptothecin (Verbiest et al., 2008). Reduction of PRMT7α and β protein expression using a genetic suppressor element (GSE)-mediated knockdown in DC-3F cells showed increased resistance towards cisplatin but hypersensitivity towards camptothecin (Bleibel et al., 2009; Gros et al., 2006).

However, over-expression of PRMT7 did not affect sensitivity of the DC-3F cells towards camptothecin (Verbiest et al., 2008). Thus, it can be suggested that there exists a threshold for optimal methylation of the specific substrates of PRMT7 and that over-expression above that threshold may not affect methylation; however, this has yet to be proven.

To date, the precise mechanism by which PRMT7 modulates response towards certain drugs remains largely unknown. However, a mechanism for conferred sensitivity has been explored. Upon symmetric dimethylation of promoter histones H2AR3 and H4R3, PRMT7 represses DNA repair genes such as POLD1 (DNA polymerase delta catalytic subunit) and APEX2 (apurinic/apyrimidinic endonuclease 2) which both repair DNA damage via base excision (Karkhanis et al., 2012). Moreover, another PRMT is most likely involved as PRMT7 is a type III PRMT incapable of symmetrically dimethylating its substrates. Repression of the DNA repair genes is dependent on the interaction between PRMT7 and the BRG1-based containing SWI/SNF chromatin remodeling complex. Thus, this group speculated that SWI/SNF complex recruitment results in remodeling of the nucleosome and subsequent recruitment of transcriptional regulators to repress the DNA repair genes. Thus, depletion of PRMT7 in NIH3T3 mouse embryo fibroblast cells results in the de-repression of the DNA repair genes, increasing resistance against cisplatin, chlorambucil, and mitomycin C, ultimately promoting cell survival. It still remains unclear how PRMT7 plays a dual role in sensitizing cells and promoting resistance against certain drugs. Further empirical experimentation may give insights as to why certain cells are more sensitive or resistant towards chemotherapy.

In addition to its role in resistance and sensitivity towards drugs, several genome-wide studies analyzing over 1200 human breast tumours have established a strong

correlation between over-expression of PRMT7 and breast cancer aggressiveness and metastasis and thus decreased survival rates. Specifically, expression of chromosome 16q22 (which contains the PRMT7 gene) is consistently up-regulated in metastatic breast cancer (Thomassen, Tan, & Kruse, 2009). Therefore, over-expression of PRMT7 may promote breast cancer cells to undergo metastasis, leading to a more aggressive and harder to treat cancer. However, these genome-wide studies are correlative and research has yet to be performed to evaluate the precise role of PRMT7 in human breast cancer. Furthermore, as PRMT7 is one of the most recently discovered PRMTs, there is limited knowledge with respect to its involvement in biological function, its protein interactome, and substrates.

As noted above, PRMTs are also known to be histone methyltransferases that regulate gene expression, thus, histones are well recognized substrates. PRMT7 is capable of methylating histones at the following arginine residues: H4R3, H2AR3, H4R17, H4R19, H3R2, H2BR29, H2BR31, and H2BR33 (S. S. Dhar et al., 2012; Y Feng et al., 2013; Karkhanis et al., 2012; Migliori et al., 2012). The majority have only been shown to be *in vitro* substrates of PRMT7. However, H4R3, H2AR3, and H3R2 have been shown to be substrates *in vivo* (S. S. Dhar et al., 2012; Karkhanis et al., 2012; Migliori et al., 2012). The only non-histone PRMT7 interactors/substrates that have been identified are as follows: CTCFL (CCCTC-Binding Factor Like), small ribonucleoprotein protein SmD3 (small nuclear ribonucleoprotein core protein D3), and eEF2 (Feng, Hadjikyriacou, & Clarke, 2014; Gonsalvez et al., 2007; Jelinic, Stehle, & Shaw, 2006; Jung et al., 2011). Interestingly, CTCFL enhances the methyltransferase activity of PRMT7 and is highly expressed in breast cancer tumours (Jelinic et al., 2006; Martin-Kleiner, 2012).

Accordingly, further identification of PRMT7-specific substrates and/or interacting proteins would aid in better understanding the protein's biological functions and how the protein is involved in cancer hallmarks; specifically, how PRMT7 promotes breast cancer aggression as suggested by a meta-analysis study (Thomassen et al., 2009).

PRMT7 also seems to be important for organismal survival. Three independent groups have developed PRMT7 null mice to better characterize the enzyme (Blanc, Vogel, Chen, Crist, & Richard, 2016; Jeong et al., 2016; Ying et al., 2015). Ying and colleagues observed post-natal death after 5-10 days in a C57BL6/129sv genetic background (Ying et al., 2015). However, both Richard's and Jong-Sun Kang's group were able to overcome early post-natal death by backcrossing the lines with wild type C57BL6 for over six generations (Blanc et al., 2016; Ying et al., 2015). These mice survived well into adulthood but with indications of obesity, defects in skeletal muscle, and developmental delays (Blanc et al., 2016).

Specifically in skeletal muscle, Blanc and colleagues observed that PRMT7 is necessary for muscle regeneration. Interestingly, in the absence of PRMT7, the satellite cells underwent premature senescence and were subsequently incapable of replenishing muscle stem cells thus exemplifying the importance of PRMT7 in maintaining muscle stem cell regenerative capabilities (Blanc et al., 2016). Furthermore, clinical work correlated loss-of-function mutations of PRMT7 with intellectual disability syndrome, microcephaly (abnormally small head), and brachydactylyl (shortened fingers/toes) (Agolini et al., 2018; Kernohan et al., 2017). As such extreme symptoms are observed, PRMT7 most likely regulates critical cellular functions.

Identifying pathways involving PRMT7 activity, its interacting proteins, or the genes that are regulated by its activity, will help in further understanding the involvement of PRMT7 in the development of metastatic breast cancer and ultimately other diseases.

1.7 Hypothesis and Research Aims

PRMTs have been recognized as important enzymes in cellular mechanisms since aberrant expression of these enzymes has been correlated with aggressive human diseases such as cancers, cardiovascular diseases, and neurodegenerative diseases (Bedford & Clarke, 2009; Blanc & Richard, 2017; Yang & Bedford, 2013). However, limited research regarding PRMT7 and cancer have been published. Furthermore, there have been many debates throughout the years regarding PRMT7's activity. As previously mentioned, PRMT7 was initially characterized as possessing type II methyltransferase activity, capable of generating both mono-methylation (Miranda et al., 2004) and symmetric di-methylation (Lee et al., 2005) of arginine residues *in vitro*. Nevertheless, two studies have provided convincing evidence indicating that PRMT7 is exclusively a type III enzyme, capable of only mono-methylating protein substrates at least in vitro (Y Feng et al., 2013, 2014; Zurita-Lopez et al., 2012). Although this is now an accepted feature of PRMT7, scientific knowledge in terms of its biological role in cellular processes required further investigation. Thus, we were determined to better characterize the role of PRMT7 in breast cancer as well as discover its protein interactome.

Though other PRMTs have been extensively studied in breast cancer and have been shown to be correlated with its aggressiveness and invasiveness, such as PRMT1, 4, 5, and 6, experiments on PRMT7 in breast cancer cell lines and tissues exploring the potential role of PRMT7 in cancer tumourigenesis had not been performed. The only study linking PRMT7 to breast cancer was correlative. Specifically, it was shown that PRMT7 mRNA expression was significantly increased in breast tumours which positively correlated with breast cancer aggressiveness and metastasis (Thomassen et al., 2009). Thus, it is likely that

increased PRMT7 mRNA expression correlates with an upregulation in PRMT7 protein expression within cancer cells.

We hypothesize that PRMT7 protein levels are upregulated in breast cancer cells and that its dysregulation contributes towards breast cancer progression and/or development by regulating and/or altering critical cancer-promoting signaling processes. This thesis aims to characterize the role of PRMT7 within breast cancer cells both in terms of biological consequences and mechanism.

The following are the two aims of research presented in this thesis, each with their own objectives:

I. Explore the potential contribution(s) of PRMT7 in breast cancer development and/or disease progression.

i. Explore PRMT7 expression in breast cancer cell lines and tissues.

ii. Determine the effects of PRMT7 knockdown on cell proliferation and invasion *in vitro*, as well as metastasis *in vivo*.

iii. Explore the mechanisms behind PRMT7's role in invasion/metastasis.

II. Identify PRMT7-specific protein interactors and/or substrates to explore a novel biological function for PRMT7 within breast cancer cells and to explore the mechanism(s) by which PRMT7 mediates its tumourigenic effect(s) in breast cancer.

i. Identify novel protein interactors of PRMT7 using quantitative mass spectrometry.

ii. Confirmation of the interacting proteins obtained from the proteomic experimentation.
iii. Explore the mechanisms and downstream pathways involving PRMT7 and its newly identified protein interactors/substrates.

Hence, by assessing the contributing role of PRMT7 as a novel mediator for breast cancer tumour development and aggressiveness, our study addresses an important knowledge gap in the field of arginine methylation regarding PRMT7 substrates and function(s), and have the potential to identify PRMT7 as a novel and promising therapeutic target for breast cancer.

CHAPTER 2: MATERIALS AND METHODS

Cell lines: Cells were purchased from the American Type Culture Collection (Manassas, VA). MDA-MB-231, 293T, BT20, and BT549 cells, were cultured in complete Dulbecco's modified Eagle's medium (DMEM) supplemented with 10% fetal bovine serum, 1% sodium pyruvate, 1% 50 IU/mL penicillin and 50 mg/mL streptomycin. MCF7 and Hs578T cells were additionally supplemented with 2.75µg/mL insulin. MCF10A cells were obtained from Drs. Marie-Chloé Boulanger and Josee Lavoie (Laval University Cancer Research Center, Laval, QC) and cultured in DMEM supplemented with 5% horse serum, 20ng/mL epidermal growth factor, 0.5µg/mL hydrocortisone, 100ng/mL cholera toxin, 10µg/mL insulin, 1% of 50 IU/mL penicillin, and 50 mg/mL streptomycin. Cells were maintained in a monolayer at 5% carbon dioxide atmosphere at 37ºC and harvested using 0.05% trypsin EDTA (Ethylenediaminetetraacetic acid; HyClone) when 80-90% confluent. A hemocytometer (Sigma-Aldrich) was used to determine the cell concentration in cells/mL.

Antibodies: PRMT7 (#14762S), eIF2α (#5324S), P- eIF2α (#3597S), Mono-Methyl Arginine (#8015S), Akt (#9272), and P-Akt (S^{473}; #9271) antibodies were purchased from Cell Signaling Technology; FMRP (#MAB2160) and puromycin (#MABE343) antibodies were purchased from EMD Millipore; GFP antibody (#sc-8334) and TIA-1 (#166247) were purchased from Santa Cruz Biotechnology; eIF2β (#A301-743A) was purchased from Bethyl Laboratories; eIF2γ antibody (#11162-1-AP) was purchased from Proteintech; GAPDH antibody (#MMS-580S) was purchased from Covance; and α-Tubulin (#T6199)

and G3BP1 (#07-1801) antibodies were purchased from Sigma Aldrich. All antibodies were used at a 1:1000 dilution overnight at 4C. Secondary antibodies conjugated with horseradish peroxidase (HRP) included goat anti-rabbit (Jackson Laboratories; used at 1:5000), goat anti-mouse (Jackson Laboratories; used at 1:25 000), and donkey anti-goat (Santa Cruz Biotechnology; used at 1:2000).

Drug treatment: Sodium arsenite (AsNaO2) was used at a final concentration of 500µM for 30 minutes or 200µM for 1 hour at 37C. Rocaglamide A was used at a final concentration of 2µM for 2 hours at 37C. Thapsigargin was used at 10µM for 2 hours at 37C. Puromycin was used at a final concentration of 91µM for 8 minutes at 37C.

Transfections: Cells were seeded at 300 000 cells/well in 6 well plates or 500 000/plate in 10 cm plates and incubated at 5% carbon dioxide in air at 37ºC overnight. The media of the cells was changed one hour prior to transfections using complete DMEM and the next day, 16h after transfections. 2µg of DNA (for 6 wells) or 10µg (for 10 cm plates) were added to 600µL of serum-free media. The reaction was incubated for 5 minutes at room temperature. PEI (polyethylenimine) was added to the mix at a ratio of 1:2 (total DNA in µg: volume of PEI at 1mg/mL). The reaction was subsequently incubated at room temperature for 20 minutes. The mix was then added, drop by drop, to the cells and cells were incubated at 5% carbon dioxide in air at 37ºC. For clonal populations, clones were picked using a pipette tip and 10µL of 0.05% trypsin EDTA, and seeded into a 96 well plate containing complete DMEM. Clonal populations were eventually scaled up to 10 cm plates.

Vectors: To over-express either C-terminal Myc-tagged or GFP-tagged PRMT7, pLenti-C-MycDDK or pLenti-C-mGFP, respectively, were purchased from Origene. A control vector expressing only GFP or Myc-DDK was created via blunt-end digestion and subsequent ligation of the pLenti-C-mGFP-PRMT7 and pLenti-C-MycDDK-PRMT7 vectors, respectively. To knockdown PRMT7, RNA interference was performed using pGIPZ vectors containing shRNA sequences against PRMT7 were also used: AGCTATGCAGTGGAGTTTC (shPRMT7-1) and GGCTTTAGTGATAAGATTA (shPRMT7-2). As a control, an shRNA proprietary sequence was used since it does not target any mRNA in the mammalian genome. Our more efficient knockdowns (whereby the experiments were all transient) were obtained using pLKO.1 vectors obtained from The RNAi Consortium containing either an shRNA with a luciferase sequence for control (5'-CAAATCACAGAATCGTCGTAT-3') or two independent PRMT7 sequences (5'-GCTAACCACTTGGAAGATAAA-3' and 5'- CGATGACTACTGCGTATGGTA-3'). Alternatively, To obtain *in vitro* knockout of PRMT7, CRISPR-Cas9 (clustered regularly interspaced short palindromic repeats-CRISPR-assocaited protein 9) was employed using sgRNA sequences designed from an online program (http://crispr.mit.edu/). Two sgRNA sequences were designed (5'-CACCGTCGGGCCAATCCGACCACG-3' and 5'-CACCGCATCGTCCCTCCC GTTGACG-3') and cloned into the lentiCRISPR-v2 vector (generous gift from Dr. David Lohnes, uOttawa). Both sequences were used simultaneously to obtain complete knockout of both alleles of PRMT7.

Proliferation/Cell viability assays: Cells were seeded into 96 well plates at 10 000 cells/well. Cells were infected the next day with either pLKO.1 non-targeting shRNA, pLKO.1 PRMT7-targeting shRNA, or sgRNA targeting PRMT7 for knockout (population). Annexin V or cytotox red reagents were also added to media. Plates were placed in an IncuCyte Zoom Live-cell imaging system where two images were taken per well every two hours for a period of 140 hours. Media-only and parental cells were used as controls. Experiments were run in triplicate for four independent experiments. Cell proliferation was analyzed via percent confluency, apoptosis via annexin V staining, and cytotoxicity via cytotox red staining. Concentrations of dyes added were used according to product data sheet (IncuCyte, Essen Bioscience).

MTT proliferation assay: Cells were seeded at 1000 cells/100µL complete DMEM per 96-well for proliferation assays and incubated at 5% carbon dioxide in air at 37ºC until each time point. Wells containing only complete DMEM were used as a control. Experiments were done in replicates of 6. At days 1, 2, 4, and 8 after initial seeding, 25µL of MTT reagent (3-(4,5-Dimethylthiazol-2-yl)-2,5-diphenyltetrazolium bromide) (MTT; Sigma-Aldrich) was added to the cells for 2 hours. Cells were lysed with 100µL of MTT lysis buffer (50% dimethylformamide and 10% sodium dodecyl sulphate) and absorbances were read at 570nm using a Synergy H1 Hybrid multi-mode plate reader (BioTek).

Lentivirus production: 293T cells were transiently transfected with packaging plasmids, pMD2.G and pPAX2 along with the expression plasmid. After 24 h, media on these cells was changed to fresh media and breast cancer cells were plated (250 000 cells in a 10cm

plate). Following an additional 24 h incubation, lentivirus was harvested from the media by filtering it through a 0.45 um syringe filter. Media containing virus with 8 µg/mL polybrene was placed on target cells and allowed to infect for 48 h. Media was then changed and cells were used for experimentations.

Cell lysis and western blot analysis: Cells were seeded at 500 000 cells and lysed the next day using lysis buffer (1M Tris (hydroxymethyl) amino methane, 5M NaCl, 0.5M EDTA, 10% Tergitol-type NP-40, 10% NaDOC (Sodium deoxycholate), 10% SDS (sodium dodecyl sulphate), pH 7.4) containing protease inhibitors (Roche). Cell lysates were vortexed, incubated on ice for 15 minutes, and spun at 13 000 revolutions per minute (rpm) for 10 minutes. Protein samples were quantified using a DC protein assay (Bio-Rad) following the manufacturer's protocol. 15µg protein samples were loaded using Laemmli dye (2M Tris, SDS, glycerol, 14.3M β-mercaptoethanol, DTT (dithiothreitol), bromophenol blue, pH 6.8) and resolved using 10% sodium-dodecyl-sulphate polyacrylamide gel electrophoresis (SDS-PAGE) for 1 hour at 200V. Proteins were transferred onto a polyvinylidene difluoride (PVDF; Millipore) membrane for 2 hours at 100V at 4ºC. The PVDF membrane was blocked overnight at 4ºC in blocking buffer (5% milk/TBST (tris-hydrochloric acid-buffered saline and 0.05% tween 20)). The membrane was probed with primary antibody at room temperature for 1 hour and washed three times for 5 minutes with TBST. The membrane was then probed with secondary antibody for 45 minutes at room temperature and washed three times for 10 minutes with TBST. Bands were detected using chemiluminescent Horseradish peroxidase (HRP) substrate (Millipore) and exposed to autoradiography film (HyBlot ES).

Cell motility and invasion assays: For Transwell chamber assays, 24 well BD Control chambers or Biocoat Matrigel invasion chambers (BD Biosciences, Mississauga, ON, Canada) were used according to the manufacturer's protocol. To measure cell motility, cells were seeded into BD Control chambers which contain a membrane with 8 μm pores at the bottom allowing for cells to migrate through to the underside of the chamber. To assess cell invasion, cells were seeded into BD Biocoat Matrigel invasion chambers. These chambers differ from the control chambers in that a Matrigel layer is applied on top of the membrane, therefore providing a physical barrier that cells are required to penetrate in order to reach the pores and the underside of the chamber membrane. Fifty thousand cells in serum-free DMEM were seeded into each chamber and placed into a well of a 24 well plate containing 500 μL complete DMEM. Cells were then incubated for 24 h (MDA-MB-231 cells) or 72 h (MCF7 cells) at 37ºC. Following incubation, cells on the upper surface of the membrane were removed by scrubbing within the chamber. Cells that reached the underside of the chamber membrane were fixed and stained using the Diff-Quik staining kit (Allegiance Inc.). A minimum of six random fields, imaged at 40X magnification, were counted to determine cell numbers.

Fluorescence microscopy: Cells were seeded at 70% confluency onto glass coverslips in a 6 well plate and incubated overnight to allow cells to adhere. Cells were washed twice with 1XPBS (phosphate-buffered saline) before fixation in 4% paraformaldehyde (10 min) at room temperature followed by cold methanol fixation for 10 minutes. Cells were then washed three times with 1XPBS and blocked for one hour with 5% donkey serum in 1XPBS. Cells were then washed once with PBS and incubated with primary antibody

(1:100 dilution) at room temperature for one hour. Following the incubation, cells were washed twice with 1XPBS and incubated with Alexa Fluor secondary antibody (1:250 dilution) for 1 hour at room temperature in the dark. Washes were performed twice with 1XPBS and coverslips were mounted onto glass slides using Vectashield Mounting Media with DAPI (4′,6-diamidino-2-phenylindole; Vector Laboratories). Images were taken at 40X magnification using a Zeiss LSM 5 Pascal/Axiovert 200 epifluorescent microscope. For stress granule experiments, within randomly imaged fields (5 fields per sample), total number of cells were counted according to DAPI staining in an unbiased manner. Subsequently, cells with at least 5 stress granules were considered as cells containing granules. The number of cells with stress granules were then divided by total number of cells, giving the percentage of cells with stress granules.

Immunohistochemistry: Tissue microarray slides were purchased from US Biomax, Inc. (Rockville, MD, USA). For PRMT7 staining, antigen retrieval was performed using sodium citrate (pH 6) and microwave treatment. Primary PRMT7 rabbit polyclonal antibody from Imgenex (Cat. # IMG-5121A, Lot# 02081856A) was used at a dilution of 1:50 and was detected with the Envision Polymer Detection System (Dako, Mississauga, ON, Canada). A scoring system from 0 to 3 based on the intensity of PRMT7 cytoplasmic staining in normal breast epithelial cells and epithelial-derived breast tumor cells was used, with 3 being the strongest staining. Distribution of PRMT7 staining in the tissue was scored from 0 to 3 as a percentage of positive cells; 0 (None), 1 (<30%), 2 (30-70%), 3 (>70%). The intensity and distribution scores were multiplied to determine the composite score used in the final assessment. Composite scores ranging from 0-2 represented low

expression, 3-5 represented moderate expression and scores 6 or greater (6+) represented high expression. Scoring was performed independently by two pathologists.

***In vivo* experimental metastasis model and *in vivo* imaging:** All the animal experiments were approved by and carried out according to the Canadian Council for Animal Care and University of Ottawa Animal Care Committee and Animal Care and Veterinary Services. Six week old female NOD.CB17-Prkdcscid/J SCID (severe combined immunodeficiency) mice (Jackson Laboratory, Bar Harbor, ME) were injected intravenously in the tail with MDA-MB-231 cells stably expressing a non-targeting control shRNA and Luciferase or a PRMT7-targeted shRNA and Luciferase. Four mice per group were randomly assigned. 500 000 cells in 100 μL of 1XPBS were injected into the tail vein of each mouse. For bioluminescence imaging, mice were given a dose of D-luciferin (150 mg/kg) in PBS by intraperitoneal injection and then anesthetised with isoflurane. At 10 min after injection, bioluminescence was detected with an *in vivo* imaging system (IVIS Spectrum, Caliper Life Sciences by PerkinElmer, Waltham, Mass, USA). Images were acquired and quantitated using Living Image 4.3.1 software. After final imaging, mice were euthanized and were dissected for lung staining and extraction. India Ink stain (15% India Ink, 85% water, 3 drops of NH_4OH/100mL) was injected through the trachea and down into the lungs. This resulted in black staining of the normal lung tissue while the tumour cell nodules were impenetrable to the stain and remained white in color. Lungs were then extracted, washed in water for 5 min and then incubated once for 5 minutes in Fekets solution (300 mL 70% ethanol, 30 mL 37% formaldehyde, 5 mL glacial acetic acid, 165mL water), followed by an overnight incubation in fresh Fekets solution at room temperature

to fix the tissue. Lungs were then imaged using a Canon digital camera and number of tumours counted in an unbiased manner by two individuals.

Reverse transcriptase polymerase chain reaction (RT-PCR) analysis: Total RNA was isolated from cells using TRIzol (Life Technologies, Burlington, ON, Canada). First strand cDNA synthesis was performed using AMV Reverse Transcriptase (Promega, Madison, WI, USA). PCRs were performed in a 15 µL reaction using GoTaq Green Master Mix (Promega). Samples were electrophoresed on a 1% agarose gel. Band densities were determined using images that were within the linear range of signal intensity and normalized to the endogenous reference gene (GAPDH). Values were then expressed as changes in expression relative to the experimental control. The following table summarizes the expected band sizes of the amplified genes, the gene name, and the forward/reverse sequence of the primers.

Table 1: Sequences and gene names of primers used for both semi and quantitative RT-PCRs

Gene	Forward sequence	Reverse sequence
GAPDH	ACCACAGTCCATGCCATCAC	TCCACCACCCTGTTGCTGTA
MMP9	TCTATGGTCCTCGCCCTGAA	TTGTATCCGGCAAACTGGCT
PRMT7	TGAACATGGGCAGCACATCGC	GCAAGGTCATCTTATGCAGAT

Quantitative RT-PCR analysis: Total RNA was extracted from cells and cDNA was generated as described above. Quantitative RT-PCR was performed in a Life Technologies Applied Biosystems (ABI) 7500 Real-time PCR system (Burlington, ON, Canada) using FastStart SYBR Green master mix (Roche, Basel, Switzerland). PCRs were performed in a 96 well plate format in triplicate. Data acquisition and analyses were performed using ABI 7500 software v2.0.6. GAPDH (glyceraldehyde 3-phosphate dehydrogenase) was used as the endogenous reference gene.

MMP array: Cells (500 000) were plated into 6 well plates in complete media. After 24 h, cells were washed and incubated in 1mL of serum free media for 48 h. Cell-conditioned media was collected and placed on membrane based MMP arrays to assess secreted protein levels (Ray Biotech, Inc, Norcross, GA, USA, Cat. #AAH-MMP). Arrays were used according to manufacturer's specifications. Briefly, conditioned media was placed on a membrane upon which MMP antibodies were present and incubated overnight at 4ºC. Following this incubation, membranes were washed and incubated with a biotinylated antibody cocktail according to manufacturer's protocol. The membranes were once again washed and then incubated with HRP-streptavidin. Following a final wash procedure, MMP proteins levels were visualized by chemiluminescence.

Gelatin Zymography: Cell-conditioned medium was analyzed for MMP9 activity by gelatin zymography. Cells were incubated in serum-free media for 24 h and then the conditioned medium was collected and concentrated *in vacuo*. Samples were prepared in non-reducing conditions in 5X sample buffer (0.625 M Tris-HCl, 10% glycerol, 2% SDS,

2% Bromophenol Blue) and resolved on 8% SDS-PAGE gels containing 0.5 mg/ml of gelatin Type A from porcine skin (Sigma-Aldrich). The gels were then washed twice in 2.5% (v/v) Triton X-100 for 15 min each at room temperature. Following this, gels were incubated in developing buffer (100 mM Tris-HCl, pH 7.9, 30 mM CaCl2, and 0.02% sodium azide) for 30 min at room temperature followed by a second incubation in fresh developing buffer overnight at 37C. The gels were then stained with SimplyBlue SafeStain solution (Life Technologies) for 15 min, followed by de-staining in water to reveal areas of activity.

Chromatin immunoprecipitation: Cells were seeded at 80-90% confluency for experiments. The day of the experiment, monolayer of cells were cross-linked with 1% formaldehyde (10 minutes at room temperature with gentle shaking). The reaction was quenched with 0.125M glycine for 5 minutes with gentle shaking. Cells were rinsed in 1XPBS, scraped and collected in a conical tube. Cells were centrifuged at 1000rpm for 5 minutes. PBS was aspirated and cells were lysed using lysis buffer (50mM Hepes-KOH pH 7.5, 140mM NaCl, 1mM EDTA, 10% glycerol, 0.75% NP-40, protease inhibitors). Cells were subjected to mechanical lysis using a type B pestle (Dounce) for 30 strokes. Nuclei were then pelleted by centrifuging at 1000rpm for 5 minutes at 4ºC. Nuclei were then washed in buffer (200mM NaCl, 1mM EDTA pH 8, 0.5mM EGTA, 10mM Tris-HCl pH 8, 0.5% sodium sarkosyl, and protease inhibitors). Nuclei were pelleted and finally resuspended in 1mM EDTA pH 8, 0.5mM EGTA (ethylene glycol-bis(β-aminoethyl ether)-N,N,N',N'-tetraacetic acid), 10mM Tris-HCl pH 8, 0.5% sodium sarkosyl, and protease inhibitors. Samples were then sonicated on ice to obtain DNA fragments between

200-300bp. 25ug of DNA was then incubated with pre-blocked A/G agarose beads for 2 hours at 4C (0.1% sodium deoxycholate and 1% NP-40 was also added to samples). A sample of the input was then saved and Myc-Trap antibody was subsequently added to the sample for immunoprecipitation (samples included either Myc-tag infected MCF7 cells or PRMT7-Myc-tag infected MCF7 cells). Samples were then washed 7 times in buffer (50mM Hepes-KOH pH 7.5, 500mM LiCl, 1mM EDTA, 0.7% sodium deoxycholate, 1% NP-40, and protease inhibitors). After the final wash, chromatin (including inputs) were reverse cross-linked overnight at 65C (including inputs). The following day, samples were treated with RNase A and proteinase K and DNA was isolated using phenol:chloroform:isoamyl-alcohol extraction. PCR amplification was then employed and products run on a 1% agarose gel to identify enriched genes.

Table 2: Sequences and gene names of primers used for chromatin immunoprecipitation experiments

Gene	Forward sequence	Reverse sequence
MMP9	GCCAGGGGGATCATTAGTTT	CAGTCTCCACTGCCAAGTCA
POLD1	CTCAGAAACAGGCCGATCC	GGACCTCATTCCCAGTTCC
E-cadherin	GTGGAATCAGAACCGTGCAG	CTCGCATAGACGCGGTGAC
GAPDH	ACCACAGTCCATGCCATCAC	TCCACCACCCTGTTGCTGTA

Senescence-Associated β-galactosidase staining: Staining was carried out as previously described (Debacq-Chainiaux, Erusalimsky, Campisi, & Toussaint, 2009). Cells were grown to sub-confluency the day of experiments. Cells were washed in 1XPBS and subsequently fixed using 1% formaldehyde and glutaraldehyde for 5 minutes at room temperature. Cells were then washed in 1X PBS and stained overnight at 37C using potassium ferrocyanide and potassium hexacyanoferrate (III). After the incubation, cells were washed twice in 1X PBS and once in methanol. Plates were then allowed to air dry. Once dry, images were obtained using a light microscope at 40X magnification.

SILAC-based affinity purification and mass spectrometry: Cells were grown in either light media (R0K0; $^{12}C_6$-Arginine/$^{12}C_6$-Lysine; Sigma) or heavy media (R6K4; $^{13}C_6$-Arginine/4,4,5,5-D4-Lysine; Cambridge Isotope Laboratories) supplemented with dialyzed FBS, penicillin/streptomycin, and insulin. After at least 5-10 cell doublings in the labeling media, cells were trypsinized and pellets were flash frozen in liquid nitrogen. Pellets were lysed using freshly-prepared lysis buffer (50 mM Tris, pH 7.5, 150 mM NaCl, 1% NP-40, 0.5% Deoxycholate, and protease inhibitors). For complete cell lysis, cell extracts were sonicated on ice (6 X 10s at full power). Protein concentrations were obtained using Bradford assay. Equal amounts of total cell extract were used for each condition and were pre-cleared with protein A/G agarose beads for 1 hour at 4C while nutating. Cleared extracts were then incubated with GFP-Trap_A agarose beads (Chromotek) and nutated for 1 hour at 4C. Beads were then washed with lysis buffer and the differentially labelled samples combined. After several more washes, bound proteins were eluted with 1% SDS, reduced using DTT, and alkylated using IAA (iodoacetamide). The eluate was separated

on an SDS-PAGE gel, stained with Simply Blue Safestain (Thermo-Fisher/Invitrogen), and cut into five equal fragments. Each fragment was further cut into small pieces for in-gel digestion using Trypsin Gold (Promega) as previously described (ref. (Trinkle-Mulcahy et al., 2008) and (Larivière et al., 2014)). An aliquot of each tryptic digest was analysed by LC-MS/MS on an LTQ Orbitrap XL hybrid MS with nanospray source (Thermo Scientific) coupled to an UltiMate 3000 RSLC nano HPLC (Dionex). Statistical and bioinformatic analyses were performed using MaxQuant software v1.2.7.4. For a more detailed protocol, refer to reference (Larivière et al., 2014; Trinkle-Mulcahy et al., 2008).

Co-immunoprecipitation: Co-immunoprecipitation experiments were carried out in a similar fashion described above. Briefly, cells were lysed in freshly-prepared lysis buffer (50 mM Tris, pH 7.5, 150 mM NaCl, 1% NP- 40, 0.5% Deoxycholate, and protease inhibitors). Lysate was pre-cleared with protein A/G agarose beads for 1 hour at 4C with end-to-end rotation. Cleared extract was then nutated at 4C with GFP-Trap_A or Myc-Trap beads (Chromotek) for 1 hour at 4C. Beads were then washed with lysis buffer. Proteins were eluted using 1% SDS and samples were run on an SDS-PAGE gel. Western blotting was performed and antibodies mentioned above were used to identify protein.

Polyribosome profiling: Cells were seeded at 80% confluency for experiments. Cells were washed in 1X PBS and lysed on ice in freshly-prepared buffer (20mM Tris-HCl, 150mM NaCl, 1.25mM $MgCl_2$, 1% NP-40, 1mM DTT, 8 U/mL RNase Out, and protease inhibitors, pH 7.4). Lysates were centrifuged and supernatant quantified for RNA content at 260nm using a NanoDrop 2000 Spectrophotometer (Thermo Scientific). 20 OD units were loaded

onto a 15-50% sucrose gradient and ultracentrifugation was performed using an Optima L-90K ultracentrifuge and SW 41Ti rotor (Beckman) at 37 000rpm for 2.5 hours at 4C. Samples were then fractionated using a Foxy R1 Fraction Collector (Brandel) and UA-6 Absorbance Detector (ISCO). For analysis, proteins were precipitated from fractions using chloroform/methanol and dried *in vacuo*. Pellets were resuspended in water and analyzed by western blotting. For co-immunoprecipitation using pooled fractions from the pre-translational complex (40, 60, 80S), samples were diluted 1:5 in lysis buffer and the aforementioned co-immunoprecipitation protocol was followed. For quantification of polysomal to pre-translational fractions, profiles were first traced above background using Adobe Illustrator. For comparison, pixels for each section were quantified via histogram densitometry (Adobe Photoshop).

Site-directed mutagenesis: Mutant eIF2α-GST protein from pGEX-4T2 vector were designed: $R^{52}R^{53}R^{54}I^{55}R^{56}$ mutated to KKK, RKK, KRR, RKR, RRK, RRRIK, RRW, and $S^{51}D$. Additionally, methyltransferase-dead mutant PRMT7 from pLenti-C-mGFP and pLenti-C-MycDDK vectors were also designed; the highly conserved PRMT sequence within the SAM binding domain of PRMT7 was mutated from $D^{70}IG \rightarrow AAA$. Primers were designed using QuickChange Primer Design by Agilent Technologies. To PCR amplify the mutations, PrimeStar polymerase was used (TaKaRa). PCR-amplified vectors were then treated with Dpn-1 enzyme to digest parental strand. Vectors were then transformed into DH5α cells and a single colony was inoculated and grown using appropriate antibiotics for selection. DNA was then isolated using a kit (Maxi Prep, Qiagen) and quantified for future experiments. Sequencing was also performed to confirm mutations were a success. The

eIF2α mutants were then sub-cloned into a pLenti-C-mGFP vector for *in vivo* methylation assays (described below). The PRMT7 wild-type and mutant sequences were also subcloned into a pCGT7 expression vector for protein purification.

Protein purification (BL-21): PRMT7 (wild-type) was purified by our collaborators Dr. Hemanta Adhikary and Dr. Jean-Yves Masson as previously described (Feng et al., 2013). Purified PRMT5 was a generous gift from Dr. Derrick Gibbings (uOttawa). GST fusion proteins (PRMT1, 3, 4, 6, 8, 9, and both wild-type and mutant eIF2α) were expressed using pGEX-4T2 vectors and purified from *E. coli* BL-21 (DES) cells (New England Biolabs). BL-21 cells were induced with a final concentration of 1 mM isopropyl-β-D-thiogalactopyranoside (IPTG). Pelleted cells were lysed in 1X PBS supplemented with protease inhibitors and sonicated on ice (5 X 30 seconds at full power). The GST (glutathione S-transferase) fusion proteins were purified using glutathione-agarose beads (Sigma Aldrich) and washed with 1XPBS. Proteins were eluted with 20mg/mL glutathione in 1XPBS. Purified proteins were then dialyzed overnight at 4C in 1X PBS. The dialyzed proteins were concentrated using centrifugal filter units (EMD Millipore) and quantified using Bradford assay. Purified recombinant histones were purchased from Sigma Aldrich.

Protein purification (293T): Methyltransferase-dead mutant PRMT7 was purified from 293T cells. Wild-type PRMT7 was also purified as a control. Note that PRMT7 purified by our collaborators were used for the majority of the *in vitro* methylation assays. 293T purified PRMT7 was used solely to compare methyltransferase-dead PRMT7 to wild-type PRMT7. Furthermore, the protocol for T7 purification of protein is described in full detail by Cazalla and colleagues (Cazalla, Sanford, & Cáceres, 2005). Briefly, 293T cells were

transfected with wild-type and methyltransferase-dead mutant PRMT7. At least 5 X 15cm plates of 293T were seeded per condition. 48h after transfection, cells were scraped and lysed in buffer (50mM sodium phosphate, pH 8, 0.5M NaCl, 5mM β-glycerophosphate, 5mM potassium fluoride, 0.1% Tween 20, and protease inhibitors. Lysates were then sonicated on ice for 30 seconds and centrifuged at 20 000g for 20 minutes at 4C. Protein was purified using T7-Agarose beads (Novagen) and nutated at 4C for 1 hour. The beads were then washed with lysis buffer and eluted with 800µL buffer (0.1M citric acid, pH 2.2, 5mM β-glycerophosphate, and 5mM potassium fluoride). Eluates were then collected in microcentrifuge tubes where an additional 200µL of 1M Tris-HCl pH 8.8 was added. Purified proteins were then dialyzed overnight at 4C in 1X PBS. The dialyzed proteins were concentrated using centrifugal filter units (EMD Millipore) and quantified using Bradford assay.

GST pulldown: Cells were lysed as in co-immunoprecipitation experiments. Lysate was incubated with 100ng of GST-purified protein for 1 hour while nutating at 4C. 40µL of glutathione beads (made in 50% slurry) were then added to the lysate and incubated for an additional 1 hour at 4C while nutating. As with co-immunoprecipitation experiments, beads were centrifuged, washed, and eluted. Input, GST control, and GST pulldown were run on an SDS-PAGE gel and Western blotting performed.

Methylation assays:

In vitro: 10µg of purified PRMT enzyme was combined with 5µg of the substrate protein (histones or eIF2α) and 1µCi µM S-adenosyl-L-[methyl-^{3}H] methionine (Perkin Elmer) in reaction buffer (50mM potassium Hepes, 10mM NaCl, and 1mM DTT, pH 7.5) for 22 hours at room temperature. Methylation was quenched using Laemmli reducing buffer (25% glycerol, 125mM Tris-HCl pH 6.8, 4& SDS, 700mM β-mercaptoethanol, 0.1% bromophenol blue) and subsequently run on an SDS-PAGE gel. The gel was then coomassie stained for 1 hour at room temperature, de-stained overnight, and then soaked in En^{3}Hance buffer (Perkin Elmer) for 30 minutes at room temperature. The gel was washed three times in water for 30 minutes and dried *in vacuo*. The ^{3}H-labelled proteins were visualized by autoradiography after a 2-week exposure at -80C.

In vivo: Cells were treated with 100µg/mL cycloheximide and 40µg/mL chloramphenicol in DMEM without methionine (Fischer Scientific). Cells were incubated for 1 hour at 37C. 33µCi/mL of L-[Methyl-^{3}H]-methionine (Perkin Elmer) was added to cells in fresh methionine-free DMEM with cycloheximide and chloramphenicol. Cells were incubated for 3 hours then subsequently lysed and resolved on an SDS-PAGE gel. The gel was coomassie stained and then soaked in En^{3}Hance buffer (Perkin Elmer) for 30 minutes at room temperature. The gel was washed three times in water for 30 minutes and dried *in vacuo*. The ^{3}H-labelled proteins were visualized by autoradiography after a 2 week exposure at -80C. As a control, an ^{35}S incorporation experiment was performed using cells either left untreated or treated with the translation inhibitors for 3 hours to ensure translation was inhibited. The lysates, once collected, were run on an SDS-PAGE gel and visualized by autoradiography and fluorography (described above).

^{35}S metabolic labelling assay: Metabolic labelling was carried out as previously described (Cunningham, Pourdehnad, Stumpf, & Ruggero, 2013). Briefly, knockdown or knockout PRMT7 cells were seeded into 6 well plates at 80% confluency. Medium was replaced with methionine/cysteine-free medium supplemented with FBS and incubated at 37C for 30 minutes. 33µCi of Express Protein Labeling Mix (Perkin Elmer) was added directly to wells and incubated for 20 minutes at 37C. As a control, cells were treated with cycloheximide for 30 minutes prior to labelling. Lysates were collected, run on an SDS-PAGE gel, transferred onto PVDF membrane, and exposed to film overnight. PVDF membrane was then used to blot for protein.

Cap binding assay: Cells were lysed and prepared similar to co-immunoprecipitation experiments. Upon pre-clearing with A/G agarose beads, lysates were incubated with immobilized γ-Aminophenyl-m7GTP agarose beads (Jena Bioscience) and nutated at 4C for 1 hour. Similar to co-immunoprecipitations, beads were washed, and proteins eluted. Eluates were then resolved on an SDS-PAGE gel followed by Western blotting.

Statistical analysis: Data are presented as mean ± standard error for the number of experiments indicated in figure legend. Statistical analysis was performed using two-tailed Student's t-test or by one way or two ANOVA using Bonferroni post-test using GraphPad Prism software where applicable. $p < 0.05$ was considered statistically significant. Immunohistochemical data was evaluated for significance using Chi squared (χ^2) test.

CHAPTER 3: RESULTS

3.1 Explore the potential contribution(s) of PRMT7 in breast cancer development and/or disease progression

3.1.1 Explore PRMT7 expression in breast cancer cell lines and tissues

It has been suggested from previous unbiased studies and through data mining of available online expression databases (OncoMINE) that PRMT7 gene expression is dysregulated in breast cancer (Thomassen et al., 2009). However, this has not been extensively examined experimentally, more specifically at the protein level. We therefore assessed PRMT7 protein expression in breast cancer tissues via immunohistochemistry. We initially thoroughly validated a PRMT7 polyclonal antibody for use in this study and have shown that it specifically detects PRMT7 in Western blots of breast cancer cell lines with no other non-specific activity. Interestingly, we detected two potential isoforms of PRMT7 at 78 and 82kDa (Figure 3A). Moreover, knockdown of PRMT7 reduced both detected bands (Figure 6A). Additionally, we observed no signal generated from our secondary antibody binding non-specifically in primary breast cancer tissues (Figure 3B). The localization of endogenous PRMT7 by immunofluorescence in breast cancer cells was shown to be predominantly cytoplasmic (Figure 3C) which was observed in previously published observations (Herrmann et al., 2009). An initial assessment of the PRMT7 staining in tissues showed similar results as our immunofluorescence images: while PRMT7 was present in the cytoplasm and nucleus of cells, a more intense staining was observed in the cytoplasm. Therefore, the cytoplasmic staining intensity was our focus for scoring.

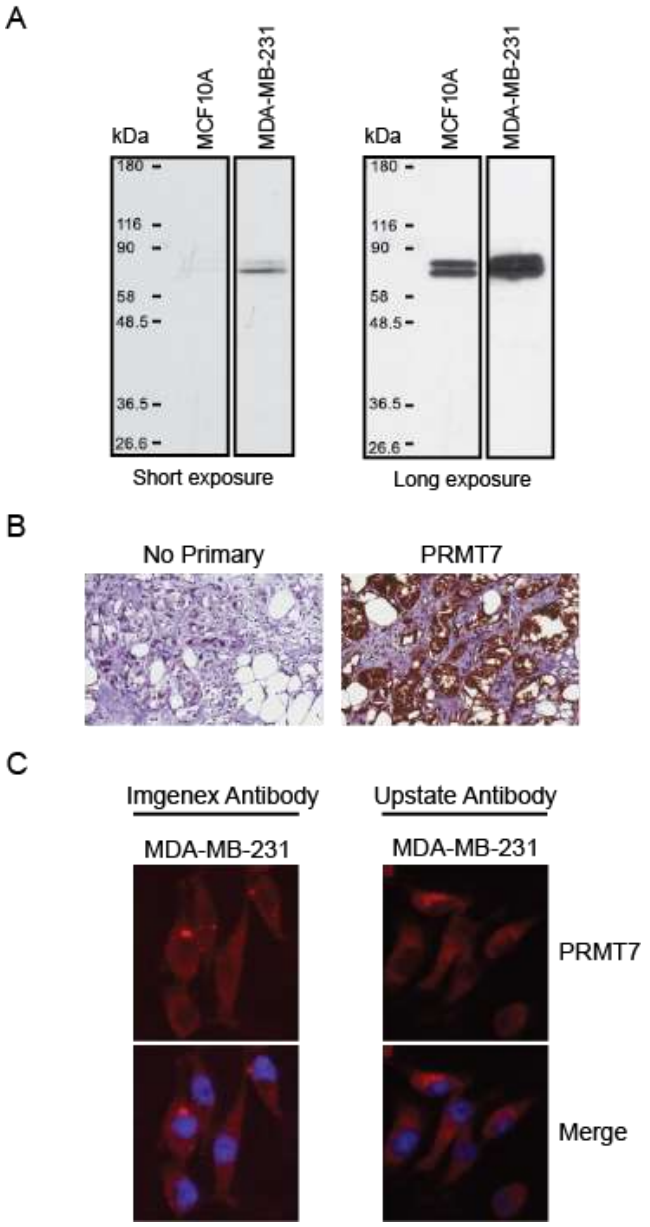

Figure 3: Use of PRMT7-specific antibody activity and specificity in immunohistochemical analyses

(A) Western blot analysis using the Imgenex Inc. PRMT7 rabbit polyclonal antibody shows specific detection of bands corresponding to PRMT7. Images of representative short and long exposures are shown. (B) Immunohistochemical staining of primary breast tumour tissue with no primary antibody as a control or using the PRMT7 rabbit polyclonal antibody. This demonstrates that the staining observed is specific to the presence of the PRMT7 antibody, with limited or no non-specific contribution from the secondary antibody. (C) Immunofluorescence for endogenous PRMT7 in MDA-MB-231 cells. This was done using two different commercially available PRMT7 antibodies: rabbit polyclonal antibody from Imgenex Inc. (Left), and rabbit polyclonal antibody from Upstate Inc. (Right). DAPI staining identifies the nucleus of cells.

To assess the expression of PRMT7 in breast cancer tissues, four commercially available high-density tissue microarrays (TMA) were used. Representative images of PRMT7 immunohistochemical staining in the tissues are shown in Figure 4A. In total, we evaluated the expression of PRMT7 in 244 tissue samples comprising of 24 normal breast tissues (a), 162 primary breast tumours (b), 48 lymph node metastases (d) and 10 normal lymph nodes (c) (Figure 4A).

Breast cancers mainly develop within the glandular cells of the breast and are characterized as epithelial-derived tumours. Therefore, the staining intensities within epithelial cells of normal breast tissues and epithelial-derived breast tumour cells were evaluated. Of note, PRMT7 staining was examined in other cell types within normal breast tissues and we found that endothelial cells had a moderate staining level while scattered fibroblasts within the connective tissue were either negative or very weakly positive. Two pathologists scored PRMT7 staining intensity and distribution within the epithelial cells of the normal breast tissues and the epithelial-derived breast tumour cells to generate a composite score (intensity score multiplied by distribution score) for each of the tissue samples examined. The mean composite scores for each of the tissue groups are shown in Figure 4B. Our results show that the mean composite score of primary breast tumours were significantly higher than normal breast tissues, at 6.10 versus 3.58, respectively. Furthermore, the expression of PRMT7 protein was elevated in lymph node metastases originating from primary breast tumours (composite score of 6.29). The PRMT7 composite scores for breast tumour tissues and metastatic tissues were not significantly different. Normal lymph nodes were completely negative for PRMT7 expression and were void of epithelial cells.

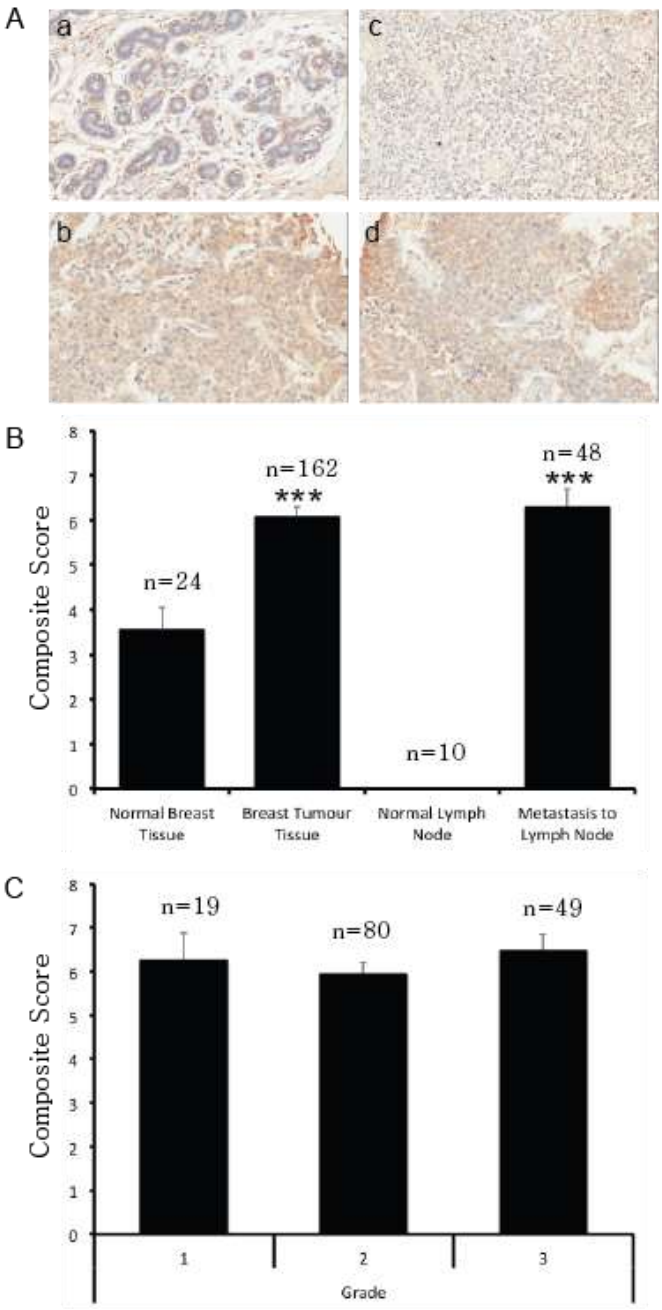

Figure 4: PRMT7 is overexpressed in breast cancer tissues

(A) High-density tissue microarrays were used to assess PRMT7 expression by immunohistochemistry in normal breast tissues (a), primary breast tumour tissues (b), normal lymph nodes (c) and lymph nodes containing metastatic breast cancer (d). Representative images of the tissue samples are shown. (B) The mean composite (intensity x distribution) score for the normal breast tissues, primary breast tumour tissues, normal lymph nodes and lymph nodes containing metastatic disease are shown. (C) An assessment of the composite scores for primary breast tumours with respect to grade was also examined. The number of samples for each of the tissue types is indicated (n). ***$p < 0.0001$.

An assessment of the composite score distribution demonstrated that a significant proportion of breast cancer tissues (68%) and lymph node metastases (68%) had a strong expression (6+ composite score) of PRMT7 (Table 3). In contrast, the majority of normal breast tissues had a weak PRMT7 expression (42%; 0-4 composite score). No differences in PRMT7 expression were observed with increasing tumour grade when comparing mean composite scores (Figure 4C). However, a slightly higher proportion (76% versus 63%) of Grade III tumour samples exhibited high PRMT7 expression (composite score equal to or greater than 6) when compared to the Grade I/II tumour group, but this did not reach significance (Table 4). This evidence suggests that PRMT7 expression may increase in early tumour development and then remain elevated in metastatic disease or that there is an elevation in tumour cells compared to normal cells.

Table 3: Summary of PRMT7 composite scoring distribution

Composite Score	Normal breast Tissue (n=24)	Primary breast tumour tissue (n=162)	Lymph node metastasis (n=68)
0-2 (low expression)	10 (42%)	16 (10%)	6 (13%)
3-5 (moderate expression)	7 (29%)	36 (22%)	9 (19%)
6+ (high expression)	7 (29%)	110 (68%)	33 (68%)
P-values	0.0002[1]	0.000035[2]	0.0033[3]

P-values calculated by χ^2 test. [1]Comparing all three groups. [2]Comparing Normal breast tissue to Primary breast tumour tissue. [3]Comparing Normal breast tissue to Lymph node metastasis.

Table 4: Summary of PRMT7 composite scoring distribution with respect to breast tumour grade

Composite Score	Grade I/II (n=99)	Grade III (n=49)
<6	37 (37%)	12 (24%)
≥ 6	62 (63%)	37 (76%)
P-value	0.11	

P-value calculated by χ^2 test.

We next examined the expression of PRMT7 in established human breast cancer cell lines in order to corroborate our observations in human breast tumour tissues and validate their use as an experimental model. To quantitate the expression levels of PRMT7 protein within these cell lines, Western blotting followed by band density analysis was performed (Figure 5A). PRMT7 protein expression was significantly higher (~3 to 5-fold) in highly invasive breast cancer cells (BT549, Hs578T, BT20, and MDA-MB-231) compared to spontaneously immortalized non-tumourigenic breast epithelial cells, MCF10A, and weakly invasive MCF7 breast cancer cells. This evidence supports our observation that PRMT7 is upregulated in breast cancer tissues, and more specifically invasive cancer cells. Interestingly, two closely migrating bands are detected for PRMT7 in several breast cancer cell lines by Western blot. Both of these bands are reduced with PRMT7-specific shRNA (see below, Figure 6A), suggesting that they both represent PRMT7 species. Additionally, using MCF10A as a control, the expression of PRMT7 was assessed by immunocytochemistry under similar conditions to the experiments performed on the human tissue samples. Consistent with our Western blot analysis, MCF7 cells had a weak staining intensity similar to MCF10A cells. In contrast, the intensity of staining in invasive breast cancer cell lines (MDA-MB-231, BT549 and BT20) was much higher compared to the aforementioned cell lines (Figure 5B).

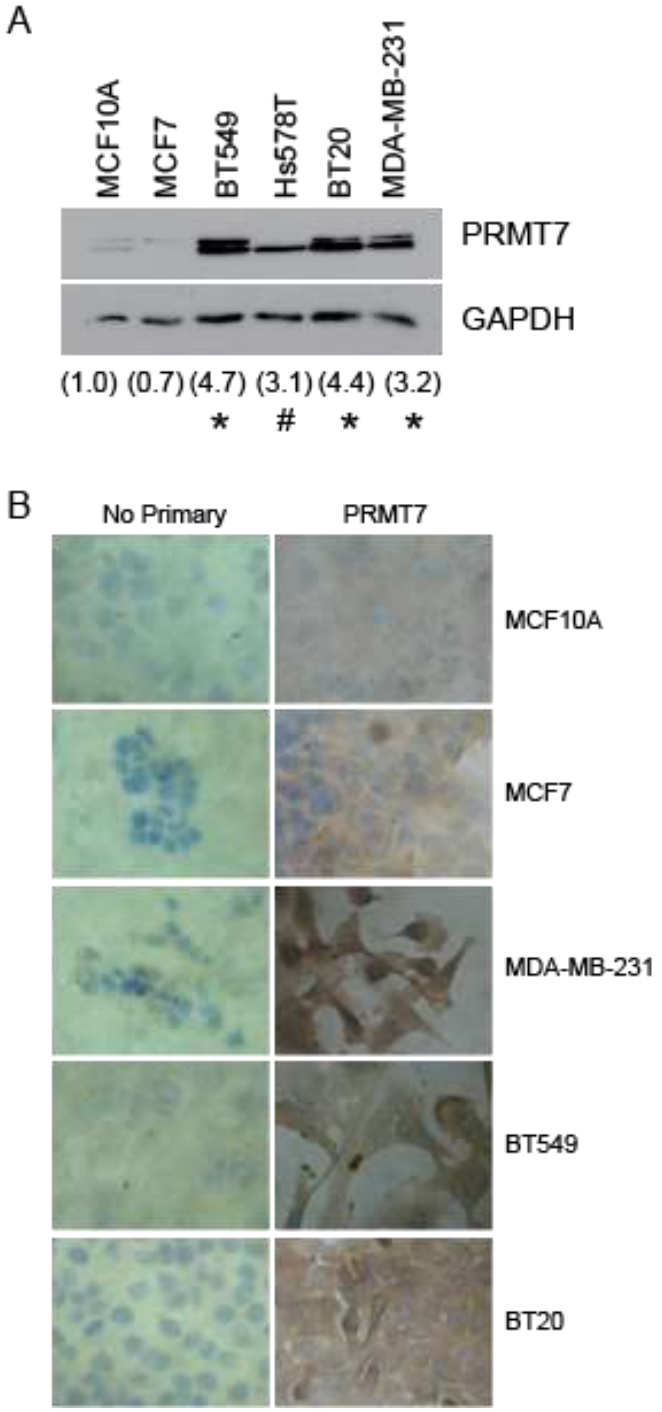

Figure 5: PRMT7 is overexpressed in breast cancer cell lines

(A) Western blot analysis for PRMT7 expression in established breast cancer cell lines. Densitometry of the band intensity (indicated below) were determined from 4 independent experiments and normalized to GAPDH and non-tumourigenic breast cells, MCF10A. *$p < 0.05$, #$p = 0.13$. (B) Immunocytochemistry for PRMT7 expression was assessed in MCF10A, MCF7, MDA-MB-231, BT549 and BT20 cells. No primary antibody (No Primary) was used as a negative control.

3.1.2 Determine the effects of PRMT7 knockdown on cell proliferation and invasion *in vitro*, as well as metastasis *in vivo*

The ability of cancer cells to metastasize comprises two main characteristics: cell migration and their capacity to penetrate through a physical barrier such as the extracellular matrix of surrounding tissues. Due to the fact that PRMT7 is upregulated in invasive breast cancer cells, we wanted to assess its importance in promoting cell invasiveness. To examine the role of PRMT7 in cancer cell motility and invasion, we used the highly invasive breast cancer cell lines, MDA-MB-231 and BT549. PRMT7 was specifically and effectively knocked down from cells using lentiviral delivered short hairpin RNA (shPRMT7-1) and stable cell populations were established following selection. This allowed for a stable reduction of PRMT7 protein expression levels in both MDA-MB-231 and BT549 cells (Figure 6A). Control cells stably expressing a non-targeting shRNA sequence (shControl) were also established. A similar knockdown was also observed using a second unrelated PRMT7 shRNA targeted sequence (shPRMT7-2) in both MDA-MB-231 and BT-459 cells (Figure 7A, B).

To assess the effect of PRMT7 on cell motility and invasion, we used Transwell chamber assays. For this, control or PRMT7-depleted cells were counted and the same numbers were plated into Transwell chambers. Cells that crossed the chamber membrane were counted after a 24h incubation. PRMT7 knockdown had a significant but limited effect on cell motility (Figure 6B, C, E). However, when using a second shRNA against PRMT7, the shPRMT7-2 stable lines showed no significant alterations in cell motility (Figure 7C, E).

To determine the effects of PRMT7 on invasion (cell motility combined with their ability to penetrate through physical barriers), we assessed the ability of invasive breast cancer cells with PRMT7 knockdown to migrate through Transwell chamber membranes coated with Matrigel (a synthetic gelatinous protein mixture similar to the ECM). PRMT7 knockdown caused a significant decrease in the number of cells that invaded through Matrigel-coated membranes compared to controls. Invasive capabilities of the cells decreased by 72% and 48% in MDA-MB-231 and BT549 cells, respectively, using shPRMT7-1 (Figure 6D, F). Similarly, knockdown of PRMT7 with shPRMT7-2 resulted in a 56% and 40% decrease in invasion in MDA-MB-231 and BT549 cells, respectively (Figure 7D, F). To further support these findings, we also isolated clonal populations of MDA-MB-231 cells stably expressing shPRMT7-1 and shPRMT7-2 (cl. 2 and cl. 3, respectively) and observed similar results (Figure 8).

It is possible that knockdown of PRMT7 affects cell proliferation which would in turn negatively influence cell invasion over the 24 hour time-point. Thus, cell proliferation was assessed over 116 hours in MDA-MB-231 cells using both shPRMT7-1 and -2 stable cell lines employing an IncuCyte Zoom proliferation assay that measures cell confluency every 10 hours. While we did observe a negative effect on cell growth in PRMT7 knockdown cells compared to controls (Figure 9), it is negligible at the time-point used for these experiments (24h).

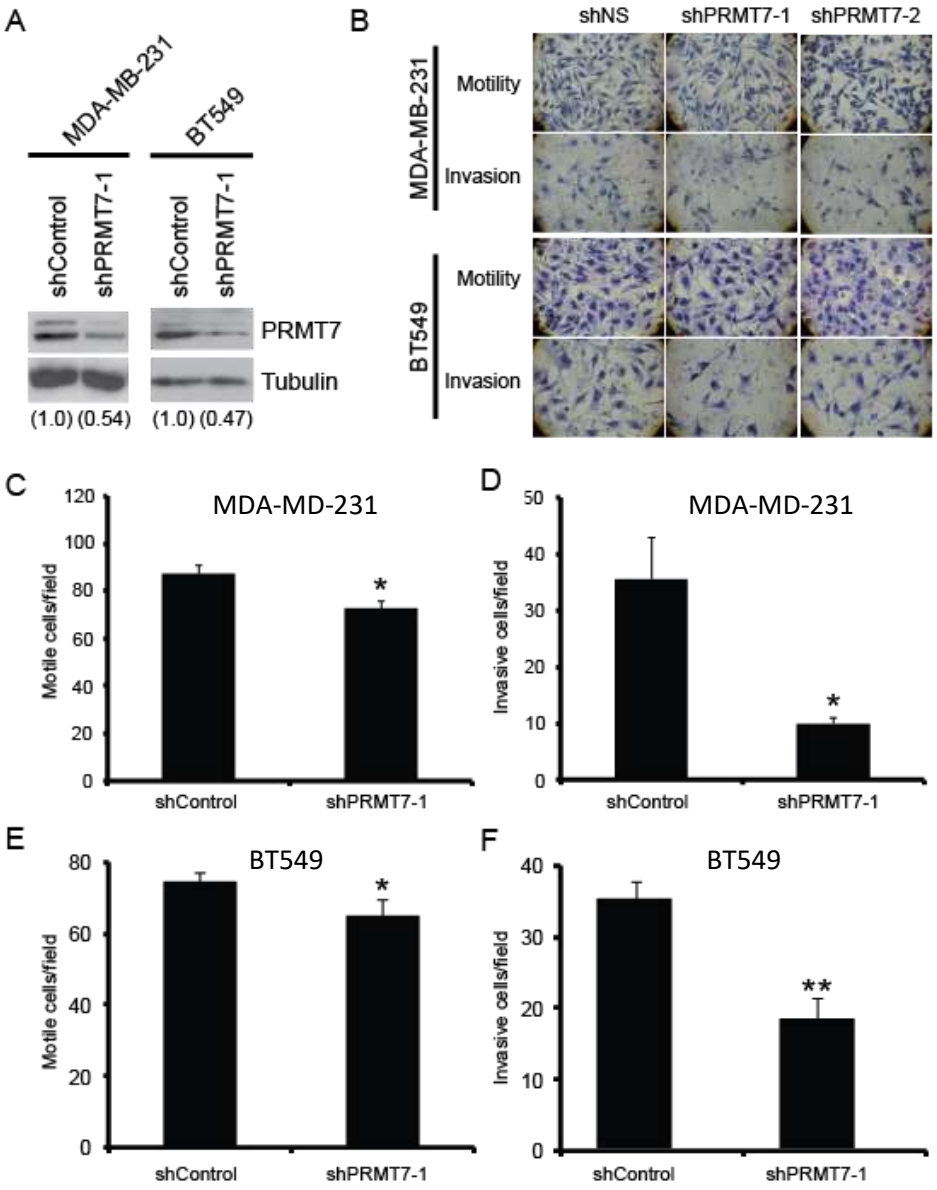

Figure 6: Knockdown of PRMT7 in invasive breast cancer cells inhibits their ability to invade

(A) Western blot analysis for PRMT7 in stably depleted MDA-MB-231 and BT549 cells. Tubulin served as a loading control. Densitometry of the band intensities are indicated below in parentheses. (B) MDA-MB-231 and BT549 cells depleted of PRMT7 were assessed for effects on motility and invasion (number of cells counted; 5 fields per chamber). Representative images of cells that have passed through the Transwell chamber ± Matrigel at 40X magnification are shown. MDA-MB-231 and BT549 cell numbers that passed through the Transwell chambers in the absence of Matrigel (C and E, respectively: motile cells/field) or in the presence of Matrigel (D, MDA-MB-231 and F, BT549: invasive cells/field) were determined. Data represents the mean ± standard error of four independent experiments for MDA-MB-231 and three independent experiments for BT549 (*$p < 0.05$, **$p < 0.01$ comparing to control).

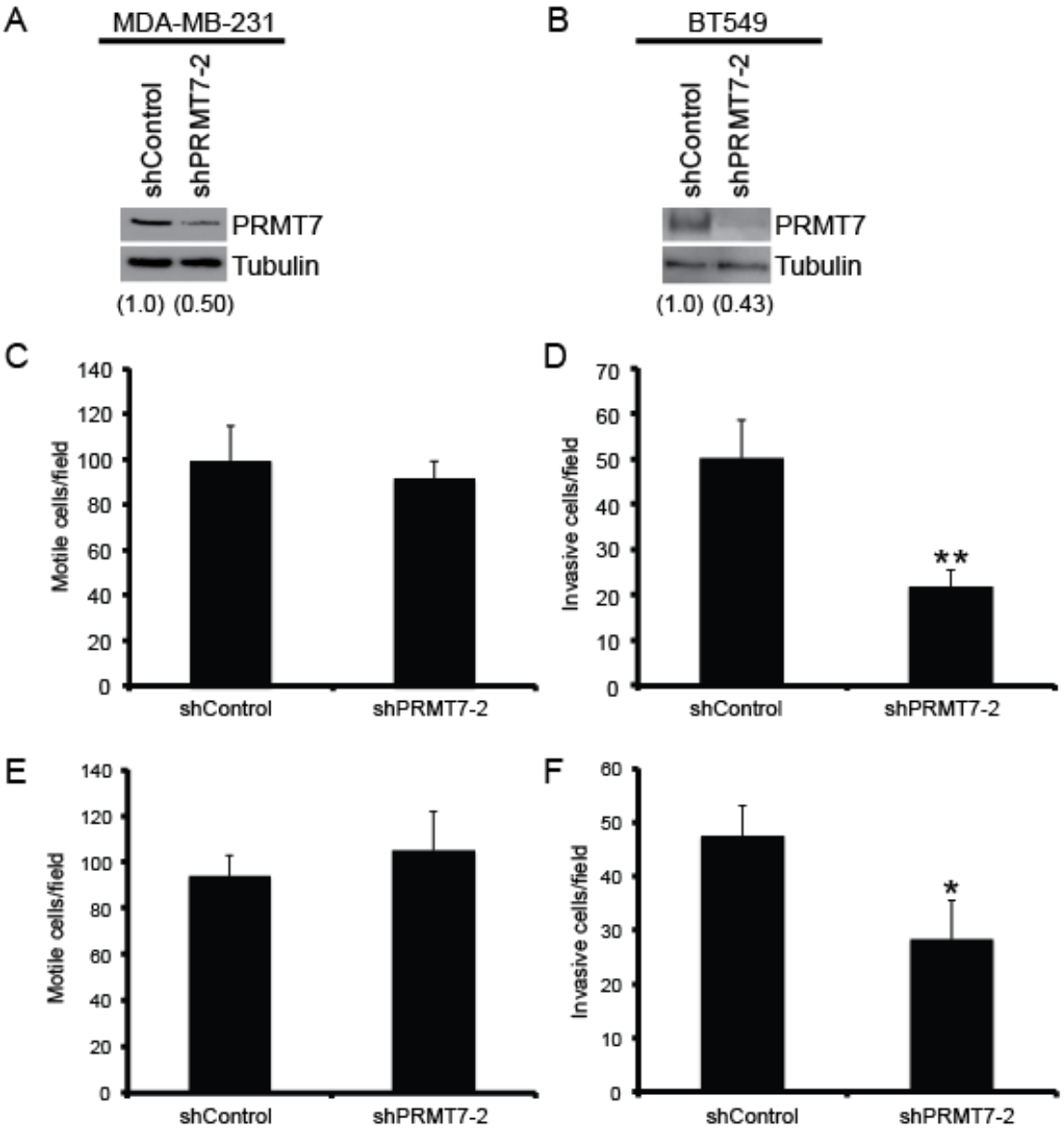

Figure 7: Assessment of motility and invasion with a second shRNA targeting PRMT7
Stable depletion of PRMT7 from MDA-MB-231 and BT549 cells using a second independent lentiviral introduced shRNA (shPRMT7-2) efficiently reduces protein levels (A and B). Densitometry of the band intensities are indicated below in parentheses. Cell motility and invasion were assessed as previously indicated in Figure 6. Depletion of PRMT7 using shPRMT7-2 did not significantly affect the motility of invasive breast cancer cells, MDA-MB-231 (C) and BT549 (E). However, a significant reduction in their ability to invade was observed (MDA-MB-231 (D) and BT549 (F)). Data represents the mean ± standard error of five independent experiments for MDA-MB-231 cells and four independent experiments for BT549 (*$p < 0.05$, **$p < 0.01$ comparing to control).

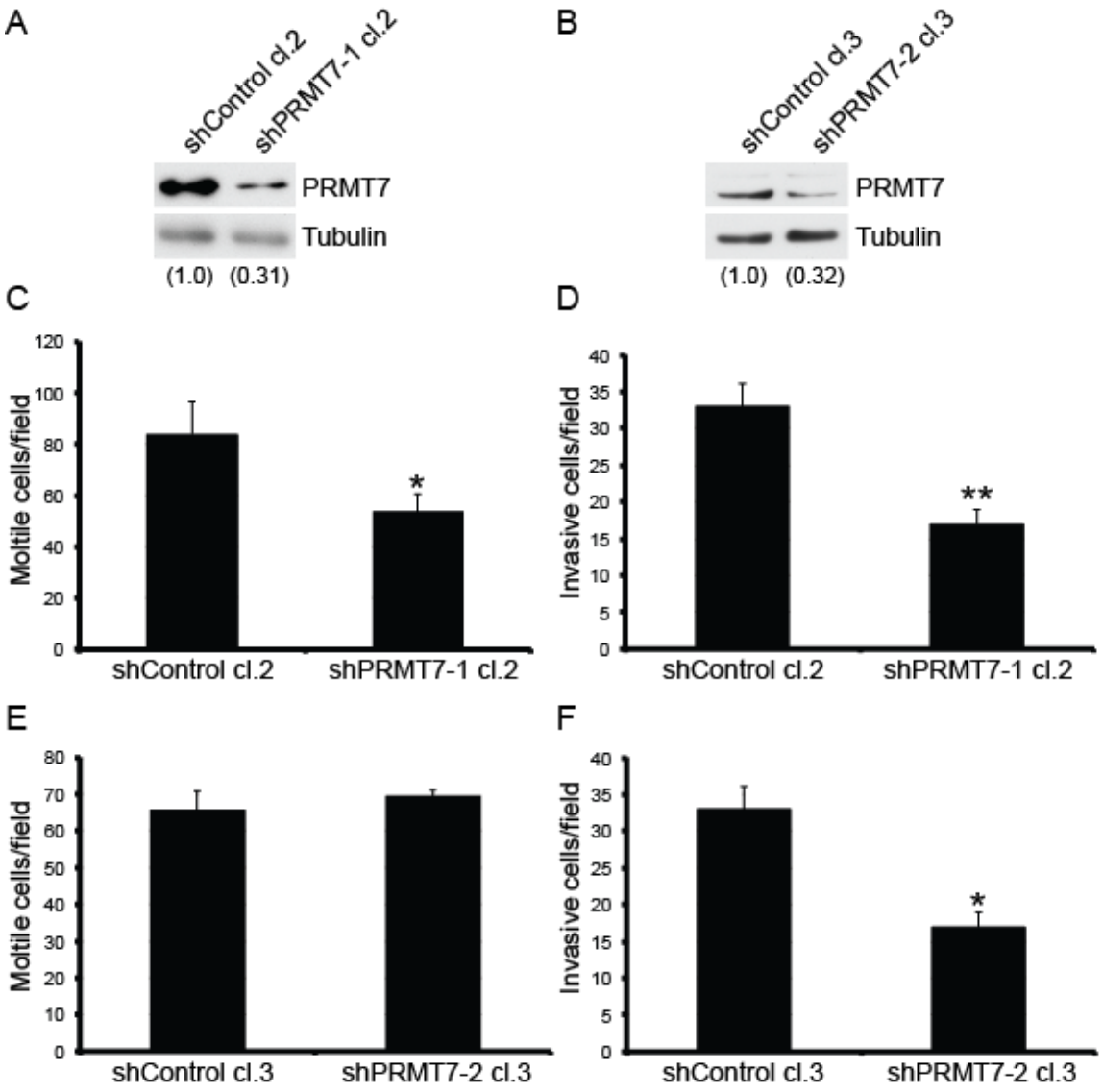

Figure 8: Assessment of motility and invasion in clonal populations of MDA-MB-231 cells stably depleted of PRMT7

Stable clones of MDA-MB-231 cells expressing non-targeting shRNA (shControl) or one of two unrelated PRMT7 targeting shRNAs (shPRMT7-1 and shPRMT7-2) were also generated by lentiviral infection and colonies were selected. Selected clonal populations show efficient PRMT7 protein depletion with shPRMT7-1 (cl. 2, A) and shPRMT7-2 (cl. 3, B). Densitometry of the band intensities are indicated below in parentheses. Cell motility and invasion was assessed as previously shown in Figure 6. Consistent with the PRMT7 depleted cell populations, clonal populations depleted of PRMT7 had a significant reduction in their ability to invade (shPRMT7-1 cl. 2 (D) and shPRMT7-2 cl. 3 (F)), with significant effects on motility in only clone 2 and not 3 (C and E). Data represents the mean ± standard error of five independent experiments for shPRMT7-1 cl. 2 cells and four independent experiments for shPRMT7-2 cl. 3 cells (*$p < 0.05$, **$p < 0.01$ comparing to control).

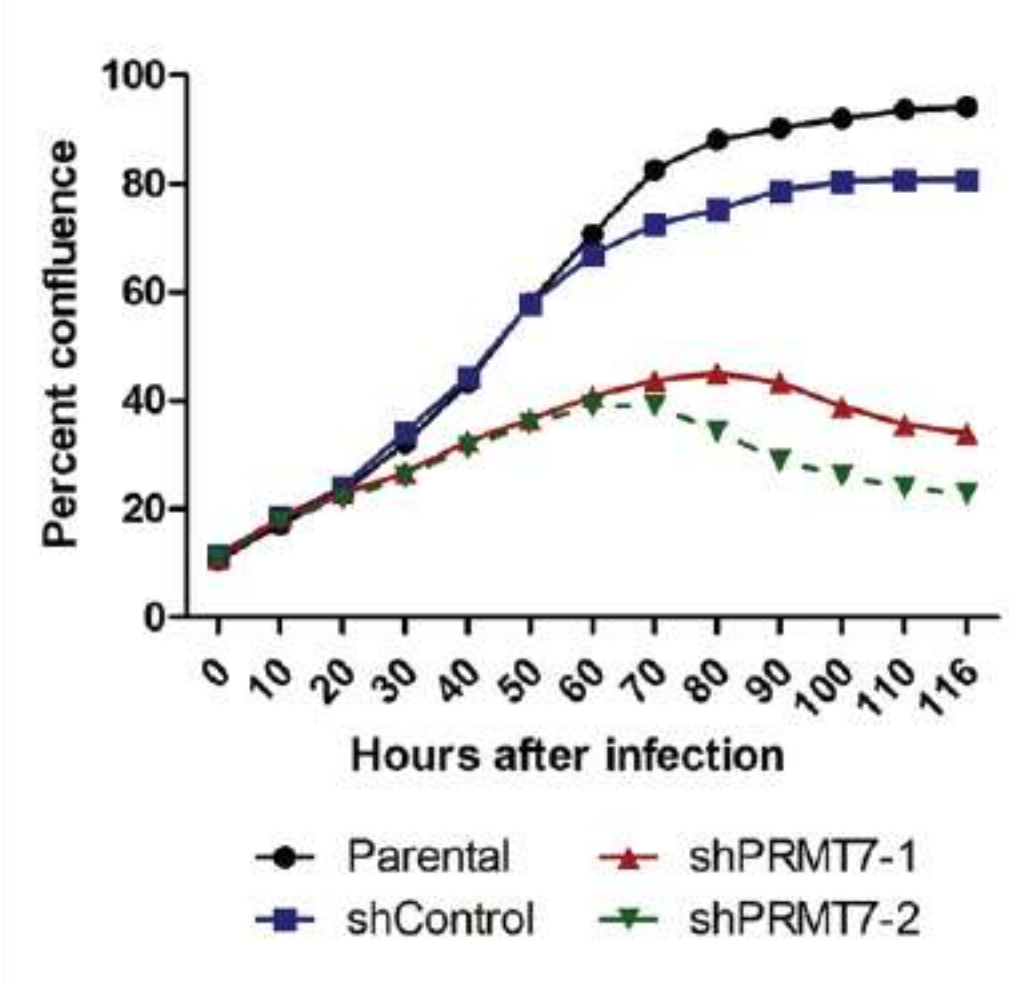

Figure 9: PRMT7 knockdown negatively affects cell proliferation rates
Cell proliferation was measured over 116 hours using calculative measurements of percent confluency on an IncuCyte Zoom Live-cell imaging system. Parental MDA-MB-231 cells (●) and MDA-MB-231 cells transfected with either a non-targeting shRNA (■) or PRMT7-shRNA (▲▼) were used for these experiments. Experiments were run in triplicate, for three independent, biological replicates (n=3; $p<0.01$).

To determine if PRMT7 could promote breast cancer cell invasion, we overexpressed PRMT7 in MCF7 cells. MCF7 cells are a well differentiated, "luminal epithelial-like" breast cancer cell line and characterized as weakly invasive breast cancer cells (Lacroix & Leclercq, 2004). Importantly, as shown above, these cells expressed low PRMT7 protein levels compared to the highly invasive breast cancer cell lines. To determine if PRMT7 is capable of enhancing the invasive capacity of these cells, we generated cell lines that stably expressed either a Myc-DDK or mGFP-tagged PRMT7 via lentiviral infection (Figure 10A). Cells expressing mGFP alone were generated as controls (Empty vector). Furthermore, the subcellular localization of our PRMT7-GFP fusion protein is consistent with what we observed for endogenous PRMT7 in breast cancer cells (Figure 10B). Once established, we examined their migration and invasion at 72h after initial seeding using Transwell chambers as cells were much less invasive. As predicted from the literature, MCF7 cells displayed a low propensity to migrate through Transwell chamber membranes, even in the absence of Matrigel (Figure 10C). However, stable overexpression of PRMT7-Myc-DDK or PRMT7-mGFP enhanced the ability of MCF7 cells to migrate by 1.9-fold and 1.5-fold, respectively, compared to controls (Figure 10C, D). Furthermore, when we assessed invasion using Transwell chambers containing Matrigel, PRMT7 overexpression significantly increased the number of cells that were able to invade (2.2-fold for PRMT7-MycDDK and 1.7-fold for PRMT7-mGFP compared to control; Figure 10C, E). We did not observe significant effects on cell proliferation upon PRMT7 overexpression, suggesting the results are independent of proliferation rates (Figure 11). Altogether, these results highly suggest that PRMT7 plays a significant role in promoting breast cancer cell invasion, a necessary characteristic leading to metastasis.

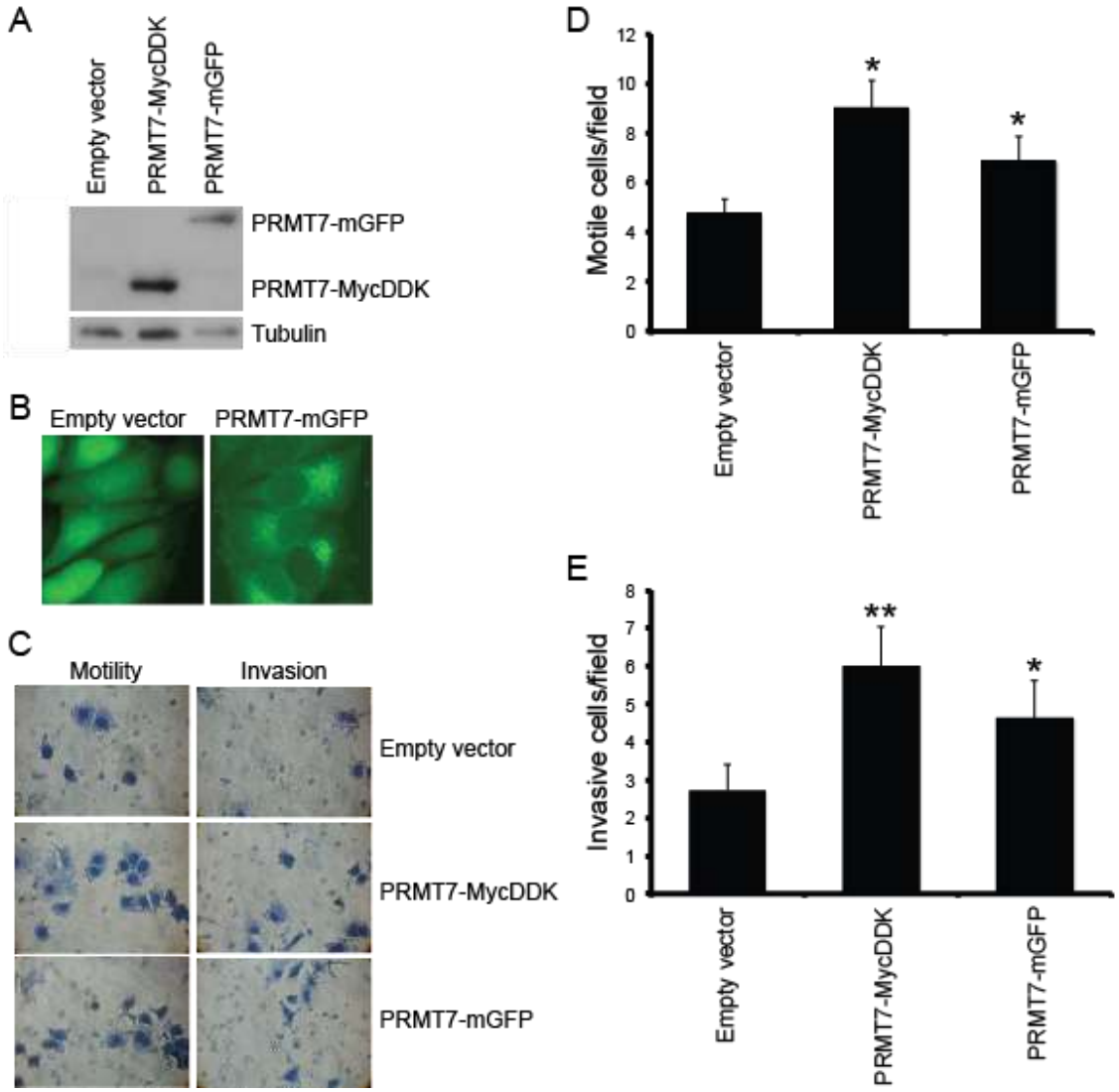

Figure 10: Overexpression of PRMT7 in non-invasive breast cancer cells promotes invasion

(A) Total protein lysates from MCF7 cells stably expressing empty vector, PRMT7-MycDDK or PRMT7-GFP were analyzed by Western blotting for PRMT7 expression. Tubulin served as a loading control. (B) Representative fluorescent images (40X) of MCF7 cells stably expressing an empty vector or PRMT7-mGFP. (C) MCF7 cells stably expressing PRMT7-MycDDK or PRMT7-mGFP were analyzed for motility and invasion at 72h using Transwell chambers. Representative images of cells that have passed through the Transwell chamber ± Matrigel at 40X magnification are shown. Cells that passed through the chamber membranes without a Matrigel layer (D: motile cells/field) or containing a Matrigel layer (E: invasive cells/field) were counted. Data represents the mean ± standard error of eleven independent experiments for PRMT7-MycDDK and nine independent experiments for PRMT7-mGFP (*$p < 0.05$, **$p < 0.01$ comparing to Empty vector control).

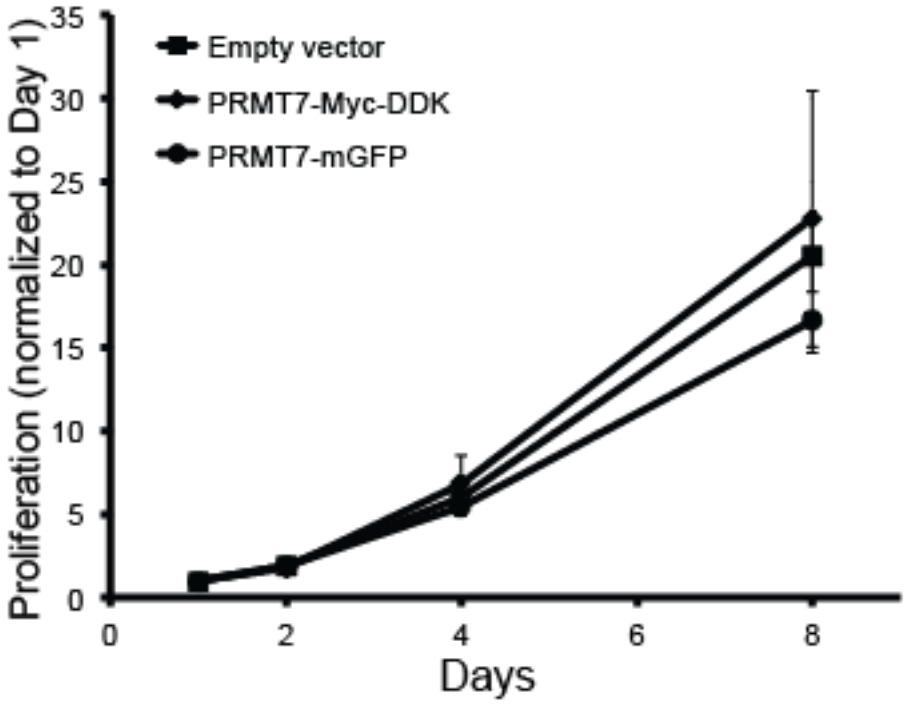

Figure 11: Cell proliferation was assessed over 8 days via MTT assay
Proliferation of MCF7 cells overexpressing PRMT7-MycDDK or PRMT7-mGFP was measured by MTT assay. Initially, cells were plated at equal numbers, lysed, and analyzed on days 1, 2, 4 and 8 post-plating. Cells expressing an empty vector were used as controls. Data is the mean ± standard error of three independent experiments, each cell line performed in 6 replicates.

To determine if PRMT7 knockdown affects breast cancer cell invasion *in vivo*, we performed an experimental metastasis study. In this model, human cancer cells were injected intravenously into the tail vein of immune compromised mice. The cells' ability to migrate through the blood stream and invade the lungs was then determined. Control MDA-MB-231 cells stably expressing either a non-targeting shRNA (shControl) or PRMT7 shRNA (shPRMT7-1) (Figure 12A) were infected with a lentivirus containing the luciferase cDNA to introduce constitutive luciferase expression and allow for visualization of these cells *in vivo* via an *in vivo* imaging system (IVIS). 500 000 control or PRMT7 knockdown cells were injected into the tail vein of NOD.CB17-Prkdcscid/NrcCrl SCID mice randomly sorted into two groups of four mice (n=4/group). On day 8 post injection, imaging was performed using IVIS to determine an initial bioluminescence signal. No signal was observed in either group at this time-point (Figure 12B). The extent of lung metastasis was evaluated 50 days post injection with the bioluminescent signal localized to the lung area, as expected. Importantly, mice injected with PRMT7-depleted cells showed a lower bioluminescent signal (photon flux: p/s/cm2/sr) compared to control mice (Figure 12B). As a non-biased approach to measure the metastatic tumour burden within the lungs, the bioluminescent photon flux for each mouse was quantitated and the mean photon flux for each group was determined. This assessment showed that the group injected with PRMT7 knockdown cells had a significantly lower photon flux compared to the control cells (Figure 12C), thus indicating a reduction in the metastatic potential of cells *in vivo* with reduced PRMT7 levels. Lungs from these mice were dissected and stained to verify the decreased presence of breast cancer cell nodules on the surface (Figure 12D). These data show that PRMT7 has a role in promoting breast cancer cell metastasis *in vivo*.

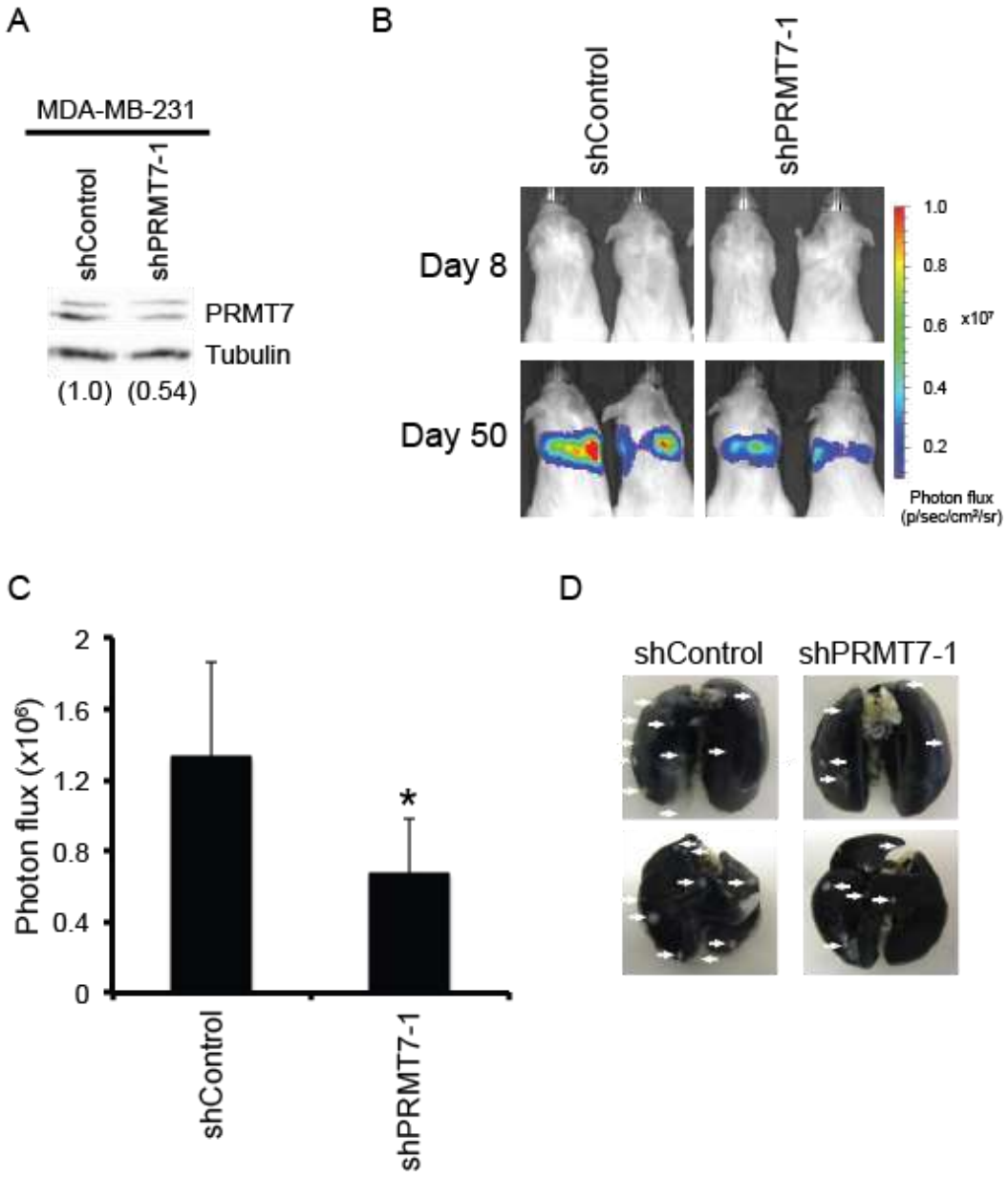

Figure 12: Knockdown of PRMT7 reduces breast cancer cell metastasis in vivo
MDA-MB-231 cells stably expressing Luciferase and a control non-targeting shRNA or a PRMT7-targeting shRNA were injected into the tail vein of six week old female NOD.CB17-Prkdcscid/J SCID mice. Four mice were injected for each group. (A) Western analysis for PRMT7 in stably depleted MDA-MB-231 into which the luciferase gene was introduced for *in vivo* imaging. Tubulin served as a loading control. Densitometry of the band intensities are indicated below in parentheses. (B) Representative images of the bioluminescence (photon flux: p/s/cm2/sr) at day 8 and 50 are shown. (C) Bioluminescence was quantitated for each mouse at day 50 by measuring the photon flux. Data represents the mean ± standard error for each group (n = 4 mice/group, *p = 0.05). (D) Representative images of whole lungs (anterior: upper image, posterior: lower image) stained with India ink, verifying the presence of cancer cell nodules upon the surface of the lungs.

3.1.3 Explore the mechanisms behind PRMT7's role in invasion/metastasis

Matrix metalloproteinases play a crucial role in cancer cell invasion (Köhrmann, Kammerer, Kapp, Dietl, & Anacker, 2009). As mentioned in the introduction, these secreted proteins are responsible for the degradation of extracellular matrix proteins which allow cancer cells to invade local tissues, intravasate and extravasate blood vessels and lymphatic vessels, and form metastatic tumours at distant sites. MMP9 is secreted as an active protein that is capable of degrading collagen type IV (Duffy, Maguire, Hill, McDermott, & O'Higgins, 2000; Kato, Yamashita, & Ishikawa, 2002; Köhrmann et al., 2009) and MMP9 has been identified as a predictive marker of breast cancer cell invasion (Vizoso et al., 2007). Therefore, we assessed the expression of MMP9 in invasive breast cancer cells depleted of PRMT7.

In PRMT7-depleted MDA-MB-231 cells, a significant reduction in MMP9 mRNA was observed using both semi-quantitative and quantitative RT-PCR analysis, 68% and 79% decrease, respectively (Figure 13A, B, C). Alternatively, in MCF7 cells stably overexpressing PRMT7-Myc-DDK, we observed a 2.1-fold increase in MMP9 mRNA expression by semi-quantitative RT-PCR (Figure 13D, E) as well as by quantitative RT-PCR (3.2-fold increase, Figure 13F).

To determine if this reduction in MMP9 mRNA expression also resulted in a decrease in MMP9 protein secretion, we used a membrane array containing MMP9 antibodies to detect protein levels in conditioned media. Conditioned media was collected from control (shControl) and PRMT7-knockdown MDA-MB-231 and BT549 cells (seeded at the same density) and assessed for MMP9 protein levels by incubation with an MMP membrane array. Consistent with the decreased mRNA expression, we also observed a

decrease in secreted MMP9 protein levels in both MDA-MB-231 and BT549 cells with PRMT7 knockdown (Figure 14A). Furthermore, consistent with a reduction in MMP9 expression and secretion, a decrease in MMP9 enzymatic activity was also observed using Gelatin zymography (Figure 14B), demonstrating the functional consequences that result from reduced expression. While the MMP arrays are able to detect other MMPs, we focused on MMP9 due to the important role it plays in breast cancer cell invasion and metastasis. This evidence reveals that PRMT7 is capable of inducing MMP9 expression, representing a mechanism through which PRMT7 can promote breast cancer cell invasion.

Lastly, to show that the observed effects were indeed the result of a change in MMP9 expression, we performed a rescue experiment in which we overexpressed MMP9 in PRMT7-knockdown cell lines. We rationalized that increasing MMP9 expression in cells that have reduced MMP9 levels (due to PRMT7 knockdown) should restore their invasive capability. MMP9 was exogenously expressed in breast cancer cells by transient transfection and assessed by PCR analysis of mRNA (Figure 15A). Following 24h of transfection, cells were re-plated at equal numbers into Matrigel-coated Transwell chambers and incubated for an additional 24h. As predicted, increased expression of MMP9 in PRMT7-depleted cells resulted in a significant, but not complete, rescue in the loss of invasion observed with PRMT7 depletion (Figure 15B). Most likely, other mechanisms are also involved to enhance cell invasion. Moreover, overexpression of MMP9 within the control lines did not further enhance invasiveness of the cells suggesting the threshold was already reached. This demonstrates the importance of MMP9 in the invasive capacity of these cells.

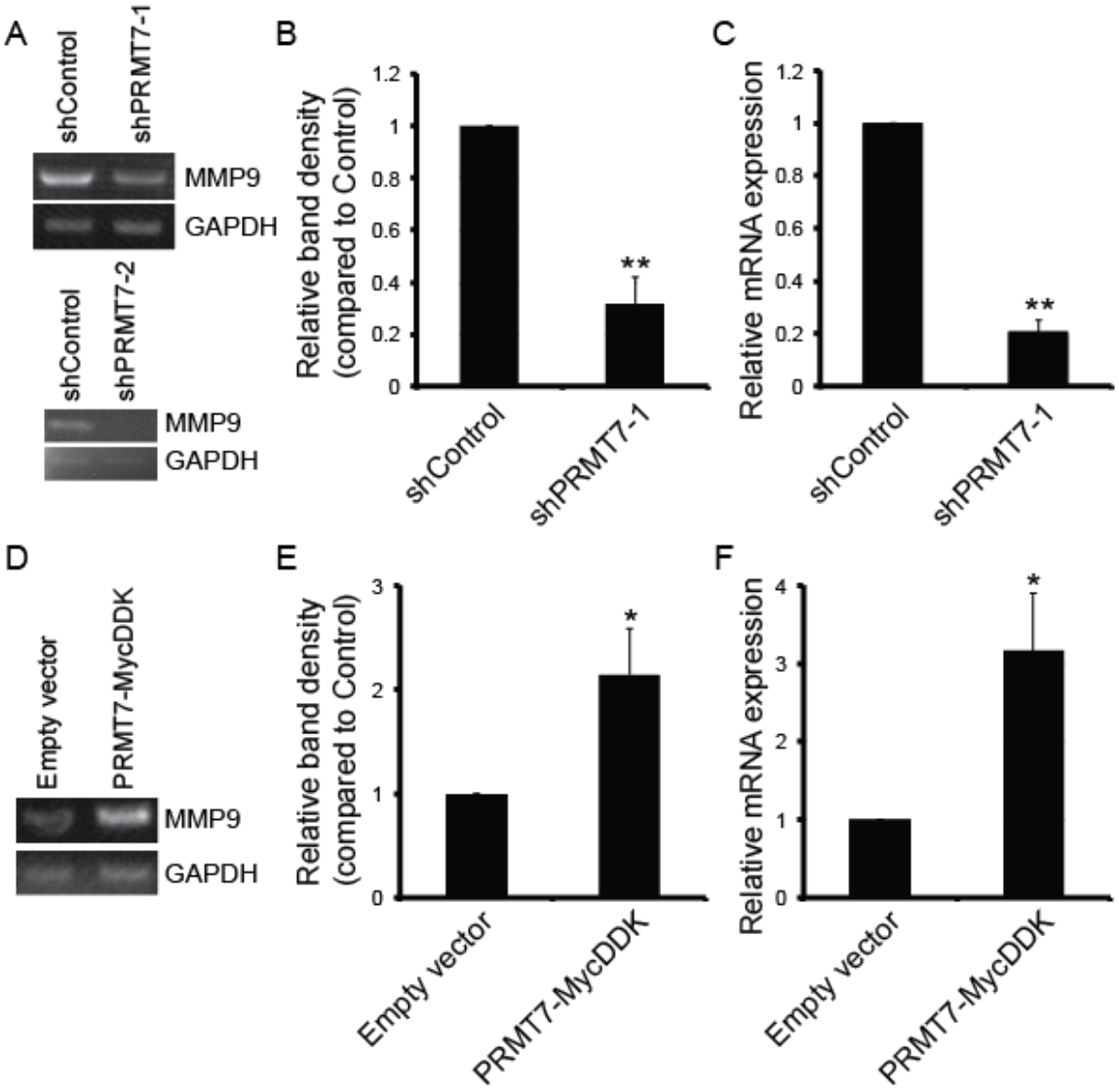

Figure 13: PRMT7 promotes MMP9 expression

Total RNA was isolated from MDA-MB-231 cells stably depleted of PRMT7 and assessed for mRNA levels by RT-PCR and quantitative RT-PCR. Representative PCR (A) and band density quantitation of MMP9 mRNA levels (B) are shown. GAPDH served as a loading control. Data represents the mean ± standard error of six independent experiments (**$p < 0.01$). (C) Quantitative RT-PCR analysis of MMP9 expression in PRMT7-depleted MDA-MB-231 cells. Data represents the mean ± standard error of five independent experiments (**$p < 0.01$). (D) Total RNA isolated from MCF7 cells stably expressing PRMT7-MycDDK was assessed for MMP9 mRNA levels by PCR analysis. Representative PCR (D) and band density quantitation of MMP9 mRNA levels (E) are shown. GAPDH served as a loading control. Data represents the mean ± standard error of four independent experiments (*$p < 0.05$). (F) Quantitative RT-PCR analysis of MMP9 expression in MCF7 cells expressing PRMT7-MycDDK compared to empty vector control. Data represents the mean ± standard error of four independent experiments (*$p < 0.05$).

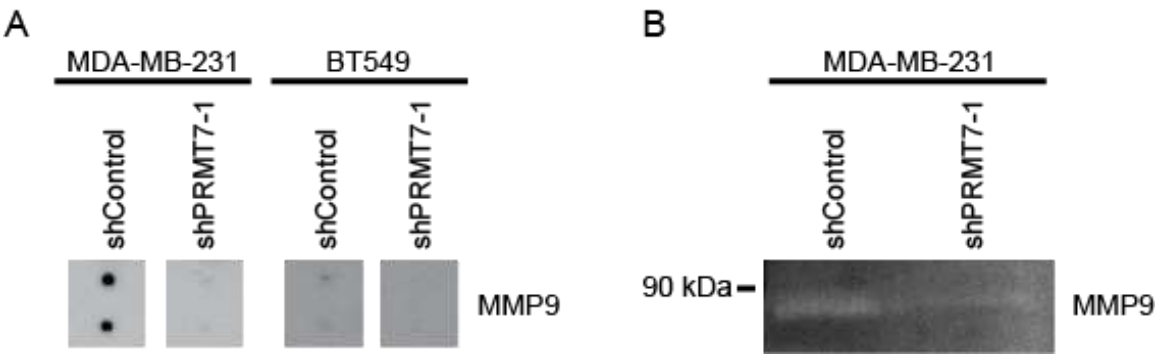

Figure 14: PRMT7 affects MMP9 secretion

(A) Secreted MMP9 protein levels were examined in conditioned media using an MMP antibody array. A reduction in secreted MMP9 protein levels was observed in both MDA-MB-231 and BT549 cells with PRMT7 knockdown. (B) Gelatin zymography was used to determine the MMP9 enzymatic activity in conditioned media collected from MDA-MB-231 cells expressing a control shRNA (non-targeting) or PRMT7-targeting shRNA. PRMT7 depletion resulted in a reduction in MMP9 enzymatic activity when comparing the white intensity to the control.

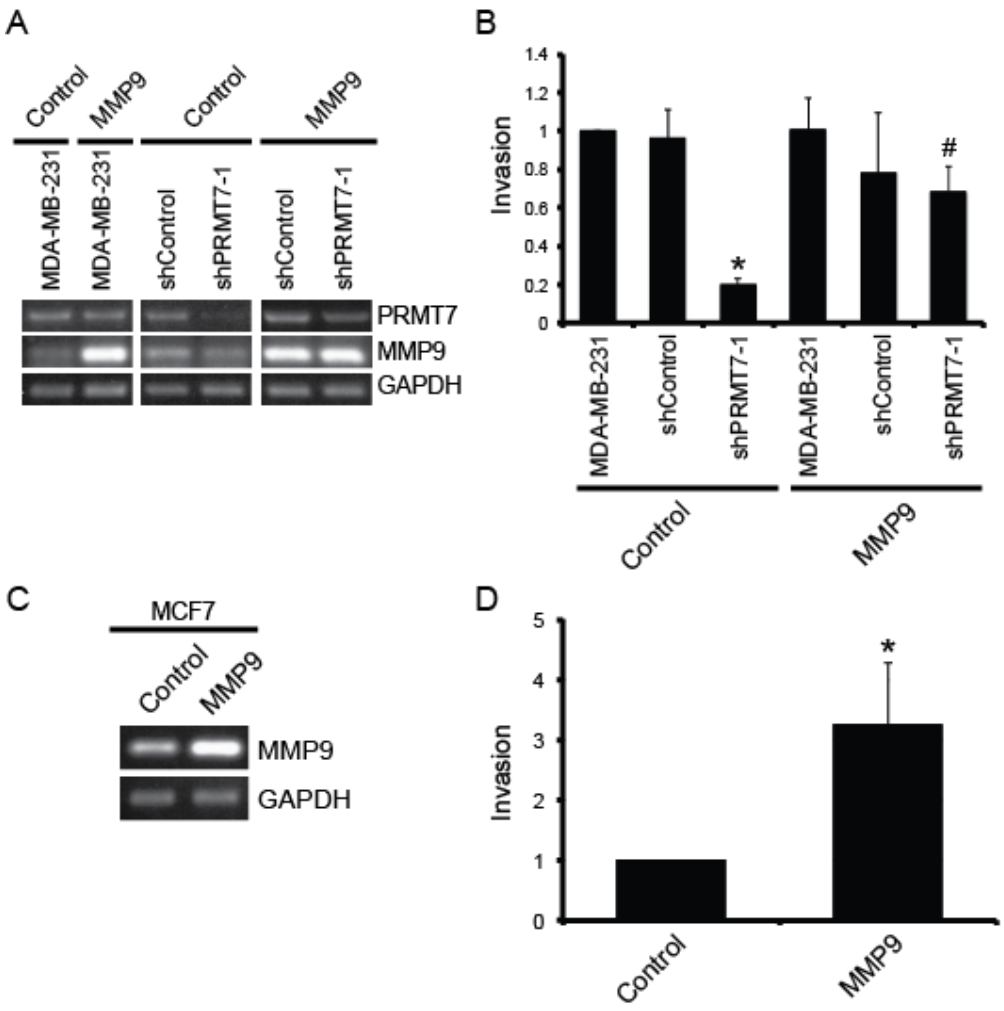

Figure 15: Overexpression of MMP9 rescues the loss of invasion in PRMT7-depleted cells

MDA-MB-231 cells stably depleted of PRMT7 were transiently transfected with an empty vector (Control) or a vector containing MMP9 cDNA. Parental MDA-MB-231 and cells expressing a non-targeting shRNA cells were used as controls. (A) Total RNA was collected 24 h post transfection and used to generate cDNA to assess PRMT7 and MMP9 expression levels. GAPDH served as a loading control. (B) To examine the effect of MMP9 overexpression on cell invasion, 24h post transfection, cells were re-plated at equal numbers into Transwell chambers containing a Matrigel layer and incubated for 24 h. Cells that passed through the chambers were counted. Data represents the mean ± standard error of 3 independent experiments. PRMT7-depleted cells exhibited decreased invasion (*$p<0.05$) but was rescued by MMP9 overexpression (#$p<0.05$). (C) MCF7 cells were transiently transfected with an empty vector (Control) or a vector containing MMP9 cDNA. Total RNA was collected 24h post transfection to assess expression. PCR analysis is shown; GAPDH was used as a loading control. (D) Similar invasion assays were performed with MCF7 cells but at 72h post-plating. Data represents the mean ± standard error of five independent experiments (*$p < 0.05$).

It is well established in the literature that an increase in MMP9 expression levels is associated with increased cancer cell invasion (Cowden Dahl et al., 2008; Köhrmann et al., 2009; Mehner et al., 2014; Mira et al., 2004; Orlichenko & Radisky, 2008; Rao et al., 2005; Wu et al., 2008; Yousef, Tahir, St-Pierre, & Gaboury, 2014). Since we observed an increase in MMP9 mRNA expression with PRMT7 overexpression in MCF7 cells which have low endogenous PRMT7 expression (Figure 13D, E, F), we wanted to know whether altering MMP9 expression alone is sufficient to affect their invasive capabilities. Indeed, MMP9 expression caused a significant enhancement of MCF7 cell invasion (Figure 15C and D), demonstrating the direct role MMP9 overexpression on breast cancer cell invasion.

As previously mentioned, PRMTs can regulate gene expression either by methylating histone tails at the promoter regions of genes, regulating ribosomes, or by regulating transcription factors (Gayatri & Bedford, 2014; Haghandish & Côté, 2016; Jahan & Davie, 2014)[1]. We sought to determine whether PRMT7 binds to the promoter region of MMP9, influencing its transcription. Through chromatin immunoprecipitation experiments, we show that PRMT7 binds -443 to -209 base pairs upstream of the MMP9 promoter (Figure 16). E-cadherin and POLD1 were used as positive controls since PRMT7 is known to bind to their promoter regions and subsequently methylate histone tails to repress their expression (Tae et al., 2011; Yao et al., 2014). PRMT7 binding to the MMP9 promoter gives insight into the mechanism by which PRMT7 promotes cell invasion and subsequent metastasis –epigenetic regulation is possible, however this needs to be further evaluated.

[1] Title and abstract of published first-authored book chapter is found in the Appendix (Haghandish & Côté, 2016).

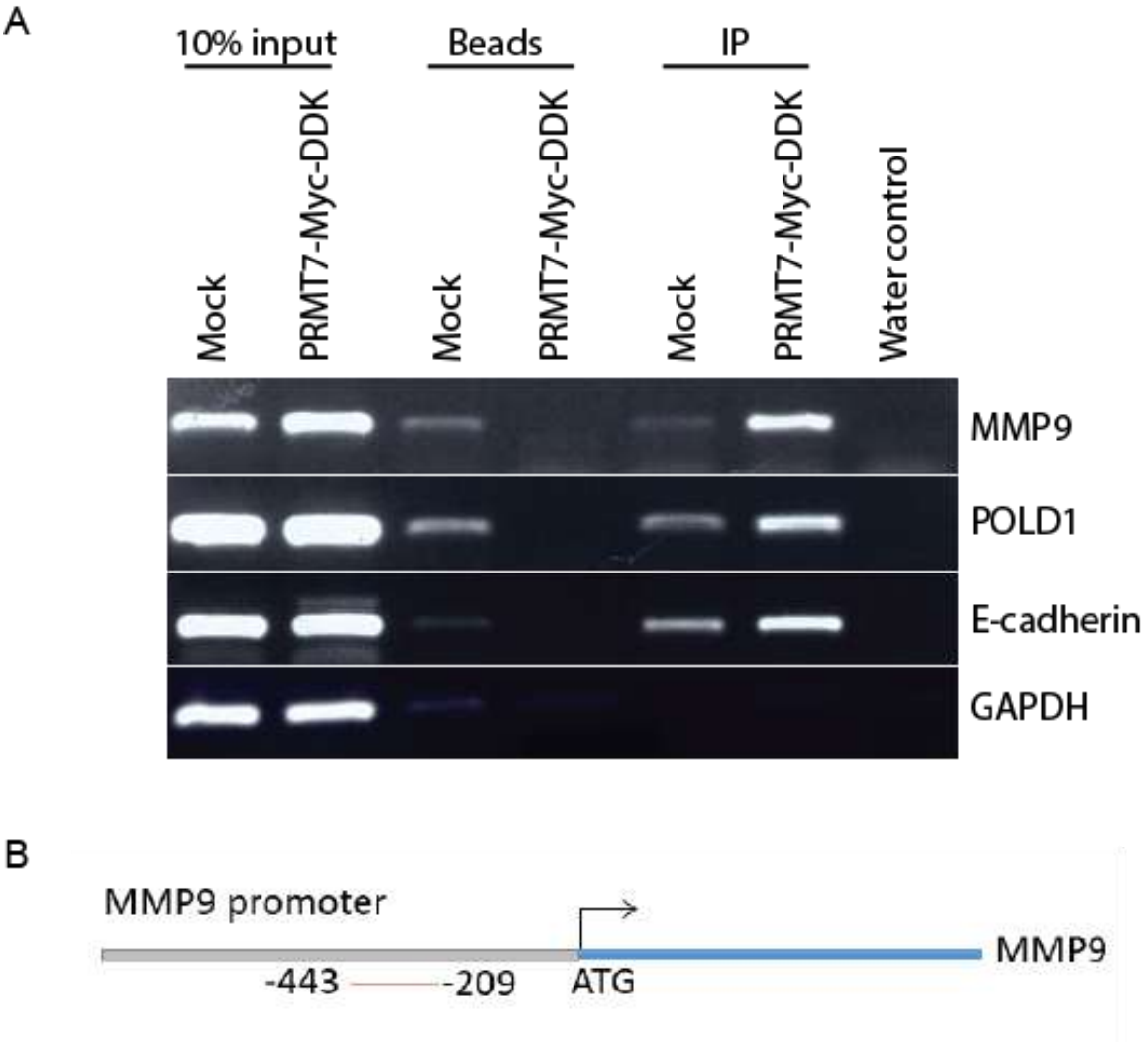

Figure 16: PRMT7 binds to the promoter region of MMP9
(A) Chromatin immunoprecipitation experiment showing that PRMT7 binds to the promoter of MMP9 within MCF7 cells. POLD1 and E-cadherin are used as positive controls as they are epigenetic targets of PRMT7 methylation (Karkhanis et al., 2012; Yao et al., 2014) and GAPDH as a negative control. (B) Schematic depicting area where PRMT7 binds to the MMP9 promoter (-443 to -209 base pairs upstream of promoter).

We next examined cell survival using a lentiviral-driven shRNA expression system different from the one previously used to efficiently knocked-down PRMT7 protein levels. We used an shRNA sequence within a replication-incompetent lentiviral vector (pLKO.1) obtained from The RNAi Consortium (Moffat et al., 2006) and obtained a more drastic depletion (80-90% depletion as opposed to 40-60% previously observed). Previously, we were able to obtain stable lines, however with these more efficient knockdowns, all of our future experiments (from this point onwards) were transient. Interestingly, whenever an 80-90% depletion of PRMT7 was acquired, drastic morphological alterations were observed. Specifically, cells were visibly flatter and larger in size. Moreover, complete knockout of PRMT7 using CRIPSR/Cas9 showed similar results (Figure 17A, B). Furthermore, the proliferation rate of PRMT7 depleted cells significantly decreased 72h after depletion (Figure 9). These observations correlated with senescence-like morphological changes – loss of a cell's ability to divide and grow. Thus, staining for senescence associated β-galactosidase (SA-β-gal) was executed to determine whether cells, upon complete ablation of PRMT7, were undergoing senescence. SA-β-gal is an enzyme that is cytochemically detectable at a pH of 6.0 using a chromogenic substrate 5-bromo-4-chloro-3-indoyl β-D-galactopyranoside (X-gal). If a cell is senescent, SA-β-gal converts X-gal into a blue, insoluble compound which can subsequently be imaged and quantitated (Debacq-Chainiaux et al., 2009; Dimri et al., 1995). Using both parental and PRMT7 knockout MDA-MB-231 cells, we observed a significant increase in SA-βgal staining after 24h post knockout, suggesting cells are undergoing senescence in the absence of PRMT7 (Figure 17C). Further experimentation needs to be performed to determine the precise percentage of cells undergoing senescence and the time course for these observed effects.

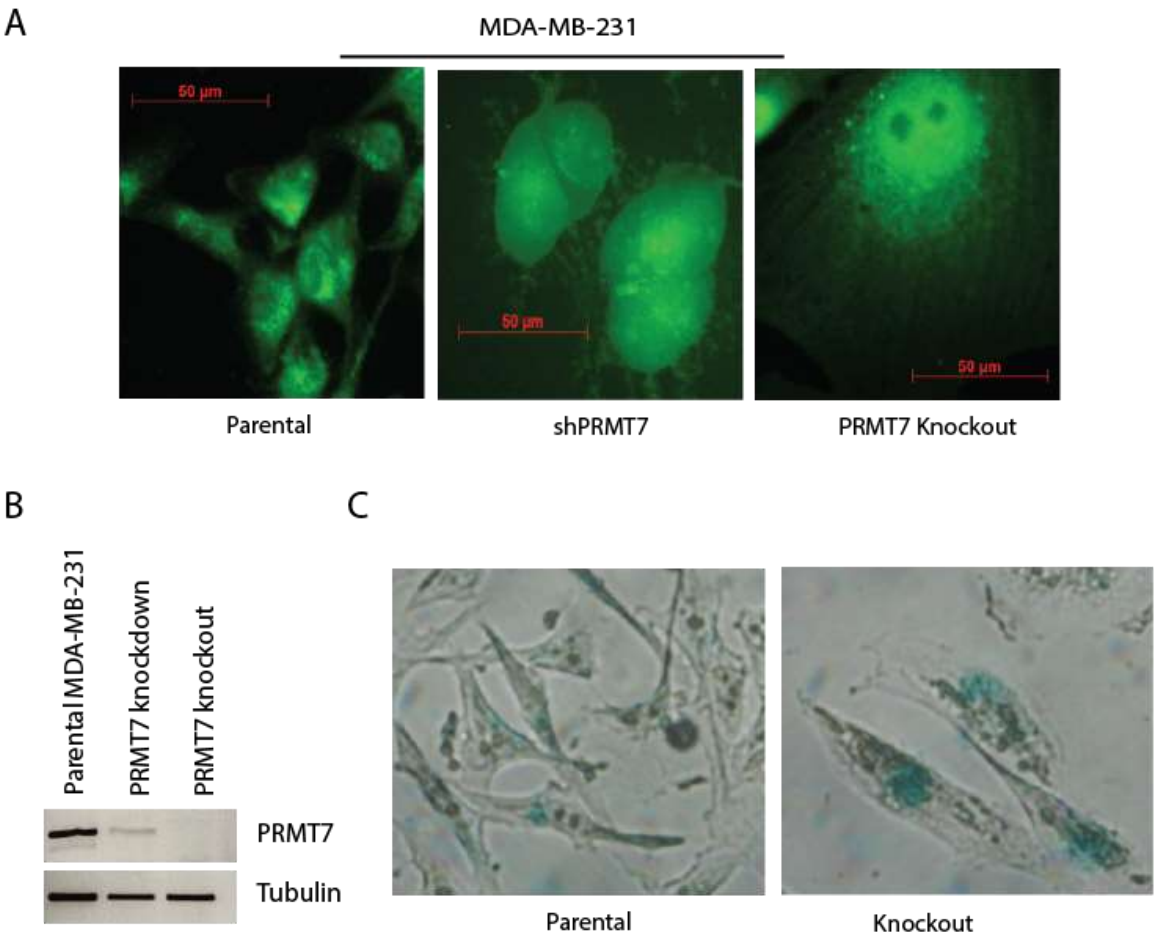

Figure 17: PRMT7 depletion drastically affects cell morphology and promotes cell senescence

(A) Immunofluorescent immaging of GFP-positive MDA-MB-231 cells with either knockdown or knockout of PRMT7 compared to parental cells. Both knockdown and knockout of PRMT7 drastically affect cell morphology. Upon depletion of PRMT7, cells become larger and flatter – senescent-like. (B) Western blot depicting representative PRMT7 knockdown and knockout MDA-MB-231 cell lines compared to parental cells. Tubulin was used as a loading control. (C) SA-β-gal staining of parental and PRMT7 knockout MDA-MB-231 cells 24h after knockout. An increase in staining is observed in knockout cells suggesting cells are undegoing senescence.

However, after a prolonged period (>72h), PRMT7-knockdown cells seemed to significantly struggle, ceasing to proliferate and eventually began to die (Figure 9). Further experimentation using IncuCyte Zoom was utilized to evaluate cell proliferation and cell death. For these assays, parental (●), shNS (■), shPRMT7 (▲), and PRMT7 knockout (▼) MDA-MB-231 cells were seeded at equal concentrations into 96-well plates. 24h after seeding, cells were infected to produce the aforementioned lines. The time of infection was termed as 0h. The percent confluency of the plate was then calculated to track cell proliferation over the course of 140h every 2 hours. A significant decrease in proliferation was observed by 72h: 38% decrease in shPRMT7 lines and 58% in PRMT7 knockout lines (Figure 18A). As a decrease in cell proliferation was observed in knockdown and knockout lines compared to both parental and shNS cells, we next evaluated general cell death using DNA intercalating markers (cytotox red; Figure 18B). Surprisingly, both PRMT7 knockdown and knockout cells almost immediately exhibited signs of cell death upon infection; however, knockout lines peaked at 12h post-infection whereas knockdown cells peaked at 88h suggesting that minimal levels of PRMT7 in knockdown cells prolonged survival. Both control lines showed no signs of significant cell death. To further explore cell death pathways, we used annexin V staining to evaluate apoptosis (Figure 18C). Knockout cells exhibited an 8 fold increase in annexin V staining by 72h whereas knockdown cells exhibited a 1.8 fold increase, suggesting that knockout cells are more prone to apoptosis than knockdown cells. As a lack of PRMT7 within breast cancer cells resulted in a drastic decrease in proliferative capabilities and eventual cell death, we proposed that PRMT7 may be essential for a critical cellular function.

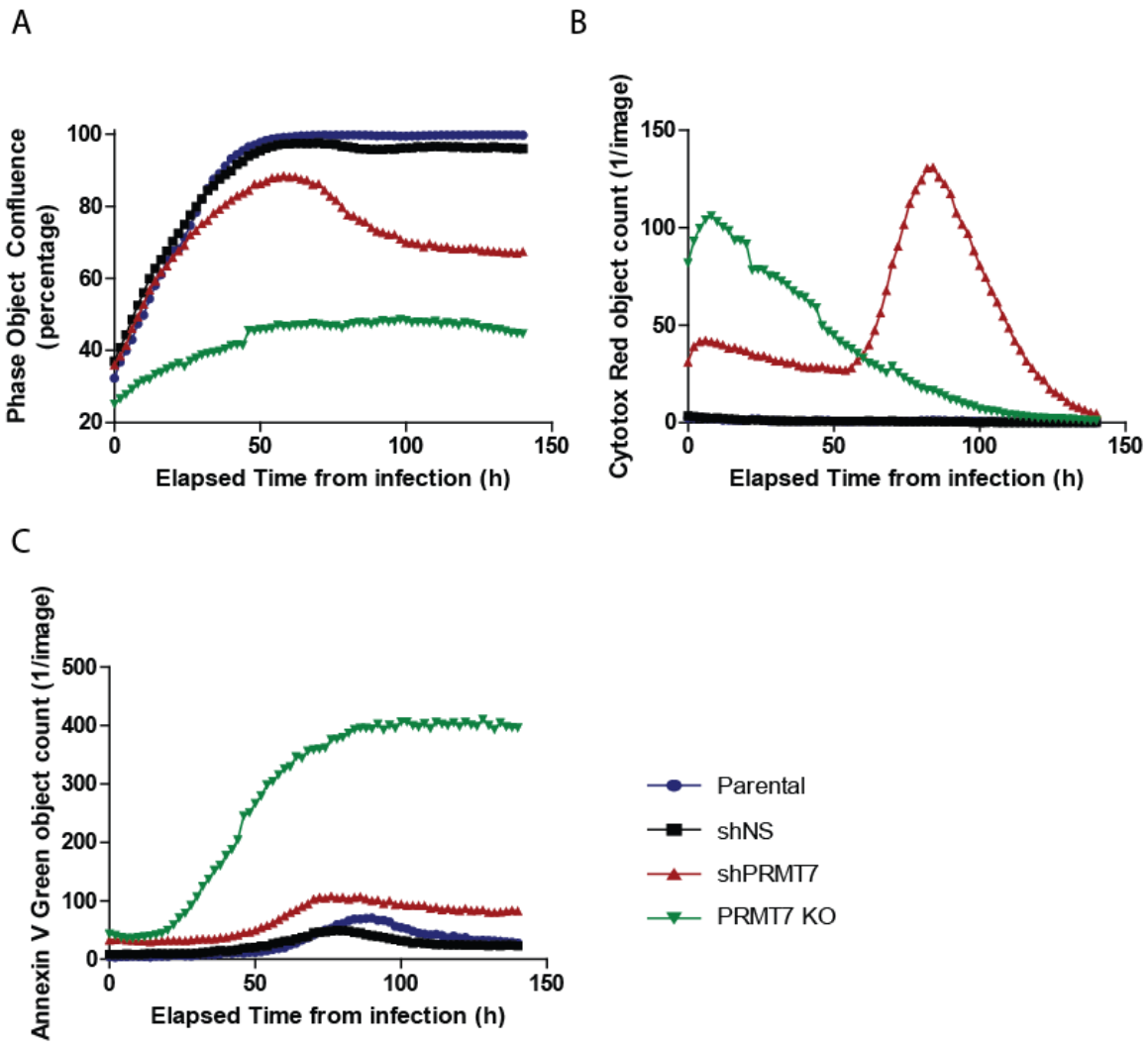

Figure 18: PRMT7 affects cell proliferation and cell death

IncuCyte Zoom experiment comparing cell proliferation by evaluating cell confluency of (A), general cell death using cytotox red DNA intercalating markers (B), and apoptosis using Annexin V staining (C) of Parental (●), shNS (■), shPRMT7 (▲), and PRMT7 knockout (▼) MDA-MB-231 cells. Data was obtained over a course of 140h after initial infection of cells and images were taken every 2 hours for n=3 (performed in six replicates). IncuCyte Zoom software was used for data analysis.

3.2 Discover novel and/or breast cancer-related biological functions of PRMT7 by identifying its protein interactome

3.2.1 Identify novel protein interactors of PRMT7 using quantitative mass spectrometry

To uncover unique substrates of PRMT7 and potentially novel functional roles for PRMT7, we performed SILAC-based quantitative mass spectrometry as previously described (Baldwin, Bejide, Trinkle-Mulcahy, & Cote, 2015; Larivière, Law, & Trinkle-Mulcahy, 2014; Trinkle-Mulcahy et al., 2008). MCF7 breast cancer cells were used to stably express either GFP as a control or PRMT7-mGFP. We used breast cancer cells for this study as they were extensively characterized in our first aim. Similar to previous publications and endogenous PRMT7 (Figure 3C), PRMT7-mGFP was found predominantly within the cytoplasm, with a weak diffused staining in the nucleus and no signal in nucleoli, in contrast to GFP which displayed a uniformly diffused staining across the whole cell (Figure 19A) (Baldwin, Haghandish, et al., 2015; Herrmann et al., 2009). GFP-expressing cells were labelled in "light" R0K0 (L) media and cells stably expressing PRMT7-mGFP, in "heavy" R6K4 (H) media. For increased confidence, we performed a second independent experiment with reciprocal labeling.

Cells were kept in culture in the isotopic-labelled media for at least five passages to obtain full incorporation of the isotopes within proteins (Larivière et al., 2014; Trinkle-Mulcahy et al., 2008). Both GFP and PRMT7-mGFP were then subsequently affinity purified from the cell lysates using GFP-Trap beads. Beads from both immunoprecipitates (GFP and PRMT7-mGFP) were combined and all bound proteins were washed and subsequently eluted. A fraction of the eluate was run on an SDS-PAGE gel alongside controls and subjected to immunoblotting to confirm that GFP and PRMT7-mGFP were

eluted in equal amounts (Figure 19B; elution lane). We observed almost complete immunodepletion of both GFP and PRMT7-mGFP from cells as noted by the absence of bands within the flowthrough lanes of the Western blot (Figure 19B; flowthrough lanes). The remainder of the eluate was then separated on an SDS-PAGE gel (two lanes), Coomassie stained, and then cut into five equal gel fragments for trypsin digestion and subsequent analysis by liquid chromatography tandem LC-MS/MS mass spectrometry (liquid chromatography–mass spectrometry; Figure 19C).

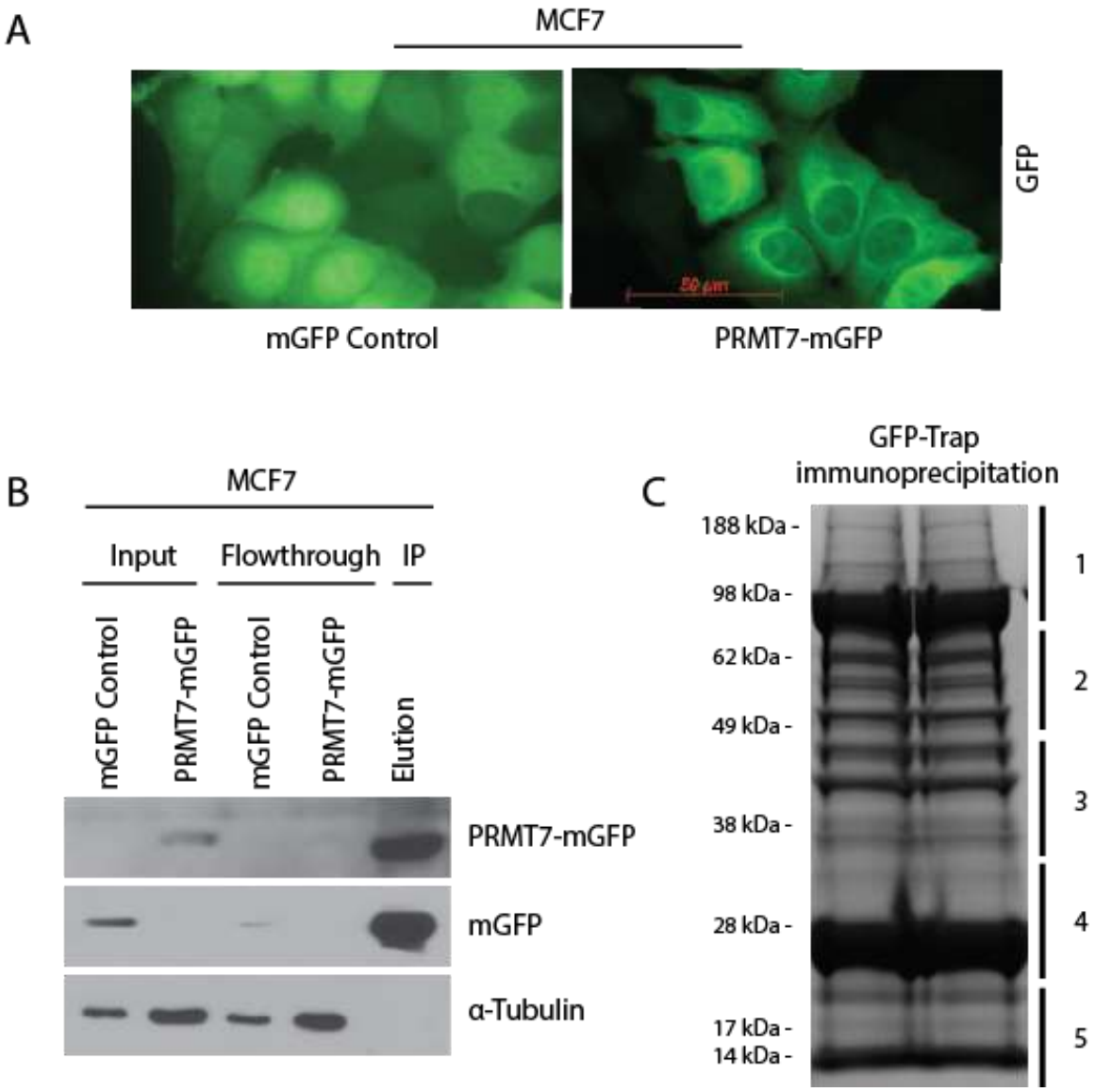

Figure 19: Preparation and confirmation of immunoprecipitation for SILAC-based quantitative mass spectrometry

(A) Representative fluorescent images of mGFP control and PRMT7-mGFP MCF7 stable cell lines showing diffused localization of PRMT7 at 40X magnification (scale bar: 50µm). (B) Confirmation of affinity immunodepletion of PRMT7-mGFP fusion protein and mGFP using GFP-Trap beads (ChromoTek) in MCF7 stable cells. (C) Coomassie-stained SDS-PAGE gel of the eluate (1:1 mixture of PRMT7-mGFP/mGFP) from affinity purification using GFP-Trap beads. The same sample was run in two lanes due to the large volume. Gel was sliced into 5 fragments to be sent for mass spectrometric analysis of co-immunoprecipitated proteins.

Database analysis (against the human Uniprot database) and quantitation were performed using MaxQuant software v1.2.7.4, as previously described (Larivière et al., 2014; Trinkle-Mulcahy et al., 2008). ProteinCenter (Proxeon Bioinformatics; a proteomics data mining and management software) was used to eliminate redundancy, compare datasets, and convert protein IDs to gene symbols. Based on the mass differences between the R0K0 and R6K4 labelled peptides, Log_2 SILAC ratios (H:L) were calculated for each identified protein. For both independent mass spectrometry experiments, the normalized Log_2 H:L ratio and normalized L:H ratio, for experiments 1 and 2 respectively, were plotted against normalized peptide intensity for each identified protein. We set a Log_2 H:L ratio of 1 log unit above the median value as a putative interactor threshold (dashed line; Figure 20) as this indicates at least a 2-fold enrichment above non-specific interactors. A total of 72 and 76 potential protein interactors of PRMT7 were identified in experiments 1 and 2 (reverse labelling), respectively (Appendix; Figure 20). Of these proteins, 41 were reproducibly pulled down in both experiments and subsequently used for our analysis. To identify specifically enriched proteins from this common set of interactors, we compared and plotted the normalized Log_2 H:L ratios of each of these proteins from both experiments (Figure 21A, B). The thresholds are indicated on the graph as red lines (1.009 for Experiment 1 and 1.26 for Experiment 2). Values less than 1 Log_2 unit of the median are more likely to represent either environmental contaminants or nonspecific interactions. As revealed from this analysis, the highly enriched PRMT7 interacting proteins from both experiments are present in the upper right quadrant of the scatter plot (Figure 21B).

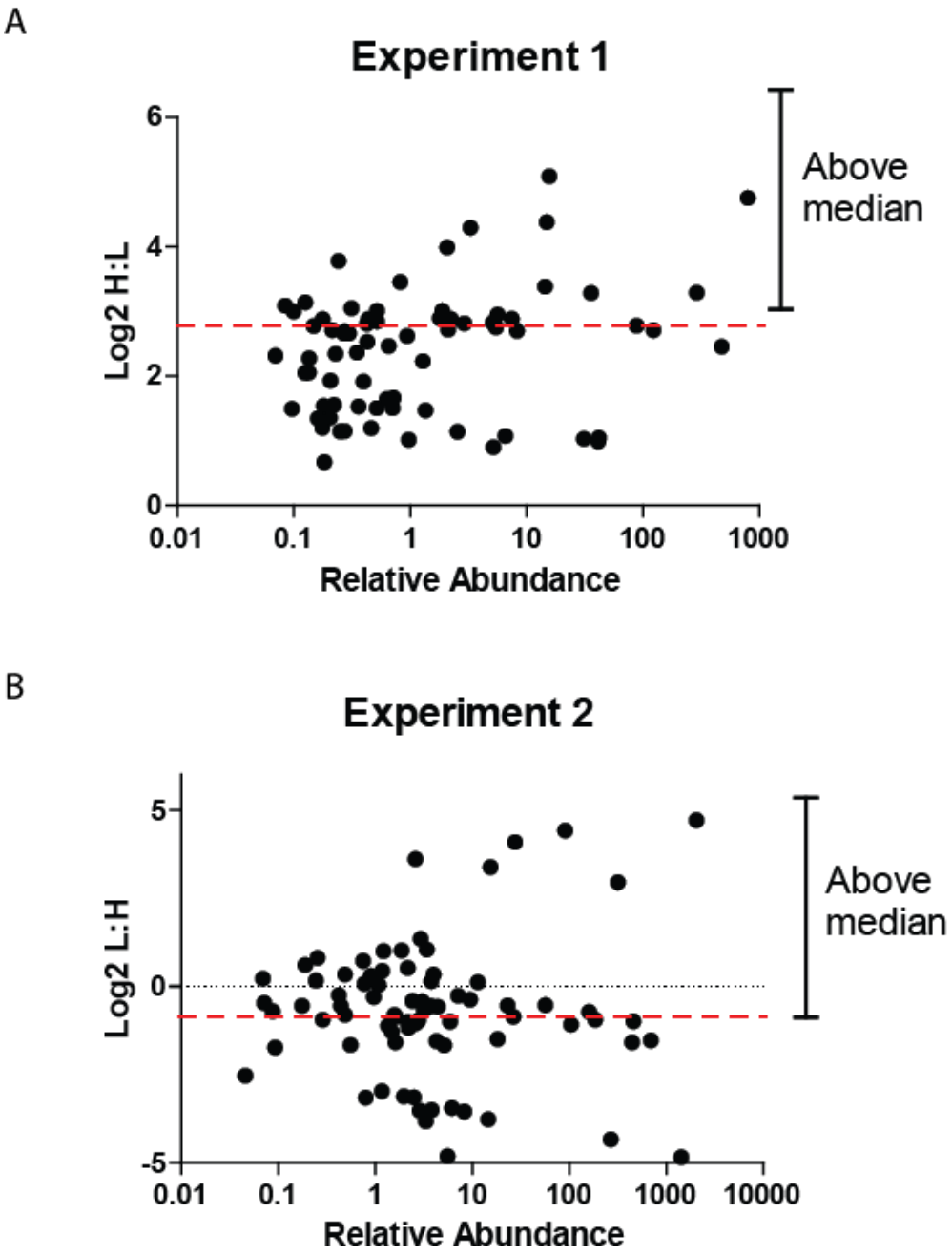

Figure 20: Analysis of SILAC-based mass spectrometry results
(A) Scatter plot showing comparison of the SILAC H:L ratio of proteins to their relative abundance within the mass spectrometry experiment (experiment 1). The median is marked by a red dashed line. (B) Similar comparison but for experiment 2 (reverse labeling; SILAC ratio is L:H).

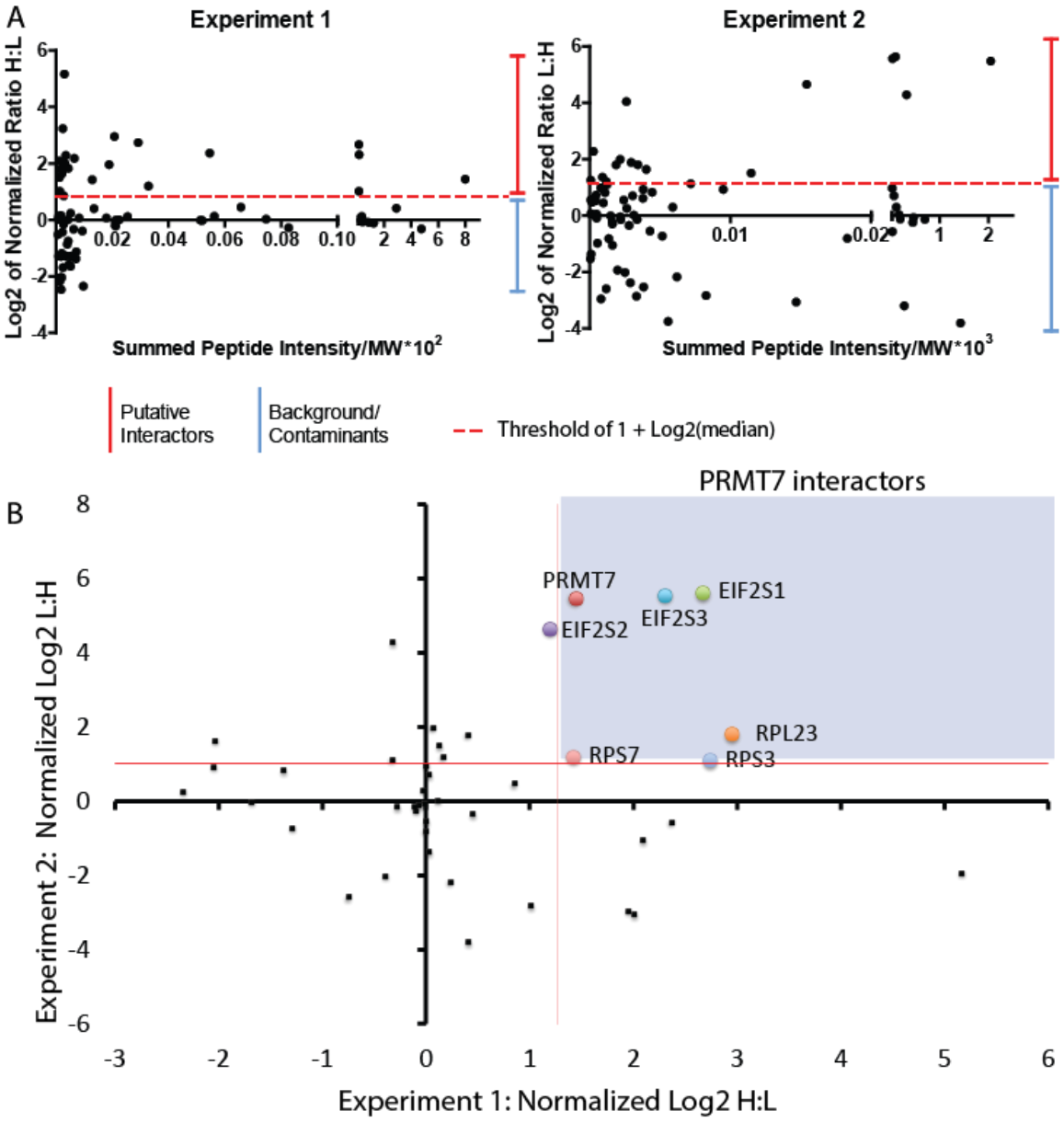

Figure 21: Analysis of SILAC-based mass spectrometry results
(A) Comparison of the normalized SILAC H:L ratio of identified proteins from the two independent mass spectrometry experiments (L:H ratio for experiment 2). Threshold for putative protein interactors are indicated by red line. (B) Scatter plot of two independent mass spectrometry experiments comparing shared interactor proteins represented as Log_2 ratios of the heavy-labelled protein to light-labelled protein. PRMT7 interactors are highlighted in purple within the graph (above red median lines).

3.2.2 Confirmation of the interacting proteins obtained from the proteomic experimentation

As shown in the table below (Table 5), amongst the most highly enriched, reproducible protein interactors of PRMT7 from both experiments were ribosomal proteins and translation initiation factors eIF2α, β, and γ. The eIF2 ternary complex (eIF2α, β, and γ)-PRMT7 interaction was validated via co-immunoprecipitation experiments (Figure 22A) and the reciprocal interaction between exogenous eIF2α-GST and endogenous PRMT7 via a GST-pulldown was also confirmed (Figure 22B).

It is important to note that if a protein is not highly enriched in both experiments, it does not mean it is not a true interactor of PRMT7. In fact, we confirmed an interaction between PRMT7 and ACTN4 (alpha actinin 4) which was enriched above background levels only in experiment 1, and strong interaction via co-immunoprecipitation was reproducible (Figure 23A). We further probed for monomethylation of arginine residues and detected a signal the same size as ACTN4. To ensure it was ACTN4 that was monomethylated, we ran two PRMT7 co-immunoprecipitations side-by-side and probed for either MMA or ACTN4 (Figure 23B). Indeed, the bands were the same size, suggesting that ACTN4 could be a potential substrate of PRMT7 or another PRMT. However, only methylation assays would truly confirm ACTN4 as a PRMT substrate.

Table 5: Summary of top 6 hits from mass spectrometry experiments

Identified protein that interact with PRMT7				
Gene Name	Experiment 1		Experiment 2	
	# Peptides	Enrichment	# Peptides	Enrichment
EIF2S1	17	2.66	14	5.63
EIF2S3	9	2.30	9	5.56
EIF2S2	11	1.20	11	4.65
RPL23	2	2.95	3	1.80
RPS3	3	2.73	2	1.10
RPS7	3	1.42	1	1.21

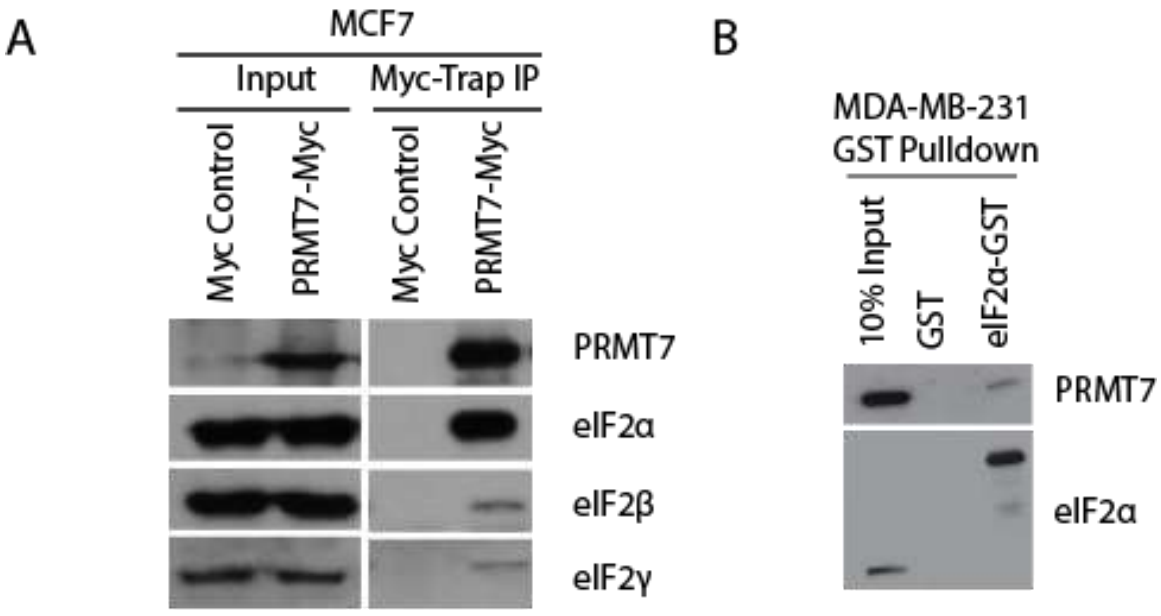

Figure 22: Identified PRMT7 interactors

(A) Co-immunoprecipitation of Myc control and PRMT7-Myc fusion protein confirms an interaction between PRMT7 and eIF2α, eIF2β, and eIF2γ in MCF7 cells. (B) GST pulldown of eIF2α-GST using MDA-MB-231 cell lysate. PRMT7 interacts with eIF2α-GST – suggesting the interaction is robust (eIF2α-GST incubated with lysate for 1 hour to see interaction).

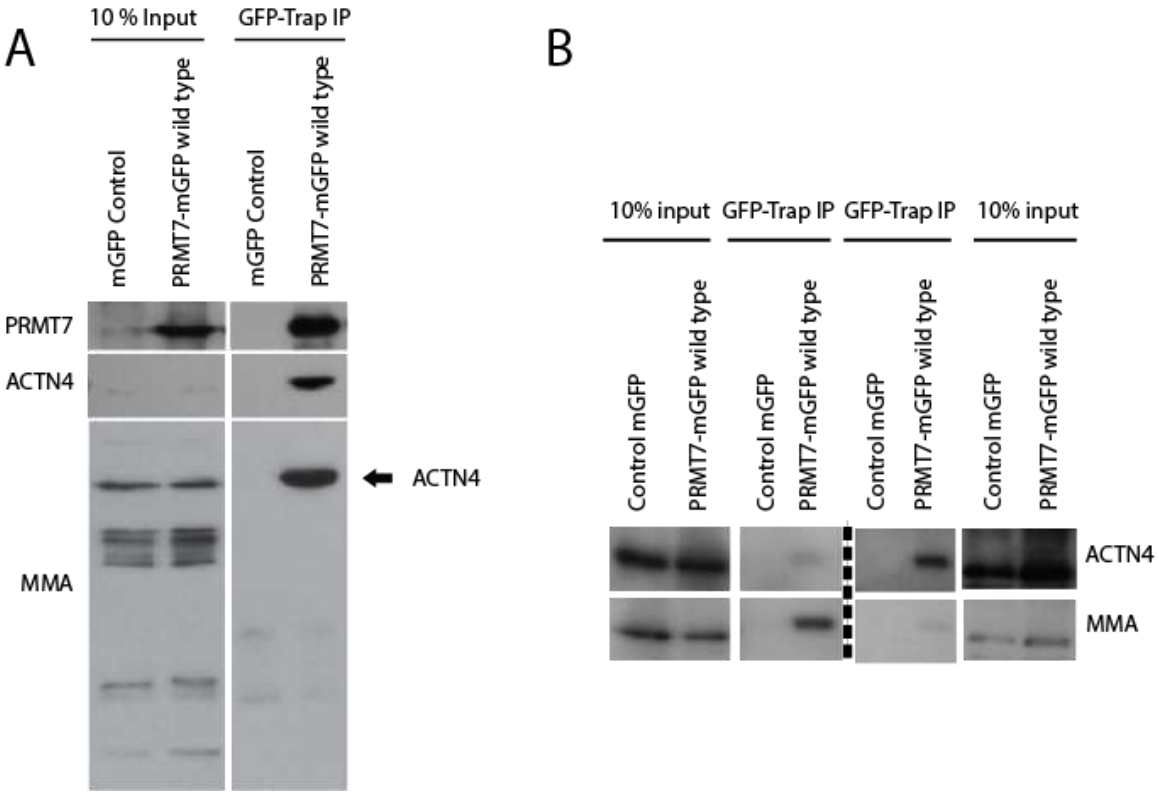

Figure 23: PRMT7 interacts with ACTN4
(A) Western blot showing interaction between PRMT7 and ACTN4 as well as strong monomethylation signal for ACTN4 within MCF7 cells. (B) Two immunoprecipitation experiments from MDA-MB-231 cells run side-by-side on a gel, the membrane was then cut after transfer, and probed for different proteins (this is done to confirm that the detected band for ACTN4 and MMA is not due to residual signal detected after stripping).

As the interaction between PRMT7 and eIF2α was highly enriched and it represents a new avenue never in terms of PRMT7 biological function, we decided to pursue a potentially novel role of PRMT7 in translational regulation and/or stress regulation via its interaction with eIF2α. To gain a better understanding into the functional role of the PRMT7-eIF2α interaction, biochemically, we first explored the presence of the interaction within the translational machinery of cells using polyribosome profiling experiments followed by fractionation of samples and Western blotting of proteins. We used highly proliferative 293T cells, to perform these experiments (Figure 24A). Since eIF2α regulates translation initiation, its protein levels are highly concentrated within the pre-translational complex (40, 60, 80S) fractions. We observed that PRMT7 co-fractionated with eIF2α within the pre-translational complex fractions. Interestingly, we also observed the presence of PRMT7 within the polysomal fractions (Figure 24B). Similarly, the association of PRMT7 with the translation machinery was also observed breast cancer cell lines MCF7 (Figure 25A), and MDA-MB-231 (Figure 25C). Western blotting of the fractionated protein samples were subsequently performed, showing that PRMT7 is present in both the pre-translational complex and polysomal fractions (Figure 25B, D).

Furthermore, our mass spectrometry results also support these observations as other ribosomal proteins (both small and large subunit proteins) were identified in both mass spectrometry screens (Appendix). Within our mass spectrometry data, we also noted the presence of unshared translation-related protein interactors. In experiment 1, eukaryotic elongation factor 1A (eEF1A) was identified but did not reach threshold levels. It is possible that eEF1A is a true interacting protein of PRMT7 or an indirect interactor but there is also the possibility that it is background/contamination. Moreover, in experiment

2, eIF4A was additionally identified and its enrichment did reach well above threshold levels (Appendix; Table 7). However, it was only identified in the second experiment and not in the first. Nevertheless, it is probable that eIF4A represents a *bona fide* PRMT7 interacting protein.

Next, to determine whether PRMT7 and eIF2α interact within the pre-translational complex fractions, co-immunoprecipitation experiments of pooled pre-translational complex fractions of MCF7 cells expressing either GFP or PRMT7-mGFP were performed (Figure 26A, B). We confirmed that PRMT7 and eIF2α not only co-fractionate with pre-translational complex fractions but also co-precipitate within the fractions, supporting the idea that PRMT7 may potentially regulate translation through a possible interaction with eIF2α (Figure 26B).

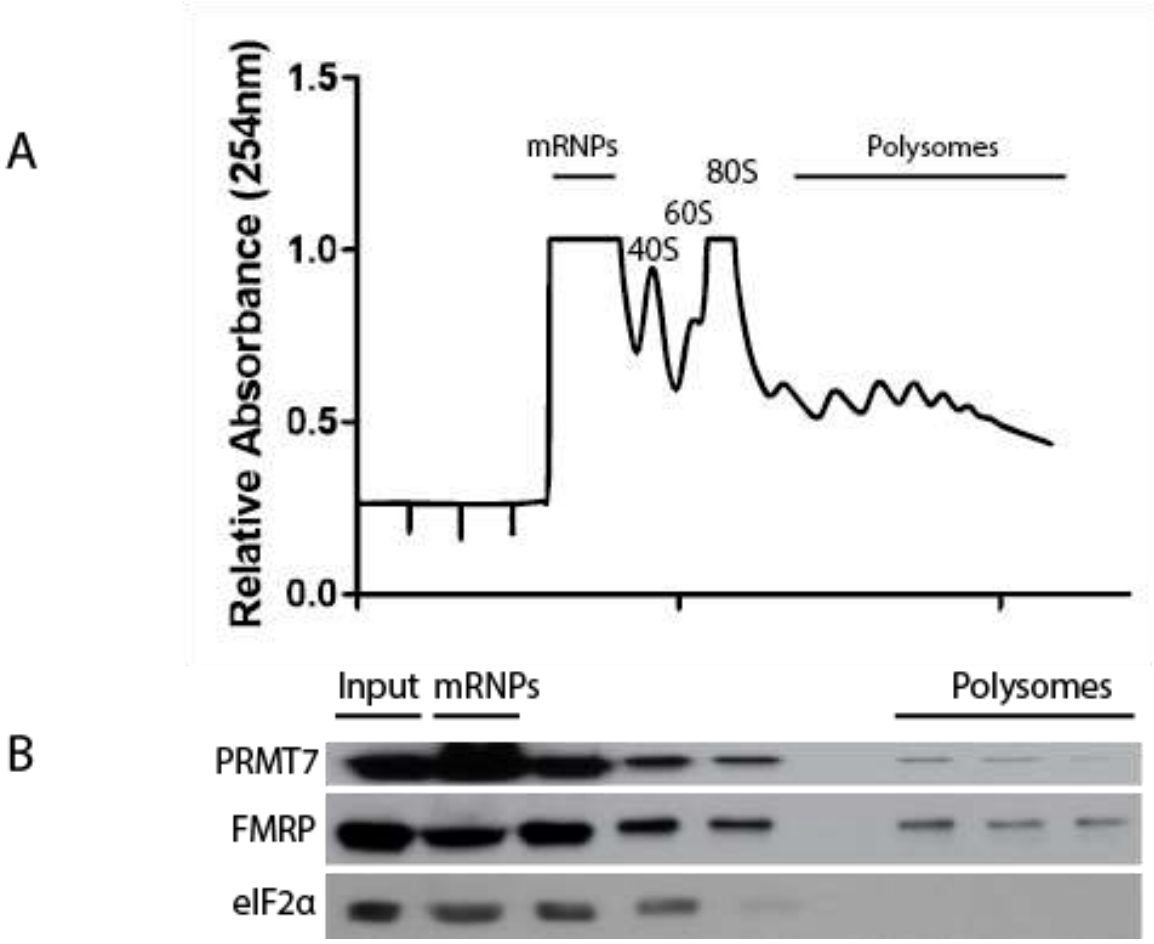

Figure 24: Presence of PRMT7 within the translational machinery
(A) Polyribosome profile of parental 293T cells. Relative absorbance of RNA was read at 254nm. (B) Polyribosome fractions were run on an SDS-PAGE gel including an input of total cell lysate. PRMT7 co-fractionates with eIF2α. FMRP was used as a positive control for pre-translation complex (40, 60, 80S) and polysomes.

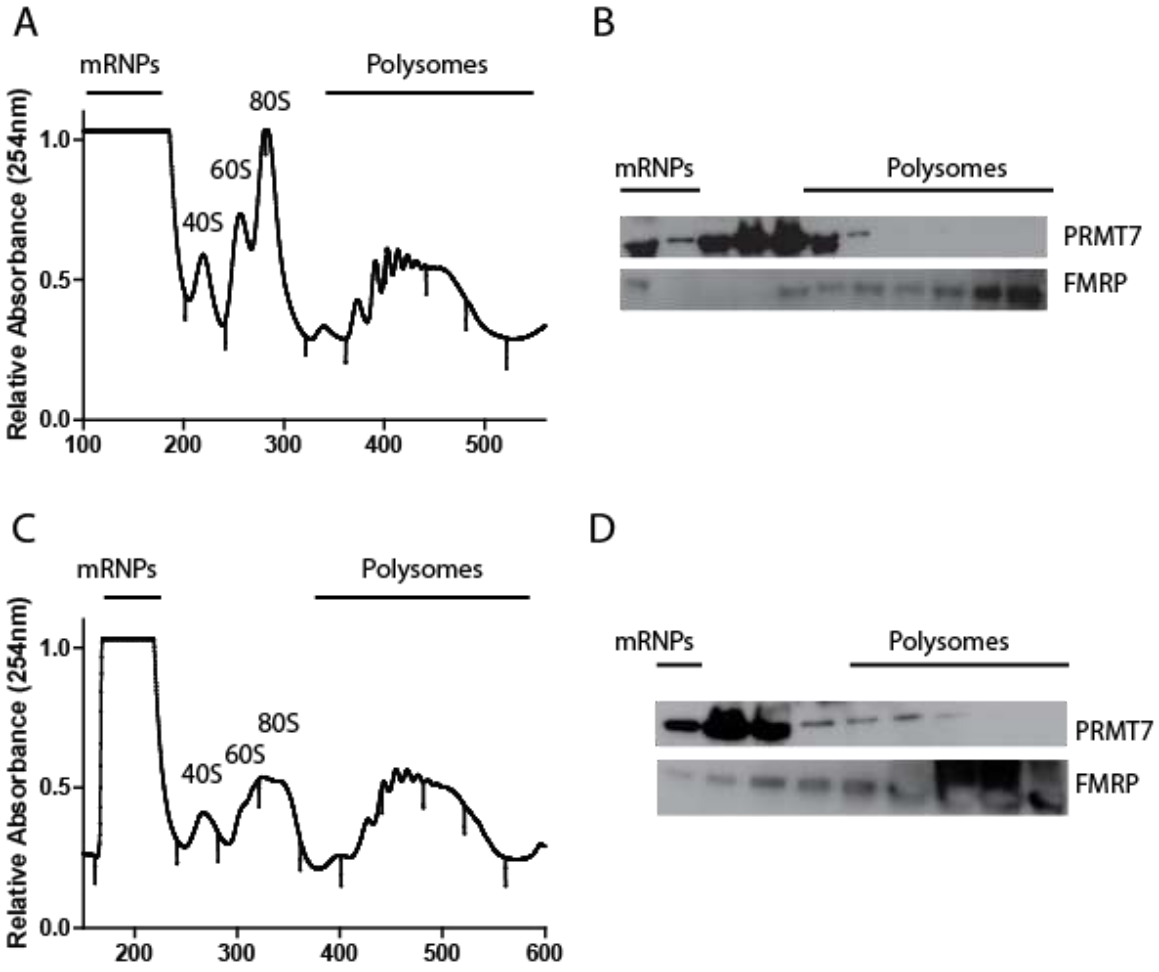

Figure 25: PRMT7 is present in translational machinery within breast cancer cell lines

Polyribosome profiles and fractions of parental MCF7 cells (A, B) and parental MDA-MB-231 cells (C, D). Relative absorbance of RNA was read at 254nm. PRMT7 co-is found within both polysomes and pre-translation complex – more so in cancer cells. FMRP was used as a positive control for the pre-translational complex and polysomes.

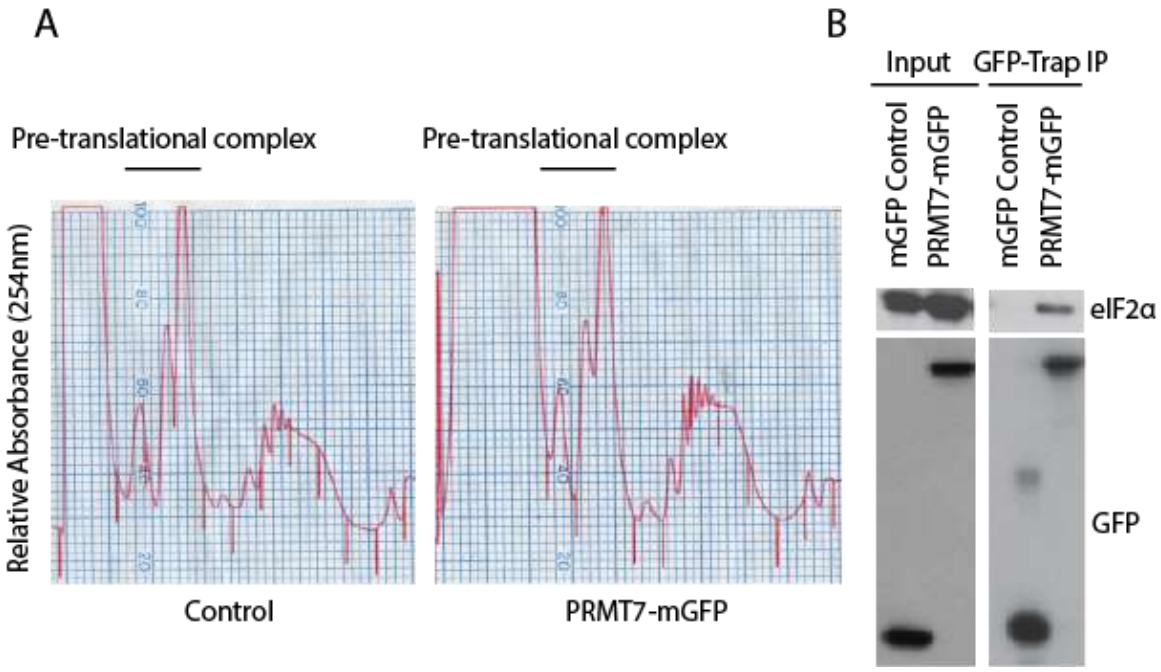

Figure 26: PRMT7 interacts with eIF2α within pre-translational complex fractions. (A) Pre-translation complex fractions were pooled from MCF7 cells expressing either mGFP or PRMT7-mGFP. (B) GFP-Trap beads were used to immunoprecipitate control mGFP and PRMT7-mGFP from pooled samples. Inputs were run alongside immunoprecipitates. PRMT7-mGFP interacts with eIF2α in pre-translational complex fractions.

Subsequently, we wanted to determine whether eIF2α is a substrate of PRMT7 since their interaction was robust and highly reproducible. PRMT7 is known to uniquely recognize and methylate an RXR motif (Y Feng et al., 2013). This motif consists of a highly basic residue (X) flanked by arginine residues (R). Our *in silico* analysis revealed that human eIF2α contains a double RXR motif, SELS^{51}**RRRI^{55}R**SINK^{60}, adjacent to the S^{51} residue – a site known for its crucial regulatory role within the cellular stress response upon phosphorylation by HRI, PKR, GCN2 or PERK kinases. Although I^{55} is not a basic residue that flanks the arginine residues within the potential RXRXR motif, the general sequence is highly basic. Using site-directed mutagenesis, the RXR sequence of eIF2α was mutated to abolish the potential PRMT7 methylation site(s). The arginine residues were mutated to lysine residues to preserve the positive charge. Several full-length mutants were thus generated: KRR, RKR, RRK, RKK, KKK, and RRRIK (Figure 27A). Additionally, an S^{51} to D phosphomimetic mutant was generated to determine whether phosphorylation at S^{51} might influence methylation of the adjacent RXRXR motif. These full-length eIF2α mutant sequences were then sub-cloned into an expression vector to purify GST fusion proteins for *in vitro* methylation assays.

Methylation assays were performed using human PRMT7 purified from insect cells, tritium-labelled SAM, wild-type and mutant eIF2α-GST proteins as potential substrates, GST as a negative control, and histones as a positive control. The autoradiography revealed that wild-type, KRR, RKR, RRRIK, and S^{51}D eIF2α-GST were methylated by PRMT7 *in vitro* since a strong signal was detected (Figure 27B; lanes 1, 2, 3, 5, and 6). As expected of the positive control, methylation of histones was also prominent (lane 10). Absence of a signal was observed for the negative GST control (lane 9), eIF2α

RKK mutant (lane 7), KKK mutant (lane 8), and RRK mutant (lane 4). Hence, within the RXR motif, the arginine residue crucial for recognition and/or methylation was identified to be R^{54} as methylation was always lost whenever this residue was mutated. Additionally, PRMT7 was still capable of methylating the $S^{51}D$ mutant suggesting that perhaps the two post-translational modifications are not mutually exclusive. Furthermore, methylation assays using purified PRMT1, 3, 4, 5, 6, 8, and 9 were performed with both wild-type and $R^{52}KK$ mutant eIF2α-GST as substrates (Figure 28A) or histone substrates as a positive control (Figure 28B). Other than the methylation of wild-type eIF2α by PRMT7, the only other signals observed were automethylation of PRMT4, 6, 7, and 8 which have been previously observed (Dillon, Rust, Thompson, & Mowen, 2013; Y Feng et al., 2014; Geng et al., 2017; Singhroy et al., 2013; L. Wang et al., 2013). These results suggest that eIF2α is a PRMT7-specific substrate. PRMT2 was excluded from these studies as its activity has been shown to be very weak within cells (Lakowski & Frankel, 2009).

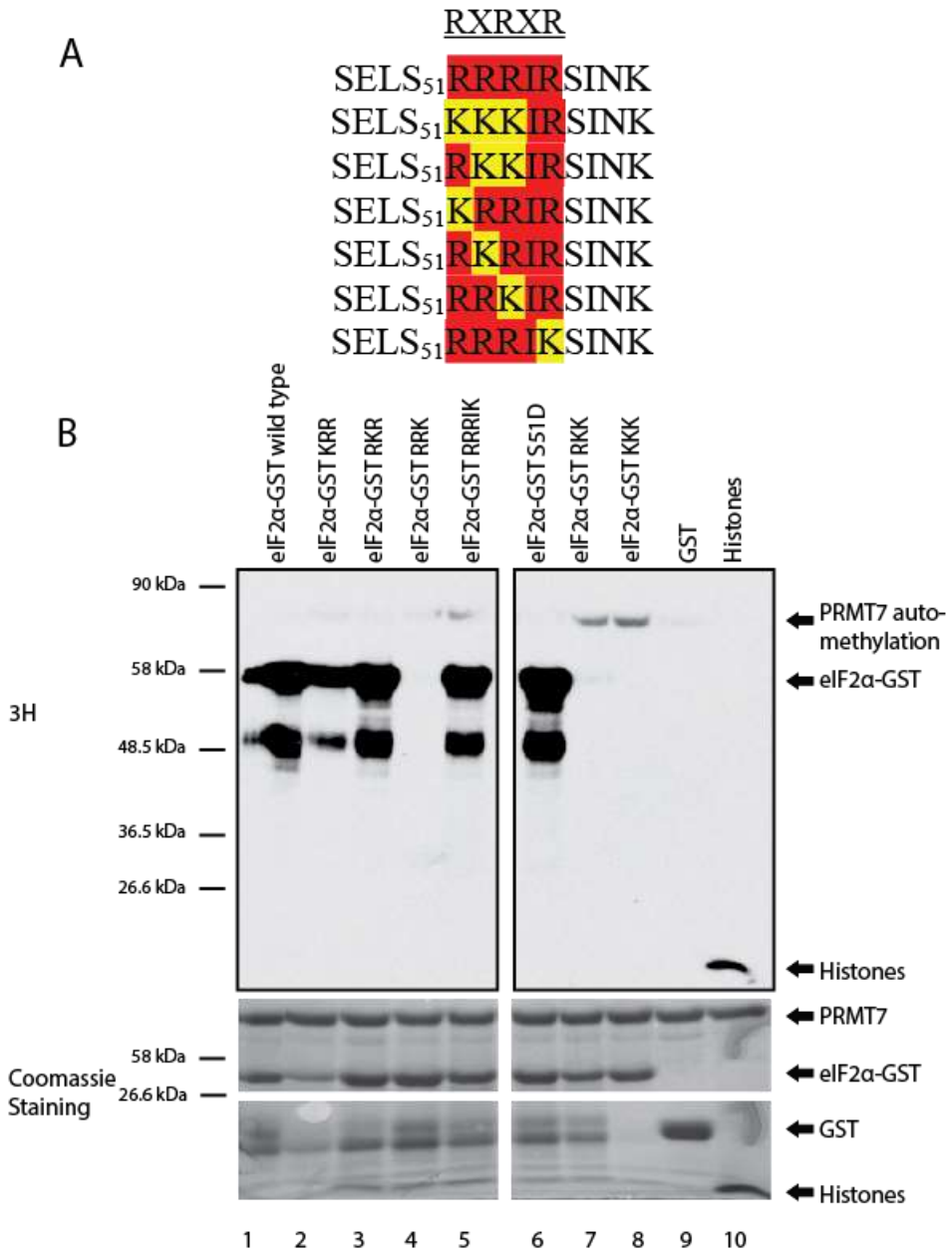

Figure 27: Confirmation that PRMT7 methylates eIF2α *in vitro*

(A) A potential motif recognized by PRMT7, RXRXR motif, exists adjacent to the regulatory S^{51} residue of eIF2α. Using site-directed mutagenesis, the arginine residues were mutated into lysine to create six mutants within the RXRXR motif. (B) Autoradiography-based methylation assays using ^{3}H-SAM as methyl-donor, PRMT7 as the enzyme, and eIF2α as a substrate. Experiments revealed that $R^{52}R^{53}R^{54}I^{55}R^{56}$ sequence motif is methylated by PRMT7 – specifically, R^{54} is critical for its methylation. Even in the presence of phosphorylation at S^{51}, using an $S^{51}D$ mutant, eIF2α was methylated. Methylation of histones was used as a positive control and GST as a negative control. Auto-methylation of PRMT7 was observed.

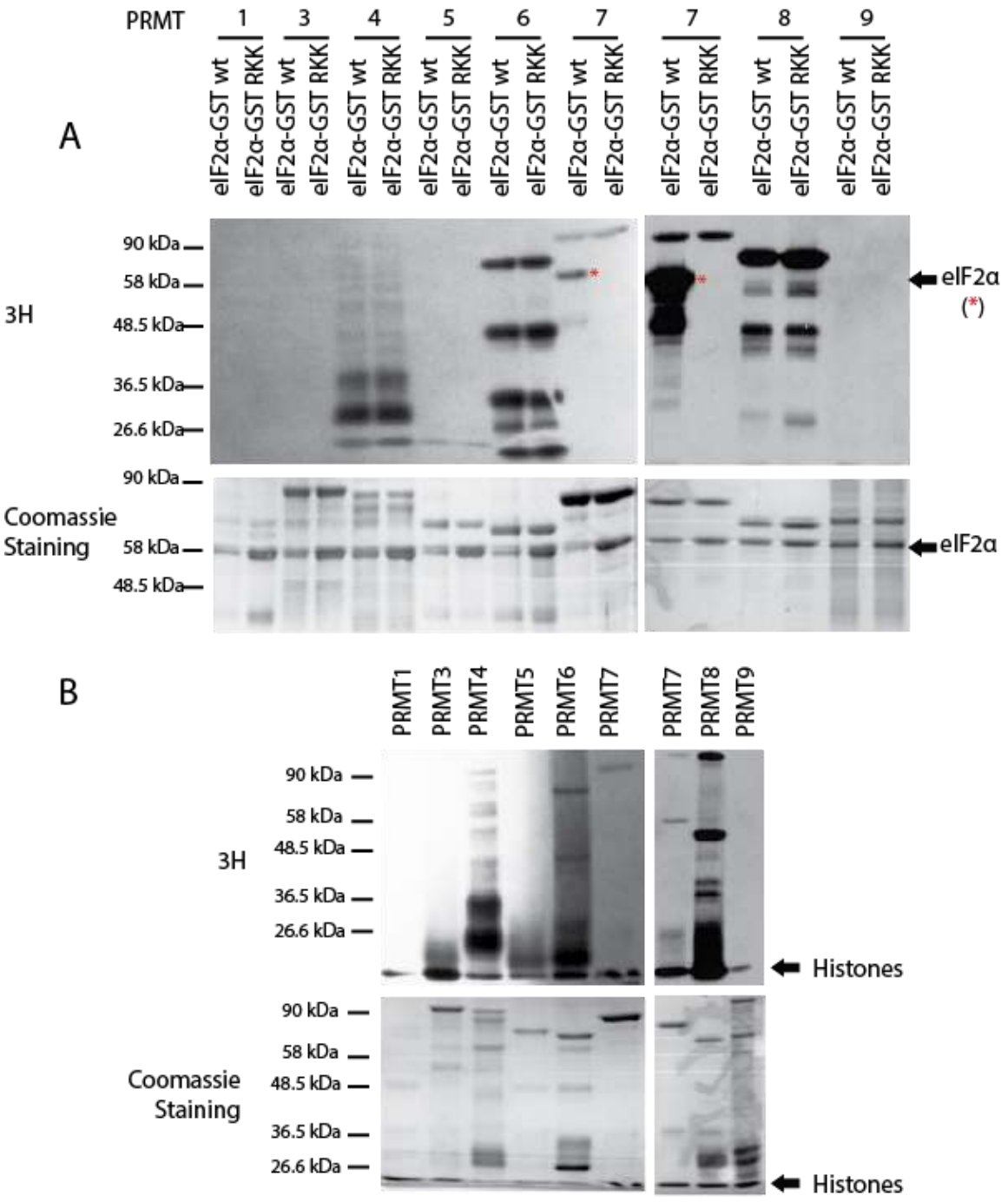

Figure 28: eIF2α is a PRMT7-specific substrate
(A) Autoradiography-based *in vitro* methylation assay using ^{3}H-SAM as a methyl-donor, PRMTs 1, 3, 4, 5, 6, 7, 8, and 9 as the enzyme, and eIF2α as a substrate (both wild-type and RKK mutant). Experiments revealed that eIF2α is a PRMT7-specific substrate (asterisks). Auto-methylation of PRMTs 4, 6, 7, and 8 were observed. (B) Methylation of histones was used as a positive control. Auto-methylation was also observed for PRMTs 4, 6, 7, and 8.

We next sought to determine whether PRMT7 was capable of methylating eIF2α *in vivo*. MDA-MB-231 cell lines expressing either wild-type eIF2α-mGFP or KRR and RRK mutants were used for methylation assays in the presence of translation inhibitors (cycloheximide/chloramphenicol) to ensure that labelling was due to post-translational methylation and not via direct incorporation of ^{3}H-methionine through protein synthesis (Figure 29A). To confirm that translation was indeed inhibited, metabolic labelling assays in MDA-MB-231 cells using ^{35}S incorporation were employed with or without the use of translation inhibitors. As expected, no incorporation of ^{35}S was observed in cells treated with the inhibitors (Figure 29B). The RRK mutant was used as the experimental mutant as a loss of methylation was observed *in vitro*; KRR was used as a negative control as no changes were observed *in vitro*. An additional cell line expressing wild-type eIF2α-mGFP with a knockdown in PRMT7 was also used to determine if PRMT7 is indeed the enzyme responsible for the methylation of eIF2α *in vivo*. Apparent by the decrease in ^{3}H signal compared to the amount immunoprecipitated (Coomassie staining), we observed a 37% decrease in methylation of wild-type eIF2α-mGFP in the PRMT7-knockdown cell line and a 62% decrease in the RRK mutant when compared to the wild-type eIF2α-mGFP cell line. However, no changes were observed in the KRR mutant compared to wild-type eIF2α-mGFP (Figure 29C, D). These findings demonstrate that PRMT7 methylates eIF2α both *in vitro* and *in vivo* and that R^{54} within the RXR motif is important for its methylation.

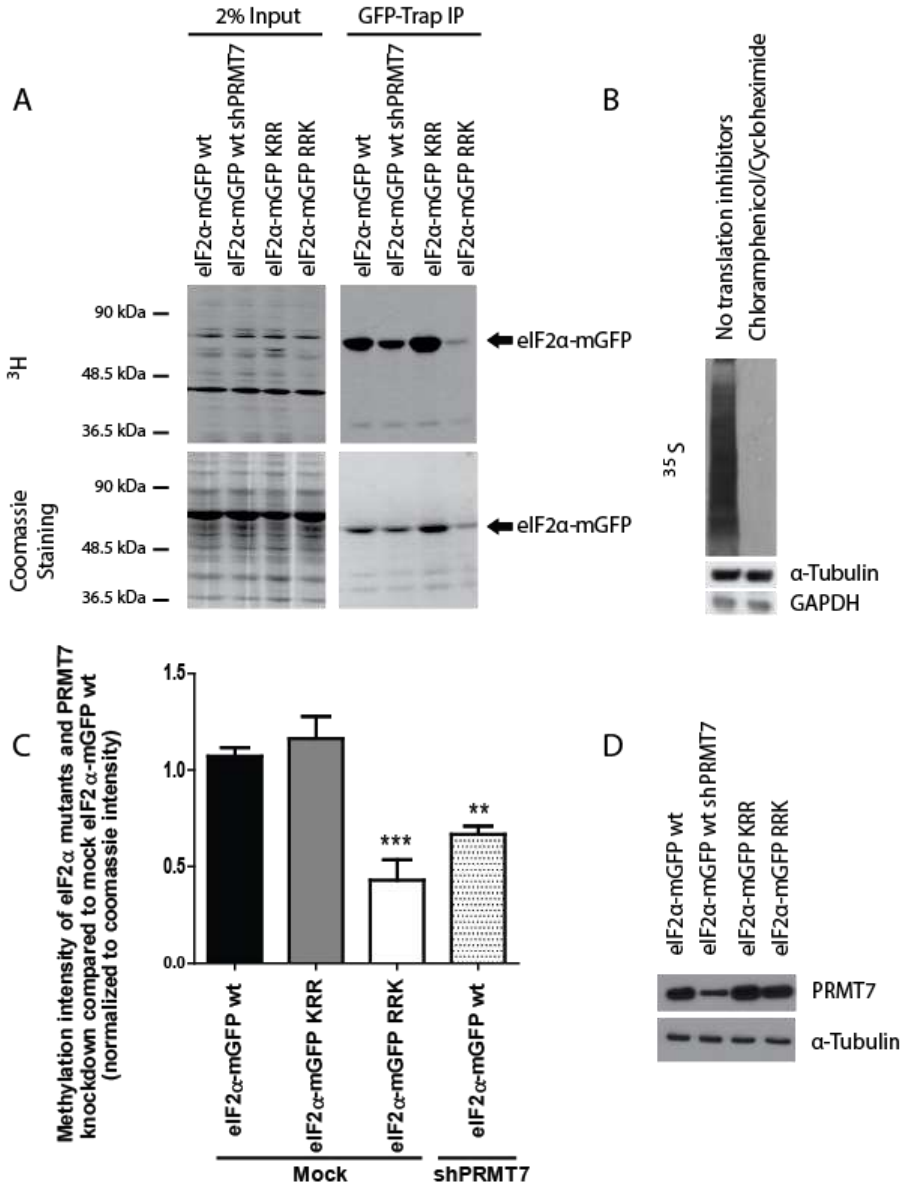

Figure 29: PRMT7 methylates eIF2α in vivo

(A) Autoradiography-based *in vivo* methylation assay using ^{3}H-methionine in MDA-MB-231 cell lines expressing either wild-type, KRR, or RRK eIF2α-mGFP. A PRMT7-knockdown cell line expressing wild-type eIF2α-mGFP was also used. (B) Autoradiography blot using ^{35}S incorporation displaying efficiency of translation inhibitors used in *in vivo* methylation assays. (C) Quantification of the methylation status of eIF2α was calculated in mutant cells lines as well as PRMT7-depleted cells and compared to mock eIF2α-mGFP wild-type cells. Methylation intensity was also normalized to Coomassie staining. A significant decrease in methylation of eIF2α was observed in the RRK mutant as well as in the PRMT7-knockdown cell line. No change was observed in the KRR mutant; data are presented as mean ± SEM for n=5, **p=0.002, ***p=0.001 (ANOVA). (D) Western blot depicting knockdown of PRMT7 in wild-type eIF2α-mGFP cell line.

3.2.3 Explore the mechanisms and downstream effects on breast cancer cells as a result of the PRMT7-eIF2α protein interaction

Since the site of methylation of eIF2α was found to be adjacent to the S^{51} residue, we anticipated a potential interplay between eIF2α phosphorylation and methylation. We first looked at the effect on S^{51} phosphorylation upon knockdown of PRMT7. Using the widely used and well established oxidative stressor, sodium arsenite (AsNaO2), we observed a 60% decrease in eIF2α phosphorylation in PRMT7-knockdown cells which was apparent via Western blot (Figure 30A) and confirmed by quantification (Figure 30B). Accordingly, we observed a 1.7-fold increase in wild-type, eIF2α-mGFP phosphorylation when over-expressing PRMT7-Myc under stressed conditions (Figure 30C, D). Lastly, we looked at the phosphorylation status of the wild-type, KRR, and RRK eIF2α-mGFP mutants upon exposure to oxidative stress (sodium arsenite). As shown in the western blots, only wild-type and KRR eIF2α were phosphorylated upon cellular stress (Figure 30E). The noted changes in eIF2α phosphorylation was not due to alterations in PRMT7 protein expression since within a time frame of one hour, the protein level of PRMT7 remained constant in cells under oxidative stress (Figure 30F). Taken together, these results indicate that arginine methylation of eIF2α (likely at R^{54}) by PRMT7 could be a prerequisite for stress-induced phosphorylation at S^{51}.

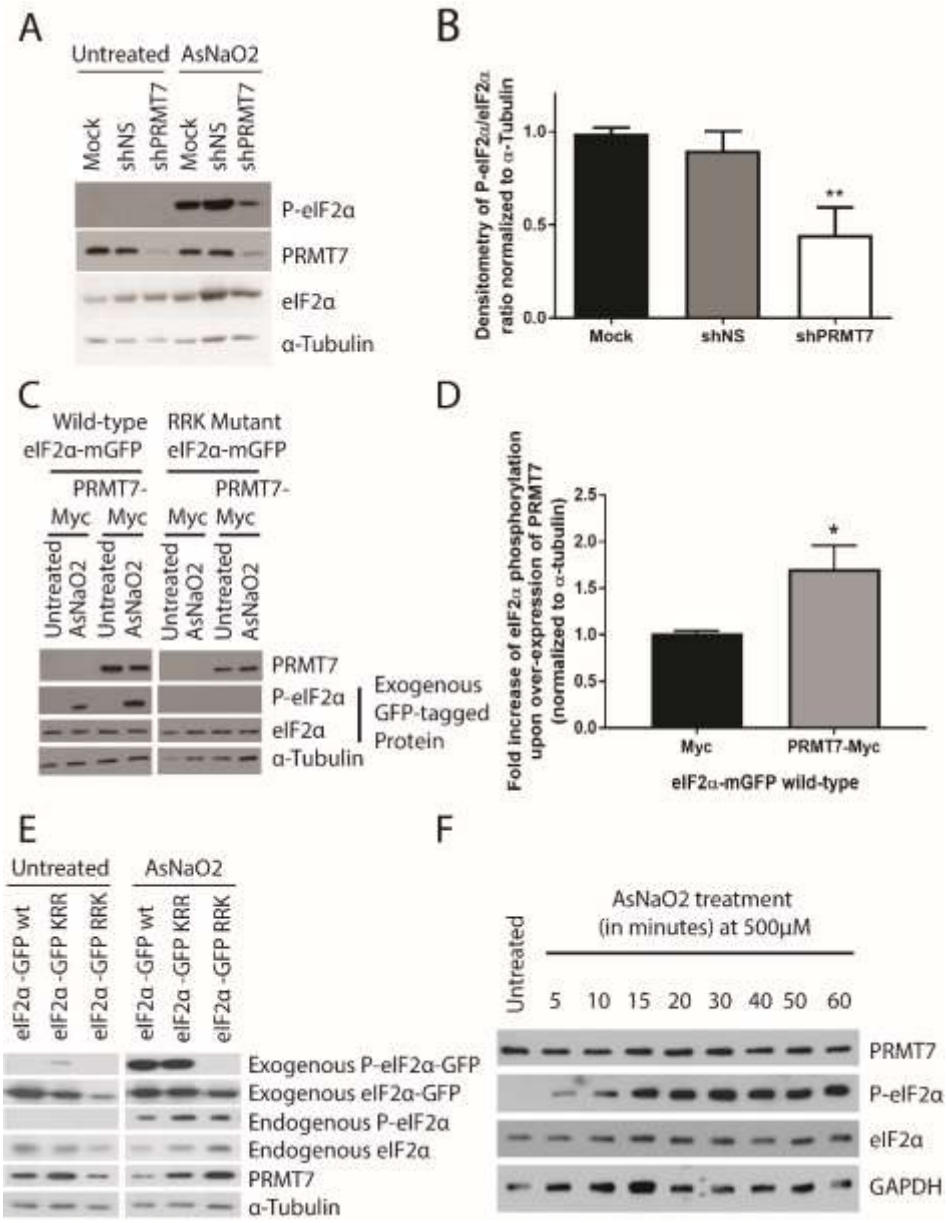

Figure 30: Interplay between eIF2α methylation and phosphorylation
(A) Phosphorylation of eIF2α decreased upon knockdown of PRMT7 as shown in the Western blot in MDA-MB-231 cells treated with 500μM AsNaO2 for 30 minutes and (B) quantification (data are presented as mean ± SEM for n=5, **p=0.01, ANOVA). (C) Representative Western blot depicts increase in eIF2α phosphorylation (only in wild-type and not RRK mutant MDA-MB-231 cells) upon over-expression of PRMT7-Myc and (D) its quantification (data are presented as mean ± SEM for n=5, *p=0.05, t-test). (E) Western blots depicting phosphorylation of wild type and KRR mutant eIF2α upon treatment with sodium arsenite for 30 minutes at 500 μM within MDA-MB-231 cells (eIF2α and P-eIF2α antibodies used). Phosphorylation is absent in the RRK mutant. (F) Western blot depicting no changes in PRMT7 expression upon exposure to at 500μM sodium arsenite from 5 minutes to one hour within MDA-MB-231 cells.

We further looked at endogenous mono-methylation levels of eIF2α under stressed conditions. For these experiments, we immunoprecipitated GFP and eIF2α-mGFP from untreated and AsNaO2-treated (500μM for 30 minutes) mammalian 293T cells and subsequently probed for monomethylation using an antibody specific for arginine monomethylation. A significant increase in eIF2α monomethylation was observed in AsNaO2 treated cells compared to untreated cells (Figure 31). Furthermore, within the AsNaO2 treated cells, PRMT7 co-immunoprecipitated with eIF2α but not the phosphorylated form of the protein. A reciprocal co-immunoprecipitation experiment further supported the finding that PRMT7 does not interact with P-eIF2α (Figure 32). Moreover, PRMT7 co-immunoprecipitated less efficiently with total eIF2α; this could be due to the majority of the eIF2α pool being phosphorylated rendering the interaction less robust.

To determine if PRMT7 more actively methylates eIF2α upon exposure to stressors, an *in vitro* methylation assay was performed using immunoprecipitated PRMT7-Myc (or Myc as a control) from untreated and AsNaO2-treated MDA-MB-231 cells as the enzyme for the reaction and wild-type eIF2α-GST as a substrate. Purified PRMT7 with either GST or eIF2α-GST as substrates were utilized as negative and positive controls, respectively, for the methylation assays. Strikingly, PRMT7-Myc immunoprecipitated from AsNaO2-treated cells more actively methylated eIF2α-GST by 2-fold (Figure 33A, B). As previously observed, these changes are not due to alterations in PRMT7 expression upon exposure to AsNaO2.

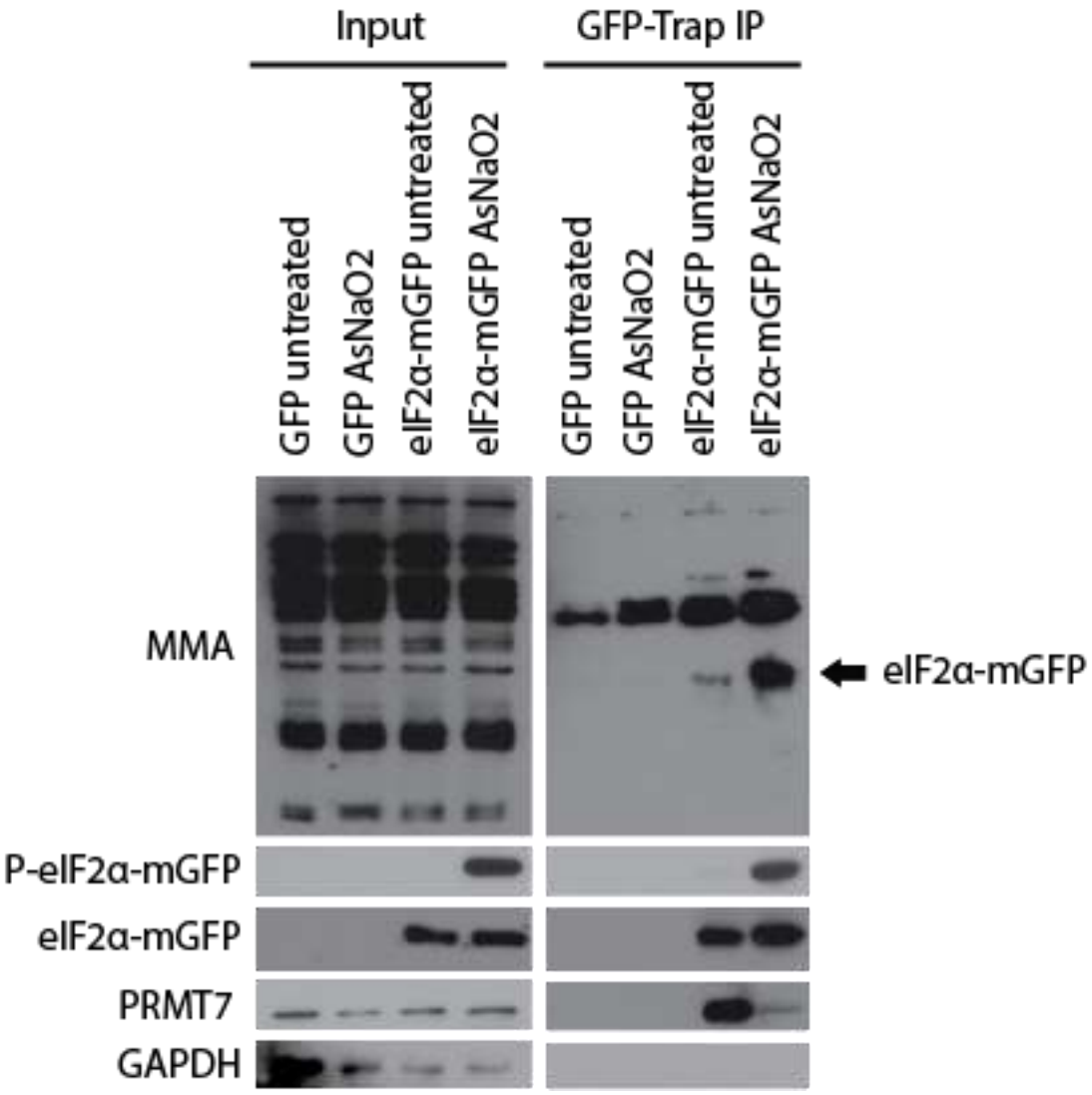

Figure 31: PRMT7 methylates eIF2α under stress conditions
(A) eIF2α-mGFP and GFP (negative control) were immunoprecipitated from untreated and AsNaO2 treated 293T cells (500µM for 30 minutes) and subsequent western blotting was performed. Western blot depicts a significant increase in eIF2α monomethylation within AsNaO2 treated cells. Furthermore, PRMT7 barely interacts with strongly monomethylated/phosphorylated eIF2α-mGFP.

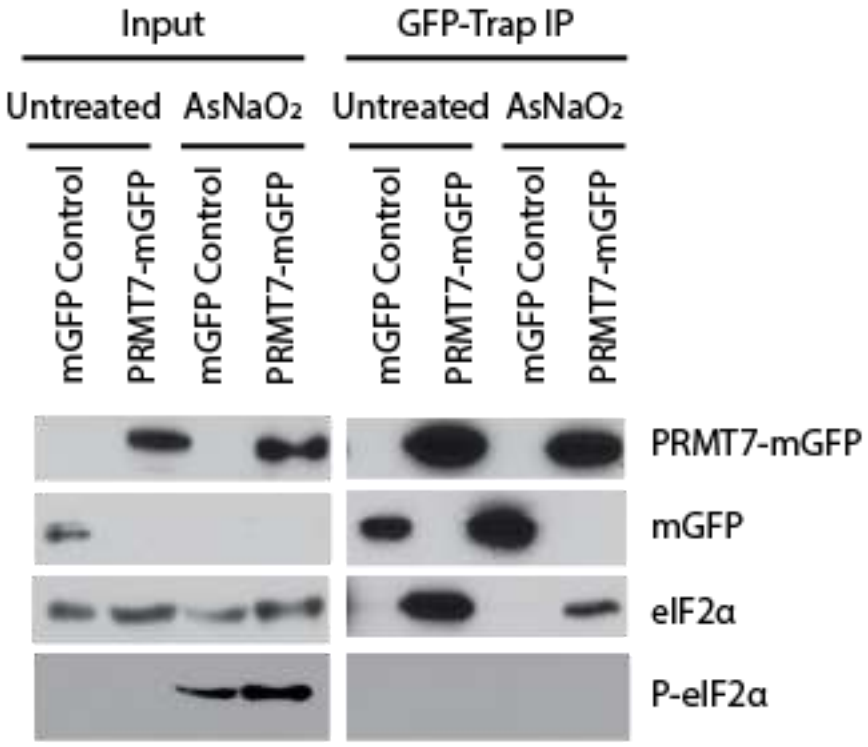

Figure 32: PRMT7 does not interact with phosphorylated eIF2α
Co-immunoprecipitation of PRMT7 from MCF7 breast cancer cells under stressed (sodium arsenite, 500µM, 30 minutes) and unstressed conditions shows that PRMT7 binds more strongly to eIF2α under unstressed conditions. Moreover, PRMT7 is incapable of binding to P-eIF2α.

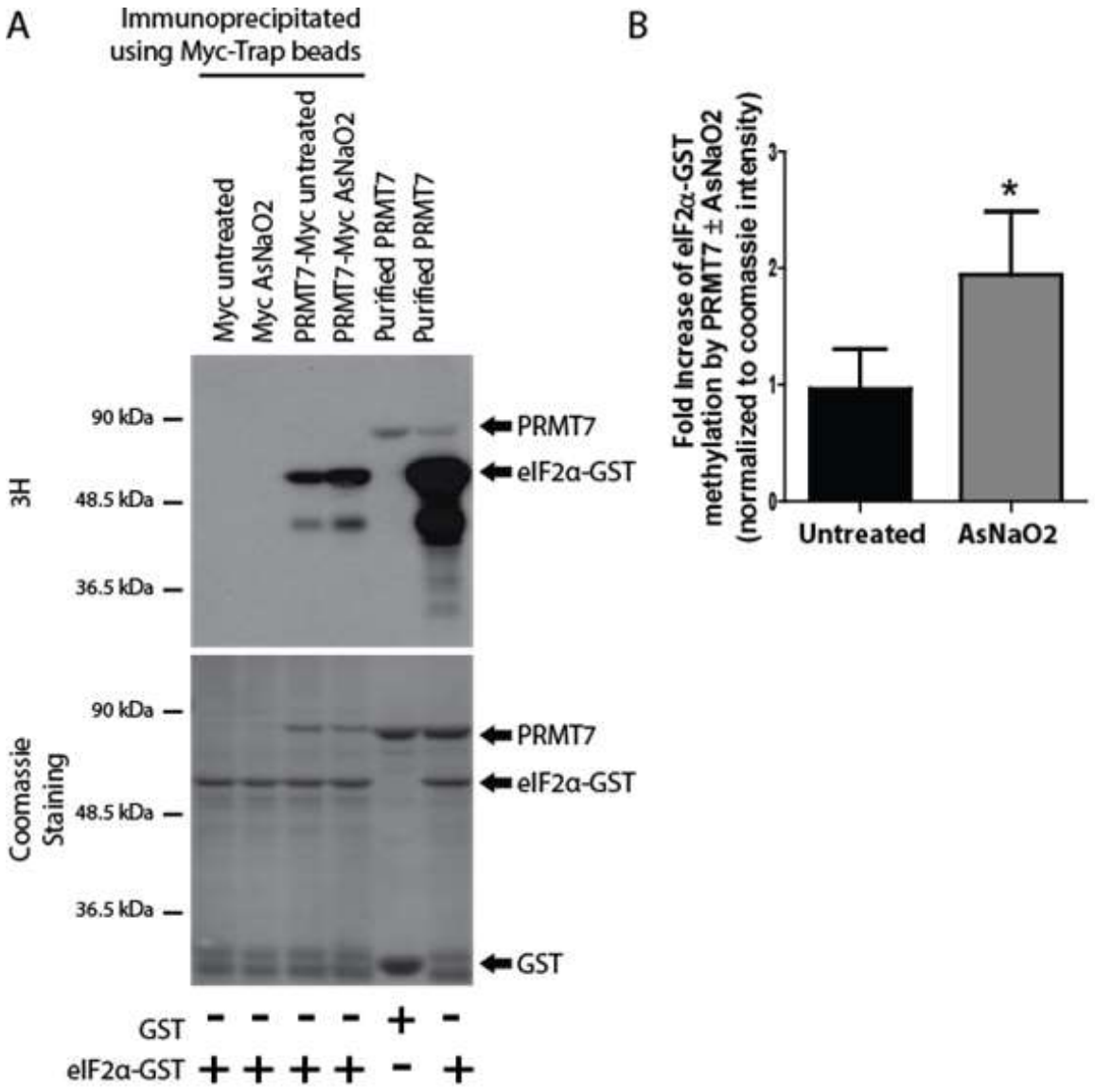

Figure 33: Under stress, PRMT7 is more active, methylating eIF2α to a higher degree. (A) Autoradiography-based *in vitro* methylation assay using ^{3}H-SAM as methyl-donor, immunoprecipitated PRMT7 from MDA-MB-231 cells untreated or treated with AsNaO2, and wild-type eIF2α-GST as a substrate. Immunoprecipiated Myc was used as a negative control. As a positive control, purified PRMT7 with either GST or wild-type eIF2α-GST was used. (B) Quantification of the methylation status of eIF2α was calculated in the AsNaO2 treated cell line. Methylation intensity was also normalized to Coomassie staining. A significant 2-fold increase in methylation of eIF2α was observed in AsNaO2-treated cells; data are presented as mean ± SEM for n=5, *p=0.02, t-test.

Geng and colleagues have shown that PRMT7 undergoes automethylation and that this MMA mark is critical for enhancing its tumourigenic potential in breast cancer (Geng et al., 2017). Thus, we performed immunoprecipitation experiments to determine whether PRMT7 automethylation status increases upon cell exposure to sodium arsenite. Strikingly, we observed the opposite: with a significant decrease in PRMT7 automethylation when cells were exposed to oxidative stress (Figure 34). However, these differing findings could be due to cell type, cell stress, or time course.

We next wanted to explore the downstream functional role of the PRMT7-eIF2α interaction. Since there exists an interplay between eIF2α arginine methylation and serine phosphorylation, we decided to explore the consequences of PRMT7 modulation on the stress response, specifically stress granule formation as it is an established downstream outcome of S^{51} phosphorylation of eIF2α. First, we employed immunofluorescence experiments to determine whether PRMT7 co-localizes with stress granule markers G3BP1, FMRP, and TIA-1. Although not always present, we did note partial co-localization of PRMT7 with both G3BP1 and FMRP (Figure 35 and 36, respectively). We additionally used TIA-1 as another stress granule marker and noted very limited co-localization (Figure 37).

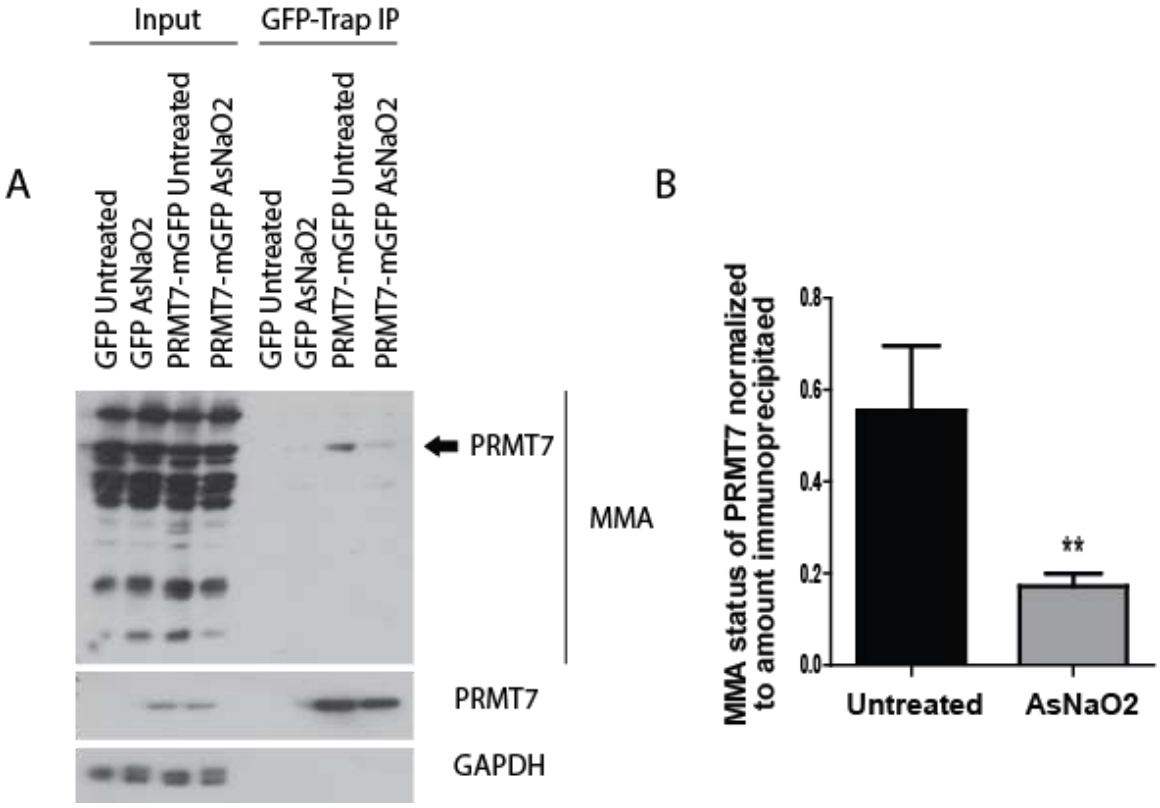

Figure 34: PRMT7 automethylation is decreased when cells are exposed to cellular stress

(A) Immunoprecipitation experiment in MDA-MB-231 cells showing decrease in monomethylation of PRMT7 when cells are exposed to AsNaO2 (500µM for 30 minutes). (B) Quantification shows a significant decrease in PRMT7 monomethylation upon exposure to AsNaO2 (n=3, **p=0.0012).

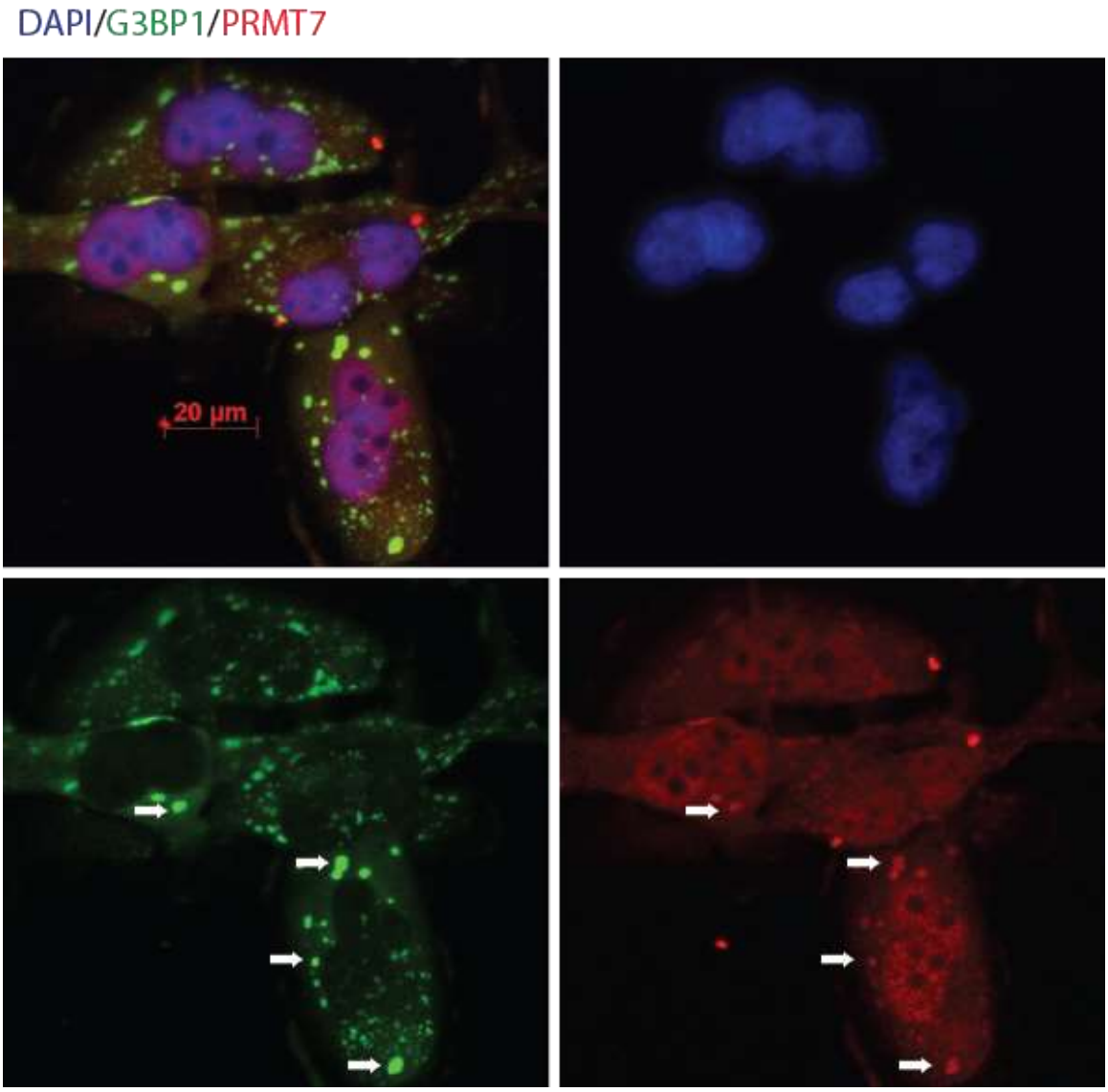

Figure 35: PRMT7 co-localizes with stress granule marker G3BP1
Representative immunofluorescent image of MDA-MB-231 cells depicting partial co-localization (white arrows) of PRMT7 (red) with stress granule marker G3BP1 (green) when cells were exposed to sodium arsenite at 500µM for 30 minutes. DAPI staining was used to indicate the nuclei of cells. Scale bar 20µm.

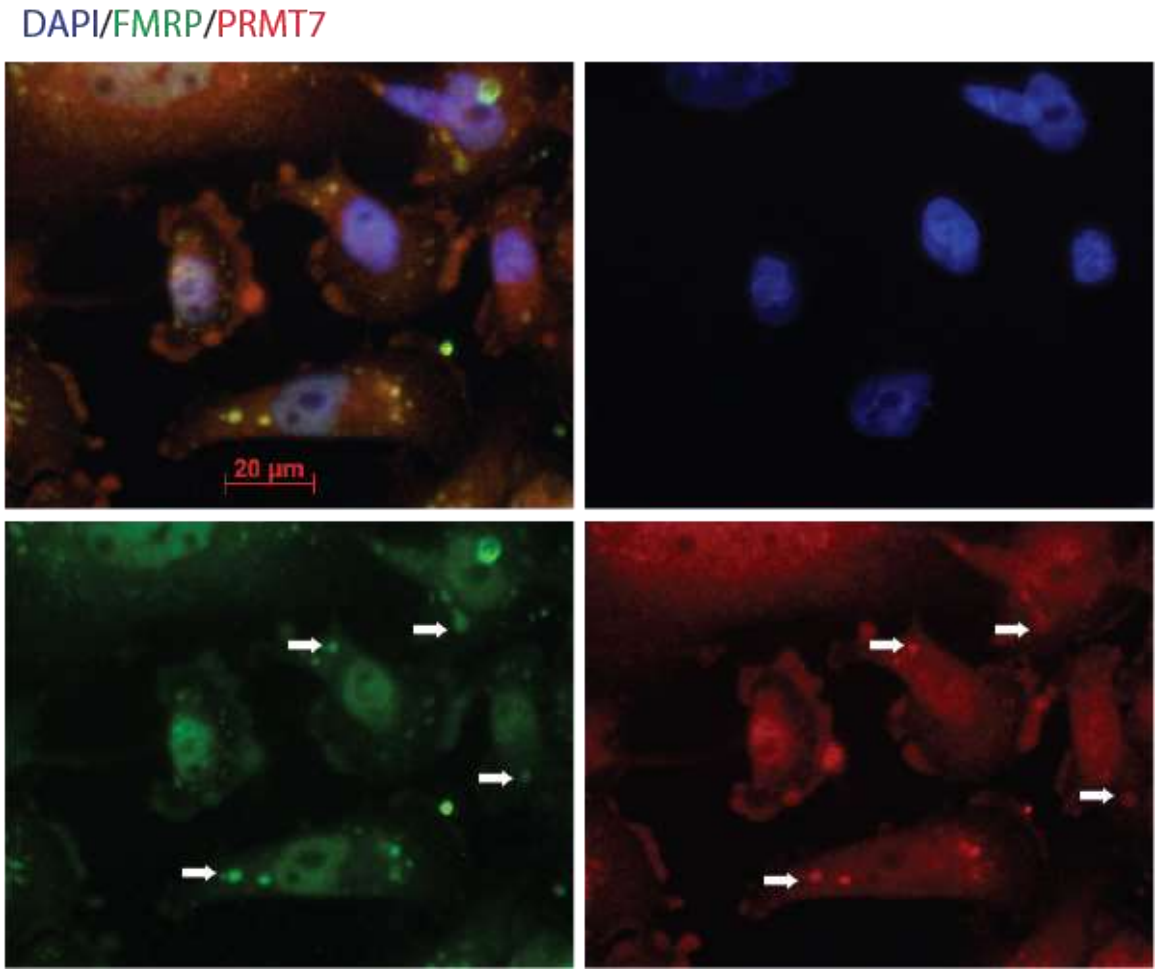

Figure 36: PRMT7 co-localizes with stress granule marker FMRP
Representative immunofluorescent image of MDA-MB-231 cells depicting partial co-localization (white arrows) of PRMT7 (red) with stress granule marker FMRP (green) when cells were exposed to sodium arsenite at 500µM for 30 minutes. DAPI staining was used to indicate the nuclei of cells. Scale bar 20µm.

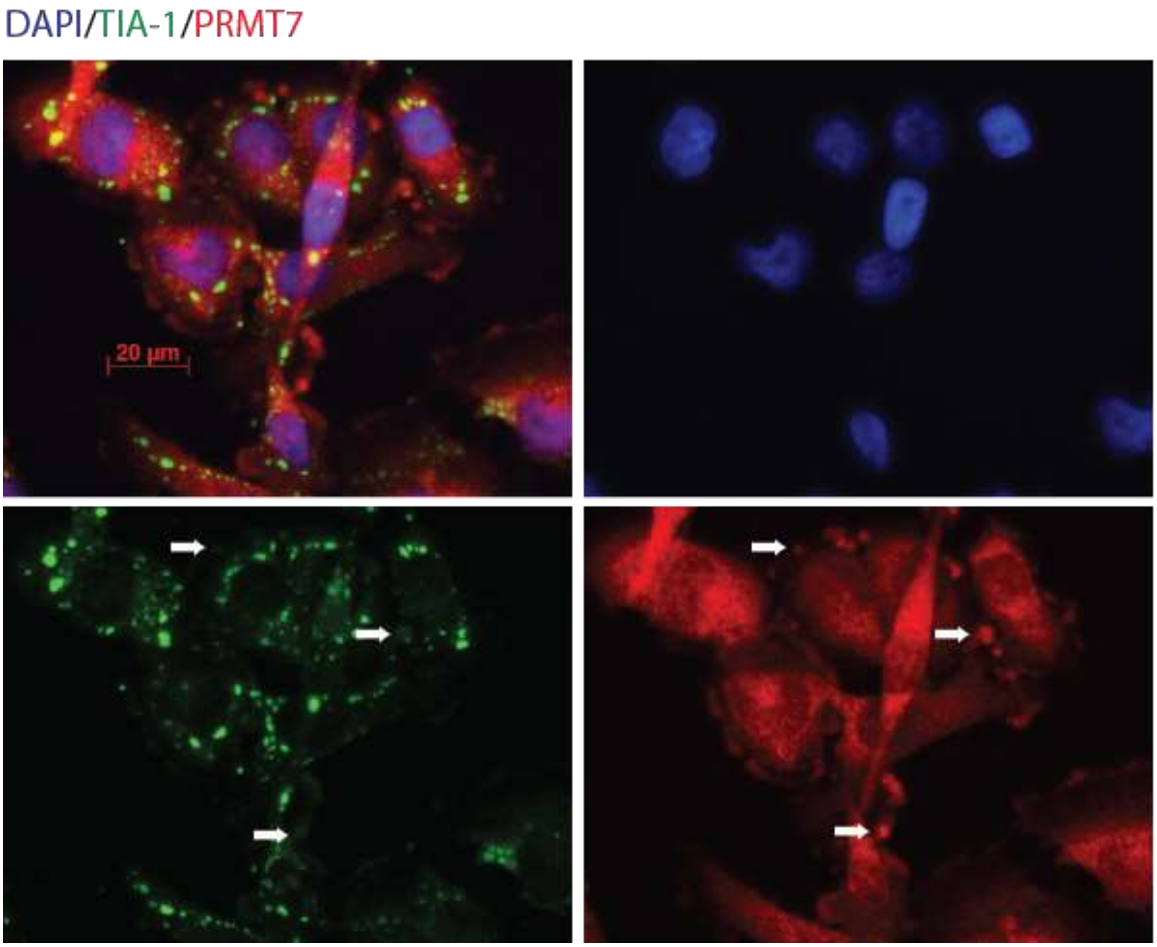

Figure 37: PRMT7 slightly co-localizes with stress granule marker TIA-1
Representative immunofluorescent image of MDA-MB-231 cells depicting partial co-localization (white arrows) of PRMT7 (red) with stress granule marker TIA-1 (green) when cells were exposed to sodium arsenite at 500µM for 30 minutes. DAPI staining was used to indicate the nuclei of cells. Scale bar 20µm.

Next, we sought to determine whether PRMT7 affects stress granule formation. Control and two independent PRMT7-knockdown cell lines were treated with two eIF2α-dependent stressors (AsNaO2 and thapsigargin) as well as an eIF2α-independent stressor rocaglamide A (activates stress granules via eIF4A). Strikingly, we observed an 80-90% reduction in the percentage of cells exhibiting stress granules upon 90% knockdown of PRMT7 compared to control MDA-MB-231 cells when using eIF2α-dependent stressors (Figure 38A, B, C). In contrast, PRMT7 knockdown had no effect on stress granule formation when cells were treated with an eIF2α-independent stressor (Figure 38A, D). These findings suggest that PRMT7 is required for the proper formation of stress granules upon exposure in an eIF2α-dependent cellular stress fashion.

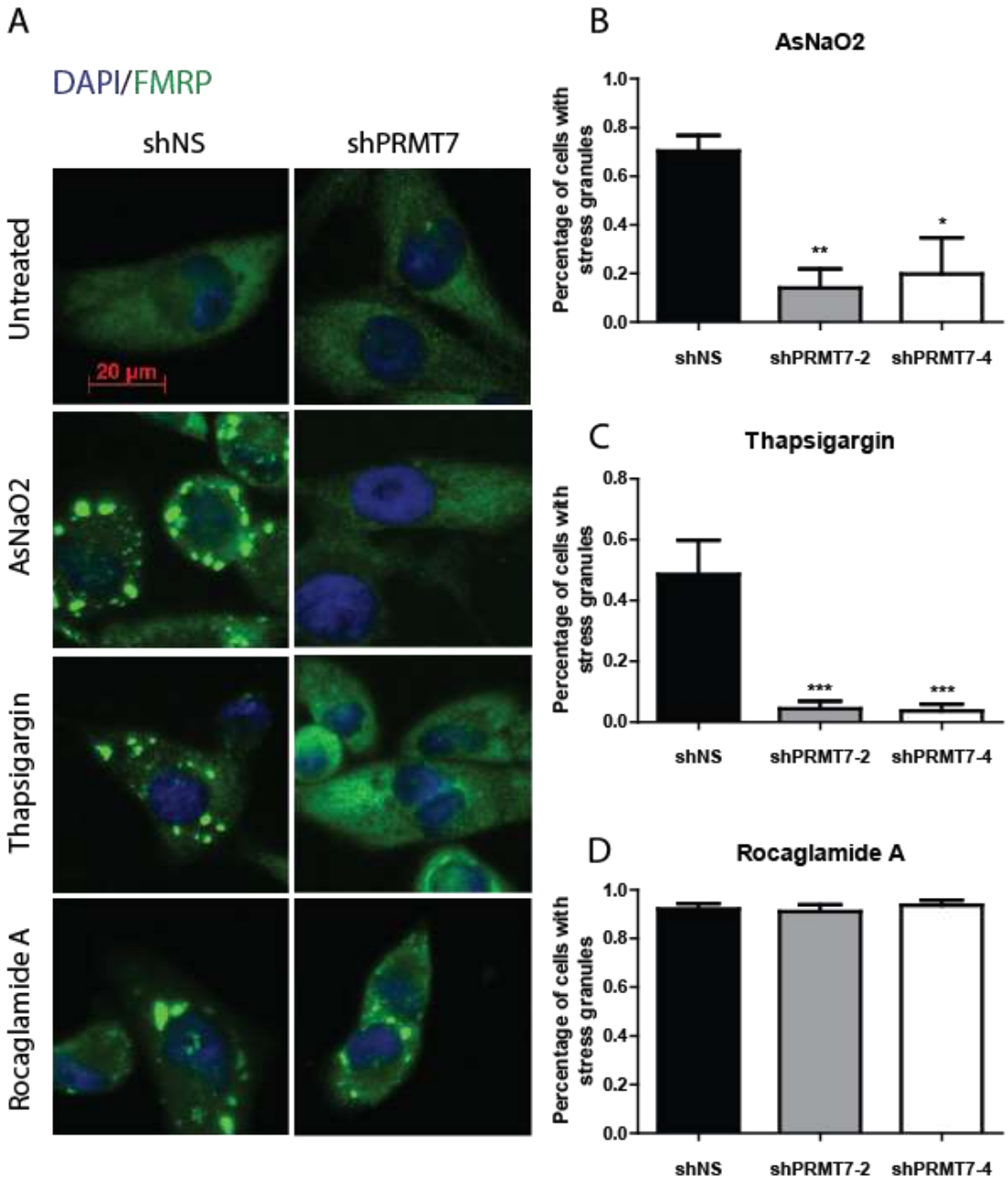

Figure 38: PRMT7 expression correlates with stress granule formation
(A) Representative immunofluorescent images of MDA-MB-231 cells depicting decreased stress granule formation upon knockdown of PRMT7 when exposed to AsNaO2 (500µM for 30 minutes) and thapsigargin (10µM for 2 hour). No change was observed when cells were treated with rocaglamide A (2µM for 2 hours). FMRP (green) was used as a stress granule marker. Scale bar 20µm. (B) Quantitation of stress granules for n=5 experiments in triplicate when treated with AsNaO2; data are presented as mean ± SEM, *p=0.04, **p=0.005 (ANOVA). (C) Similar quantitation was performed when treating with thapsigargin, ***p=0.0001 (ANOVA), and (D) rocaglamide A (not significant).

To further explore the mechanism involving PRMT7 and stress granule formation, we utilized wild-type mouse embryonic fibroblast cells (SS MEFs) and $S^{51}A$ MEF cells (AA MEFs) for our immunofluorescence experiments. These cell lines have been previously used in biochemical experiments to pinpoint S^{51} phosphorylation dependent pathways (Kedersha et al., 2005; Mielke et al., 2011; Muaddi et al., 2010). When using an eIF2α-dependent stressor, eIF2α is incapable of being phosphorylated in AA cells, thus, stress granules are not observed. Hence, we expressed wild-type and KRR, RKR, RRK, and RRRIK mutant eIF2α-mGFP in AA cells to try to rescue their inability in forming stress granules. The goal of this experiment was to determine whether the methylation in the RXRXR motif of eIF2α is required to observe stress granule formation. We demonstrated that upon expression of wild-type, RRK, and RRRIK eIF2α-mGFP, a complete rescue in stress granule formation was observed. Partial rescue was observed in RKR cells and, surprisingly, stress granule formation was completely absent in KRR cells (Figure 39).

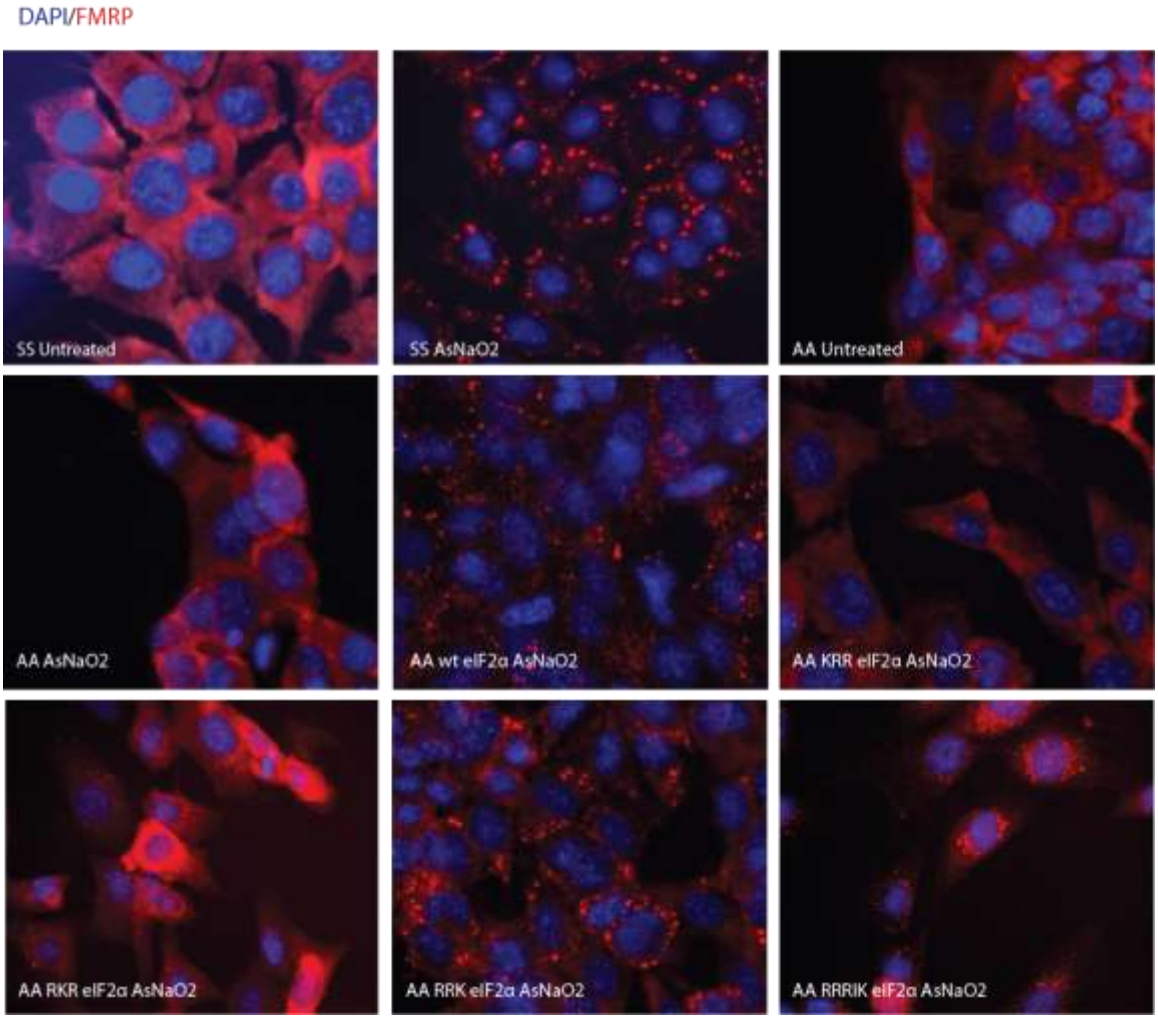

Figure 39: Expression of mutant eIF2α to rescue stress granule defects in AA MEF cells

Representative immunofluorescent images of SS and AA MEF cells in both untreated and AsNaO2 conditions (500µM for 30 minutes). For AA cells, wild-type and mutant eIF2α were expressed and cells were treated with AsNaO2 to examine which mutants rescue the stress granule defects in the cell line. Complete rescue of stress granules were observed in wild-type, RRK, and RRRIK cells. Partial rescue was observed in RKR cells. KRR cells did not rescue stress granule formation. FMRP was used as a marker for stress granules and DAPI for DNA staining (n=3).

Since eIF2α is first and foremost a translation initiation factor, we next wanted to determine whether PRMT7 regulates protein translation. Since PRMT7 both co-fractionated and interacted with eIF2α within the pre-translational complex fractions of cells, we sought to determine whether modulating PRMT7 protein levels would affect the polyribosome profiles of MDA-MB-231 cells. We efficiently knocked-down PRMT7 protein levels using a lentiviral-driven shRNA expression system, as previously described. However, upon knockdown of PRMT7, no drastic changes in the ribosomal profiles were observed (Figure 40A, C). Similarly, using MCF7 breast cancer cell lines, alterations in the polyribosome profiles were very minimal (Figure 40B, C). However, upon quantification of the polysomal to pre-translational complex fractions, we did note a 39% decrease in this ratio in MDA-MB-231 cells and 32% in MCF7 cells (Figure 41). This suggests that although the results are not strikingly obvious, a slight alteration in translation is occurring in cells deficient of PRMT7 protein expression – further supporting the importance of PRMT7 in protein synthesis.

Accordingly, as the alterations were very subtle, it could be possible that only a subset of mRNAs are finely regulated by PRMT7 not visible by drastic changes in polyribosome profiles. To further explore PRMT7's regulatory role in protein synthesis, metabolic labelling assays using ^{35}S-labelled methionine and cysteine were performed. For these experiments, highly metabolically active MDA-MB-231 cells with a knockdown in PRMT7 were used to compare global translation rates with shNS control cells. Additionally, cells treated with cycloheximide were used as a negative control. We noted that upon knockdown of PRMT7 (shPRMT7), a 56% decrease in global translation was

observed (Figure 42A, B). Experiments using puromycylation showed similar results (Figure 42C).

To further explore the importance of S^{51} phosphorylation and translation regulation in the absence of PRMT7, we performed the ^{35}S metabolic assay using SS and AA MEF cells. In untreated conditions, knockdown of PRMT7 resulted in a significant decrease in ^{35}S incorporation similar to MDA-MB-231 cells. A 49% decrease was observed in SS MEF cells and 46% decrease in AA MEF cells (Figure 42D). Interestingly, when cells were treated with AsNaO2 for 30 minutes, a 48% decrease in protein synthesis was observed in SS MEF cells but no changes were observed in the AA MEF cells (Figure 42E). Thus, there could be eIF2α-independent pathways that compensates for the loss of translation under stressed conditions.

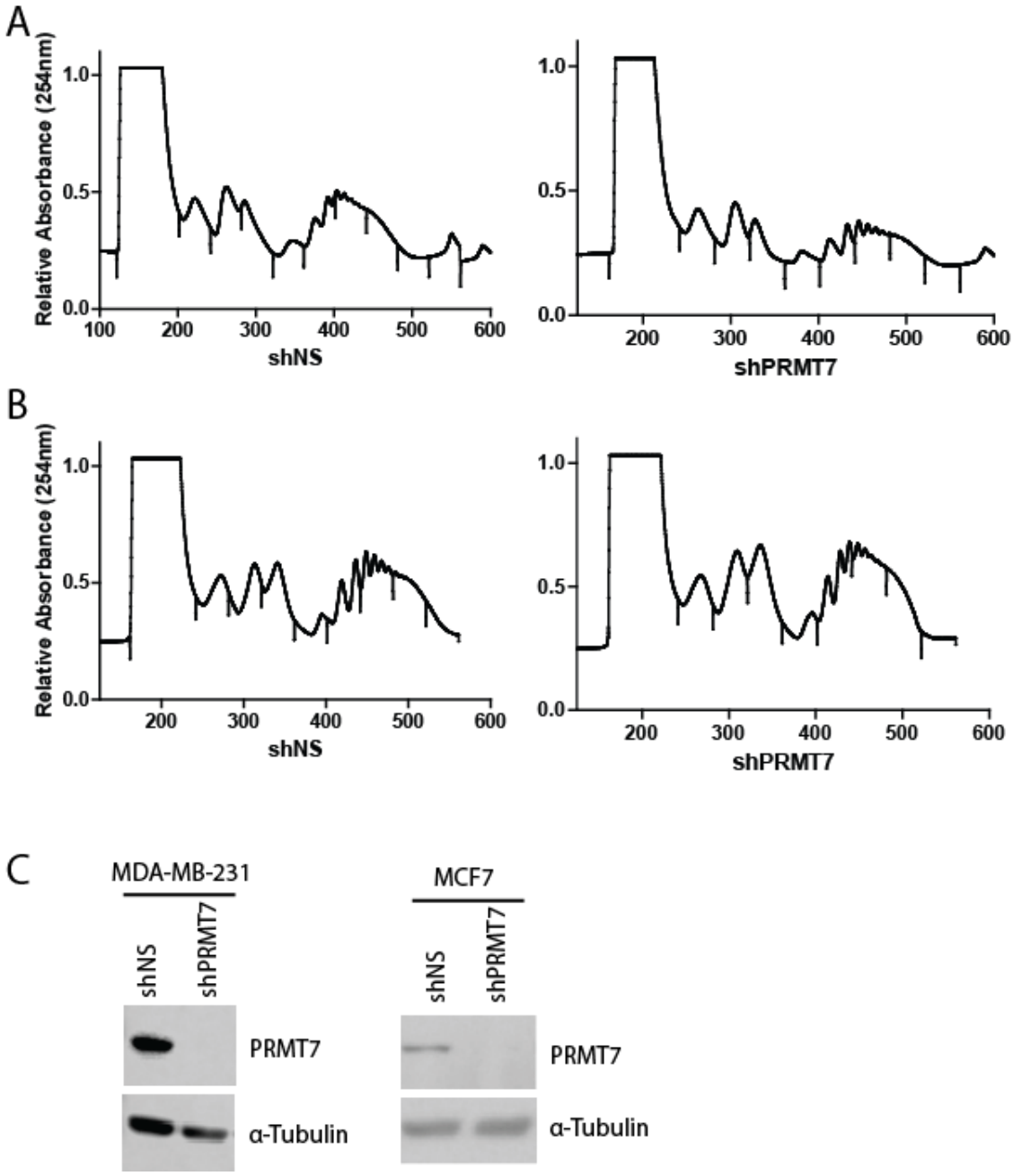

Figure 40: PRMT7 knockdown does not affect polyribosome profile
(A) Polyribosome profiles of control shNS MDA-MB-231 cells compared to PRMT7 knockdown MDA-MB-231 cells. (B) Polyribosome profiles of control shNS MCF7 cells compared to PRMT7 knockdown MCF7 cells. Relative absorbance of RNA was read at 254nm. (C) Western blots depict extent of knockdown in shPRMT7 cell lines compared to shNS control.

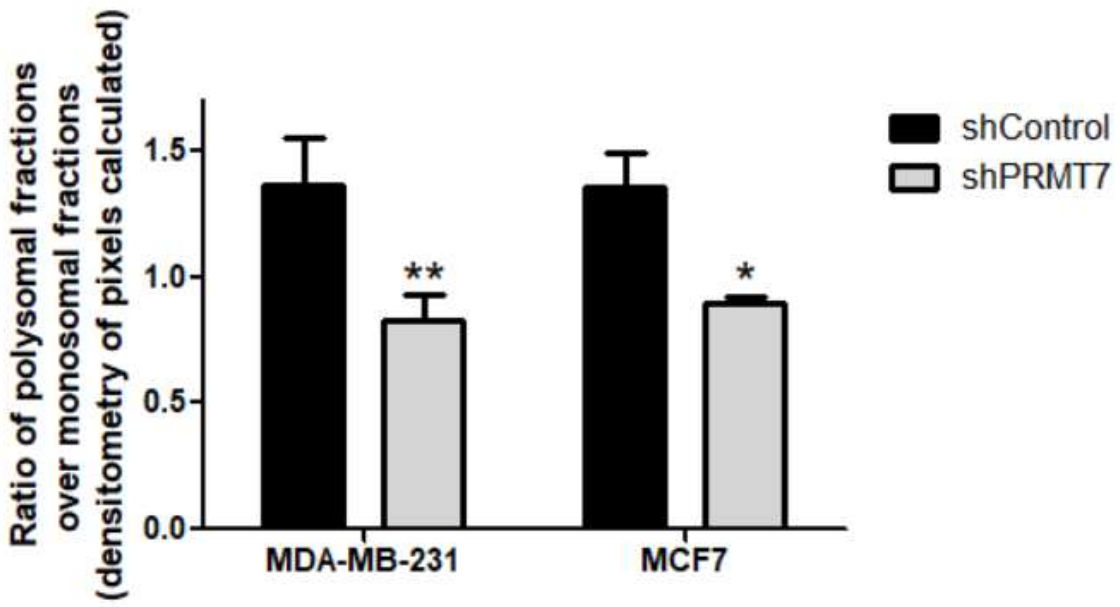

Figure 41: Knockdown of PRMT7 affects polysomal to pre-translational complex ratio

Polyribosome profiling for MDA-MB-231 and MCF7 with a knockdown in PRMT7 was performed and subsequently fractionated. The profiles were then traced and densitometry of polysomal and pre-translational complex fractions were quantified. The ratio of polysomes to pre-translational complex were then computed. As observed by the graph, a knockdown of PRMT7 within MDA-MB-231 cells caused a 36% significant reduction in the polysomal to pre-translational complex ratio and a 32% reduction in MCF7 cells (**p=0.01; *p=0.03, n=3, ANOVA).

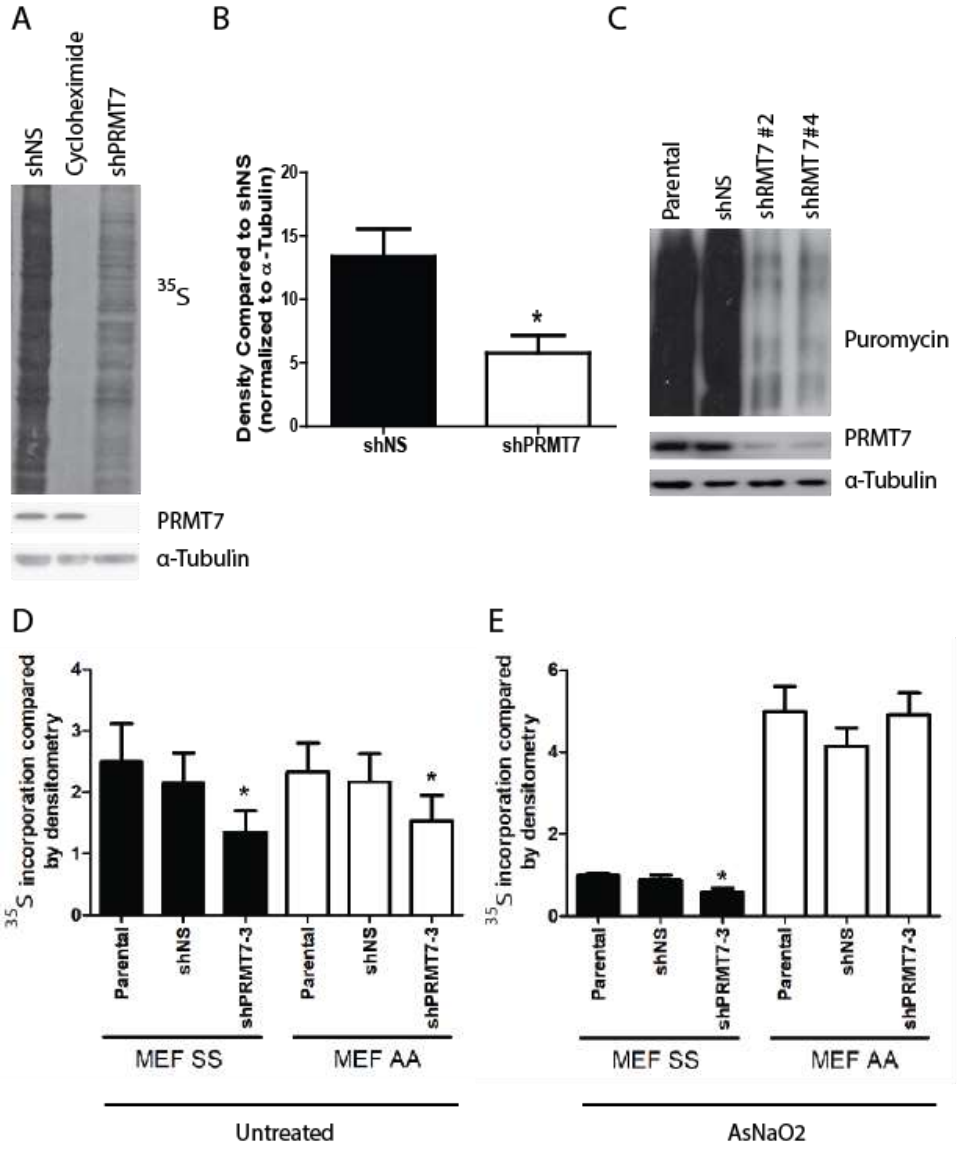

Figure 42: PRMT7 positively regulates translation

(A) Metabolic labelling assay using ^{35}S-labelled methionine and cysteine shows a decrease in ^{35}S-incorporation within PRMT7 knockdown MDA-MB-231. Cells treated with cycloheximide were used as a positive control. (B) Quantification of the metabolic assays comparing shPRMT7 to shNS (data are presented as mean ± SEM for n=6, *p=0.04). (C) Puromycylation of parental, shNS, or shPRMT7 MDA-MB-231 cells shows decreased incorporation of puromycin into the nascent polypeptide chains in PRMT7-knockdown cells compared to both parental and shNS cells. (D) Metabolic labelling assay using ^{35}S-labelled methionine and cysteine within wild-type MEF cells (SS) or S^{51}A mutant MEF cells (AA) shows a decrease in ^{35}S-incorporation in PRMT7 knockdown cells under normal conditions. (E) Under stressed conditions (using sodium arsenite), SS cells still exhibited a decrease in ^{35}S-incorporation, however, AA cells showed no significant change; n=7, $p<0.05$.

We additionally looked at eIF4F complex formation. As previously mentioned, this complex is critical for proper formation of the 48S ribosomal subunit. We therefore wanted to determine whether this complex is also affected via knockdown of PRMT7. Since eIF4A was identified as a potential interacting protein of PRMT7 (Appendix; Table 7), we wanted to determine whether the formation of the eIF4F complex upon knockdown of PRMT7 would be affected. Hence, we performed cap affinity pull-down assays using immobilized γ-aminophenyl-m7GTP beads that mimic the mRNA cap. This experiment precipitates proteins that bind to the mRNA cap. Control and PRMT7 knockdown MDA-MB-231 cells were used to determine if binding of the eIF4F complex to mRNA is affected upon PRMT7 knockdown. Interestingly, we observed a decrease in eIF4G and eIF4A binding to the cap in cells lacking PRMT7 (Figure 43). In fact, eIF4A was completely absent from the cap in the knockdown PRMT7 lysates. Unfortunately, our eIF4E antibody was too dirty to detect bands.

Furthermore, as mentioned in the introduction, eIF2α seems to regulate cell survival. Specifically, the PI3K-Akt survival pathway downstream of P-eIF2α is affected upon knockdown of PRMT7. We saw an 85% decrease in P-Akt (S^{473}) levels but no change in total Akt upon knockdown of PRMT7 (Figure 44). Thus, there seems to be an overarching mechanism responsible for cell survival dependent on P-eIF2α.

Altogether, these results suggest that PRMT7 is a novel regulator of eIF2α-dependent translation and stress granule formation. In terms of stress regulation, we proposed that methylation of eIF2α by PRMT7 may be a prerequisite for phosphorylation for proper stress granule formation to occur upon cellular stress.

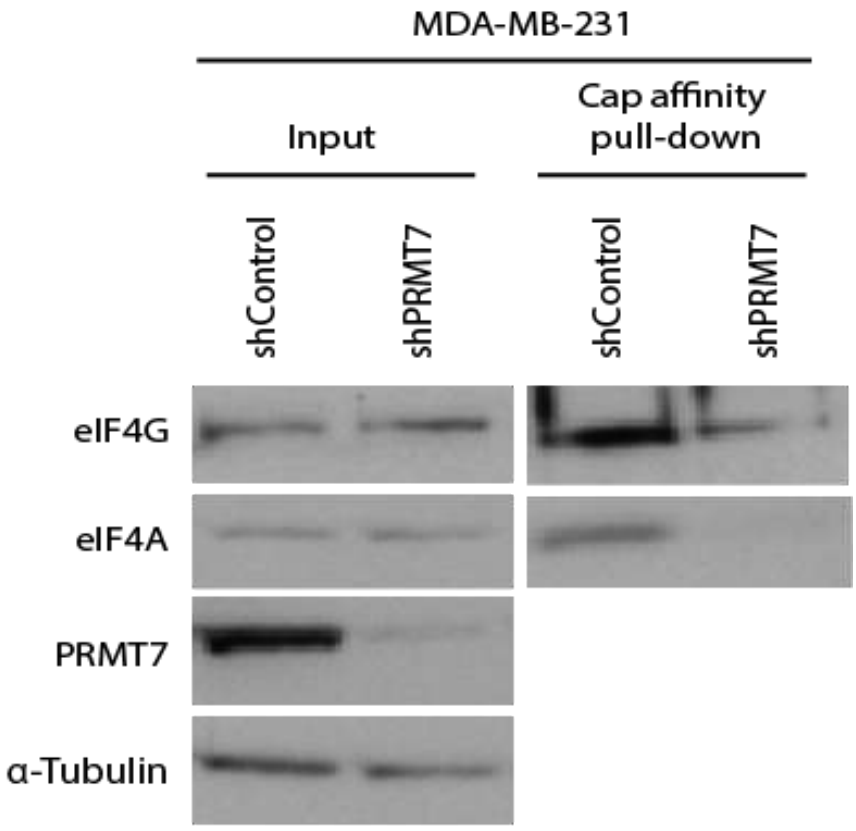

Figure 43: PRMT7 affects the eIF4F complex binding to mRNA cap
Cap affinity pull-down in shControl or shPRMT7 MDA-MB-231 cells using beads mimicking the 5' mRNA cap was employed. A decrease in eIF4G and eIF4A binding to the cap is apparent in knockdown cells. There seems to be a decrease in binding of these factors to the mRNA cap suggesting that PRMT7 may be important for efficient translation via the recruitment of translation factors.

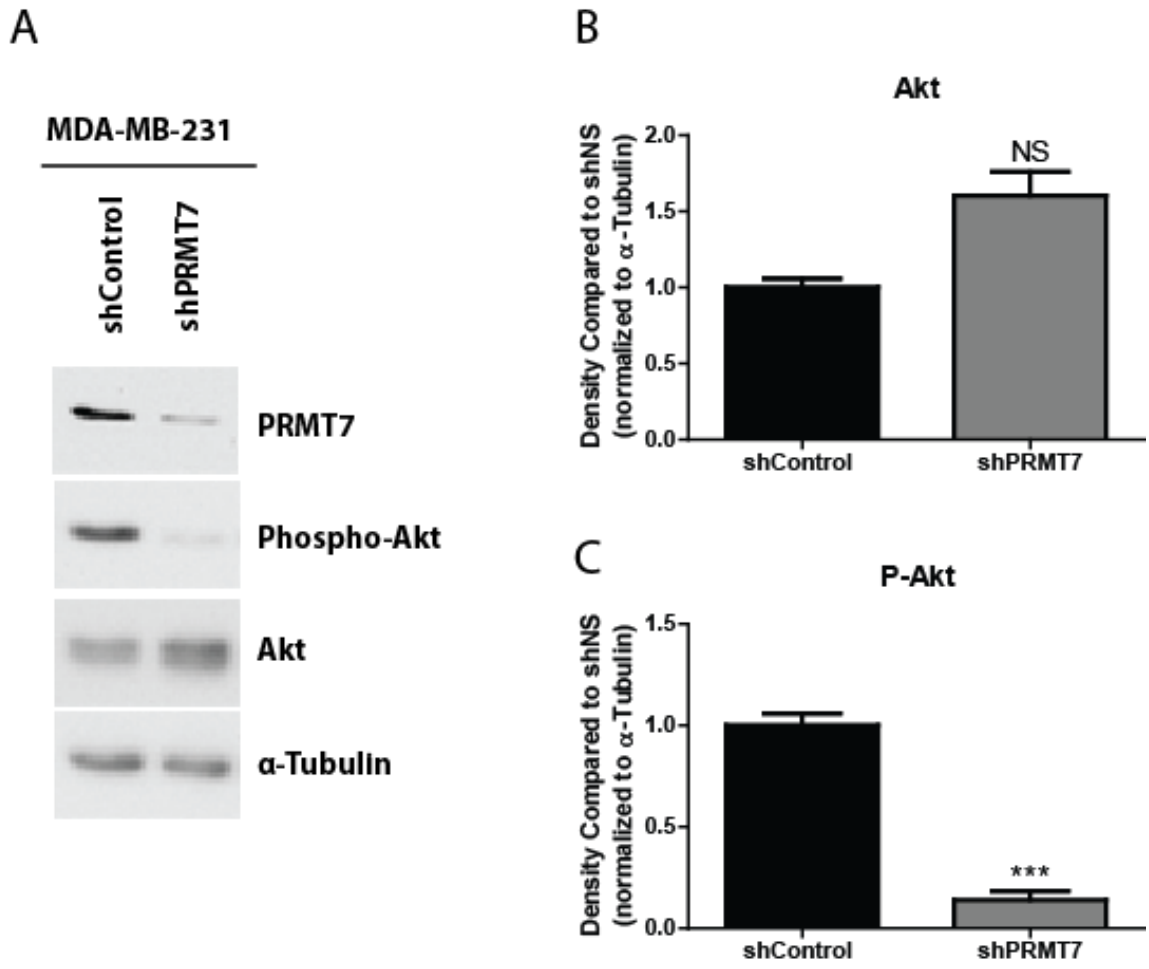

Figure 44: PRMT7 affects phosphorylation of Akt at S473
(A) Representative western blot showing a decrease in phosphorylated Akt levels at S^{473} upon PRMT7 knockdown. (B) Quantification of total Akt levels in shControl MDA-MB-231 cells and PRMT7 knockdown cells show no significant difference. (C) However, there is a significant decrease (>80%) in P-Akt levels upon knockdown of PRMT7 (n=3, p=0.0007).

CHAPTER 4: DISCUSSION AND CONCLUSIONS

4.1 Summary

In this study we have shown that PRMT7 plays a functional role in promoting breast cancer cell invasion, stress granule regulation, and protein translation. Previous studies have associated PRMT7 expression with cellular sensitivity and resistance towards chemotherapeutic drugs (Bleibel et al., 2009; Gros et al., 2003; Karkhanis et al., 2012; Verbiest et al., 2008). Furthermore, a meta-analysis correlated PRMT7 mRNA expression with breast cancer aggressiveness and metastasis (Thomassen et al., 2009). Although mostly correlative, these studies demonstrate the possibility that PRMT7 plays a noteworthy role in promoting breast cancer metastasis and cell survival under stressed conditions such as the use of chemotherapeutic drugs.

Our study adds to the aforementioned work, showing that PRMT7 protein promotes breast cancer cell invasion and metastasis. Mechanistically, we found that PRMT7 induces MMP9 transcription and that this induction could be through epigenetic arginine methylation of histone tails within the promoter region of MMP9. We also observed that PRMT7 ablation affects cellular proliferation, promotes senescence, and induces cellular death. Furthermore, as there is a very limited number of known substrates of PRMT7, we additionally performed mass spectrometry experiments to expand the current knowledge on PRMT7's interactome. We identified 76 interacting proteins which are all listed in the Appendix. Pursuing the eIF2α-PRMT7 interaction, we identified a novel role for PRMT7 in both stress granule regulation and protein translation. In terms of stress granule regulation, we observed an interplay between serine phosphorylation and arginine methylation of eIF2α. We additionally observed the requirement of PRMT7 for stress

granule formation. Furthermore, we noted that protein translation and other survival pathways such as the PI3K/Akt pathway are negatively affected by PRMT7 depletion.

Together, our observations suggest that PRMT7 is a critical player in both basic cellular functions such as cell survival and protein translation as well as in the cellular stress response. Thus, targeting PRMT7 could prove to be beneficial in reducing breast cancer metastasis and tumour cell survival. The use of a cocktail of chemotherapeutic drugs as well as PRMT7 inhibitors could turn out to be efficient in the treatment of breast cancer. Moreover, this study is a stepping stone in further expanding our knowledge on arginine methylation and exploring the implications of this post-translational modification in human disease and cellular mechanisms.

4.2 PRMT7 expression in breast cancer cell lines and tissues

Our immunohistochemical study of PRMT7 protein expression is the first to demonstrate that PRMT7 protein expression is significantly increased in primary breast tumours and lymph node metastases compared to normal breast tissues. PRMT7 expression was mainly localized to the cytoplasm of normal breast epithelial cells and breast tumour cells. This is consistent with the predominantly cytoplasmic localization of PRMT7 that has been established in various transformed cell lines in previous studies (Gros et al., 2003, 2006; Herrmann et al., 2009).

We have shown that a significantly higher number of primary breast tumours and lymph node metastatic disease cases display high expression of PRMT7. Consistent with this observation, established breast cancer cell lines, that are classified as highly invasive, poorly differentiated 'mesenchymal-like' cell lines, expressed significantly higher PRMT7 protein levels compared to normal breast epithelial cells. These results suggest that PRMT7 expression may promote breast cancer tumourigenesis and cell transformation as well. Although our results did not reach statistical significance with our specific sample size, we also noted a slightly higher proportion (76% versus 63%) of Grade III tumour samples exhibiting high PRMT7 expression when compared to the Grade I/II tumour group. Our results suggest that PRMT7 levels are increased at an early stage in breast tumour development where it plays a role in promoting tumourigenesis. Elevated PRMT7 expression is maintained within the tumours potentially contributing to progression of metastatic disease.

Increased expression was observed in cell lines classified as more invasive with a 'mesenchymal-like' morphology (BT549, Hs578T, BT20 and MDA-MB-231) in contrast

to the weakly invasive, 'luminal epithelial-like' cells, MCF7, which expressed PRMT7 protein levels similar to normal MCF10A cells. Interestingly, each of the invasive cell lines examined is characterized genetically as triple negative (ER-, PR-, HER2-), whereas MCF7 cells are hormone receptor positive (ER+, PR+, HER2-) (Kao et al., 2009). Thus these results support the association of increased PRMT7 expression in aggressive triple negative breast cancer cells and that PRMT7 may promote breast cancer tumourigenesis in a non-hormonal manner.

A positive correlation exists between breast cancer invasiveness/aggression and PRMT7 mRNA levels (Thomassen et al., 2009) and now we have shown similar correlations at the protein levels. Thus, as we are detecting higher levels of PRMT7 in TNBC, PRMT7 presents a potential biomarker for the use of non-hormonal therapies against breast cancer. Moreover, PRMT7 could be a predictor of therapeutic options in terms of cellular response towards chemotherapeutic drugs. For instance, if high levels of PRMT7 are detected, then it is reasonable to conclude that camptothecin and bleomycin would be an inefficient therapy since PRMT7 promotes resistance to these compounds (Verbiest et al., 2008). However, cisplatin, mitomycin C, and chlorambucin present possible therapies as PRMT7 promotes sensitivity towards these drugs (Karkhanis et al., 2012). Thus, by evaluating the expression levels of PRMT7, a more efficient and beneficial therapy regimen can be designed.

Our analysis of PRMT7 protein expression in breast cancer cells has also possibly uncovered an additional unique feature of PRMT7: the potential existence of alternative species. The presence of alternative isoforms is not uncommon amongst the PRMTs, as alternatively spliced isoforms have been identified for PRMT1, PRMT2 and CARM1

(Isabelle Goulet et al., 2007; Ohkura, Takahashi, Yaguchi, Nagamura, & Tsukada, 2005; L. Wang et al., 2013; Zhong et al., 2011, 2012). These isoforms potentially have distinct roles in cancer cells (Baldwin, Morettin, & Cote, 2014). We observed two closely migrating bands on Western blots that were detected by PRMT7 antibodies. Intriguingly, we observed differential expression of these PRMT7 species. MCF7 cells only expressed the higher molecular weight band (~82kDa) and Hs578T exclusively expressed the lower molecular weight band (~78kDa). The remaining breast cancer cell lines tested exhibited both bands with the lower band being more intense. The significance of this differential expression is not currently known in human cells. We believe that both these bands represent PRMT7 species because PRMT7-targeted shRNAs are capable of knocking down both species. Originally, in hamster cells, it was found that the PRMT7 gene encoded two proteins, p77 (78kDa) and p82 (82kDa), that were highly homologous, and later designated PRMT7α and β, respectively (Gros et al., 2003, 2006). Several theories exist as to the origin of these two proteins. In Chinese hamster cells, it is thought that these two isoforms are generated by the use of distinct 5' translation initiation codons within the primary transcript, with the PRMT7β isoform containing an additional 37 amino acids at the N-terminus.

In human tissues, only a single PRMT7 transcript was detected (~3.6 kb) and one protein, at 78kDa, was detected in two human cancer cell lines (HeLa and HuH7). This transcript was shown to share the greatest homology to the PRMT7α isoform (Gros et al., 2006; Lee et al., 2005; Miranda et al., 2004). However, the limited subset of cell lines used to conclude this cannot completely rule out the existence of the PRMT7β isoform expression in other human cell types. Furthermore, it is quite possible that the PRMT7β

isoform may only be present in a certain subtype of cells as this isoform may be tissue specific in terms of expression. Secondly, a survey within both NCBI and Ensembl databases predicts the existence of at least 2 alternatively spliced PRMT7 isoforms that can be produced from the human PRMT7 gene. These two isoforms have the same N- and C-terminal regions however one has an in frame deletion of exon 5. Importantly, this may affect methyltransferase activity because it removes the post I domain required for formation of the methyltransferase domain.

Finally, we cannot rule out the possibility that the higher molecular weight band is the result of one or more posttranslational modifications or that proteolytic cleavage is occurring to yield the lower molecular weight band. Furthermore, it could be possible that the lower molecular weight band is the more “tumourigenic” band as it is more highly expressed in the aggressive breast cancer cell lines. Further studies into the precise nature and origin of these species are required in order to determine their nature and specific functional roles in cells. Additionally, it would be interesting to determine whether these isoforms are localized to different cellular compartments in human cells as is that case with hamster cells.

4.3 PRMT7 expression affects cell invasion and metastasis

The association of PRMT7 expression with primary breast tumours and metastatic breast cancer led us to investigate whether PRMT7 directly affects breast cancer cell invasion. Metastasis of the primary tumour to distant sites is the major cause of mortality amongst breast cancer patients (Weigelt, Peterse, & van 't Veer, 2005). Here, we have shown that PRMT7 plays a direct role in promoting human breast cancer cell invasion. Depletion of PRMT7 in highly invasive breast cancer cells, MDA-MB-231 and BT549, caused a significant reduction in the ability of these cells to invade through an extracellular matrix-like barrier *in vitro* but had minimal effects on cell motility. Alternatively, overexpression of PRMT7 in MCF7 cells, a weakly invasive breast cancer cell line, was sufficient to enhance their invasive capability as well as cell motility. The discrepancy in the observed effects on cell motility could be due to different signaling cascades between breast cancer cell lines or differences in the threshold of PRMT7 required to observe an effect on cell motility. Nevertheless, this needs to be further pursued.

To explore the role of PRMT7 in promoting metastasis, we used RNA interference in breast cancer cell lines and evaluated lung metastases using a well-established mouse tail vein injection model. We showed that PRMT7 knockdown in MDA-MB-231 cells significantly reduced their ability to metastasize *in vivo*. Specifically, we observed a significant decrease in lung metastases formed by cells with a knockdown in PRMT7 compared to controls. These findings suggest that reduction of PRMT7 within breast cancer cells can significantly impede cell invasion and metastasis. Importantly, we found that PRMT7's effects on cell invasion are due to an induction in MMP9 expression.

A cancer cell's capacity to invade and metastasize is dependent on its ability to manipulate the tumour microenvironment in which it resides (Kessenbrock et al., 2010). Key molecular mediators of tumour cells that promote cellular invasion are the matrix metalloproteinase family of zinc-dependent endopeptidases (Köhrmann et al., 2009). MMP9 production and secretion by tumour cells is a critical element involved in promoting metastasis (Mehner et al., 2014). MMP9 has been the focus of many studies due to the fact that it degrades Type IV collagen which is an abundant component of the basement membrane of epithelial cell layers. In breast cancer, MMP9 status is an important indicator of breast cancer prognosis (Kato et al., 2002; Pellikainen et al., 2004). MMP9 expression is significantly associated with higher grade breast tumours (grades II and III) (Köhrmann et al., 2009; Li et al., 2004). Elevated levels of MMP9 expression is also associated with shortened relapse-free survival in breast cancer patients and a high rate of distant metastases (Vizoso et al., 2007). Direct targeting of MMP9 expression in invasive breast cancer cells was shown to significantly inhibit cell invasion and metastasis *in vitro* and *in vivo*, respectively (Hallett et al., 2013; Mehner et al., 2014). The activity of MMP9 has also been shown to play a crucial role in breast cancer metastasis to the bone (Nannuru et al., 2010). In an *in vivo* experimental model of bone metastasis, the presence of active MMP9 at the tumour-bone interface was important for bone destruction, a necessary process for tumour formation.

Our assessment of MMP9 expression in invasive breast cancer cells showed that PRMT7 knockdown caused a significant decrease in MMP9 mRNA levels, secreted MMP9 protein amounts, and decreased enzymatic activity. In turn, overexpression of PRMT7 in MCF7 cells resulted in a significant increase in MMP9 expression and invasion. A

comparison of MMP9 enzymatic activity, by gelatin zymography, between MCF10A, MCF7 and MDA-MB-231 cells demonstrated MCF10A and MCF7 possess little or no activity, whereas MDA-MB-231 cells have a high activity levels (X. Wang et al., 2011). This potentially reflects a lower amount of MMP9 protein being produced in MCF10A and MCF7 compared to MDA-MB-231 cells. Importantly, the MMP9 activity from these cell lines directly correlates with the amount of PRMT7 expressed within them and provides additional support for PRMT7 regulation of MMP9 expression. Furthermore, in a gene expression analysis performed in NIH 3T3 cells in which PRMT7 was knocked down, MMP9 expression was downregulated by 2.3-fold (Karkhanis et al., 2012); however, this result was not validated further. This does, however, suggest that the regulation of MMP9 expression by PRMT7 may be consistent across cell types and species. Importantly, we have shown that expression of MMP9 in PRMT7-depleted cells rescued their invasive ability. This demonstrates that the reduction in cell invasion resulting from PRMT7 depletion is due, at least in part, to the reduced expression and activity of MMP9 expression. The rescue observed here was partial, suggesting that PRMT7 may also regulate additional mechanisms and cellular pathways to induce breast cancer cell invasion.

The precise mechanism through which PRMT7 induces MMP9 expression within breast cancer cells requires further clarification. There is evidence supporting both direct and indirect mechanisms through which PRMT7 may be acting. PRMT7 can influence gene expression through the methylation of histone proteins, as it has been shown to be involved in the methylation of N-terminal tail regions of histones H2A, H2B, H3 and H4 (Gayatri & Bedford, 2014). Specifically, PRMT7 affects the methylation of histone H2AR3, H2BR29, 30 and 31, H3R2 and H4R3, 17 and 19 (Y Feng et al., 2013; Karkhanis

et al., 2012; Migliori et al., 2012; Tweedie-Cullen et al., 2012). Importantly, MMP9 expression has been shown to be influenced by arginine methylation of histone proteins. Ma and colleagues have shown that methylation of histones H4R3, H3R26, and H3R17 are involved in Phorbol 12-myristate 12-acetate (PMA)-induced transcriptional activation of MMP9 (Ma, Shah, Chang, & Benveniste, 2004). Thus, PRMT7 may play a direct role in the regulation of MMP9 expression through its involvement in the methylation of histone H4R3. Indeed, we found that PRMT7 binds to the promoter of MMP9, supporting that epigenetic regulation may be taking place. Thus, it is highly likely that PRMT7 transcriptionally activates MMP9 by methylating H4R3, a previously identified target of PRMT7, to induce its expression (S. S. Dhar et al., 2012; Karkhanis et al., 2012). However, H4R3 is di-methylated and as PRMT7 has been shown to solely exhibit monomethylation activity, it could be possible that another PRMT is also involved. In fact, PRMT5 and PRMT4 are potential candidates as they methylate H4R3 and H3R17/26, respectively (Schurter et al., 2001; Zhao et al., 2009). Thus, PRMT7 may prime histone 4 via monomethylation to subsequently allow PRMT5 to dimethylate H4R3. In the case of PRMT4, its methyl mark may be occurring as a separate reaction from H4R3 or may be due to the recruitment of other factors such as transcription factors and histone remodelling factors as a result of H4R3 methylation which ultimately promote H3R17/26 methylation by PRMT4. It is also possible that PRMT7 simply acts as a scaffolding protein within the promoter of MMP9 to recruit histone writers and transcription factors. Rescue experiments using PRMT7 mutants that lack methyltransferase activity would address this question. Nevertheless, additional biochemical experimentations are required to fully understand the consequence of PRMT7 binding to the promoter of MMP9.

While we were in the later stages of publishing our work, a study essentially corroborating our findings was published (Yao et al., 2014). In support of, and complementary to our findings, Yao and colleagues also observed that PRMT7 protein expression is upregulated in breast cancer tissues and cell lines. They additionally found that PRMT7 is more highly expressed in ER- as opposed to ER+ breast cancer tissues and highly expressed in basal-like breast cancer tissues. Thus, Yao and colleagues have demonstrated that PRMT7 expression levels positively correlate with clinicopathological features of aggressive breast tumours, including ER negative status and basal-like pathology (Yao et al., 2014). Conversely, Yao's findings support the idea that PRMT7 is increasingly expressed in higher grade breast tumours, specifically grade III tumours. We found no such correlation. In fact, we found that PRMT7 levels remain consistent in grade I/II as well as in grade III tumours. This discrepancy between ours and Yao's study could be due to scoring method. As mentioned above, we focused more on cytoplasmic staining of PRMT7. Yao and colleagues used a more holistic method for scoring, looking at both nuclear and cytoplasmic staining (Yao et al., 2014). Although we also detected nuclear staining, we focused more on analyzing cytoplasmic staining as it was more prominent. This could possibly affect the observed results and could explain the differences observed between our findings and theirs. Furthermore, we focused on epithelial cell staining for score. It is possible that Yao and colleagues looked at more than one cell type. Lastly, it could also be due to antibody detection. The antibody used in our study detected two bands for PRMT7 in Western blotting, while Yao and colleagues detect a single band. Thus, epitope detection could also contribute to the discrepancies in our immunihistochemical

experiments. Nonetheless, we both conclude that PRMT7 is highly expressed in primary breast tumours as well as metastases.

Yao and colleagues also performed *in vivo* experiments but instead executed the reverse methodology whereby PRMT7 was over-expressed and subsequent lung metastases examined (Yao et al., 2014). They observed a drastic increase in lung metastases. These results suggest that PRMT7 could represent a potential oncogene. In fact, it is highly likely to be the case since Yao and colleagues also demonstrated PRMT7's ability to promote cell transformation by inducing EMT via E-cadherin repression. Importantly, the cellular process of EMT positively regulates the invasion and metastasis cancer hallmark as cells that obtain this feature can more readily acquire further traits to induce invasion, resisting of apoptosis, and dissemination of cells throughout the body (Hanahan & Weinberg, 2011). Mechanistically, it was observed that PRMT7, as part of a ternary complex consisting of YY1 (Ying Yang 1) and HDAC3 (histone deacetylase), methylated H4R3 within the promoter region of E-cadherin (Yao et al., 2014). The H4R3 mark was negatively correlated with H3K4 tri-methylation and H4Ac (both activating marks of gene expression). Again, the classification of PRMT7 as a Type III arginine methyltransferase suggests that it may work in concert with other PRMT enzymes to produce the symmetric H4R3 dimethylarginine mark. The group further demonstrated that over-expression of PRMT7 in MCF10A breast cancer cells resulted in repression of E-cadherin and subsequent transformation of the cells (van Roy & Berx, 2008; Yao et al., 2014). This again supports the hypothesis that PRMT7 may be a potential oncogene (through transcriptional regulation) since by simply over-expressing the enzyme in normal cells, cell transformation and ultimately tumourigenesis is induced via alterations in gene

expression. Ultimately, by inducing EMT and MMP9 expression, PRMT7 can potentially promote breast cancer metastasis.

To determine whether PRMT7 truly is an oncogenic protein, further experiments are required. First, since oncogenes are dysregulated or activated genes, it is crucial to determine whether this is the case with PRMT7. Genome studies to identify the existence of either activating mutations within the *PRMT7* gene or gene amplifications in breast cancer patients are necessary. Furthermore, the creation of a transgenic mouse model that expresses active PRMT7 within the mammary glands would aid in determining whether PRMT7 activity is sufficient to induce breast cancer in mice. Lastly, because over-expression transforms "immortalized" cells, it is likely that PRMT7 exhibits oncogenic properties. It would also be critical to determine whether over-expression of PRMT7 in primary fibroblast cells would also induce the same transformation and development of the noted cancer hallmark: invasion/metastasis.

Interestingly, E-cadherin has been shown to affect MMP9 expression (Nawrocki-Raby, Gilles, Polette, Martinella-Catusse, et al., 2003). Thus, it is possible that PRMT7 additionally regulates MMP9 expression indirectly through E-cadherin regulation. Overexpression of E-cadherin in E-cadherin-null invasive lung epithelial tumour cell lines resulted in a decrease in MMP9 expression and secreted protein levels (Nawrocki-Raby, Gilles, Polette, Martinella-Catusse, et al., 2003). This also caused a reduction in their invasiveness. Conversely, loss of E-cadherin protein expression in MCF10A cells resulted in a significant increase in MMP9 expression (A. Chen et al., 2014). Therefore, PRMT7 could potentially induce MMP9 expression indirectly through its repressive effects on E-cadherin. However, this has yet to be proven whether these effects are PRMT7-dependent.

Intriguingly, there appears to be an additional relationship between E-cadherin and MMP9. MMP9 has been shown to promote cleavage of E-cadherin generating a soluble extracellular E-cadherin fragment (sE-cadherin: 80kDa) (David & Rajasekaran, 2012; Symowicz et al., 2007). sE-cadherin has been shown to not only have oncogenic activities itself (S M Brouxhon et al., 2014; Sabine M. Brouxhon et al., 2014), but it is also capable of upregulating MMP9 expression (Nawrocki-Raby, Gilles, Polette, Bruyneel, et al., 2003; Nawrocki-Raby, Gilles, Polette, Martinella-Catusse, et al., 2003). Thus, PRMT7 could promote a positive feedback loop which could contribute to rapidly increasing the aggressiveness and invasiveness of tumour cells by promoting cell invasion.

It seems as though PRMT7 methyltransferase activity is required for its tumourigenic role in breast cancer (Geng et al., 2017). Specifically, automethylation of PRMT7 at R^{531} is critical in inducing EMT and cell invasion. Furthermore, Geng and colleagues observed that tumour metastases were almost abolished with the introduction of an un-methylatable PRMT7 ($R^{531}K$ mutant). This suggests the importance of both PRMT7 activity and automethylation in breast cancer aggression. This automethylation activation of PRMTs is not unique for PRMT7. In fact, other PRMTs (such as PRMT4, 6, and 8) have been shown to be either over-active or its activity towards certain substrates regulated upon automethylation (Dillon et al., 2013; Kuhn et al., 2011; Singhroy et al., 2013). As methyltransferase activity seems to be critical for its tumourigenic properties (Geng et al., 2017), the use of PRMT7-specific inhibitors could ultimately slow or regress breast cancer tumourigenesis. In fact, identification of the molecular pathways that contribute to breast cancer development and progression has shifted the therapeutic focus to a more targeted approach (Di Cosimo & Baselga, 2008). Targeted therapeutic strategies

offer a more refined and specific approach to the treatment of breast cancer in an attempt to reduce possible recurrence and metastasis. Our results, taken together with those of Yao and colleagues, as well as Geng and colleagues clearly establishes PRMT7 as a key mediator of breast cancer cell invasiveness and demonstrate that PRMT7 represents a novel biomarker and may be a promising new therapeutic target.

4.4 PRMT7 deficiency results in cellular senescence and cell death

We consistently observed significant defects in cell proliferation upon knockdown of PRMT7. Specifically, we noted that cells underwent cellular senescence as noted by increased SA-β-gal staining compared to controls. Conversely, over-expression of PRMT7 had no positive effects on cell growth. This suggests that there is a threshold of PRMT7 expression and activity that is required for efficient cell proliferation. Thus, in MCF7 cells, either the threshold has been reached and cells are undergoing maximal proliferation or that the threshold has yet to be reached suggesting that additional PRMT7 is required to observe an effect on proliferation. Within the invasive cells, once PRMT7 protein levels are below this threshold, cells begin to senesce. Although we did not explore the mechanisms behind cellular senescence, a group published findings demonstrating PRMT7 as an epigenetic regulator of senescence (Blanc et al., 2016).

Blanc and colleagues have observed that absence of PRMT7 within quiescent muscle stem cells results in cellular senescence and the inability of these cells to regenerate injured muscles and maintain self-renewal capabilities (Blanc et al., 2016). Mechanistically, the group found that PRMT7 epigenetically regulates p21 by methylating H4R3 near the CpG islands of *Cdkn1a* promoter (to silence p21 expression). The group additionally found that PRMT7 positively regulates DNMT3b (DNA methyltrasnferase 3b) expression to subsequently recognize the H4R3 methylation at the CpG islands of *Cdkn1* to hypermethylate the DNA. Thus, in addition to the epigenetic regulation of p21, loss of PRMT7 causes decreased DNMT3b expression which results in hypomethylation of the CpG islands within the *Cdkn1a* promoter leading to an increased expression of p21. Eventually, p21 induces cellular senescence which impedes self-renewal capacity. Looking

closely at their data, the group looked specifically into H4R3 symmetric dimethylation. Thus, it is highly likely that PRMT5 is additionally involved in maintaining muscle stem cell regenerative capabilities as an additional enzyme is required to dimethylate H4R3. To support this proposition, it is known that H4R3 symmetric dimethylation by PRMT5 can recruit DNMT3a to regulate gene silencing (Zhao et al., 2009). Indeed, PRMT5 has been shown to be a critical player in regulating muscle stem cell expansion via epigenetic silencing of p21 (Zhang et al., 2015). Thus, it could be possible that PRMT5 is additionally recruited to epigenetically regulate p21 and/or recruit DNMT3b through allosteric regulation of histone marks alongside PRMT7.

Cells lacking PRMT7 also eventually underwent apoptosis. The effects were more drastic when using a knockout cell line as opposed to knockdown. Due to these effects, our experiments were all transient. These observations are reasonable in that knockdown cells are likely able to cope with cell survival with residual levels of PRMT7 protein remaining. In terms of apoptosis, we currently have not pursued the mechanism through which this is occurring. However, this represents a new potential cancer hallmark role for PRMT7: evasion of apoptosis. Thus, not only does PRMT7 promote cell invasion and metastasis, but it also promotes cell survival. As mentioned in the introduction, PRMT7 knockout mice tend to live for about 5-10 days (Blanc et al., 2016; Jeong et al., 2016; Ying et al., 2015). Thus, it seems as though there is some compensatory mechanisms occurring to prolong the life of the mice in the absence of PRMT7. In fact, it is well known that PRMTs share many substrates and that the loss of one PRMT can promote others to compensate for substrate methylation (Dhar et al., 2013). However, even some compensation may not be sufficient for “normal” growth and development of cells. Thus, the death of the mice after 5-10 days

is unavoidable. Furthermore, there is the possibility that PRMT7 expression is more critical in certain cell types and tissues. Thus, the observed death after 5-10 days suggests that the organ or tissue that is affected by the absence of PRMT7 may allow for some coping to occur for a short interval. Further empirical experimentation is necessary to better elucidate the importance of PRMT7 in promoting cell survival.

Since PRMT7 has been shown to be involved in regulating the response of cells to cytotoxic and chemotherapeutic agents, it is possible that PRMT7 further regulates evasion of apoptosis by regulating sensitivity towards drugs. We have shown that lack of PRMT7 promotes both cellular senescence and apoptosis. Furthermore, a reduction in PRMT7 expression causes increased sensitivity of Chinese hamster cells to UV radiation, bleomycin and camptothecin (Gros et al., 2006). In human cancer cells (HeLa), downregulation of PRMT7 expression conferred sensitivity towards camptothecin treatment (Verbiest et al., 2008) and in NIH3T3 cells, depletion of PRMT7 was shown to cause resistance to cisplatin, mitomycin C and chlorambucil (Karkhanis et al., 2012). These studies have revealed that PRMT7 is involved in regulating the cellular response to treatment with cytotoxic agents. Although the studies are not all consistent, contrasting findings may be due to cell type and/or drug metabolism. Further studies examining the effects of targeting PRMT7 in combination with chemotherapeutic drugs, specifically in breast and other cancer cell types, will help determine its full therapeutic value, and notably as a potential biomarker for aggressive breast cancer.

Future work would include determining whether PRMT7 can be detected in tissues as a prognostic factor and whether decreasing PRMT7 protein levels in “normal” cells would be detrimental. It is possible that cancer cells are more sensitive to the loss of

PRMT7 as they are addicted to its increased activity and biological function in cells. Thus, loss of PRMT7 in cancerous cells leads to extreme stress. However, normal cells may also apoptose upon depletion of PRMT7, thus targeted therapies specifically against cancer cells should be developed. Nonetheless, this needs to be tested if therapies using small molecule inhibitors are to be used against PRMT7. Moreover, specifically targeting PRMT7 in resistant tumours may sensitize them to apoptosis as the survival mechanism can be prevented. The results of this project can be eventually extended to *in vivo* work for future studies of the role of PRMT7 in tumourigenesis. Specifically, mouse xenografts in the mammary fat pad can be employed to better imitate the progression of breast cancer. Better yet, a transgenic mouse line with a constitutively active PRMT7 can also be used to better study its role in tumorigenesis. This study can be extended to other cancer types as well since PRMT7 may also be implicated in a variety of different cancers. In fact, PRMT7 was recently shown to participate in endometrial carcinoma and could be a potential biomarker of endometrial serous carcinoma (Y. Chen, Wang, Lan, Zhou, & Wu, 2018). Furthermore, in the Human Protein Atlas (https://www.proteinatlas.org/), RNA expression of PRMT7 was shown to be strongly expressed in colorectal adenocarcinomas, pancreatic cancer, and lymphomas. Moreover, PRMT7 protein levels were upregulated in the endocrine system, the gastrointestinal tracts, male tissues, and the immune system. When dysregulated, PRMT7 expression could drastically affect organ function, thus, further research is required.

4.5 eIF2α is a novel substrate of PRMT7

PRMT7 is still not well characterized functionally; thus, further studies are necessary to better elucidate its role in human diseases such as breast cancer. To better characterize its role in breast cancer, it is important to go back to the basics, biochemically. Thus, the second objective of this work was to gain some insight into the biological functions of PRMT7 by identifying its protein interactors and potential substrates. The goal was to then divulge a novel cellular process that is dependent on PRMT7 expression and/or activity in the hopes of better characterizing the enzyme. Hence, we performed SILAC-based quantitative mass spectrometry.

We identified 76 interacting proteins of PRMT7 and validated many of them. However, we opted to focus on a novel substrate of PRMT7: the eukaryotic translation initiation factor eIF2α. Importantly, we identified eIF2α as a unique substrate of PRMT7 with its methylation site pinpointed to be within a duplicate RXR motif (SELS^{51}**RRRIR**SINK^{60}) adjacent to the S^{51} residue, a site important for eIF2α's role in the cellular stress response. As previously mentioned, PRMT7 is a type III PRMT capable of forming MMA final products whereas other PRMTs are involved in dimethylation. Generally, it is presumed that the MMA product is a transient modification which is subsequently dimethylated by either the same PRMT or another family member suggesting that the MMA mark acts as a priming post-translational modification (PTM) via allosteric regulation (Jain et al., 2017; Yang & Bedford, 2013). In our *in vitro* methylation assays, we noted that the only PRMT capable of methylating eIF2α was PRMT7. However, more experimentation needs to be performed to determine whether the other PRMTs could methylate eIF2α *in vivo* and/or *in vitro* upon priming by PRMT7 within cells/tissues.

Nonetheless, it could be possible that MMA marks play important roles *in vivo*. In fact, a LC-MS/MS study used monomethyl arginine antibodies to identify MMA-modified proteins (A. Guo et al., 2014). Confirming our results, the supplemental data from this experiment revealed eIF2α to be monomethylated and not asymmetrically dimethylated in mouse brain and embryo (note that symmetric dimethylation of arginine residues was not explored and could be a possibility). Furthermore, this mass spectrometry experiment identified both R^{53} and R^{54} as methylation sites. However, neither site was identified in their screen using mammalian colorectal carcinoma cells. We found that R^{54} played a critical role in eIF2α methylation status in human cell lines but found no such correlation with R^{53}. It could be possible that methylation sites differ according to the cellular mechanisms, cell type, cell state (normal vs cancerous cells), as well as species. This also raises the question as to whether MMA can behave as a final product under certain conditions and/or model systems. Nonetheless, mass spectrometry experimentations would resolve the question of whether the methylation sites are shared across species and/or tissues. Furthermore, it would be pertinent to determine if the function or structure of eIF2α is affected upon methylation.

Notably, in our *in vivo* methylation assays, we observed a decrease in methylation status of eIF2α by knocking down PRMT7. These findings suggest that PRMT7 is responsible for a major methylation site on eIF2α. A more drastic decrease in methylation status was observed in the RRK mutant compared to the knockdown cell line suggesting that there is residual PRMT7 still capable of methylating eIF2α in the knockdown cell line. The use of a CRIPSR-Cas9 knockout cell line was not possible since addition of translation inhibitors, as required by the protocol, resulted in massive cell stress and death within 48

hours in the complete absence of PRMT7. Furthermore, an incomplete loss of methylation in the RRK mutant suggests that there are potentially other sites of methylation within eIF2α to be further identified – lysine methylation is also a possibility. Moreover, methylation by other PRMTs through scavenging could occur. Even though we have shown that the other PRMTs do not methylate eIF2α *in vitro,* this does not eliminate the possibility of methylation occurring *in vivo.* Thus, future experiments should include looking into whether eIF2α is a shared substrate *in vivo* amongst the PRMT family of enzymes and whether substrate scavenging occurs with PRMT7 as it does with PRMT1 (Dhar et. al., 2013).

Looking more closely at the RXR motif, methylation was reduced and phosphorylation of eIF2α was lost when R^{54} was mutated to a lysine residue (RRK). However, introduction of the KRR and RRRIK mutants had no impact on methylation of eIF2α. One proposition is that within the duplicate RXR motif, $SELS^{51}$**RRRIR**$SINK^{60}$, only R^{54} is important for recognition since if mutated, both RXR motifs are abolished. For instance, the KRR mutant still maintains an RXR motif, KR**RIR,** as does the **RRR**IK mutant. Conversely, the RRK mutant no longer contains any RXR motif: RRKIR. Moreover, as the KR**RIR** mutant is still methylated, this suggests that neutral residues may still be recognized within an RXR motif if the general region is extremely basic.

Although we did not confirm any of the other identified PRMT7 interactors as substrates, we predict that ACTN4 is a novel substrate of PRMT7 for two reasons. Firstly, the interaction between PRMT7 and ACTN4 is extremely robust. Furthermore, when using an MMA specific antibody, we detect a strong signal at the molecular size of ACTN4, suggesting the protein is monomethylated *in vivo.* This finding also supports our previous

suggestion that MMA is a final mark and should no longer be assumed to be intermediary. Secondly, upon performing *in silico* experimentation, a single RXR motif was identified within the primary amino acid sequence of ACTN4: $R^{205}HR$. Thus, it is imperative to mutate this region and perform *in vitro* methylation assays to determine whether ACTN4 is a *bona fide* substrate of PRMT7. In addition to the identification of ACTN4, gamma actin monomers (ACTG1) were additionally identified in the mass spectrometry screens, thus it is possible that PRMT7 regulates cytoskeletal organization of cells. This could explain the drastic morphological changes observed upon knockdown and knockout of PRMT7.

We had also identified 76 additional putative interactors of PRMT7, which 41 were reproduced in both mass spectrometry experiments. Thus, there are still many other avenues concerning PRMT7's functional role in breast cancer that are left undiscovered. Moreover, these novel interactions could be extended to other cancer types as well as normal cellular mechanisms to better understand the biochemical and molecular importance of this enzyme. Since abnormalities such as intellectual disability syndrome were observed in patients with autosomal recessive mutations in PRMT7, it could be possible to develop drugs that could help improve these symptoms if the interactome of PRMT7 is better understood (Agolini et al., 2018; Kernohan et al., 2017). Furthermore, extensive studies should be performed to determine how these mutation in PRMT7 affect its activity in cells.

4.6 Interplay between eIF2α arginine methylation and serine phosphorylation

As there are many instances where PTMs can be either mutually exclusive or synergistic, we wanted to determine whether phosphorylation of eIF2α was affected by methylation. First, we observed that absence of PRMT7 when cells were under oxidative stress resulted in decreased phosphorylation of eIF2α whereas over-expression of PRMT7 resulted in an increase in phosphorylation. Furthermore, when the RXR motif of eIF2α was mutated, specifically at R^{54}, the protein was incapable of being phosphorylated upon exposure to oxidative stress. It could be possible that eIF2α methylation is required for phosphorylation to take place in stressed conditions – specifically, that phosphorylation succeeds eIF2α methylation. Interestingly, we observed that PRMT7 is incapable of interacting with P-eIF2α. Likewise, the PRMT7-eIF2α interaction is drastically reduced in stressed cells. This suggests that the majority of the eIF2α pool is phosphorylated in stressed cells, thereby resulting in a less robust interaction with PRMT7. These findings were observed in both eIF2α and PRMT7 immunoprecipitation experiments. No matter which of the two proteins were immunopurified from the lysate, the interaction was significantly diminished when cells were exposed to stress. Interestingly, in our *in vitro* methylation assays, PRMT7 was still capable of methylating the $S^{51}D$ phosphomimetic mutant. This discrepancy could be due to differences observed *in vitro* and *in vivo.* Specifically, cell compartmentalization may negatively impact the PRMT7-P-eIF2α protein interactions *in vivo*. Thus, upon exposure to cellular stress, eIF2α and PRMT7 may be found in different cellular compartments which prevent their interaction. Furthermore, a phosphomimetic does not exactly mimic an *in vivo* phosphorylation structure. The observed difference may simply be an issue with amino acid chemistry.

Moreover, because we see an increase in eIF2α arginine monomethylation upon exposure to cellular stress, this suggests that PRMT7 more actively methylates eIF2α under stressed conditions. Since MMA of eIF2α is required for S^{51} phosphorylation to take place, we propose that following monomethylation, eIF2α kinases displace PRMT7, allowing for the kinase to bind and subsequently phosphorylate the S^{51} residue. However, more studies are required to show that the PRMT7-eIF2α interaction is physically displaced by kinases. PTMs are known to affect protein-protein interactions as the chemistry of proteins are altered. In fact, positive crosstalk between arginine methylation and serine phosphorylation has been observed previously for other PRMTs. For instance, methylation of apoptosis signal-regulating kinase 1 (ASK1) by PRMT5 at R^{89} enhances the ASK1-Akt interaction resulting in phosphorylation of ASK1 at S^{83} to inhibit endothelial cell apoptosis (Chen et al., 2016). Thus, it is imperative to determine whether kinases bind more favourably to methylated eIF2α over non-methylated eIF2α.

Crystal structures of eIF2α when bound to its kinases would aid in determining whether R^{54} is critical for binding and how monomethylation at that site would affect the interaction between eIF2α and its kinases. In fact, Dhaliwal and Hoffman modelled the eIF2α structure in *Saccharomyces cerevisiae* and identified the side chains of both R^{52} and R^{54} make contact with other protein molecules within the crystal (Dhaliwal & Hoffman, 2003). Since proteins are dynamic, it could be possible that R^{52} and R^{54} are involved in intermolecular interactions with eIF2α kinases. Furthermore, the group proposed that the highly basic arginine rich sequence and the $lysine^{60}$ residue near the S^{51} residue (SELS^{51}**RRR**I**R**SIN**K**^{60}) balance the negative charge of the phosphate group added by eIF2α kinases and are additionally involved in sequence recognition by eIF2α kinases.

Hence, it is possible that the RXRXR sequence is critical in stabilizing the added negative charge of the phosphate group on S^{51} and in promoting intermolecular interactions. Moreover, monomethylation could slightly alter the structure of the residue and thus either positively or negatively affect the residue's interaction with other factors. Methylation of arginine residues does not affect the charge of the residue, thus the balancing effect on the negative phosphate group would not be affected. But, interaction of eIF2α with other protein molecules could significantly be affected upon arginine monomethylation. In our study, the introduction of an unmethylatable eIF2α (RRK mutant) prevented S^{51} phosphorylation. Thus, perhaps the MMA mark is required for the intermolecular interaction between eIF2α and its kinases to promote S^{51} phosphorylation.

We have additionally shown that the increase in eIF2α methylation upon cellular stress may be due to the fact that PRMT7 is more active under stressed conditions. Importantly, this is not due to alterations in PRMT7 expression as its levels remained consistent under stress. These results supports the idea that eIF2α is not constitutively methylated and that this reaction is induced by stress. Importantly, examples of stress-induced arginine methylation remains unexplored. Nonetheless, it is necessary to determine what causes PRMT7 activation under stressed conditions to promote eIF2α methylation and subsequent phosphorylation by its kinases. Interestingly, we observed a decrease in PRMT7 automethylation upon exposure to cellular stress. As mentioned previously, PRMT7's tumourigenic role in promoting breast cancer invasion and metastasis is dependent upon the activating automethylation of PRMT7 (Geng et al., 2017). However, we observed that there is a decrease in automethylation in stressed conditions at the 30 minute time point used for all our experiments. We were expecting an increase rather

than a decrease since we observed increased PRMT7 activity upon exposure to oxidative stress. Upon speculation, it could be possible that the activation of PRMT7 is extremely transient. Since signaling cascades tend to occur quickly, it is conceivable that PRMT7 monomethylation is enhanced within the first few moments of cellular stress. This monomethylation then triggers PRMT7 to methylate eIF2α to subsequently allow for serine phosphorylation to occur by eIF2α kinases. Thus, automethylation should be examined at the initial stages of cellular stress and followed closely over time. Since signaling cascades are highly regulated, after activation of PRMT7, demethylases could feedback inhibit the cascade. This would allow cells to reset the system to return to a state of homeostasis so that if cell stress is sensed once again, the cascade will then be triggered once more. Conversely, protein turnover rather than post-translational modifications may be responsible for the decreased MMA mark. Thus, pulse-chase experimentation should be performed over the same time points to determine whether there is an increase in protein turnover rate upon exposure to cellular stress. Furthermore, looking upstream this signaling cascade would better aid in understanding the stress-induced activation. Additional empirical studies are necessary to determine whether this phenomenon is applicable to normal tissues or whether it is tissue-specific. These studies would aid in better understanding the functional output of eIF2α's post-translational marks.

4.7 Novel role for PRMT7 in stress granule formation

Since eIF2α plays a major role in stress regulation, we further explored the consequences of PRMT7 modulation on a downstream eIF2α readout: stress granule formation. First, we observed partial co-localization of PRMT7 with stress granule markers G3BP1, FMRP, and to a lesser extent TIA-1. This could be due to the fact that PRMT7 may be present/required in a certain subtype of stress granules under specific stressors. In fact, depending on the stressor used, the composition, assembly, and dynamics of stress granules differ (Aulas et al., 2017). Additionally, there is the possibility that co-localization with specific stress granule markers is time dependent. Thus, live-cell imagining could aid in better understanding this phenomenon.

Interestingly, upon knockdown of PRMT7, we observed a drastic decrease in stress granule formation within cells treated with eIF2α-dependent stressors but saw no alterations when using an eIF2α-independent stressor. These results suggest that PRMT7 regulates stress granule formation in an eIF2α-dependent manner. Either the interaction of PRMT7 with eIF2α or methylation of eIF2α by PRMT7 may be required for eIF2α phosphorylation and subsequent stress granule formation. Hence, reduction of PRMT7 via knockdown most likely resulted in inefficient formation of stress granules as the lack of methylation diminishes S^{51} phosphorylation. Furthermore, different mechanisms may exist as a more drastic effect was observed when using thapsigargin (ER stress) as opposed to sodium arsenite (oxidative stress). Thus, it could be possible that PRMT7 more strongly regulates a certain subset of stresses or the differing components of stress granules depending on the stress. As these results are mostly correlative, there could be a possibility that PRMT7 does not play a direct role in stress granule formation. A sequence of signaling

cascades to promote the formation of stress granules is definitely a possibility and should be further explored. For instance, other stress granule promoting factors may be regulated via methylation by PRMT7 to promote aggregation of the stress granule components. Further experiments will be required to determine whether PRMT7 methylates stress granule components or plays additional role(s) within stress granule assembly since arginine methylation has been shown to be a critical player in stress granule formation (W. C. Tsai et al., 2017). For instance, arginine methylation of core constituents of stress granules have been observed, such as with FMRP (Xie & Denman, 2011). Furthermore, methylation seems to impact stress granule dynamics (I. Goulet, Boisvenue, Mokas, Mazroui, & Cote, 2008). It was observed that methyl-arginine readers such as Tudor domain-containing protein 3 (TDRD3), a protein known to recognize and bind methylated arginine residues via its Tudor domain, similarly localizes to stress granules. (I Goulet et al., 2008; Linder et al., 2008). By simply over-expressing TDRD3, stress granules are induced whereby TDRD3 co-localizes with FMRP within the cytoplasmic granules (Linder et al., 2008). This suggests that TDRD3, as a methyl-reader, is recruited to stress granules upon recognition of arginine methylated proteins within the stress granule core. In terms of arginine demethylation, G3BP1 demethylation by JMJD6 is critical for stress granule formation (W.-C. Tsai et al., 2016; W. C. Tsai et al., 2017). Thus, both methylation and demethylation are important reactions for the fine tuning of stress granule components. It is apparent that a fine balance between methylation and demethylation is essential for appropriate stress granule formation and that PRMT7 may be involved in this regulatory role.

In AA MEF cells, since there is an $S^{51}A$ mutation, the formation of P-eIF2α-dependent stress granule formation is not possible. Interestingly, when we tried to rescue P-eIF2α-dependent stress granule formation in AA MEF cells by expressing wild-type and mutant eIF2α, we observed stress granules when using all mutants (wild-type, RKR, RRK, and RRRIK) except for the KRR mutant. This was surprising since we were expecting a lack of stress granules only with the RRK mutant as it is incapable of being methylated and phosphorylated in human cells. This discrepancy suggests that mouse cells and human cells may have different mechanisms or substrate recognition motifs (in terms of PRMT7 methylation) *in vivo.* As previously mentioned, a mass spectrometry study found that R^{53} and R^{54} were methylated in mouse brain samples. However, in our study, we found that only R^{54} was critical for both methylation and phosphorylation. Thus, it is a possibility that the different residues may have differing effects on stress granule formation. Another distinction is the fact that MEF cells are immortalized fibroblasts and are not transformed (as is the case with our breast cancer cell lines). Thus, this discrepancy can also be due to the different cell characteristics. To better resolve this inconsistency, phosphorylation status and methylation of the eIF2α mutants should be further explored in mouse cells to determine whether these effects are specific to human cells or can be applied to mouse cell lines as well.

4.8 Novel role for PRMT7 in translation

Notably, eIF2α is first and foremost a translation initiation factor. Moreover, since PRMT7 and eIF2α both co-fractionated and interacted within pre-translational complex fractions of breast cancer cells and since PRMT7 further prevailed within polysomal fractions, we wanted to further explore the potential role of PRMT7 as a regulator of translation. We first compared polyribosome profiles from PRMT7 knockdown and control cells and did not observe any clear alterations. However, upon analyzing the polysomal-to- pre-translational complex ratios, we observed a significant decrease in relative polysome abundance in both MDA-MB-231 (36%) and MCF7 (32%) cells. Since the profiles were slightly more affected in MDA-MB-231 cells, this suggests that PRMT7's role in promoting translation may be cancer-subtype specific. For instance, it is possible that TNBC lines are more "addicted" to PRMT7 expression and thus any alterations in its levels more significantly alters the biological functions of the cell. Furthermore, since we saw that PRMT7 affects eIF2α phosphorylation, which is a signal for global translation inhibition, we predict more drastic changes when using stressors. Possibly, in the absence of PRMT7, the cells would not be able to respond to the cellular stress and ultimately die – resulting in flattening of the profiles. Conversely, if performed before the massive cell death observed upon PRMT7 knockdown, depletion of PRMT7 would impede eIF2α phosphorylation and thus translation would not be inhibited. Thus, we could expect a decrease in polysomal peaks only in the control cells and not the PRMT7 knockdown cells since the latter would be incapable of responding to the stress via translation inhibition. Furthermore, these effects may differ depending on the stressors used.

Although the identification of eIF2α as a substrate of PRMT7 is novel, other PRMT7 substrates and other PRMTs have previously been linked with translation. For instance, eukaryotic elongation factor 2 (eEF2) is a substrate of PRMT7 and the methylation reaction is coordinated by PRMT5 (Jung et al., 2011). However, the downstream functional effects of eEF2 methylation have yet to be discovered. PRMT5 methylates heterogeneous nuclear ribonucleoprotein (hnRNP) A1. Importantly, hnRNP A1 is a transactivating factor that regulates cap-independent translation, or in other words internal ribosomal entry sites (IRES)-dependent mRNA translation, of cyclin D1 and c-Myc and its interaction with IRES RNA is facilitated by arginine methylation catalyzed by PRMT5 (Gao, Dhar, & Bedford, 2017). Moreover, as mentioned in the introduction, PRMT1 methylates RNA binding protein Aven to regulate the translation of *mixed lineage leukemia* (MLL) 1/4 (Thandapani et al., 2015). PRMT3 additionally regulates 80S ribosome maturation, required for translation elongation, by catalyzing the methylation of rpS2 (Miyata, Mori, & Tohyama, 2010; Swiercz, Person, & Bedford, 2005). Thus, it is to no surprise that PRMT7 may also regulate translation.

We observed between a 46-56% decrease in global translation in breast cancer and MEF cells lacking PRMT7 using both ^{35}S metabolic assays and puromycylation assays. These findings further provide evidence that PRMT7 regulates basic, bulk protein translation. Although translation is evidently affected upon knockdown of PRMT7, it remains unclear how PRMT7 modulates translation. It is likely that PRMT7 positively regulates the formation or assembly of the ternary complex through its interaction with and/or methylation of the eIF2 complex. Furthermore, whether PRMT7 regulates global

translation efficiency or the translation of only a subset of mRNAs that are eIF2α-dependent remains unclear and necessitates further exploration.

It is also possible that PRMT7 regulates P-eIF2α dependent translation under stressed conditions, specifically with mRNAs containing long 5'UTRs harbouring multiple uORFs. The presence of these uORFs drastically alters the translation of the specific protein. For instance, under normal conditions, the abundance of the ternary complex allows for translation initiation to occur at the mRNA uORFs, inhibiting the translational expression of the protein. However, under stressed conditions, ribosome scanning occurs past the uORFs until the main/strong ORF is found whereby the residual active ternary complex binds and allows for the translation of the main protein (Holcik & Sonenberg, 2005; Martin Holcik, 2015). Thus, phosphorylation of eIF2α enhances the translation of these specific mRNAs. One such example is ATF4 which, once translated, enhances the transcription of cancer-promoting and stress-response/adaptive proteins such as autophagy-related genes (B'chir et al., 2013). Once expressed, these proteins could promote cell survival. Thus, it would be beneficial to determine whether modulating PRMT7 protein levels affects P-eIF2α-dependent translation under stressed conditions since it affects eIF2α phosphorylation status.

Protein synthesis rates of AA MEF cells remained unchanged under oxidative stress since the inhibition of bulk translation was attenuated as the phosphorylation cascade is absent due to the $S^{51}A$ mutation in eIF2α. However, it is puzzling that the decrease in translation is absent under stressed conditions even in PRMT7 knockdown cells. This observation could be due to a compensatory mechanism such as over-activation of HRI under stressed conditions. Since HRI cannot phosphorylate mutant eIF2α, its activated

levels remains high. Moreover, it could be speculated that it is through HRI activation that PRMT7 activity is increased. Thus, as HRI is over-stimulated, this results in over-activation of the residual PRMT7 in our knockdown lines, ultimately leading to unchanged protein synthesis. The use of PRMT7 knockout cell lines would aid in better unfolding this mystery. Moreover, there is a possibility that under stressed conditions, a P-eIF2α-independent translation mechanism is activated such as IRES-mediated translation. Nonetheless, it is hard to decipher the mechanism behind these observations unless RNA sequencing on the actively translated mRNAs are performed to identify the alterations in translation.

Seeing as eIF4A was identified as a PRMT7-specific protein interactor in experiment 2 of the mass spectrometry analysis, we next performed mRNA cap binding assays. Surprisingly, upon knockdown of PRMT7, we observed a complete loss of eIF4A binding to the mRNA cap. The scaffolding protein, eIF4G was also significantly lost in our pulldown assays. These findings suggest that PRMT7 may also promote eIF4F complex formation. Thus, the significant decrease in translation observed in the absence of PRMT7 may be due to inhibition of cap-dependent translation as the eIF4F complex is inefficiently formed. This, however, does not rule out the possibility that PRMT7 could regulate cap-independent translation. Interestingly, within both mass spectrometry experiments, many hnRNP proteins were identified, specifically those that are known to be IRES-transactivating factors (ITAFs) such as hnRNP A1 (Appendix, Table 7). Therefore, it is highly possible that PRMT7 regulates both cap-dependent and cap-independent translation.

As mentioned in the introduction, two groups have found that P-eIF2α positively regulates the Akt pathway to promote cell survival under stressed conditions (Rajesh et al.,

2015; Tenkerian et al., 2015). Interestingly, we found that ablation of PRMT7 resulted in a significant decrease in Akt phosphorylation which correlated with decreased cell survival. As it was not further explored, PRMT7 could either directly or indirectly regulate Akt phosphorylation. As an indirect pathway, it could be proposed that PRMT7 promotes eIF2α phosphorylation which subsequently inhibits the mTORC1 negative regulatory feedback loop on PI3K-Akt. Ultimately, this leads to increased activation of the PI3K-Akt pathway, promoting cell survival. Furthermore, downstream of the PI3K-Akt pathway, eIF4E inhibition by its binding protein (4E-BP) is relieved, resulting in enhanced protein synthesis. Thus, this could present another mechanism through which PRMT7 promotes both cell survival and protein synthesis. Nevertheless, more empirical studies examining the P-eIF2α/PI3K-Akt signaling pathway is warranted.

Overall, regarding the PRMT7-eIF2α interaction, our model suggests that PRMT7 plays a major regulatory role in both translation and stress granule formation (Figure 45). In brief, under stressed conditions, upon methylation by PRMT7, phosphorylation of eIF2α ensues which subsequently promotes the formation of stress granules. PRMT7 may additionally regulate stress granules at their core as the enzyme co-localizes with several stress granule proteins. Furthermore, through an unknown mechanism, translation is also regulated by PRMT7. Whether this biological function is dependent on methyltransferase activity remains to be explored. In essence, a decrease in PRMT7 protein levels results in both inefficient stress granule formation as well as a significant decrease in protein translation. These results suggest the importance of PRMT7 in maintaining cellular homeostasis. With the dysregulation of PRMT7 in breast cancer, the cellular stress

response and translation regulation could be greatly impaired resulting in abnormal cellular functions which ultimately lead to disease progression.

Additional empirical experimentations are required to identify the precise mechanisms through which PRMT7 positively regulates the stress response and protein synthesis and whether this role is enhanced within breast cancer cells, other cancer types, and/or normal tissues. In terms of translation, it is vital to determine whether it is translation efficiency or a subset of mRNAs that are affected upon modulation of PRMT7. In fact, we have already taken the next steps to identify the mRNAs whose translation is affected by PRMT7 expression. We pooled polysomal fractions from knockdown PRMT7 and control cells and isolated RNA samples to perform RNA sequencing (Appendix; Figure 46). This experiment would identify the mRNAs that are dependent on PRMT7 expression and/or activity. One could argue that the effects on protein translation upon knockdown of PRMT7 could be due to the observed effects on cell survival, senescence, and proliferation. However, throughout the experiments, the observed effects on protein synthesis were performed at time points prior to the observed proliferative and survival defects observed upon knockdown of PRMT7. Nevertheless, more empirical experimentation must be performed to isolate these effects.

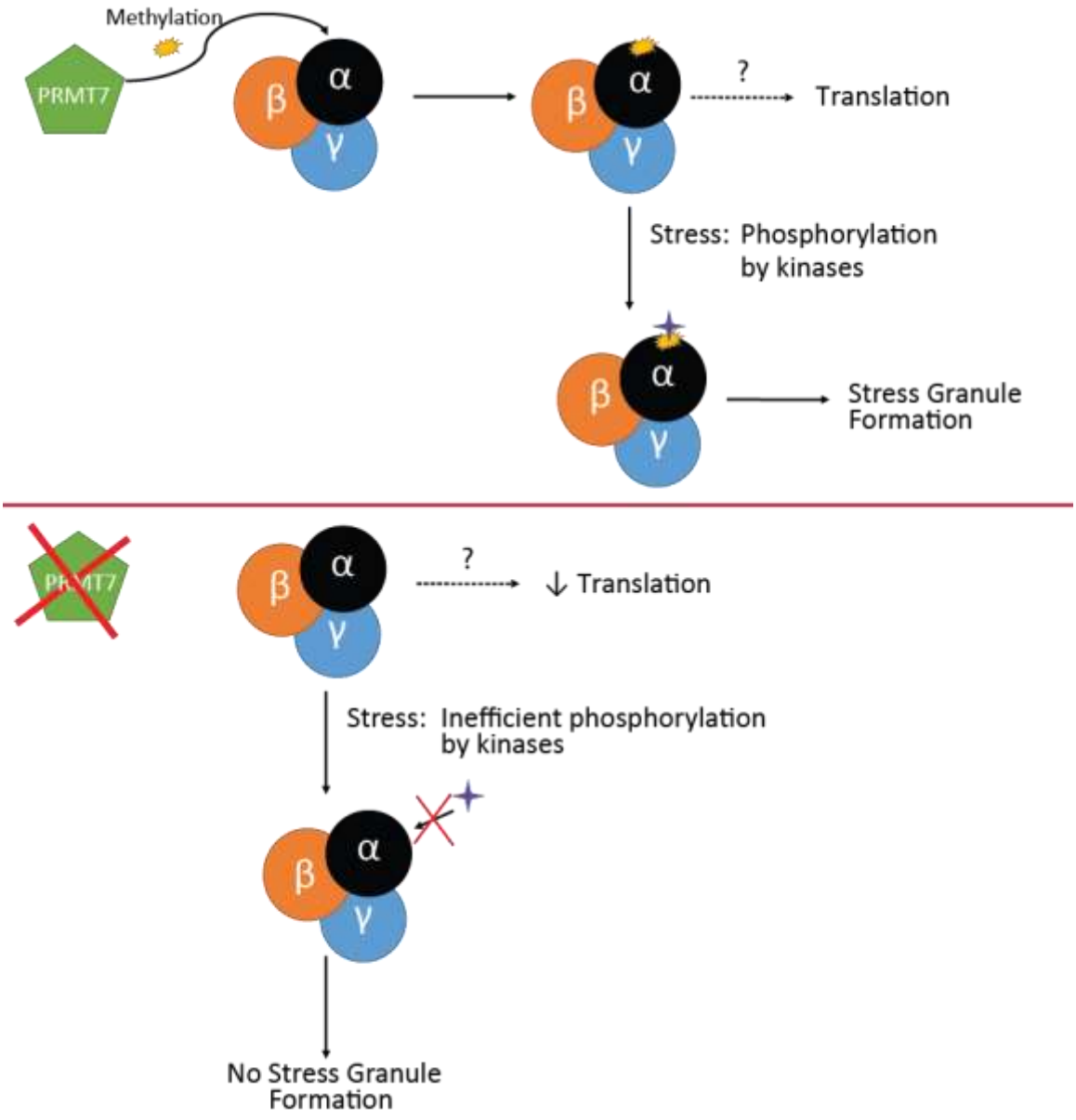

Figure 45: Working model for PRMT7 in translation and stress granule formation
PRMT7 positively regulates translation through an unknown mechanism. Furthermore, upon exposure to stress such as oxidative stress, phosphorylation of eIF2α occurs to induce stress granule formation. Methylation of eIF2α by PRMT7 may be involved in promoting phosphorylation of eIF2α. Thus, lack of PRMT7 and subsequent lack of methylated eIF2α may prevent phosphorylation from occurring and therefore result in the absence of stress granule formation.

Future studies would include using a methyltransferase dead mutant to determine if the loss in translation and stress granule formation due to PRMT7 knockdown could be rescued. This would give us an idea as to whether the enzymatic function of PRMT7 is the cause for the observed effects. We have created a methyltransferase-dead mutant PRMT7 by mutating the highly conserved PRMT SAM-binding domain ($D^{70}IG \rightarrow AAA$) and subsequently performed *in vitro* methylation assays to confirm the mutant is catalytically dead (Appendix; Figure 47A). Interestingly, this mutant behaves completely differently from wild-type PRMT7 in that it does not interact with any of the identified proteins from this study (Appendix; Figure 47B). However, localization of the enzyme resembled wild-type PRMT7 (Appendix; Figure 47C). This finding suggests that SAM binding to PRMT7 is critical for optimal conformational changes to occur to ultimately allow for substrate binding and subsequent methylation. Indeed, this model was shown with PRMT1: SAM binding alters the interaction between PRMT1 and its substrate histone H4 (You Feng et al., 2011). Thus, in the case of PRMT7, mutation of the SAM binding domain may prevent further conformational changes to promote substrate binding. Crystal structures of the methyltransferase-dead mutant PRMT7 should also be compared to wild-type PRMT7 to confirm these speculations.

4.9 Implications of the eIF2α/PRMT7 interaction

We showed that PRMT7 expression is upregulated in breast cancer tissues and cell lines. Interestingly, eIF2α also seems to be implicated in several cancers. eIF2α protein levels are upregulated in malignant melanocytic and colonic epithelial neoplasms, thyroid carcinomas, and non-Hodgkin's lymphomas (Rosenwald, Wang, Savas, Woda, & Pullman, 2003; S. Wang et al., 1999, 2001). Phosphorylated eIF2α is similarly upregulated in triple negative breast cancer and was proposed to represent a novel prognostic factor (Guo et al., 2017). Furthermore, P-eIF2α is implicated in promoting survival of tumour cells under stressed conditions (Rajesh et al., 2015; Tenkerian et al., 2015). Importantly, P-eIF2α and PRMT7 are both upregulated in TNBC. This supports our hypothesis that with more PRMT7 present in breast cancer, eIF2α methylation and subsequent phosphorylation will be increased under stressed conditions. Nevertheless, this is hypothetical and requires additional experimentation to be proven correct.

Stress granules additionally promote cell survival in the presence of cellular stressors. Interestingly, several chemotherapeutic drugs (bortezomib, 5-fluorouracil, 6-thioguanine, and 5-azacytidine) have been shown to induce stress granule formation thereby resulting in the cells resisting drug-induced apoptosis (Anderson et al., 2015; Fournier et al., 2010; Kaehler et al., 2014). Several stressors that induce stress granules (hypoxia, UV irradiation, nutrient deprivation, and oxidative stress) could contribute to resistance against standard therapy regimens, ultimately resulting in tumour recurrence after treatment. It is possible that PRMT7 confers resistance towards such chemotherapeutic drugs through stress granule formation. For instance, stress granules have been shown to exist in breast tumour cells at the hypoxic core, promoting cell survival

(Baguet et al., 2007; Moeller & Dewhirst, 2006). It is highly likely that the hypoxic core of the tumours induces stress-like conditions to activate PRMT7 which in turn enhances methylation of eIF2α resulting in an increase in P-eIF2α and stress granule formation to promote survival. Thus, targeting PRMT7 in breast cancer using small molecule inhibitors to prevent its methyltransferase activity could lead towards the synthesis of more effective therapeutic agents in the treatment of cancer.

Finally, the interaction between eIF2α and PRMT7 most likely does not only affect translational regulation and stress dynamics. Two independent groups have found that PRMT7 and eIF2α regulate muscle stem cell quiescence and self-renewal (Blanc et al., 2016; Zismanov et al., 2016). Although the two groups have observed these results independently of each other, it could be possible that PRMT7 and eIF2α work in conjunction to regulate muscle stem cell activation and differentiation. Skeletal muscle stem cells incapable of phosphorylating eIF2α exit the quiescent state and subsequently undergo differentiation (Zismanov et al., 2016). Consistent with this, PRMT7 is necessary for muscle regeneration; more specifically, cells undergo premature senescence in the absence of PRMT7 and are subsequently incapable of replenishing muscle stem cells (Blanc et al., 2016). Hypothetically, it is possible that PRMT7 aids in promoting muscle stem cell self-renewal by promoting eIF2α phosphorylation via methylation. Thus, cells deficient in PRMT7 would lack phosphorylation of eIF2α resulting in exiting of the quiescent state as both PRMT7 and P-eIF2α are required for the maintenance of muscle stem cell self-renewal. Overall, there could be other molecular functions dependent on the PRMT7-eIF2α interaction that have yet to be discovered.

4.10 Conclusions

We demonstrated that an excess of PRMT7 promotes breast cancer cell invasion and metastasis through the induction of MMP9. Our results suggest that PRMT7 presents a potential oncogene and biomarker in aggressive breast cancer. Thus, small molecule inhibitors targeting PRMT7 could prove to be beneficial in the treatment or prevention of breast cancer. Although a PRMT7-specific inhibitor has not yet been developed, a dual PRMT5/PRMT7 inhibitor exists (Smil et al., 2015). Future experiments using this dual inhibitor would aid in better exploring the therapeutic potential of PRMT7.

It is unclear why PRMT7 is upregulated in aggressive and highly invasive breast cancers. Some possibilities include gene duplication, misregulation of PRMT7's upstream transcriptional regulators, post-transcriptional regulation, and mutations within its promoter. Future research should focus on identifying causes of PRMT7 dysregulation in breast cancer. The ultimate goal would be to regulate PRMT7 protein expression to prevent tumourigenesis and to restore cellular homeostasis.

We additionally uncovered the protein interactome of PRMT7 to better understand the enzyme's biological functions in breast cancer cells. We specifically observed that PRMT7 regulates two essential cellular processes through its interaction with eIF2α: the cellular stress response and protein translation. The identification of the protein interactome of PRMT7 allows for further biological characterization of the enzyme. Our results underline the importance of arginine methylation in regulating the intricate web of cellular processes, and highlight the implications of arginine monomethylation in molecular biology.

REFERENCES

Adjibade, P., St-Sauveur, V. G., Huberdeau, M. Q., Fournier, M. J., Savard, A., Coudert, L., … Mazroui, R. (2015). Sorafenib, a multikinase inhibitor, induces formation of stress granules in hepatocarcinoma cells. *Oncotarget*, *6*, 43927–43943.

Agolini, E., Dentici, M. L., Bellacchio, E., Alesi, V., Radio, F. C., Torella, A., … Novelli, A. (2018). Expanding the clinical and molecular spectrum of *PRMT7* mutations: 3 additional patients and review. *Clinical Genetics*, *93*(3), 675–681. https://doi.org/10.1111/cge.13137

Anderson, P., Kedersha, N., & Ivanov, P. (2015). Stress granules, P-bodies and cancer. *Biochim Biophys Acta*, *1849*, 861–870. https://doi.org/10.1016/j.bbagrm.2014.11.009

Antonysamy, S., Bonday, Z., Campbell, R. M., Doyle, B., Druzina, Z., Gheyi, T., … Emtage, S. (2012). Crystal structure of the human PRMT5:MEP50 complex. *Proceedings of the National Academy of Sciences*, *109*, 17960–17965. https://doi.org/10.1073/pnas.1209814109

Aulas, A., Fay, M. M., Lyons, S. M., Achorn, C. A., Kedersha, N., Anderson, P., & Ivanov, P. (2017). Stress-specific differences in assembly and composition of stress granules and related foci. *Journal of Cell Science*, *130*(5), 927–937. https://doi.org/10.1242/jcs.199240

Avery, T. P. (2018). Triple-Negative Breast Cancer. In M. Howard-McNatt (Ed.), *Changing Paradigms in the Management of Breast Cancer* (pp. 155–166). Cham: Springer International Publishing. https://doi.org/10.1007/978-3-319-60336-0_11 LB - Avery2018

B'chir, W., Maurin, A.-C., Carraro, V., Averous, J., Jousse, C., Muranishi, Y., … Bruhat, A. (2013). The eIF2α/ATF4 pathway is essential for stress-induced autophagy gene expression. *Nucleic Acids Research*, *41*(16), 7683–7699. https://doi.org/10.1093/nar/gkt563

Bachand, F., & Silver, P. A. (2004). PRMT3 is a ribosomal protein methyltransferase that affects

the cellular levels of ribosomal subunits. *The EMBO Journal*, *23*(13), 2641–2650. https://doi.org/10.1038/sj.emboj.7600265

Baguet, A., Degot, S., Cougot, N., Bertrand, E., Chenard, M.-P., Wendling, C., … Tomasetto, C. (2007). The exon-junction-complex-component metastatic lymph node 51 functions in stress-granule assembly. *Journal of Cell Science*, *120*, 2774. Retrieved from http://jcs.biologists.org/content/120/16/2774.abstract

Baird, T. D., & Wek, R. C. (2012). Eukaryotic initiation factor 2 phosphorylation and translational control in metabolism. *Adv Nutr*, *3*, 307–321. https://doi.org/10.3945/an.112.002113

Balagopal, V., & Parker, R. (2009). Polysomes, P bodies and stress granules: states and fates of eukaryotic mRNAs. *Curr Opin Cell Biol*, *21*, 403–408. https://doi.org/10.1016/j.ceb.2009.03.005

Baldwin, R. M., Bejide, M., Trinkle-Mulcahy, L., & Cote, J. (2015). Identification of the PRMT1v1 and PRMT1v2 specific interactomes by quantitative mass spectrometry in breast cancer cells. *Proteomics*, *15*, 2187–2197. https://doi.org/10.1002/pmic.201400209

Baldwin, R. M., Haghandish, N., Daneshmand, M., Amin, S., Paris, G., Falls, T. J., … Côté, J. (2015). Protein arginine methyltransferase 7 promotes breast cancer cell invasion through the induction of MMP9 expression. *Oncotarget*, *6*, 3013–3032. https://doi.org/10.18632/oncotarget.3072

Baldwin, R. M., Morettin, A., & Cote, J. (2014). Role of PRMTs in cancer: Could minor isoforms be leaving a mark? *World J Biol Chem*, *5*, 115–129. https://doi.org/10.4331/wjbc.v5.i2.115

Baldwin, R. M., Morettin, A., Paris, G., Goulet, I., & Cote, J. (2012). Alternatively spliced protein arginine methyltransferase 1 isoform PRMT1v2 promotes the survival and invasiveness of

breast cancer cells. *Cell Cycle*, *11*, 4597–4612. https://doi.org/10.4161/cc.22871

Bedford, M. T. (2007). Arginine methylation at a glance. *J Cell Sci*, *120*, 4243–4246. https://doi.org/10.1242/jcs.019885

Bedford, M. T., & Clarke, S. G. (2009). Protein arginine methylation in mammals: who, what, and why. *Mol Cell*, *33*, 1–13. https://doi.org/10.1016/j.molcel.2008.12.013

Bedford, M. T., & Richard, S. (2005). Arginine methylation an emerging regulator of protein function. *Mol Cell*, *18*, 263–272. https://doi.org/10.1016/j.molcel.2005.04.003

Bianchini, G., Balko, J. M., Mayer, I. A., Sanders, M. E., & Gianni, L. (2016). Triple-negative breast cancer: challenges and opportunities of a heterogeneous disease. *Nat Rev Clin Oncol*, *13*, 674–690. https://doi.org/10.1038/nrclinonc.2016.66

Blanc, R. S., & Richard, S. (2017). Arginine Methylation: The Coming of Age. *Mol Cell*, *65*, 8–24. https://doi.org/10.1016/j.molcel.2016.11.003

Blanc, R. S., Vogel, G., Chen, T., Crist, C., & Richard, S. (2016). PRMT7 Preserves Satellite Cell Regenerative Capacity. *Cell Rep*, *14*, 1528–1539. https://doi.org/10.1016/j.celrep.2016.01.022

Bleibel, W. K., Duan, S., Huang, R. S., Kistner, E. O., Shukla, S. J., Wu, X., … Dolan, M. E. (2009). Identification of genomic regions contributing to etoposide-induced cytotoxicity. *Hum Genet*, *125*, 173–180. https://doi.org/10.1007/s00439-008-0607-4

Bogorad, A. M., Lin, K. Y., & Marintchev, A. (2017). Novel mechanisms of eIF2B action and regulation by eIF2α phosphorylation. *Nucleic Acids Research*, *45*(20), 11962–11979. https://doi.org/10.1093/nar/gkx845

Böttger A, Islam MS, Chowdhury R, Schofield CJ, Wolf A. The oxygenase Jmjd6--a case study in conflicting assignments. Biochem J. 2015 Jun 1;468(2):191-202. doi: 10.1042/BJ20150278. Review. PubMed PMID: 25997831.

Brouxhon, S. M., Kyrkanides, S., Teng, X., Athar, M., Ghazizadeh, S., Simon, M., … Ma, L. (2014). Soluble E-cadherin: a critical oncogene modulating receptor tyrosine kinases, MAPK and PI3K/Akt/mTOR signaling. *Oncogene*, *33*(2), 225–235. https://doi.org/10.1038/onc.2012.563

Brouxhon, S. M., Kyrkanides, S., Teng, X., O'Banion, M. K., Clarke, R., Byers, S., & Ma, L. (2014). Soluble-E-cadherin activates HER and IAP family members in HER2+ and TNBC human breast cancers. *Molecular Carcinogenesis*, *53*(11), 893–906. https://doi.org/10.1002/mc.22048

Buchan, J. R., & Parker, R. (2009). Eukaryotic stress granules: the ins and outs of translation. *Mol Cell*, *36*, 932–941. https://doi.org/10.1016/j.molcel.2009.11.020

Buchan, J. R., Yoon, J.-H., & Parker, R. (2011). Stress-specific composition, assembly and kinetics of stress granules in Saccharomyces cerevisiae. *Journal of Cell Science*, *124*(2), 228–239. https://doi.org/10.1242/jcs.078444

Cáceres, T. B., Thakur, A., Price, O. M., Ippolito, N., Li, J., Qu, J., … Hevel, J. M. (2018). Phe71 in Type III Trypanosomal Protein Arginine Methyltransferase 7 (TbPRMT7) Restricts the Enzyme to Monomethylation. *Biochemistry*, *57*(8), 1349–1359. https://doi.org/10.1021/acs.biochem.7b01265

Cazalla, D., Sanford, J. R., & Cáceres, J. F. (2005). A rapid and eYcient protocol to purify biologically active recombinant proteins from mammalian cells. *Protein Expression and PuriWcation*, *42*, 54–58. https://doi.org/10.1016/j.pep.2005.03.035

Cazzaniga, M., & Bonanni, B. (2012). Breast cancer chemoprevention: old and new approaches. *J Biomed Biotechnol*, *2012*, 985620. https://doi.org/10.1155/2012/985620

Cha, B., & Jho, E. H. (2012). Protein arginine methyltransferases (PRMTs) as therapeutic targets. *Expert Opin Ther Targets*, *16*, 651–664. https://doi.org/10.1517/14728222.2012.688030

Chang, B., Chen, Y., Zhao, Y., & Bruick, R. K. (2007). JMJD6 Is a Histone Arginine Demethylase. *Science*, *318*(5849), 444–447. https://doi.org/10.1126/science.1145801

Chen, A., Beetham, H., Black, M. A., Priya, R., Telford, B. J., Guest, J., … Guilford, P. J. (2014). E-cadherin loss alters cytoskeletal organization and adhesion in non-malignant breast cells but is insufficient to induce an epithelial-mesenchymal transition. *BMC Cancer*, *14*(1), 552. https://doi.org/10.1186/1471-2407-14-552

Chen, M., Qu, X., Zhang, Z., Wu, H., Qin, X., Li, F., … Shu, W. (2016). Cross-talk between Arg methylation and Ser phosphorylation modulates apoptosis signal–regulating kinase 1 activation in endothelial cells. *Mol Biol Cell*, *27*, 1358–1366. https://doi.org/10.1091/mbc.E15-10-0738

Chen, Y., Wang, B., Lan, X., Zhou, Z., & Wu, X. (2018). Increased protein arginine methyl transferase 7 expression is correlated with the occurrence and development of endometrial carcinoma. *Int J Clin Exp Med*, *11*(5), 4883–4890. Retrieved from www.ijcem.com

Chiang, K., Zielinska, A. E., Shaaban, A. M., Sanchez-Bailon, M. P., Jarrold, J., Clarke, T. L., … Davies, C. C. (2017). PRMT5 Is a Critical Regulator of Breast Cancer Stem Cell Function via Histone Methylation and FOXP1 Expression. *Cell Rep*, *21*, 3498–3513. https://doi.org/10.1016/j.celrep.2017.11.096

Colina, R., Costa-Mattioli, M., Dowling, R. J., Jaramillo, M., Tai, L. H., Breitbach, C. J., … Sonenberg,

N. (2008). Translational control of the innate immune response through IRF-7. *Nature*, *452*, 323–328. https://doi.org/10.1038/nature06730

Comen, E. A. (2012). Tracking the seed and tending the soil: evolving concepts in metastatic breast cancer. *Discovery Medicine*, *14*(75), 97–104. Retrieved from http://www.ncbi.nlm.nih.gov/pubmed/22935206

Cowden Dahl, K. D., Symowicz, J., Ning, Y., Gutierrez, E., Fishman, D. A., Adley, B. P., … Hudson, L. G. (2008). Matrix Metalloproteinase 9 Is a Mediator of Epidermal Growth Factor-Dependent E-Cadherin Loss in Ovarian Carcinoma Cells. *Cancer Research*, *68*(12), 4606–4613. https://doi.org/10.1158/0008-5472.CAN-07-5046

Cunningham, J. T., Pourdehnad, M., Stumpf, C. R., & Ruggero, D. (2013). Investigating Myc-Dependent Translational Regulation in Normal and Cancer Cells. *Methods Mol Biol*, *1012*, 201–212. https://doi.org/10.1007/978-1-62703-429-6_13

Cura, V., Troffer-Charlier, N., Lambert, M. A., Bonnefond, L., & Cavarelli, J. (2014). Cloning, expression, purification and preliminary X-ray crystallographic analysis of mouse protein arginine methyltransferase 7. *Acta Crystallogr F Struct Biol Commun*, *70*, 80–86. https://doi.org/10.1107/S2053230X13032871

Cura, V., Troffer-Charlier, N., Wurtz, J. M., Bonnefond, L., & Cavarelli, J. (2014). Structural insight into arginine methylation by the mouse protein arginine methyltransferase 7: a zinc finger freezes the mimic of the dimeric state into a single active site. *Acta Crystallogr D Biol Crystallogr*, *70*, 2401–2412. https://doi.org/10.1107/S1399004714014278

David, J. M., & Rajasekaran, A. K. (2012). Dishonorable Discharge: The Oncogenic Roles of Cleaved E-Cadherin Fragments. *Cancer Research*, *72*(12), 2917–2923. https://doi.org/10.1158/0008-

5472.CAN-11-3498

Debacq-Chainiaux, F., Erusalimsky, J. D., Campisi, J., & Toussaint, O. (2009). Protocols to detect senescence-associated beta-galactosidase (SA-betagal) activity, a biomarker of senescent cells in culture and in vivo. *Nature Protocols*, *4*(12), 1798–1806. https://doi.org/10.1038/nprot.2009.191

Deribe, Y. L., Pawson, T., & Dikic, I. (2010). Post-translational modifications in signal integration. *Nat Struct Mol Biol*, *17*, 666–672. https://doi.org/10.1038/nsmb.1842

Dhaliwal, S., & Hoffman, D. W. (2003). The Crystal Structure of the N-terminal Region of the Alpha Subunit of Translation Initiation Factor 2 (eIF2α) from Saccharomyces cerevisiae Provides a View of the Loop Containing Serine 51, the Target of the eIF2α-specific Kinases. *Journal of Molecular Biology*, *334*(2), 187–195. https://doi.org/10.1016/J.JMB.2003.09.045

Dhar, S. S., Lee, S. H., Kan, P. Y., Voigt, P., Ma, L., Shi, X., … Lee, M. G. (2012). Trans-tail regulation of MLL4-catalyzed H3K4 methylation by H4R3 symmetric dimethylation is mediated by a tandem PHD of MLL4. *Genes Dev*, *26*, 2749–2762. https://doi.org/10.1101/gad.203356.112

Dhar, S., Vemulapalli, V., Patananan, A. N., Huang, G. L., Di Lorenzo, A., Richard, S., … Bedford, M. T. (2013). Loss of the major Type I arginine methyltransferase PRMT1 causes substrate scavenging by other PRMTs. *Sci Rep*, *3*, 1311. https://doi.org/10.1038/srep01311

Di Cosimo, S., & Baselga, J. (2008). Targeted therapies in breast cancer: Where are we now? *European Journal of Cancer*, *44*(18), 2781–2790. https://doi.org/10.1016/j.ejca.2008.09.026

Dillon, M. B., Rust, H. L., Thompson, P. R., & Mowen, K. A. (2013). Automethylation of protein arginine methyltransferase 8 (PRMT8) regulates activity by impeding S-adenosylmethionine sensitivity. *J Biol Chem*, *288*, 27872–27880. https://doi.org/10.1074/jbc.M113.491092

Dimri, G. P., Lee, X., Basile, G., Acosta, M., Scott, G., Roskelley, C., … Pereira-Smith, O. (1995). A biomarker that identifies senescent human cells in culture and in aging skin in vivo. *Proceedings of the National Academy of Sciences of the United States of America*, *92*(20), 9363–9367. Retrieved from http://www.ncbi.nlm.nih.gov/pubmed/7568133

Duan, G., & Walther, D. (2015). The roles of post-translational modifications in the context of protein interaction networks. *PLoS Computational Biology*, *11*(2), e1004049. https://doi.org/10.1371/journal.pcbi.1004049

Duffy, M. J., Maguire, T. M., Hill, A., McDermott, E., & O'Higgins, N. (2000). Metalloproteinases: role in breast carcinogenesis, invasion and metastasis. *Breast Cancer Research : BCR*, *2*(4), 252–257. Retrieved from http://www.ncbi.nlm.nih.gov/pubmed/11250717

Feng, Y., Hadjikyriacou, A., & Clarke, S. G. (2014). Substrate specificity of human protein arginine methyltransferase 7 (PRMT7): the importance of acidic residues in the double E loop. *J Biol Chem*, *289*, 32604–32616. https://doi.org/10.1074/jbc.M114.609271

Feng, Y., Maity, R., Whitelegge, J. P., Hadjikyriacou, A., Li, Z., Zurita-Lopez, C., … Clarke, S. G. (2013). Mammalian protein arginine methyltransferase 7 (PRMT7) specifically targets RXR sites in lysine- and arginine-rich regions. *J Biol Chem*, *288*, 37010–37025. https://doi.org/10.1074/jbc.M113.525345

Feng, Y., Xie, N., Jin, M., Stahley, M. R., Stivers, J. T., & Zheng, Y. G. (2011). A transient kinetic analysis of PRMT1 catalysis. *Biochemistry*, *50*(32), 7033–7044. https://doi.org/10.1021/bi200456u

Figueira, R. C. S., Gomes, L. R., Neto, J. S., Silva, F. C., Silva, I. D. C. G., & Sogayar, M. C. (2009). Correlation between MMPs and their inhibitors in breast cancer tumor tissue specimens and

in cell lines with different metastatic potential. *BMC Cancer*, *9*, 20. https://doi.org/10.1186/1471-2407-9-20

Fisk, J. C., Sayegh, J., Zurita-Lopez, C., Menon, S., Presnyak, V., Clarke, S. G., & Read, L. K. (2009). A type III protein arginine methyltransferase from the protozoan parasite Trypanosoma brucei. *J Biol Chem*, *284*, 11590–11600. https://doi.org/10.1074/jbc.M807279200

Fournier, M. J., Gareau, C., & Mazroui, R. (2010). The chemotherapeutic agent bortezomib induces the formation of stress granules. *Cancer Cell Int*, *10*, 12. https://doi.org/10.1186/1475-2867-10-12

Gao, G., Dhar, S., & Bedford, M. T. (2017). PRMT5 regulates IRES-dependent translation via methylation of hnRNP A1. *Nucleic Acids Research*, *45*(8), gkw1367. https://doi.org/10.1093/nar/gkw1367

Gao, Y., Zhao, Y., Zhang, J., Lu, Y., Liu, X., Geng, P., … Lu, J. (2016). The dual function of PRMT1 in modulating epithelial-mesenchymal transition and cellular senescence in breast cancer cells through regulation of ZEB1. *Sci Rep*, *6*, 19874. https://doi.org/10.1038/srep19874

Gary, J. D., & Clarke, S. (1998). RNA and Protein Interactions Modulated by Protein Arginine Methylation. *Progress in Nucleic Acid Research and Molecular Biology*, *61*, 65–131. https://doi.org/10.1016/S0079-6603(08)60825-9

Gayatri, S., & Bedford, M. T. (2014). Readers of histone methylarginine marks. *Biochim Biophys Acta*, *1839*, 702–710. https://doi.org/10.1016/j.bbagrm.2014.02.015

Geng, P., Zhang, Y., Liu, X. X., Zhang, N., Liu, Y., Liu, X. X., … Lu, J. (2017). Automethylation of protein arginine methyltransferase 7 and its impact on breast cancer progression. *Faseb J*, *31*(6), 2287–2300. https://doi.org/10.1096/fj.201601196R

Gerlitz, G., Jagus, R., & Elroy-Stein, O. (2002). Phosphorylation of initiation factor-2 alpha is required for activation of internal translation initiation during cell differentiation. *European Journal of Biochemistry*, *269*(11), 2810–2819. Retrieved from http://www.ncbi.nlm.nih.gov/pubmed/12047392

Giannelli, G., Erriquez, R., Fransvea, E., Daniele, A., Trerotoli, P., Schittulli, F., … Antonaci, S. (2004). Proteolytic imbalance is reversed after therapeutic surgery in breast cancer patients. *International Journal of Cancer*, *109*(5), 782–785. https://doi.org/10.1002/ijc.20009

Gonsalvez, G. B., Tian, L., Ospina, J. K., Boisvert, F. M., Lamond, A. I., & Matera, A. G. (2007). Two distinct arginine methyltransferases are required for biogenesis of Sm-class ribonucleoproteins. *J Cell Biol*, *178*, 733–740. https://doi.org/10.1083/jcb.200702147

Goulet, I., Boisvenue, S., Mokas, S., Mazroui, R., & Cote, J. (2008). TDRD3, a novel Tudor domain-containing protein, localizes to cytoplasmic stress granules. *Hum Mol Genet*, *17*, 3055–3074. https://doi.org/10.1093/hmg/ddn203

Goulet, I., Boisvenue, S., Mokas, S., Mazroui, R., & Cote, J. (2008). TDRD3, a novel Tudor domain-containing protein, localizes to cytoplasmic stress granules. *Human Molecular Genetics*, *17*(19), 3055–3074. https://doi.org/10.1093/hmg/ddn203

Goulet, I., Gauvin, G., Boisvenue, S., & Côté, J. (2007). Alternative Splicing Yields Protein Arginine Methyltransferase 1 Isoforms with Distinct Activity, Substrate Specificity, and Subcellular Localization. *Journal of Biological Chemistry*, *282*(45), 33009–33021. https://doi.org/10.1074/jbc.M704349200

Graber, T. E., & Holcik, M. (2007). Cap-independent regulation of gene expression in apoptosis. *Molecular BioSystems*, *3*(12), 825. https://doi.org/10.1039/b708867a

Gros, L., Delaporte, C., Frey, S., Decesse, J., de Saint-Vincent, B. R., Cavarec, L., … Jacquemin-Sablon, A. (2003). Identification of new drug sensitivity genes using genetic suppressor elements: protein arginine N-methyltransferase mediates cell sensitivity to DNA-damaging agents. *Cancer Res*, *63*, 164–171. Retrieved from internal-pdf://217.215.157.54/Gros-1.pdf internal-pdf://1960848155/Bleibel.pdf

Gros, L., Renodon-Corniere, A., de Saint Vincent, B. R., Feder, M., Bujnicki, J. M., & Jacquemin-Sablon, A. (2006). Characterization of prmt7alpha and beta isozymes from Chinese hamster cells sensitive and resistant to topoisomerase II inhibitors. *Biochim Biophys Acta*, *1760*, 1646–1656. https://doi.org/10.1016/j.bbagen.2006.08.026

Guo, A., Gu, H., Zhou, J., Mulhern, D., Wang, Y., Lee, K. A., … Comb, M. J. (2014). Immunoaffinity Enrichment and Mass Spectrometry Analysis of Protein Methylation. *Mol Cell Proteomics*, *13*, 372–387. https://doi.org/10.1074/mcp.O113.027870

Guo, L., Chi, Y., Xue, J., Ma, L., Shao, Z., & Wu, J. (2017). Phosphorylated eIF2alpha predicts disease-free survival in triple-negative breast cancer patients. *Sci Rep*, *7*, 44674. https://doi.org/10.1038/srep44674

Haghandish, N., & Côté, J. (2016). The Role of Histone Mark Writers in Chromatin Signaling: Protein Arginine Methyltransferases. In O. B. and M. E. Fernandez-Zapico (Ed.), *Chromatin Signaling and Diseases* (pp. 55–74). Oxford: Elsevier.

Hallett, M. A., Teng, B., Hasegawa, H., Schwab, L. P., Seagroves, T. N., & Pourmotabbed, T. (2013). Anti-matrix metalloproteinase-9 DNAzyme decreases tumor growth in the MMTV-PyMT mouse model of breast cancer. *Breast Cancer Research : BCR*, *15*(1), R12. https://doi.org/10.1186/bcr3385

Hanahan, D., & Weinberg, R. A. (2000). The hallmarks of cancer. *Cell*, *100*, 57–70.

Hanahan, D., & Weinberg, R. A. (2011). Hallmarks of cancer: the next generation. *Cell*, *144*, 646–674. https://doi.org/10.1016/j.cell.2011.02.013

Harding, H. P., Zhang, Y., Bertolotti, A., Zeng, H., & Ron, D. (2000). Perk is essential for translational regulation and cell survival during the unfolded protein response. *Molecular Cell*, *5*(5), 897–904. Retrieved from http://www.ncbi.nlm.nih.gov/pubmed/10882126

Hasegawa, M., Toma-Fukai, S., Kim, J.-D. D., Fukamizu, A., & Shimizu, T. (2014). Protein arginine methyltransferase 7 has a novel homodimer-like structure formed by tandem repeats. *FEBS Lett*, *588*(10), 1942–1948. https://doi.org/10.1016/j.febslet.2014.03.053

Herrmann, F., Pably, P., Eckerich, C., Bedford, M. T., & Fackelmayer, F. O. (2009). Human protein arginine methyltransferases in vivo--distinct properties of eight canonical members of the PRMT family. *J Cell Sci*, *122*(5), 667–677. https://doi.org/10.1242/jcs.039933

Hofweber, M., Hutten, S., Bourgeois, B., Spreitzer, E., Niedner-Boblenz, A., Schifferer, M., … Dormann, D. (2018). Phase Separation of FUS Is Suppressed by Its Nuclear Import Receptor and Arginine Methylation. *Cell*, *173*(3), 706–719.e13. https://doi.org/10.1016/J.CELL.2018.03.004

Holcik, M. (2015). Could the eIF2α-Independent Translation Be the Achilles Heel of Cancer? *Frontiers in Oncology*, *5*, 264. https://doi.org/10.3389/fonc.2015.00264

Holcik, M., & Sonenberg, N. (2005). Translational control in stress and apoptosis. *Nat Rev Mol Cell Biol*, *6*, 318–327. https://doi.org/10.1038/nrm1618

Hsu, J. H.-R., Hubbell-Engler, B., Adelmant, G., Huang, J., Joyce, C. E., Vazquez, F., … Orkin, S. H. (2017). PRMT1-Mediated Translation Regulation Is a Crucial Vulnerability of Cancer. *Cancer*

Research, *77*(17), 4613–4625. https://doi.org/10.1158/0008-5472.CAN-17-0216

Iorns, E., Drews-Elger, K., Ward, T. M., Dean, S., Clarke, J., Berry, D., … Lippman, M. (2012). A new mouse model for the study of human breast cancer metastasis. *PloS One*, *7*(10), e47995. https://doi.org/10.1371/journal.pone.0047995

Iurlaro, R., Leon-Annicchiarico, C. L., & Munoz-Pinedo, C. (2014). Regulation of cancer metabolism by oncogenes and tumor suppressors. *Methods Enzymol*, *542*, 59–80. https://doi.org/10.1016/b978-0-12-416618-9.00003-0

Jackson, R. J., Hellen, C. U., & Pestova, T. V. (2010). The mechanism of eukaryotic translation initiation and principles of its regulation. *Nat Rev Mol Cell Biol*, *11*, 113–127. https://doi.org/10.1038/nrm2838

Jahan, S., & Davie, J. R. (2014). Protein arginine methyltransferases (PRMTs): Role in chromatin organization. *Adv Biol Regul*. https://doi.org/10.1016/j.jbior.2014.09.003

Jain, K., Jin, C. Y., & Clarke, S. G. (2017). Epigenetic control via allosteric regulation of mammalian protein arginine methyltransferases. *Proc Natl Acad Sci U S A*, *114*(38), 10101–10106. https://doi.org/10.1073/pnas.1706978114

Jelinic, P., Stehle, J. C., & Shaw, P. (2006). The testis-specific factor CTCFL cooperates with the protein methyltransferase PRMT7 in H19 imprinting control region methylation. *PLoS Biol*, *4*, e355. https://doi.org/10.1371/journal.pbio.0040355

Jeong, H. J., Lee, H. J., Vuong, T. A., Choi, K. S., Choi, D., Koo, S. H., … Kang, J. S. (2016). Prmt7 Deficiency Causes Reduced Skeletal Muscle Oxidative Metabolism and Age-Related Obesity. *Diabetes*, *65*, 1868–1882. https://doi.org/10.2337/db15-1500

Jin, H., & Zangar, R. C. (2009). Protein Modifications as Potential Biomarkers in Breast Cancer.

Biomark Insights, *4*, 191–200.

Jung, G. A., Shin, B. S., Jang, Y. S., Sohn, J. B., Woo, S. R., Kim, J. E., … Park, G. H. (2011). Methylation of eukaryotic elongation factor 2 induced by basic fibroblast growth factor via mitogen-activated protein kinase. *Exp Mol Med*, *43*, 550–560. https://doi.org/10.3858/emm.2011.43.10.061

Kaehler, C., Isensee, J., Hucho, T., Lehrach, H., & Krobitsch, S. (2014). 5-Fluorouracil affects assembly of stress granules based on RNA incorporation. *Nucleic Acids Research*, *42*(10), 6436–6447. https://doi.org/10.1093/nar/gku264

Kalluri, R., & Weinberg, R. A. (2009). The basics of epithelial-mesenchymal transition. *The Journal of Clinical Investigation*, *119*(6), 1420–1428. https://doi.org/10.1172/JCI39104

Kao, J., Salari, K., Bocanegra, M., Choi, Y.-L., Girard, L., Gandhi, J., … Pollack, J. R. (2009). Molecular Profiling of Breast Cancer Cell Lines Defines Relevant Tumor Models and Provides a Resource for Cancer Gene Discovery. *PLoS ONE*, *4*(7), e6146. https://doi.org/10.1371/journal.pone.0006146

Karkhanis, V., Wang, L., Tae, S., Hu, Y. J., Imbalzano, A. N., & Sif, S. (2012). Protein arginine methyltransferase 7 regulates cellular response to DNA damage by methylating promoter histones H2A and H4 of the polymerase delta catalytic subunit gene, POLD1. *J Biol Chem*, *287*, 29801–29814. https://doi.org/10.1074/jbc.M112.378281

Kashiwagi, K., Ito, T., & Yokoyama, S. (2017). Crystal structure of eIF2B and insights into eIF2-eIF2B interactions. *The FEBS Journal*, *284*(6), 868–874. https://doi.org/10.1111/febs.13896

Kato, Y., Yamashita, T., & Ishikawa, M. (2002). Relationship between expression of matrix metalloproteinase-2 and matrix metalloproteinase-9 and invasion ability of cervical cancer

cells. *Oncology Reports*. https://doi.org/10.3892/or.9.3.565

Kedersha, N., Stoecklin, G., Ayodele, M., Yacono, P., Lykke-Andersen, J., Fritzler, M. J., … Anderson, P. (2005). Stress granules and processing bodies are dynamically linked sites of mRNP remodeling. *The Journal of Cell Biology*, *169*(6), 871–884. https://doi.org/10.1083/jcb.200502088

Kernohan, K. D., McBride, A., Xi, Y., Martin, N., Schwartzentruber, J., Dyment, D. A., … Chitayat, D. (2017). Loss of the arginine methyltranserase PRMT7 causes syndromic intellectual disability with microcephaly and brachydactyly. *Clinical Genetics*, *91*(5), 708–716. https://doi.org/10.1111/cge.12884

Kessenbrock, K., Plaks, V., & Werb, Z. (2010). Matrix metalloproteinases: regulators of the tumor microenvironment. *Cell*, *141*(1), 52–67. https://doi.org/10.1016/j.cell.2010.03.015

Kevil, C. G., De Benedetti, A., Payne, D. K., Coe, L. L., Laroux, F. S., & Alexander, J. S. (1996). Translational regulation of vascular permeability factor by eukaryotic initiation factor 4E: implications for tumor angiogenesis. *Int J Cancer*, *65*, 785–790. https://doi.org/10.1002/(sici)1097-0215(19960315)65:6<785::aid-ijc14>3.0.co;2-3

Khan, S. A., Reddy, D., & Gupta, S. (2015). Global histone post-translational modifications and cancer: Biomarkers for diagnosis, prognosis and treatment? *World J Biol Chem*, *6*, 333–345. https://doi.org/10.4331/wjbc.v6.i4.333

Kim, K. Y., Wang, D. H., Campbell, M., Huerta, S. B., Shevchenko, B., Izumiya, C., & Izumiya, Y. (2015). PRMT4-Mediated Arginine Methylation Negatively Regulates Retinoblastoma Tumor Suppressor Protein and Promotes E2F-1 Dissociation. *Mol Cell Biol*, *35*, 238–248. https://doi.org/10.1128/mcb.00945-14

Klausner, R. D. (2002). The fabric of cancer cell biology-Weaving together the strands. *Cancer Cell*, *1*, 3–10.

Kleinschmidt, M. A., Streubel, G., Samans, B., Krause, M., & Bauer, U. M. (2008). The protein arginine methyltransferases CARM1 and PRMT1 cooperate in gene regulation. *Nucleic Acids Res*, *36*, 3202–3213. https://doi.org/10.1093/nar/gkn166

Kohn, E. C., Alessandro, R., Spoonster, J., Wersto, R. P., & Liotta, L. A. (1995). Angiogenesis: role of calcium-mediated signal transduction. *Proc Natl Acad Sci U S A*, *92*(5), 1307–1311. https://doi.org/10.1073/PNAS.92.5.1307

Köhrmann, A., Kammerer, U., Kapp, M., Dietl, J., & Anacker, J. (2009). Expression of matrix metalloproteinases (MMPs) in primary human breast cancer and breast cancer cell lines: New findings and review of the literature. *BMC Cancer*, *9*(1), 188. https://doi.org/10.1186/1471-2407-9-188

Komar, A. A., & Hatzoglou, M. (2011). Cellular IRES-mediated translation: the war of ITAFs in pathophysiological states. *Cell Cycle (Georgetown, Tex.)*, *10*(2), 229–240. https://doi.org/10.4161/cc.10.2.14472

Kuhn, P., Chumanov, R., Wang, Y., Ge, Y., Burgess, R. R., & Xu, W. (2011). Automethylation of CARM1 allows coupling of transcription and mRNA splicing. *Nucleic Acids Research*, *39*(7), 2717–2726. https://doi.org/10.1093/nar/gkq1246

Lacroix, M., & Leclercq, G. (2004). Relevance of Breast Cancer Cell Lines as Models for Breast Tumours: An Update. *Breast Cancer Research and Treatment*, *83*(3), 249–289. https://doi.org/10.1023/B:BREA.0000014042.54925.cc

Lakowski, T. M., & Frankel, A. (2009). Kinetic analysis of human protein arginine N-

methyltransferase 2: formation of monomethyl- and asymmetric dimethyl-arginine residues on histone H4. *Biochem J*, *421*, 253–261. https://doi.org/10.1042/bj20090268

Larivière, N., Law, J., & Trinkle-Mulcahy, L. (2014). Dissection of a Novel Autocrine Signaling Pathway via Quantitative Secretome and Interactome Mapping. *Journal of Proteome Research*, *13*, 3432–3443. https://doi.org/10.1021/pr500392m

Larsson, O., Li, S., Issaenko, O. A., Avdulov, S., Peterson, M., Smith, K., … Polunovsky, V. A. (2007). Eukaryotic translation initiation factor 4E induced progression of primary human mammary epithelial cells along the cancer pathway is associated with targeted translational deregulation of oncogenic drivers and inhibitors. *Cancer Res*, *67*, 6814–6824. https://doi.org/10.1158/0008-5472.can-07-0752

Le Romancer, M., Treilleux, I., Leconte, N., Robin-Lespinasse, Y., Sentis, S., Bouchekioua-Bouzaghou, K., … Corbo, L. (2008). Regulation of Estrogen Rapid Signaling through Arginine Methylation by PRMT1. *Molecular Cell*, *31*, 212–221. https://doi.org/10.1016/j.molcel.2008.05.025

Lee, J. H., Cook, J. R., Yang, Z. H., Mirochnitchenko, O., Gunderson, S. I., Felix, A. M., … Pestka, S. (2005). PRMT7, a new protein arginine methyltransferase that synthesizes symmetric dimethylarginine. *J Biol Chem*, *280*, 3656–3664. https://doi.org/10.1074/jbc.M405295200

Leiper, J., & Nandi, M. (2011). The therapeutic potential of targeting endogenous inhibitors of nitric oxide synthesis. *Nat Rev Drug Discov*, *10*, 277–291. https://doi.org/10.1038/nrd3358

Levy, A. T., Cioce, V., Sobel, M. E., Garbisa, S., Grigioni, W. F., Liotta, L. A., & Stetler-Stevenson, W. G. (1991). Increased expression of the Mr 72,000 type IV collagenase in human colonic adenocarcinoma. *Cancer Res*, *51*(1), 439–444. Retrieved from

http://www.ncbi.nlm.nih.gov/pubmed/1846313

Li, H., Cao, D., Liu, Y., Hou, Y., Wu, J., Lu, J., … Shao, Z. (2004). Prognostic value of matrix metalloproteinases (MMP-2 and MMP-9) in patients with lymph node-negative breast carcinoma. *Breast Cancer Research and Treatment*, *88*(1), 75–85. https://doi.org/10.1007/s10549-004-1200-8

Linder, B., Plöttner, O., Kroiss, M., Hartmann, E., Laggerbauer, B., Meister, G., … Fischer, U. (2008). Tdrd3 is a novel stress granule-associated protein interacting with the Fragile-X syndrome protein FMRP. *Human Molecular Genetics*, *17*(20), 3236–3246. https://doi.org/10.1093/hmg/ddn219

Ma, Z., Shah, R. C., Chang, M. J., & Benveniste, E. N. (2004). Coordination of cell signaling, chromatin remodeling, histone modifications, and regulator recruitment in human matrix metalloproteinase 9 gene transcription. *Mol Cell Biol*, *24*, 5496–5509. https://doi.org/10.1128/mcb.24.12.5496-5509.2004

Machesky, L. M. (2008). Lamellipodia and filopodia in metastasis and invasion. *FEBS Letters*, *582*(14), 2102–2111. https://doi.org/10.1016/j.febslet.2008.03.039

Majumder, S., Alinari, L., Roy, S., Miller, T., Datta, J., Sif, S., … Jacob, S. T. (2010). Methylation of histone H3 and H4 by PRMT5 regulates ribosomal RNA gene transcription. *J Cell Biochem*, *109*, 553–563. https://doi.org/10.1002/jcb.22432

Mann, M., & Jensen, O. N. (2003). Proteomic analysis of post-translational modifications. *Nat Biotechnol*, *21*, 255–261. https://doi.org/10.1038/nbt0303-255

Martin-Kleiner, I. (2012). BORIS in human cancers -- a review. *Eur J Cancer*, *48*, 929–935. https://doi.org/10.1016/j.ejca.2011.09.009

McEwen, E., Kedersha, N., Song, B., Scheuner, D., Gilks, N., Han, A., … Kaufman, R. J. (2005). Heme-regulated Inhibitor Kinase-mediated Phosphorylation of Eukaryotic Translation Initiation Factor 2 Inhibits Translation, Induces Stress Granule Formation, and Mediates Survival upon Arsenite Exposure. *Journal of Biological Chemistry*, *280*(17), 16925–16933. https://doi.org/10.1074/jbc.M412882200

Mehner, C., Hockla, A., Miller, E., Ran, S., Radisky, D. C., & Radisky, E. S. (2014). Tumor cell-produced matrix metalloproteinase 9 (MMP-9) drives malignant progression and metastasis of basal-like triple negative breast cancer. *Oncotarget*, *5*(9), 2736–2749. https://doi.org/10.18632/oncotarget.1932

Mielke, N., Schwarzer, R., Calkhoven, C. F., Kaufman, R. J., Dörken, B., Leutz, A., & Jundt, F. (2011). Eukaryotic initiation factor 2alpha phosphorylation is required for B-cell maturation and function in mice. *Haematologica*, *96*(9), 1261–1268. https://doi.org/10.3324/haematol.2011.042853

Migliori, V., Muller, J., Phalke, S., Low, D., Bezzi, M., Mok, W. C., … Guccione, E. (2012). Symmetric dimethylation of H3R2 is a newly identified histone mark that supports euchromatin maintenance. *Nat Struct Mol Biol*, *19*, 136–144. https://doi.org/10.1038/nsmb.2209

Mira, E., Lacalle, R. A., Buesa, J. M., de Buitrago, G. G., Jiménez-Baranda, S., Gómez-Moutón, C., … Mañes, S. (2004). Secreted MMP9 promotes angiogenesis more efficiently than constitutive active MMP9 bound to the tumor cell surface. *Journal of Cell Science*, *117*(9), 1847–1857. https://doi.org/10.1242/jcs.01035

Miranda, T. B., Miranda, M., Frankel, A., & Clarke, S. (2004). PRMT7 is a member of the protein arginine methyltransferase family with a distinct substrate specificity. *J Biol Chem*, *279*, 22902–22907. https://doi.org/10.1074/jbc.M312904200

Miyata, S., Mori, Y., & Tohyama, M. (2010). PRMT3 is essential for dendritic spine maturation in rat hippocampal neurons. *Brain Research*, *1352*, 11–20. https://doi.org/10.1016/j.brainres.2010.07.033

Moeller, B. J., & Dewhirst, M. W. (2006). HIF-1 and tumour radiosensitivity. *Br J Cancer*, *95*, 1–5. https://doi.org/10.1038/sj.bjc.6603201

Moffat, J., Grueneberg, D. A., Yang, X., Kim, S. Y., Kloepfer, A. M., Hinkle, G., … Root, D. E. (2006). A Lentiviral RNAi Library for Human and Mouse Genes Applied to an Arrayed Viral High-Content Screen. *Cell*, *124*(6), 1283–1298. https://doi.org/10.1016/j.cell.2006.01.040

Monteagudo, C., Merino, M. J., San-Juan, J., Liotta, L. A., & Stetler-Stevenson, W. G. (1990). Immunohistochemical distribution of type IV collagenase in normal, benign, and malignant breast tissue. *Am J Pathol*, *136*(3), 585–592. Retrieved from http://www.ncbi.nlm.nih.gov/pubmed/2156430

Muaddi, H., Majumder, M., Peidis, P., Papadakis, A. I., Holcik, M., & Scheuner, D. (2010). Phosphorylation of eIF2alpha at serine 51 is an important determinant of cell survival and adaptation to glucose deficiency. *Mol Biol Cell*, *21*, 3220–3231.

Nagase, H., & Woessner, J. F. (1999). Matrix metalloproteinases. *The Journal of Biological Chemistry*, *274*(31), 21491–21494. Retrieved from http://www.ncbi.nlm.nih.gov/pubmed/10419448

Nakakido, M., Deng, Z., Suzuki, T., Dohmae, N., Nakamura, Y., & Hamamoto, R. (2015). PRMT6 increases cytoplasmic localization of p21CDKN1A in cancer cells through arginine methylation and makes more resistant to cytotoxic agents. *Oncotarget*, *6*, 30957–30967. https://doi.org/10.18632/oncotarget.5143

Nannuru, K. C., Futakuchi, M., Varney, M. L., Vincent, T. M., Marcusson, E. G., & Singh, R. K. (2010). Matrix Metalloproteinase (MMP)-13 Regulates Mammary Tumor-Induced Osteolysis by Activating MMP9 and Transforming Growth Factor- Signaling at the Tumor-Bone Interface. *Cancer Research*, *70*(9), 3494–3504. https://doi.org/10.1158/0008-5472.CAN-09-3251

Nawrocki-Raby, B., Gilles, C., Polette, M., Bruyneel, E., Laronze, J.-Y., Bonnet, N., … Birembaut, P. (2003). Upregulation of MMPs by soluble E-cadherin in human lung tumor cells. *International Journal of Cancer*, *105*(6), 790–795. https://doi.org/10.1002/ijc.11168

Nawrocki-Raby, B., Gilles, C., Polette, M., Martinella-Catusse, C., Bonnet, N., Puchelle, E., … Birembaut, P. (2003). E-Cadherin Mediates MMP Down-Regulation in Highly Invasive Bronchial Tumor Cells. *The American Journal of Pathology*, *163*(2), 653–661. https://doi.org/10.1016/S0002-9440(10)63692-9

Neault, M., Mallette, F. A., Vogel, G., Michaud-Levesque, J., & Richard, S. (2012). Ablation of PRMT6 reveals a role as a negative transcriptional regulator of the p53 tumor suppressor. *Nucleic Acids Res*, *40*, 9513–9521. https://doi.org/10.1093/nar/gks764

Nguyen, D. X., Bos, P. D., & Massagué, J. (2009). Metastasis: from dissemination to organ-specific colonization. *Nature Reviews. Cancer*, *9*(4), 274–284. https://doi.org/10.1038/nrc2622

Ohkura, N., Takahashi, M., Yaguchi, H., Nagamura, Y., & Tsukada, T. (2005). Coactivator-associated arginine methyltransferase 1, CARM1, affects pre-mRNA splicing in an isoform-specific manner. *The Journal of Biological Chemistry*, *280*(32), 28927–28935. https://doi.org/10.1074/jbc.M502173200

Ohn, T., & Anderson, P. (2010). The role of posttranslational modifications in the assembly of stress granules. *Wiley Interdiscip Rev RNA*, *1*, 486–493. https://doi.org/10.1002/wrna.23

Orlichenko, L. S., & Radisky, D. C. (2008). Matrix metalloproteinases stimulate epithelial-mesenchymal transition during tumor development. *Clinical & Experimental Metastasis*, *25*(6), 593–600. https://doi.org/10.1007/s10585-008-9143-9

Panas, M. D., Ivanov, P., & Anderson, P. (2016). Mechanistic insights into mammalian stress granule dynamics. *The Journal of Cell Biology*, *215*(3), 313–323. https://doi.org/10.1083/jcb.201609081

Pelletier, J., Graff, J., Ruggero, D., & Sonenberg, N. (2015). Targeting the eIF4F translation initiation complex: a critical nexus for cancer development. *Cancer Research*, *75*(2), 250–263. https://doi.org/10.1158/0008-5472.CAN-14-2789

Pellikainen, J. M., Ropponen, K. M., Kataja, V. V, Kellokoski, J. K., Eskelinen, M. J., & Kosma, V.-M. (2004). Expression of Matrix Metalloproteinase (MMP)-2 and MMP-9 in Breast Cancer with a Special Reference to Activator Protein-2, HER2, and Prognosis. *Clinical Cancer Research*, *10*(22), 7621–7628. https://doi.org/10.1158/1078-0432.CCR-04-1061

Pestova, T. V, de Breyne, S., Pisarev, A. V, Abaeva, I. S., & Hellen, C. U. T. (2008). eIF2-dependent and eIF2-independent modes of initiation on the CSFV IRES: a common role of domain II. *The EMBO Journal*, *27*(7), 1060–1072. https://doi.org/10.1038/emboj.2008.49

Polunovsky, V. A., Rosenwald, I. B., Tan, A. T., White, J., Chiang, L., Sonenberg, N., & Bitterman, P. B. (1996). Translational control of programmed cell death: eukaryotic translation initiation factor 4E blocks apoptosis in growth-factor-restricted fibroblasts with physiologically expressed or deregulated Myc. *Mol Cell Biol*, *16*, 6573–6581.

Qamar, S., Wang, G., Randle, S. J., Ruggeri, F. S., Varela, J. A., Lin, J. Q., … St George-Hyslop, P. (2018). FUS Phase Separation Is Modulated by a Molecular Chaperone and Methylation of

Arginine Cation-π Interactions. *Cell*, *173*(3), 720–734.e15. https://doi.org/10.1016/J.CELL.2018.03.056

Rajesh, K., Krishnamoorthy, J., Kazimierczak, U., Tenkerian, C., Papadakis, A. I., Wang, S., … Koromilas, A. E. (2015). Phosphorylation of the translation initiation factor eIF2alpha at serine 51 determines the cell fate decisions of Akt in response to oxidative stress. *Cell Death Dis*, *6*(1), e1591. https://doi.org/10.1038/cddis.2014.554

Rao, J. S., Gondi, C., Chetty, C., Chittivelu, S., Joseph, P. A., & Lakka, S. S. (2005). Inhibition of invasion, angiogenesis, tumor growth, and metastasis by adenovirus-mediated transfer of antisense uPAR and MMP-9 in non-small cell lung cancer cells. *Molecular Cancer Therapeutics*, *4*(9), 1399–1408. https://doi.org/10.1158/1535-7163.MCT-05-0082

Robert, F., Kapp, L. D., Khan, S. N., Acker, M. G., Kolitz, S., Kazemi, S., … Pelletier, J. (2006). Initiation of protein synthesis by hepatitis C virus is refractory to reduced eIF2.GTP.Met-tRNA(i)(Met) ternary complex availability. *Molecular Biology of the Cell*, *17*(11), 4632–4644. https://doi.org/10.1091/mbc.E06-06-0478

Rosenwald, I. B., Wang, S., Savas, L., Woda, B., & Pullman, J. (2003). Expression of translation initiation factor eIF-2alpha is increased in benign and malignant melanocytic and colonic epithelial neoplasms. *Cancer*, *98*, 1080–1088. https://doi.org/10.1002/cncr.11619

Roskoski, R. (2012). ERK1/2 MAP kinases: Structure, function, and regulation. *Pharmacological Research*, *66*(2), 105–143. https://doi.org/10.1016/j.phrs.2012.04.005

Ruggero, D. (2013). Translational control in cancer etiology. *Cold Spring Harb Perspect Biol*, *5*. https://doi.org/10.1101/cshperspect.a012336

Schurter, B. T., Koh, S. S., Chen, D., Bunick, G. J., Harp, J. M., Hanson, B. L., … Aswad, D. W. (2001).

Methylation of histone H3 by coactivator-associated arginine methyltransferase 1. *Biochemistry*, *40*, 5747–5756.

Silvera, D., Formenti, S. C., & Schneider, R. J. (2010). Translational control in cancer. *Nat Rev Cancer*, *10*, 254–266. https://doi.org/10.1038/nrc2824

Singhroy, D. N., Mesplede, T., Sabbah, A., Quashie, P. K., Falgueyret, J. P., & Wainberg, M. A. (2013). Automethylation of protein arginine methyltransferase 6 (PRMT6) regulates its stability and its anti-HIV-1 activity. *Retrovirology*, *10*, 73. https://doi.org/10.1186/1742-4690-10-73

Smil, D., Eram, M. S., Li, F., Kennedy, S., Szewczyk, M. M., Brown, P. J., … Schapira, M. (2015). Discovery of a Dual PRMT5-PRMT7 Inhibitor. *ACS Med Chem Lett*, *6*, 408–412. https://doi.org/10.1021/ml500467h

Srivastava, S. P., Kumar, K. U., & Kaufman, R. J. (1998). Phosphorylation of eukaryotic translation initiation factor 2 mediates apoptosis in response to activation of the double-stranded RNA-dependent protein kinase. *The Journal of Biological Chemistry*, *273*(4), 2416–2423. https://doi.org/10.1074/JBC.273.4.2416

SWIERCZ, R., PERSON, M. D., & BEDFORD, M. T. (2005). Ribosomal protein S2 is a substrate for mammalian PRMT3 (protein arginine methyltransferase 3). *Biochemical Journal*, *386*(1), 85–91. https://doi.org/10.1042/BJ20041466

Symowicz, J., Adley, B. P., Gleason, K. J., Johnson, J. J., Ghosh, S., Fishman, D. A., … Stack, M. S. (2007). Engagement of Collagen-Binding Integrins Promotes Matrix Metalloproteinase-9-Dependent E-Cadherin Ectodomain Shedding in Ovarian Carcinoma Cells. *Cancer Research*, *67*(5), 2030–2039. https://doi.org/10.1158/0008-5472.CAN-06-2808

Tae, S., Karkhanis, V., Velasco, K., Yaneva, M., Erdjument-Bromage, H., Tempst, P., & Sif, S. (2011). Bromodomain protein 7 interacts with PRMT5 and PRC2, and is involved in transcriptional repression of their target genes. *Nucleic Acids Res*, *39*, 5424–5438. https://doi.org/10.1093/nar/gkr170

Tenkerian, C., Krishnamoorthy, J., Mounir, Z., Kazimierczak, U., Khoutorsky, A., Staschke, K. A., … Koromilas, A. E. (2015). mTORC2 Balances AKT Activation and eIF2alpha Serine 51 Phosphorylation to Promote Survival under Stress. *Mol Cancer Res*, *13*(10), 1377–1388. https://doi.org/10.1158/1541-7786.mcr-15-0184-t

Thandapani, P., Song, J., Gandin, V., Cai, Y., Rouleau, S. G., Garant, J.-M., … Richard, S. (2015). Aven recognition of RNA G-quadruplexes regulates translation of the mixed lineage leukemia protooncogenes. *ELife*, *4*, e06234. https://doi.org/10.7554/eLife.06234

Thomassen, M., Tan, Q., & Kruse, T. A. (2009). Gene expression meta-analysis identifies chromosomal regions and candidate genes involved in breast cancer metastasis. *Breast Cancer Res Treat*, *113*, 239–249. https://doi.org/10.1007/s10549-008-9927-2

Thompson, P. R., & Fast, W. (2006). Histone citrullination by protein arginine deiminase: is arginine methylation a green light or a roadblock? *ACS Chem Biol*, *1*(7), 433–441. https://doi.org/10.1021/cb6002306

Tradewell, M. L., Yu, Z., Tibshirani, M., Boulanger, M. C., Durham, H. D., & Richard, S. (2012). Arginine methylation by PRMT1 regulates nuclear-cytoplasmic localization and toxicity of FUS/TLS harbouring ALS-linked mutations. *Hum Mol Genet*, *21*, 136–149. https://doi.org/10.1093/hmg/ddr448

Trinkle-Mulcahy, L., Boulon, S., Lam, Y. W., Urcia, R., Boisvert, F.-M., Vandermoere, F., … Lamond,

A. (2008). Identifying specific protein interaction partners using quantitative mass spectrometry and bead proteomes. *The Journal of Cell Biology*, *183*, 223–239. https://doi.org/10.1083/jcb.200805092

Tsai, W.-C., Gayatri, S., Reineke, L. C., Sbardella, G., Bedford, M. T., & Lloyd, R. E. (2016). Arginine Demethylation of G3BP1 Promotes Stress Granule Assembly. *Journal of Biological Chemistry*, *291*(43), 22671–22685. https://doi.org/10.1074/jbc.M116.739573

Tsai, W. C., Reineke, L. C., Jain, A., Jung, S. Y., & Lloyd, R. E. (2017). Histone arginine demethylase JMJD6 is linked to stress granule assembly through demethylation of the stress granule nucleating protein G3BP1. *J Biol Chem*. https://doi.org/10.1074/jbc.M117.800706

Tweedie-Cullen, R. Y., Brunner, A. M., Grossmann, J., Mohanna, S., Sichau, D., Nanni, P., … Mansuy, I. M. (2012). Identification of combinatorial patterns of post-translational modifications on individual histones in the mouse brain. *PLoS One*, *7*, e36980. https://doi.org/10.1371/journal.pone.0036980

van Roy, F., & Berx, G. (2008). The cell-cell adhesion molecule E-cadherin. *Cell Mol Life Sci*, *65*, 3756–3788. https://doi.org/10.1007/s00018-008-8281-1

Vattem, K. M., & Wek, R. C. (2004). Reinitiation involving upstream ORFs regulates ATF4 mRNA translation in mammalian cells. *Proceedings of the National Academy of Sciences of the United States of America*, *101*(31), 11269–11274. https://doi.org/10.1073/pnas.0400541101

Verbiest, V., Montaudon, D., Tautu, M. T., Moukarzel, J., Portail, J. P., Markovits, J., … Pourquier, P. (2008). Protein arginine (N)-methyl transferase 7 (PRMT7) as a potential target for the sensitization of tumor cells to camptothecins. *FEBS Lett*, *582*, 1483–1489.

https://doi.org/10.1016/j.febslet.2008.03.031

Vivanco, I., & Sawyers, C. L. (2002). The phosphatidylinositol 3-Kinase AKT pathway in human cancer. *Nature Reviews. Cancer*, *2*(7), 489–501. https://doi.org/10.1038/nrc839

Vizoso, F. J., González, L. O., Corte, M. D., Rodríguez, J. C., Vázquez, J., Lamelas, M. L., … García-Muñiz, J. L. (2007). Study of matrix metalloproteinases and their inhibitors in breast cancer. *British Journal of Cancer*, *96*(6), 903–911. https://doi.org/10.1038/sj.bjc.6603666

Walport, L. J., Hopkinson, R. J., & Chowdhury, R. (2016). Arginine demethylation is catalysed by a subset of JmjC histone lysine demethylases, *7*, 11974. https://doi.org/10.1038/ncomms11974

Wang, L., Charoensuksai, P., Watson, N. J., Wang, X., Zhao, Z., Coriano, C. G., … Xu, W. (2013). CARM1 automethylation is controlled at the level of alternative splicing. *Nucleic Acids Res*, *41*(14), 6870–6880. https://doi.org/10.1093/nar/gkt415

Wang, S., Lloyd, R. V, Hutzler, M. J., Rosenwald, I. B., Safran, M. S., Patwardhan, N. A., & Khan, A. (2001). Expression of eukaryotic translation initiation factors 4E and 2alpha correlates with the progression of thyroid carcinoma. *Thyroid*, *11*, 1101–1107. https://doi.org/10.1089/10507250152740939

Wang, S., Rosenwald, I. B., Hutzler, M. J., Pihan, G. A., Savas, L., Chen, J. J., & Woda, B. A. (1999). Expression of the eukaryotic translation initiation factors 4E and 2alpha in non-Hodgkin's lymphomas. *Am J Pathol*, *155*, 247–255.

Wang, X., Lu, H., Urvalek, A. M., Li, T., Yu, L., Lamar, J., … Zhao, J. (2011). KLF8 promotes human breast cancer cell invasion and metastasis by transcriptional activation of MMP9. *Oncogene*, *30*(16), 1901–1911. https://doi.org/10.1038/onc.2010.563

Weigelt, B., Peterse, J. L., & van ’t Veer, L. J. (2005). Breast cancer metastasis: markers and models. *Nat Rev Cancer*, *5*, 591–602. https://doi.org/10.1038/nrc1670

Wek, S. A., Zhu, S., & Wek, R. C. (1995). The histidyl-tRNA synthetase-related sequence in the eIF-2 alpha protein kinase GCN2 interacts with tRNA and is required for activation in response to starvation for different amino acids. *Molecular and Cellular Biology*, *15*(8), 4497–4506. Retrieved from http://www.ncbi.nlm.nih.gov/pubmed/7623840

Wu, Z.-S., Wu, Q., Yang, J.-H., Wang, H.-Q., Ding, X.-D., Yang, F., & Xu, X.-C. (2008). Prognostic significance of MMP-9 and TIMP-1 serum and tissue expression in breast cancer. *International Journal of Cancer*, *122*(9), 2050–2056. https://doi.org/10.1002/ijc.23337

Xie, W., & Denman, R. B. (2011). Protein methylation and stress granules: posttranslational remodeler or innocent bystander? *Mol Biol Int*, *2011*, 137459. https://doi.org/10.4061/2011/137459

Yamaguchi, A., & Kitajo, K. (2012). The effect of PRMT1-mediated arginine methylation on the subcellular localization, stress granules, and detergent-insoluble aggregates of FUS/TLS. *PLoS One*, *7*, e49267. https://doi.org/10.1371/journal.pone.0049267

Yamaguchi, H., Wyckoff, J., & Condeelis, J. (2005). Cell migration in tumors. *Curr Opin Cell Biol*, *17*, 559–564. https://doi.org/10.1016/j.ceb.2005.08.002

Yamasaki, S., & Anderson, P. (2008). Reprogramming mRNA translation during stress. *Curr Opin Cell Biol*, *20*, 222–226. https://doi.org/10.1016/j.ceb.2008.01.013

Yang, Y., & Bedford, M. T. (2013). Protein arginine methyltransferases and cancer. *Nat Rev Cancer*, *13*, 37–50. https://doi.org/10.1038/nrc3409

Yang, Y., Hadjikyriacou, A., & Xia, Z. (2015). PRMT9 is a type II methyltransferase that methylates

the splicing factor SAP145, *6*, 6428. https://doi.org/10.1038/ncomms7428

Yao, R., Jiang, H., Ma, Y., Wang, L., Wang, L., Du, J., … Lu, J. (2014). PRMT7 induces epithelial-to-mesenchymal transition and promotes metastasis in breast cancer. *Cancer Res*, *74*, 5656–5667. https://doi.org/10.1158/0008-5472.can-14-0800

Ying, Z., Mei, M., Zhang, P., Liu, C., He, H., Gao, F., & Bao, S. (2015). Histone Arginine Methylation by PRMT7 Controls Germinal Center Formation via Regulating Bcl6 Transcription. *J Immunol*, *195*, 1538–1547. https://doi.org/10.4049/jimmunol.1500224

Yousef, E. M., Tahir, M. R., St-Pierre, Y., & Gaboury, L. A. (2014). MMP-9 expression varies according to molecular subtypes of breast cancer. *BMC Cancer*, *14*(1), 609. https://doi.org/10.1186/1471-2407-14-609

Zhang, T., Günther, S., Looso, M., Künne, C., Krüger, M., Kim, J., … Braun, T. (2015). Prmt5 is a regulator of muscle stem cell expansion in adult mice. *Nature Communications*, *6*(1), 7140. https://doi.org/10.1038/ncomms8140

Zhao, Q., Rank, G., Tan, Y. T., Li, H., Moritz, R. L., Simpson, R. J., … Jane, S. M. (2009). PRMT5-mediated methylation of histone H4R3 recruits DNMT3A, coupling histone and DNA methylation in gene silencing. *Nat Struct Mol Biol*, *16*, 304–311. https://doi.org/10.1038/nsmb.1568

Zheng, S., Moehlenbrink, J., Lu, Y.-C., Zalmas, L.-P., Sagum, C. A., Carr, S., … La Thangue, N. B. (2013). Arginine Methylation-Dependent Reader-Writer Interplay Governs Growth Control by E2F-1. *Molecular Cell*, *52*(1), 37–51. https://doi.org/10.1016/j.molcel.2013.08.039

Zhong, J., Cao, R.-X., Hong, T., Yang, J., Zu, X.-Y., Xiao, X.-H., … Wen, G.-B. (2011). Identification and expression analysis of a novel transcript of the human PRMT2 gene resulted from

alternative polyadenylation in breast cancer. *Gene*, *487*(1), 1–9. https://doi.org/10.1016/j.gene.2011.06.022

Zhong, J., Cao, R.-X., Zu, X.-Y., Hong, T., Yang, J., Liu, L., … Wen, G.-B. (2012). Identification and characterization of novel spliced variants of PRMT2 in breast carcinoma. *FEBS Journal*, *279*(2), 316–335. https://doi.org/10.1111/j.1742-4658.2011.08426.x

Zurita-Lopez, C. I., Sandberg, T., Kelly, R., & Clarke, S. G. (2012). Human protein arginine methyltransferase 7 (PRMT7) is a type III enzyme forming omega-NG-monomethylated arginine residues. *J Biol Chem*, *287*, 7859–7870. https://doi.org/10.1074/jbc.M111.336271

APPENDIX

ACADEMIC PRESS

Chromatin Signaling and Diseases

2016, Pages 55–74

Chapter 3 – The Role of Histone Mark Writers in Chromatin Signaling: Protein Arginine Methyltransferases

N. Haghandish, J. Côté

University of Ottawa, Ottawa, ON, Canada

Available online 12 August 2016

https://doi.org/10.1016/B978-0-12-802389-1.00003-4

Abstract

Protein arginine methyltransferases (PRMTs) are enzymes that catalyze the methylation of arginine residues within proteins, resulting in changes in several biological processes such as RNA regulation, signal transduction, and chromatin regulation. As histones are common substrates of PRMTs, their methylation can alter the histone code. The modified structure of histones results in changes in gene expression by altering their interaction with other proteins and by generating docking sites for chromatin-associated proteins. Dysregulation of this group of enzymes can result in aberrant gene expression which may eventually lead to human disease. This chapter outlines the general properties of mammalian PRMTs, the resulting changes in gene expression upon methylation of specific arginine residues within histone tails, and specific diseases that may arise due to the dysregulation of histone methylation.

OUTLINE

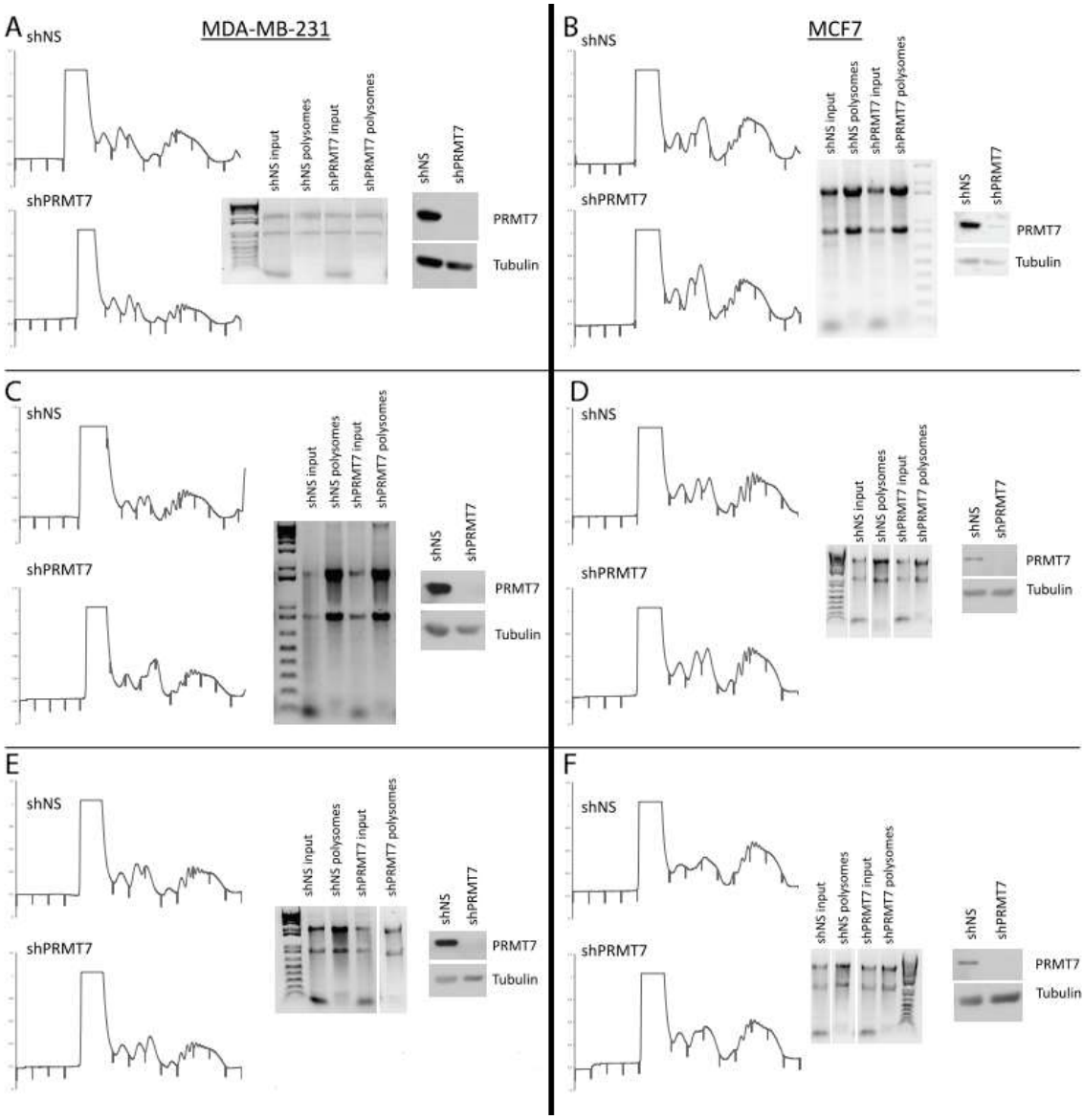

Figure 46: Future work for RNA-sequencing analysis
Triplicate MDA-MB-231 and MCF7 cell lysates with a knockdown in PRMT7 protein were used for polyribosome profiling experiments. RNA was isolated from pooled polysomal fractions and run on an agarose gel to ensure purity and lack of degradation. Inputs were also collected. Western blots depict extent of PRMT7 knockdown.

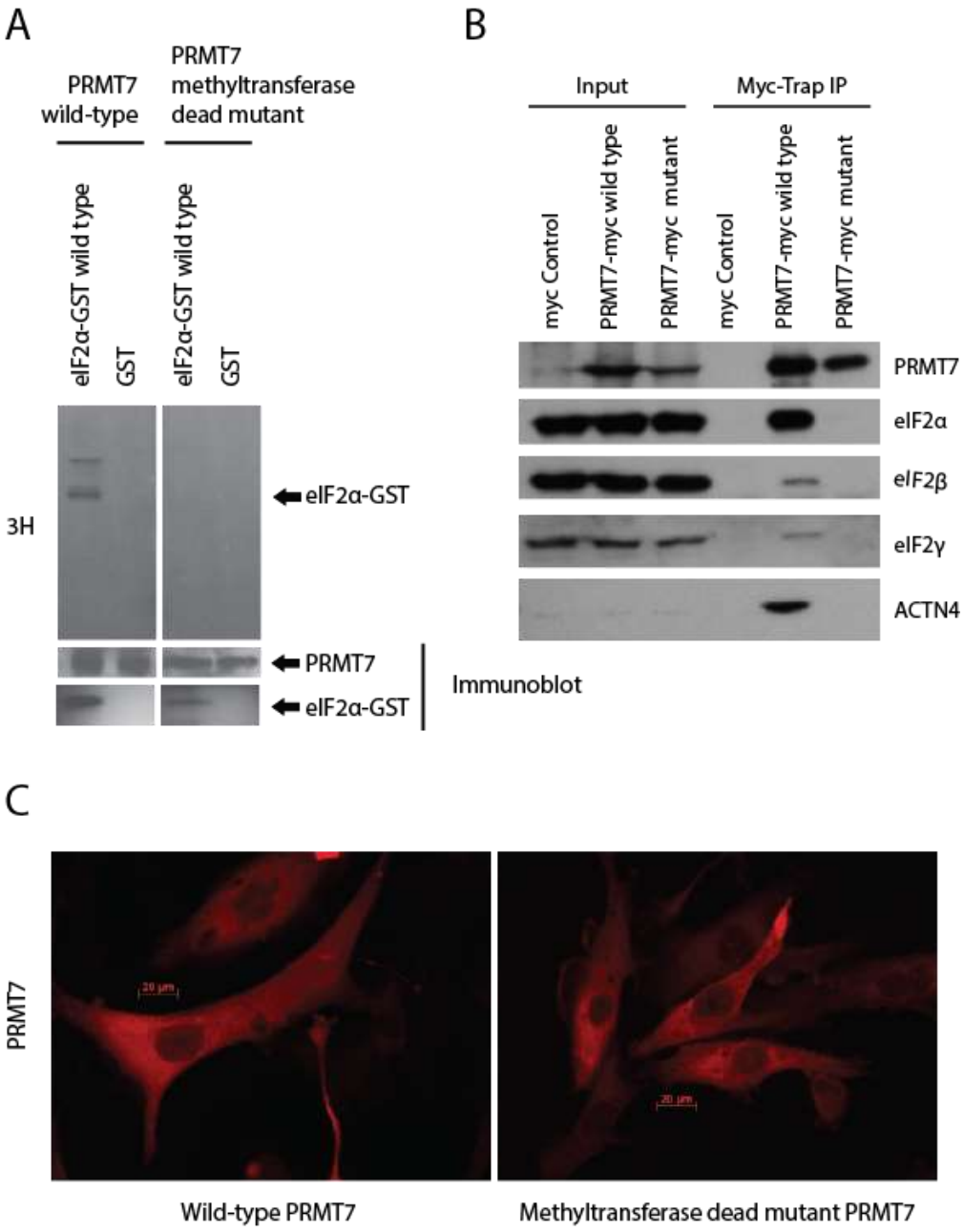

Figure 47: Methyltransferase-dead PRMT7 mutant is truly catalytically inactive
(A) *In vitro* methylation assay of purified wild-type and methyltransferase-dead PRMT7 mutant using eIF2α-GST as a substrate. Assay demonstrates the inability of mutant PRMT7 from methylating its substrate. (B) Co-immunoprecipitation of confirmed protien interactors of PRMT7 using both wild-type and mutant PRMT7 within MCF7 cells. Methyltransferase-dead mutant is incapable of binding to its substrates. (C) Immunofluorescence imagining of wild-type and mutant PRMT7 in MCF7 cells shows similar localized which is consistent with endogenous localization of PRMT7 (as shown in this thesis, Figure 3C); scale bar 20µm.

Mass Spectrometry Data:

The mass spectrometry data are presented in the following six tables:

- All identified proteins from experiment 1
- All identified protein from experiment 2
- Categorized proteins identified from experiment 1
- Categorized proteins identified from experiment 2
- List of proteins from experiment 2 that are common with experiment 2
- List of proteins from experiment 2 that are common with experiment 1

Note that data analysis was performed by L. Trinkle-Mulcahy (Tables 6 and 7) and R. M. Baldwin (Tables 8, 9, 10, and 11).

Table 6: All identified proteins from experiment 1

Proteins identified from experiment 1 are listed below in order of PRMT7 to GFP enrichment (log2 H:L ratio, Log2 HL). GFP was labelled in light (L) isotopes and PRMT7 in heavy (H). HLn represent normalized values against molecular weight. Intensity is also normalized against molecular weight (MW) of the protein. The number of peptides identified in the mass spectrometry experiment for each protein are listed below. A total of 72 proteins were identified.

Gene names	# Peptide	MW [kDa]	Ratio HL	Log2 HL	Ratio HLn	Log2 HLn	Intensity	Norm Int
SFXN1	1	35.619	101.38	6.664	1.755	0.8115	8.7E+09	244.886
EIF2S3	9	51.109	33.957	5.086	4.9411	2.3048	8E+08	15.6937
PRMT7	**28**	**78.458**	**26.941**	4.752	2.7121	1.4394	6.3E+10	799.026
EIF2S1	17	36.112	20.755	4.375	6.3481	2.6663	5.4E+08	14.9266
EIF2S2	11	38.388	19.585	4.292	2.2929	1.1972	1.3E+08	3.29087
RPL23	2	14.865	15.836	3.985	7.7124	2.9472	3.1E+07	2.07851
ACTN1	8	107.14	13.726	3.779	9.398	3.2324	2.6E+07	0.24241
SMARCD1	1	36.849	10.965	3.455	1.0441	0.0623	3E+07	0.8226
ACTN4	18	104.85	10.43	3.383	2.0159	1.0114	1.5E+09	14.4158
ACTG1	24	41.792	9.7766	3.289	1.3277	0.4089	1.2E+10	290.462
ACTBL2	4	42.003	9.7185	3.281	1.0854	0.1182	1.5E+09	35.7927
AIF1L	2	20.015	8.8124	3.14	4.2433	2.0852	2517100	0.12576
IQGAP1	2	189.25	8.5101	3.089	1.0175	0.025	1.6E+07	0.08462
CALM	2	20.762	8.2702	3.048	4.0278	2.01	6512700	0.31368
MYO1B	9	131.98	8.0547	3.01	3.8698	1.9523	2.5E+08	1.88794
CAPZA2	3	32.949	8.0333	3.006	1.1741	0.2316	1.7E+07	0.51868
LAD1	2	58.677	7.9852	2.997	1.092	0.127	5836700	0.09947
HSPA8	13	70.897	7.7209	2.949	1.0921	0.1271	4E+08	5.6252
HSPA1	9	77.405	7.4342	2.894	1.044	0.0621	1.4E+08	1.79084
TUBB4	16	49.83	7.3756	2.883	1.0164	0.0235	3.7E+08	7.46779
RPS16	2	17.107	7.3533	2.878	3.5433	1.8251	7448500	0.43541
ARPC4-TTLL3	3	71.718	7.3526	2.878	3.5054	1.8096	1.3E+07	0.1769
TUBB	13	49.67	7.3488	2.878	1.0003	0.0004	1.1E+08	2.24562
MYO6	3	148.83	7.1805	2.844	0.31909	-1.648	7.7E+07	0.52071
TAB3	1	78.682	7.0692	2.822	0.99361	-0.009	4E+08	5.1351
NEFM	1	102.47	7.0469	2.817	0.99818	-0.002	2.2E+08	2.13477
RPS3	3	26.688	7.0248	2.812	6.6428	2.7318	7.8E+07	2.92274
ATP5A1	4	59.75	7.0062	2.809	1.0015	0.0022	2.5E+07	0.42623
KRT18	21	48.057	6.8642	2.779	0.93605	-0.095	4.2E+09	88.368

LMNA	3	74.139	6.8323	2.772	0.99416	-0.008	1.1E+07	0.14844
HSPB1	2	22.782	6.7408	2.753	5.1488	2.3642	1.2E+08	5.46133
EEF1A1	4	50.14	6.5885	2.72	0.85715	-0.222	1.1E+08	2.11867
MYL12	2	19.779	6.542	2.71	3.1189	1.641	4241100	0.21442
KRT8	30	56.608	6.5217	2.705	0.9225	-0.116	7E+09	123.136
TUBA	8	57.73	6.4792	2.696	0.82291	-0.281	4.8E+08	8.26797
TUFM	2	49.541	6.4322	2.685	0.90609	-0.142	1.4E+07	0.27361
HSP90A	3	98.16	6.3168	2.659	0.90296	-0.147	2.7E+07	0.27057
CAPZB	2	37.455	6.3047	2.656	35.824	5.1629	1.1E+07	0.29686
TMOD3	6	39.594	6.1409	2.618	0.75997	-0.396	3.7E+07	0.93885
MYH9	6	226.53	5.7735	2.529	0.59338	-0.753	9.7E+07	0.42898
GSN	4	85.696	5.5123	2.463	4.5241	2.1776	5.6E+07	0.65266
GFP	**2**	**28.106**	**5.4766**	**2.453**	**0.80046**	**-0.321**	**1.3E+10**	**475.735**
SLC25A10	2	48.099	5.1473	2.364	4.8674	2.2832	1.7E+07	0.35015
DDX5	4	69.147	5.0633	2.34	0.73676	-0.440	1.6E+07	0.22918
LRRFIP2	1	82.17	4.9591	2.31	0.69703	-0.520	5723200	0.06965
SFPQ	2	76.149	4.8247	2.27	0.22099	-2.177	1E+07	0.13575
RPS7	3	22.127	4.6759	2.225	2.6742	1.4191	2.9E+07	1.29032
RPS12	1	14.515	4.1508	2.053	2.0215	1.0154	1953400	0.13458
SPTAN1	4	284.94	4.1292	2.046	2.8271	1.4993	3.6E+07	0.12547
HNRNPH	2	51.229	3.8035	1.927	0.43983	-1.185	1.1E+07	0.20664
RBM14	4	69.491	3.7693	1.914	0.54848	-0.866	2.8E+07	0.3975
HSPA9	8	73.68	3.163	1.661	0.45603	-1.132	5.3E+07	0.72037
NPM1	1	32.575	3.1237	1.643	0.79472	-0.331	2E+07	0.62751
NOP58	3	59.578	2.9367	1.554	0.41238	-1.278	1.3E+07	0.22228
HNRNPK	3	51.028	2.9027	1.537	0.40761	-1.294	9215500	0.1806
NOP56	4	66.049	2.8789	1.526	0.41153	-1.280	2.4E+07	0.36135
HNRNPF	3	45.671	2.8333	1.502	0.40912	-1.289	2.4E+07	0.51523
HNRNPA2B1	2	37.429	2.831	1.501	0.38436	-1.379	2.6E+07	0.70707
DKC1	3	57.673	2.8126	1.492	0.40926	-1.288	5577600	0.09671
MIF	2	12.476	2.7656	1.468	1.3185	0.3989	1.7E+07	1.35524
RPLP0	2	34.273	2.5551	1.353	0.24331	-2.039	6995000	0.2041
HNRNPC	2	33.67	2.537	1.343	0.24159	-2.049	5423900	0.16109
RPL12	2	17.818	2.2952	1.199	1.1178	0.1607	3131500	0.17575
TAF15	3	61.829	2.2891	1.195	0.33308	-1.586	2.9E+07	0.46139
HIST1H1C	2	21.364	2.2137	1.146	1.8017	0.8494	5852400	0.27394
HSPA5	5	72.332	2.2093	1.144	0.31024	-1.688	1.8E+07	0.25112
HIST1H2	4	13.904	2.2024	1.139	1.0817	0.1133	3.5E+07	2.54632
HIST1H3	3	15.404	2.0996	1.07	1.3605	0.4441	1E+08	6.57037
HIST2H2BF	4	18.041	2.0604	1.043	1.011	0.0158	7.5E+08	41.6917

HIST1H4A	6	11.367	2.0389	1.028	0.98421	-0.023	3.5E+08	31.112
H2AFY	3	39.617	2.0187	1.013	0.19649	-2.347	3.9E+07	0.97304
HIST1H2AG	4	14.091	1.9833	0.988	0.95248	-0.070	5.8E+08	41.2703
UBC	2	77.028	1.86	0.895	0.98113	-0.027	4E+08	5.19759
RBMX	2	42.331	1.5897	0.669	0.18076	-2.467	7747200	0.18301

Table 7: All identified proteins from experiment 2

Proteins identified from experiment 2 are listed below in order of PRMT7 to GFP enrichment (Log2 H:L ratio, Log2 HL). GFP was labelled in heavy (H) isotopes and PRMT7 in light (L) which is why the HL ratios of the highly enriched proteins are negative. HLn represent normalized ratios, against molecular weight. Intensity is normalized against molecular weight (MW) of the protein. The number of peptides identified in the mass spectrometry experiment for each protein are listed below. A total of 76 proteins were identified.

Gene names	# Peptide	MW [kDa]	Ratio HL	Log2 HL	Ratio HLn	Log2 HLn	Intensity	Norm int
PRMT7	**23**	**78.458**	**0.03804**	**-4.716**	**0.022466**	**-5.476**	**1.6E+11**	**2044.53**
EIF2S1	14	36.112	0.04689	-4.415	0.020194	-5.63	3.3E+09	91.0667
EIF2S3	9	51.109	0.05866	-4.091	0.021195	-5.56	1.4E+09	27.637
KRT2	10	65.432	0.08187	-3.61	0.060689	-4.042	1.7E+08	2.60316
EIF2S2	11	38.388	0.09613	-3.379	0.039743	-4.653	5.9E+08	15.4103
GFP	**2**	**28.106**	**0.12885**	**-2.956**	**0.05149**	**-4.28**	**8.9E+09**	**316.85**
RPS15A	2	14.839	0.3921	-1.351	0.27096	-1.884	4.4E+07	2.94171
RPL23	3	14.865	0.48515	-1.043	0.28665	-1.803	5.1E+07	3.40848
MIF	2	12.476	0.49372	-1.018	0.2874	-1.799	2.3E+07	1.86975
RPS3	2	26.688	0.5001	-1	0.46598	-1.102	3.2E+07	1.21294
CCT4	1	57.924	0.57185	-0.806	0.2066	-2.275	1.5E+07	0.25428
RPS7	1	22.127	0.60553	-0.724	0.43307	-1.207	1.7E+07	0.75256
CCT2	2	57.488	0.65912	-0.601	0.23813	-2.07	1.1E+07	0.18955
HSPA1	5	77.405	0.69382	-0.527	0.25067	-1.996	1.7E+08	2.16433
RPL12	3	17.818	0.73868	-0.437	0.43321	-1.207	2.1E+07	1.18212
RPLP0	4	34.273	0.79044	-0.339	0.32043	-1.642	1.4E+08	4.01045
YBX1	1	41.905	0.7913	-0.338	0.96065	-0.058	2E+07	0.48856
RPL6	2	32.728	0.81185	-0.301	0.38865	-1.363	2.9E+07	0.89929
DDX3X	2	73.243	0.85681	-0.223	0.41882	-1.256	5071900	0.06925
SEC11A	1	21.454	0.89074	-0.167	0.66503	-0.589	5232500	0.24389
RPS14	5	16.273	0.90217	-0.149	0.52516	-0.929	6.2E+07	3.79672
HSPA	8	70.897	0.91781	-0.124	0.3516	-1.508	8.1E+08	11.4713
NCL	1	76.613	0.94958	-0.075	0.50459	-0.987	5.9E+07	0.77582
RPS24	2	32.43	0.96939	-0.045	0.56851	-0.815	3.5E+07	1.08144
SNRPD3	2	13.916	1.1881	0.2487	0.69677	-0.521	5862300	0.42126
NPM1	4	32.575	1.2041	0.268	0.45618	-1.132	2.3E+08	7.17544
RPLP2	2	11.665	1.2357	0.3053	0.73012	-0.454	1.1E+07	0.96597
HNRNPC	3	33.67	1.2946	0.3725	0.52482	-0.93	3.2E+08	9.48708
RPS11	1	18.431	1.3345	0.4163	0.6801	-0.556	4.5E+07	2.41799

HNRNPA1	1	38.746	1.351	0.434	0.61291	-0.706	1.2E+08	3.05141
HIST1H1E	2	21.865	1.3814	0.4661	0.6809	-0.554	1564900	0.07157
TUBB4	16	49.83	1.449	0.5351	0.61314	-0.706	2.8E+09	56.9536
TUBB	15	49.67	1.45	0.5361	0.50968	-0.972	1.1E+09	23.1427
EIF4A	2	46.153	1.462	0.5479	0.60387	-0.728	2E+07	0.44222
HIST1H1C	2	21.364	1.4644	0.5503	0.7218	-0.47	3756600	0.17584
HNRNPA3	4	39.594	1.4706	0.5564	0.65342	-0.614	1.5E+08	3.7786
HNRNPA2B1	5	37.429	1.4965	0.5816	0.56277	-0.829	1.7E+08	4.42812
SLC25A5	2	32.852	1.5264	0.6101	1.0998	0.1372	1.1E+08	3.36113
BANF1	2	10.058	1.5449	0.6275	0.98714	-0.019	3.2E+07	3.13889
MYH7	1	223.47	1.6339	0.7083	0.95111	-0.072	1.9E+07	0.08713
HIST1H2B	6	13.904	1.6499	0.7224	0.97486	-0.037	2.2E+09	160.35
ARF3	3	23.346	1.7482	0.8059	1.0638	0.0892	1.1E+07	0.48638
TUBG	2	51.169	1.7504	0.8077	1.1577	0.2113	8.1E+07	1.58303
HSPB1	3	22.782	1.8146	0.8597	1.4799	0.5655	6.1E+08	26.6355
H2A	5	15.144	1.8307	0.8724	1.2277	0.296	2.4E+07	1.61067
LOXHD1	1	252.56	1.921	0.9419	0.97895	-0.031	7.3E+07	0.28757
HIST1H2A	7	14.091	1.926	0.9456	1.0871	0.1205	2.6E+09	185.047
HIST1H3	3	15.404	1.9426	0.958	1.2691	0.3438	4.3E+07	2.79603
HIST1H4A	9	11.367	1.9821	0.987	1.0507	0.0714	5.2E+09	459.638
UBC	1	77.028	2.0011	1.0008	0.81226	-0.3	4.5E+08	5.89072
HIST1H2A	6	14.135	2.0127	1.0091	1.0257	0.0366	3.1E+07	2.16795
H2AFY	3	39.617	2.0627	1.0445	0.83618	-0.258	1E+08	2.62387
TUBA1	13	50.135	2.119	1.0834	0.81167	-0.301	5.2E+09	104.522
HNRNPU	4	90.583	2.1669	1.1156	1.7555	0.8119	1.2E+08	1.35025
TUBA1	12	57.73	2.2587	1.1755	1.1041	0.1429	1.3E+08	2.20111
HSPA5	3	72.332	2.4308	1.2814	1.0035	0.005	1.1E+08	1.48717
TAB3	1	78.682	2.8087	1.4899	1.7427	0.8013	1.4E+09	18.3079
KRT8	34	56.608	2.8922	1.5322	1.0939	0.1295	3.9E+10	693.824
NEFM	1	102.47	2.9307	1.5512	1.4615	0.5474	4.4E+08	4.28457
AIF1L	2	20.015	2.9996	1.5848	2.0728	1.0516	3.2E+07	1.61359
CFL1	3	22.728	3.1516	1.6561	1.9665	0.9756	1.3E+07	0.55416
HNRNPF	2	45.671	3.1865	1.672	1.6499	0.7224	2.4E+08	5.14681
IQGAP1	2	189.25	3.3312	1.736	2.571	1.3623	1.8E+07	0.09299
ACTR3	1	47.371	5.771	2.5288	2.878	1.5251	2166000	0.04572
MYH9	13	226.53	7.8391	2.9707	6.0183	2.5894	2.7E+08	1.17044
CAPZB	2	37.455	8.6565	3.1138	3.8102	1.9299	7.4E+07	1.97877
TMOD3	7	39.594	8.8148	3.1399	4.0255	2.0092	9.9E+07	2.50278
MYO1B	5	131.98	8.922	3.1574	7.7231	2.9492	1E+08	0.79482
CAPZA2	4	32.949	10.896	3.4457	4.5006	2.1701	2E+08	6.1929

DBN1	5	76.299	11.321	3.5009	5.7628	2.5268	2.9E+08	3.82207
PPP1CA	4	38.631	11.453	3.5177	5.1959	2.3774	1.1E+08	2.87748
ACTN4	14	104.85	11.695	3.5478	7.0968	2.8272	8.7E+08	8.26638
CALM2	6	20.762	13.59	3.7645	8.3427	3.0605	3E+08	14.671
MYL6	3	26.707	14.149	3.8226	7.2104	2.8501	8.9E+07	3.32482
ACTC1	13	42.019	20.174	4.3344	9.1527	3.1942	1.1E+10	268.045
CAPZA1	4	32.922	28.154	4.8153	13.39	3.7431	1.8E+08	5.57196
ACTG1	21	41.792	28.673	4.8416	13.948	3.802	6E+10	1426.88

Table 8: Categorized proteins identified from experiment 1

White shading represents experiment 1 specific proteins. Orange shading represents shared proteins identified in both experiments 1 and 2. The protein are listed in order of PRMT7 (heavy isotopes; H) to GFP (light isotopes; L) enrichment (Log2 HLn – normalized Log2 H:L ratio). Dark grey shading represents proteins immunoprecipitated from experiment (PRMT7 and GFP). GFP was labelled in light (L) isotopes and PRMT7 in heavy (H).

Gene names	Peptides	Ratio HL normalized	Log2 HLn	Fold Enrichment
CAPZB	2	35.824	5.1629	573.650503
ACTN1	8	9.398	3.2324	359.150419
RPL23	2	7.7124	2.9472	327.464431
RPS3	3	6.6428	2.7318	303.532387
EIF2S1	17	6.3481	2.6663	296.258317
HSPB1	2	5.1488	2.3642	262.692915
EIF2S3	9	4.9411	2.3048	256.092473
SLC25A10	2	4.8674	2.2832	253.683482
GSN	4	4.5241	2.1776	241.95898
AIF1L	2	4.2433	2.0852	231.687409
CALM2	2	4.0278	2.01	223.33245
MYO1B	9	3.8698	1.9523	216.917667
RPS16	2	3.5433	1.8251	202.78818
ARPC4-TTLL3	3	3.5054	1.8096	201.064342
MYL12B	2	3.1189	1.641	182.337477
SPTAN1	4	2.8271	1.4993	166.591435
PRMT7	**28**	2.7121	1.4394	159.934486
RPS7	3	2.6742	1.4191	157.678596
EIF2S2	11	2.2929	1.1972	133.019271
RPS12	1	2.0215	1.0154	112.825134
ACTN4	18	2.0159	1.0114	112.380453
HIST1H1C	2	1.8017	0.8494	94.373201
SFXN1	1	1.755	0.8115	90.1634478
HIST1H3	3	1.3605	0.4441	49.3485507
ACTG1	24	1.3277	0.4089	45.4365778
MIF	2	1.3185	0.3989	44.3219524
CAPZA2	3	1.1741	0.2316	25.7283656
RPL12	2	1.1178	0.1607	17.8513422
HSPA8	13	1.0921	0.1271	14.1227739
LAD1	2	1.092	0.127	14.1080951

ACTBL2	4	1.0854	0.1182	13.1363126
HIST1H2B	4	1.0817	0.1133	12.5889373
SMARCD1	1	1.0441	0.0623	6.91776605
HSPA1B	9	1.044	0.0621	6.90241243
IQGAP1	2	1.0175	0.025	2.78097717
TUBB4	16	1.0164	0.0235	2.60758672
HIST2H2B	4	1.011	0.0158	1.75366636
ATP5A1	4	1.0015	0.0022	0.24026902
TUBB	13	1.0003	0.0004	0.04808262
NEFM	1	0.99818	-0.0026	-0.2920108
LMNA	3	0.99416	-0.0085	-0.938893
TAB3	1	0.99361	-0.0092	-1.0276002
HIST1H4A	6	0.98421	-0.023	-2.5513244
UBC	2	0.98113	-0.0275	-3.0537543
HIST1H2AG	4	0.95248	-0.0702	-7.8043662
KRT18	21	0.93605	-0.0953	-10.593611
KRT8	30	0.9225	-0.1164	-12.93102
TUFM	2	0.90609	-0.1423	-15.808193
HSP90AA1	3	0.90296	-0.1473	-16.362891
EEF1A	4	0.85715	-0.2224	-24.708933
TUBA1C	8	0.82291	-0.2812	-31.243716
GFP	**2**	**0.80046**	**-0.3211**	-35.677643
NPM1	1	0.79472	-0.3315	-36.831271
TMOD3	6	0.75997	-0.396	-43.998403
DDX5	4	0.73676	-0.4407	-48.970373
LRRFIP2	1	0.69703	-0.5207	-57.856372
MYH9	6	0.59338	-0.753	-83.663533
RBM14	4	0.54848	-0.8665	-96.276564
HSPA9	8	0.45603	-1.1328	-125.8666
HNRNPH	2	0.43983	-1.185	-131.66468
NOP58	3	0.41238	-1.278	-141.99486
NOP56	4	0.41153	-1.2809	-142.32561
DKC1	3	0.40926	-1.2889	-143.21227
HNRNPF	3	0.40912	-1.2894	-143.26711
HNRNPK	3	0.40761	-1.2947	-143.85985
HNRNPA2B1	2	0.38436	-1.3795	-153.27443
TAF15	3	0.33308	-1.5861	-176.22882
MYO6	3	0.31909	-1.648	-183.10719
HSPA5	5	0.31024	-1.6885	-187.61593
RPLP0	2	0.24331	-2.0391	-226.57028

HNRNPC	2	0.24159	-2.0494	-227.70748
SFPQ	2	0.22099	-2.1779	-241.99411
H2AFY	3	0.19649	-2.3475	-260.83024
RBMX	2	0.18076	-2.4679	-274.20585

Table 9: Categorized proteins identified from experiment 2

White shading represents experiment 2 specific proteins. Orange shading represents shared proteins identified in both experiments 1 and 2. The protein are listed in order of PRMT7 to GFP enrichment (Log2 HLn – normalized Log2 H:L ratio). Dark grey shading represents proteins immunoprecipitated from experiment (PRMT7 and GFP). GFP was labelled in heavy (H) isotopes and PRMT7 in light (L). The inverse Log HLn ratio is also listed below to be able to compare with experiment 1 since the values were previously negative.

Gene names	Peptides	Ratio HLn	Log2 HLn	1/HLn	Log2 1/HLn	Fold Enrichment
EIF2S1	14	0.020194	-5.63	49.52	5.629929	21.6535749
EIF2S3	9	0.021195	-5.56	47.18	5.560132	21.3851239
PRMT7	**23**	**0.022466**	**-5.476**	44.51	5.476113	21.0619727
EIF2S2	11	0.039743	-4.653	25.16	4.653155	17.8967516
GFP	**2**	**0.05149**	**-4.28**	19.42	4.279564	16.4598612
KRT2	10	0.060689	-4.042	16.48	4.042421	15.5477736
CCT4	1	0.2066	-2.275	4.84	2.275088	8.75033785
CCT2	2	0.23813	-2.07	4.199	2.070179	7.96222581
HSPA1	5	0.25067	-1.996	3.989	1.996139	7.67745673
RPS15A	2	0.27096	-1.884	3.691	1.883848	7.24557001
RPL23	3	0.28665	-1.803	3.489	1.802638	6.93322237
MIF	2	0.2874	-1.799	3.479	1.798868	6.9187232
RPLP0	4	0.32043	-1.642	3.121	1.641919	6.31507258
HSPA8	8	0.3516	-1.508	2.844	1.507993	5.79997317
RPL6	2	0.38865	-1.363	2.573	1.363457	5.24406376
DDX3X	2	0.41882	-1.256	2.388	1.255598	4.82922214
RPS7	1	0.43307	-1.207	2.309	1.207328	4.64356869
RPL12	3	0.43321	-1.207	2.308	1.206862	4.64177519
NPM1	4	0.45618	-1.132	2.192	1.132325	4.35509576
RPS3	2	0.46598	-1.102	2.146	1.10166	4.23715408
NCL	1	0.50459	-0.987	1.982	0.986816	3.795448
TUBB	15	0.50968	-0.972	1.962	0.972336	3.7397552
HNRNPC	3	0.52482	-0.93	1.905	0.930105	3.57732844
RPS14	5	0.52516	-0.929	1.904	0.929171	3.57373485
HNRNPA2B1	5	0.56277	-0.829	1.777	0.829383	3.18993335
RPS24	2	0.56851	-0.815	1.759	0.814742	3.1336245
EIF4A1	2	0.60387	-0.728	1.656	0.72769	2.79880805
HNRNPA1	1	0.61291	-0.706	1.632	0.706253	2.71635712
TUBB4B	16	0.61314	-0.706	1.631	0.705712	2.71427526

HNRNPA3	4	0.65342	-0.614	1.53	0.613917	2.36122108
SEC11A	1	0.66503	-0.589	1.504	0.588509	2.26349489
RPS11	1	0.6801	-0.556	1.47	0.556181	2.13915847
HIST1H1E	2	0.6809	-0.554	1.469	0.554485	2.13263524
SNRPD3	2	0.69677	-0.521	1.435	0.521246	2.00479072
HIST1H1C	2	0.7218	-0.47	1.385	0.470329	1.80895751
RPLP2	2	0.73012	-0.454	1.37	0.453794	1.74536344
TUBA1	13	0.81167	-0.301	1.232	0.301035	1.15782617
UBC	1	0.81226	-0.3	1.231	0.299986	1.15379421
H2AFY	3	0.83618	-0.258	1.196	0.258115	0.9927483
MYH7	1	0.95111	-0.072	1.051	0.072316	0.27813804
YBX1	1	0.96065	-0.058	1.041	0.057917	0.22275844
HIST1H2B	6	0.97486	-0.037	1.026	0.036733	0.14128095
LOXHD1	1	0.97895	-0.031	1.022	0.030693	0.11804969
BANF1	2	0.98714	-0.019	1.013	0.018673	0.07182072
HSPA5	3	1.0035	0.005	0.997	-0.00504	-0.01938699
HIST1H2A	6	1.0257	0.0366	0.975	-0.03661	-0.14080319
HIST1H4A	9	1.0507	0.0714	0.952	-0.07135	-0.27442617
ARF3	3	1.0638	0.0892	0.94	-0.08923	-0.34318055
HIST1H2A	7	1.0871	0.1205	0.92	-0.12048	-0.46340253
KRT8	34	1.0939	0.1295	0.914	-0.12948	-0.4980033
SLC25A5	2	1.0998	0.1372	0.909	-0.13724	-0.52785074
TUBA1	12	1.1041	0.1429	0.906	-0.14287	-0.54950325
TUBG	2	1.1577	0.2113	0.864	-0.21126	-0.81254404
KRT18	21	1.1816	0.2407	0.846	-0.24074	-0.92592974
H2AFX	5	1.2277	0.296	0.815	-0.29596	-1.13830026
HIST1H3A	3	1.2691	0.3438	0.788	-0.34381	-1.32232982
HSPB1	3	1.4799	0.5655	0.676	-0.5655	-2.17499882
HNRNPF	2	1.6499	0.7224	0.606	-0.72238	-2.77837918
HNRNPU	4	1.7555	0.8119	0.57	-0.81188	-3.12262306
CFL1	3	1.9665	0.9756	0.509	-0.97563	-3.75242379
AIF1L	2	2.0728	1.0516	0.482	-1.05158	-4.044542
IQGAP1	2	2.571	1.3623	0.389	-1.36233	-5.23972927
ACTR3	1	2.878	1.5251	0.347	-1.52507	-5.86564074
CAPZB	2	3.8102	1.9299	0.262	-1.92987	-7.42256434
TMOD3	7	4.0255	2.0092	0.248	-2.00917	-7.72756919
CAPZA2	4	4.5006	2.1701	0.222	-2.17012	-8.34660518
PPP1CA	4	5.1959	2.3774	0.192	-2.37737	-9.14374487
DBN1	5	5.7628	2.5268	0.174	-2.52677	-9.71834597
MYH9	13	6.0183	2.5894	0.166	-2.58936	-9.95906163

ACTN4	14	7.0968	2.8272	0.141	-2.82717	-10.8737256
MYL6	3	7.2104	2.8501	0.139	-2.85008	-10.9618434
MYO1B	5	7.7231	2.9492	0.129	-2.94918	-11.3430002
CALM	6	8.3427	3.0605	0.12	-3.06051	-11.7712091
ACTC1	13	9.1527	3.1942	0.109	-3.1942	-12.2853746
CAPZA1	4	13.39	3.7431	0.075	-3.74308	-14.3964771
ACTG1	21	13.948	3.802	0.072	-3.80199	-14.6230245

Table 10: List of proteins from experiment 1 that are common with experiment 2
Only the 41 shared proteins are listed below. Only the values from experiment 1 are listed. Threshold for experiment 1 was 1.009. Green shading represents the proteins from experiment 1 that were above threshold and were also identified to be above the threshold in experiment 2 (1.26). White shading represents proteins from experiment 1 that were not above both experiment 1 threshold (1.009) and experiment 2 threshold (1.26). Either case, these represent contaminant/background in either experiment 1 or both experiments. Dark grey shading represents proteins immunoprecipitated from experiment (PRMT7 and GFP). GFP was labelled in light (L) isotopes and PRMT7 in heavy (H).

Gene names	Peptides	Ratio HL normalized	log HLn	Fold above threshold
CAPZB	2	35.824	5.1629	573.650503
RPL23	2	7.7124	2.9472	327.464431
RPS3	3	6.6428	2.7318	303.532387
EIF2S1	17	6.3481	2.6663	296.258317
HSPB1	2	5.1488	2.3642	262.692915
EIF2S3	9	4.9411	2.3048	256.092473
AIF1L	2	4.2433	2.0852	231.687409
CALM	2	4.0278	2.01	223.33245
MYO1B	9	3.8698	1.9523	216.917667
PRMT7	**28**	2.7121	1.4394	159.934486
RPS7	3	2.6742	1.4191	157.678596
EIF2S2	11	2.2929	1.1972	133.019271
ACTN4	18	2.0159	1.0114	112.380453
HIST1H1C	2	1.8017	0.8494	94.373201
HIST1H3	3	1.3605	0.4441	49.3485507
ACTG1	24	1.3277	0.4089	45.4365778
MIF	2	1.3185	0.3989	44.3219524
CAPZA2	3	1.1741	0.2316	25.7283656
RPL12	2	1.1178	0.1607	17.8513422
HSPA8	13	1.0921	0.1271	14.1227739
HIST1H2B	4	1.0817	0.1133	12.5889373
HSPA1	9	1.044	0.0621	6.90241243
IQGAP1	2	1.0175	0.025	2.78097717
TUBB4	16	1.0164	0.0235	2.60758672
TUBB	13	1.0003	0.0004	0.04808262
NEFM	1	0.99818	-0.0026	-0.2920108
TAB3	1	0.99361	-0.0092	-1.0276002
HIST1H4A	6	0.98421	-0.023	-2.5513244

UBC	2	0.98113	-0.0275	-3.0537543
HIST1H2A	4	0.95248	-0.0702	-7.8043662
KRT18	21	0.93605	-0.0953	-10.593611
KRT8	30	0.9225	-0.1164	-12.93102
TUBA1	8	0.82291	-0.2812	-31.243716
GFP	**2**	**0.80046**	**-0.3211**	-35.677643
NPM1	1	0.79472	-0.3315	-36.831271
TMOD3	6	0.75997	-0.396	-43.998403
MYH9	6	0.59338	-0.753	-83.663533
HNRNPF	3	0.40912	-1.2894	-143.26711
HNRNPA2B1	2	0.38436	-1.3795	-153.27443
HSPA5	5	0.31024	-1.6885	-187.61593
RPLP0	2	0.24331	-2.0391	-226.57028
HNRNPC	2	0.24159	-2.0494	-227.70748
H2AFY	3	0.19649	-2.3475	-260.83024

Table 11: List of proteins from experiment 2 that are common with experiment 1
Only the 41 shared proteins identified are listed below. Only the values from experiment 2 are listed. Threshold for experiment 2 was 1.26. Green shading represents the proteins from experiment 2 that were above threshold and were also identified to be above the threshold in experiment 1 (1.009). White shading represents proteins from experiment 1 that were not above both experiment 1 threshold (1.009) and experiment 2 threshold (1.26). Either case, these represent contaminant/background in either experiment 2 or both experiments. Dark grey shading represents proteins immunoprecipitated from experiment (PRMT7 and GFP). GFP was labelled in heavy (H) isotopes and PRMT7 in light (L). Since the labelling was reversed, the inverse Log ratios were compared in order to be able to properly compared threshold levels between both experiments.

Gene names	Peptides	Ratio HL normalized	log HLn	1/HLn	Log2 (1/HLn)	Fold above threshold
EIF2S1	14	0.020194	-5.6299	49.52	5.629929	21.65357494
EIF2S3	9	0.021195	-5.5601	47.18	5.560132	21.38512394
PRMT7	**23**	**0.022466**	**-5.4761**	44.51	5.476113	21.06197273
EIF2S2	11	0.039743	-4.6532	25.16	4.653155	17.89675158
GFP	**2**	**0.05149**	**-4.2796**	19.42	4.279564	16.45986123
HSPA1	5	0.25067	-1.9961	3.989	1.996139	7.677456727
RPL23	3	0.28665	-1.8026	3.489	1.802638	6.933222369
MIF	2	0.2874	-1.7989	3.479	1.798868	6.918723204
RPLP0	4	0.32043	-1.6419	3.121	1.641919	6.315072576
HSPA8	8	0.3516	-1.508	2.844	1.507993	5.799973171
RPS7	1	0.43307	-1.2073	2.309	1.207328	4.643568687
RPL12	3	0.43321	-1.2069	2.308	1.206862	4.641775189
NPM1	4	0.45618	-1.1323	2.192	1.132325	4.355095761
RPS3	2	0.46598	-1.1017	2.146	1.10166	4.237154075
TUBB	15	0.50968	-0.9723	1.962	0.972336	3.739755201
HNRNPC	3	0.52482	-0.9301	1.905	0.930105	3.577328443
HNRNPA2B1	5	0.56277	-0.8294	1.777	0.829383	3.18993335
TUBB4	16	0.61314	-0.7057	1.631	0.705712	2.714275264
HIST1H1C	2	0.7218	-0.4703	1.385	0.470329	1.808957506
UBC	1	0.81226	-0.3	1.231	0.299986	1.153794211
H2AFY	3	0.83618	-0.2581	1.196	0.258115	0.9927483
HIST1H2B	6	0.97486	-0.0367	1.026	0.036733	0.14128095
HSPA5	3	1.0035	0.005	0.997	-0.00504	-0.01938698
HIST1H4A	9	1.0507	0.0714	0.952	-0.07135	-0.27442617
HIST1H2A	7	1.0871	0.1205	0.92	-0.12048	-0.46340252
KRT8	34	1.0939	0.1295	0.914	-0.12948	-0.49800330

TUBA1	12	1.1041	0.1429	0.906	-0.14287	-0.54950325
KRT18	21	1.1816	0.2407	0.846	-0.24074	-0.92592973
HIST1H3	3	1.2691	0.3438	0.788	-0.34381	-1.32232981
NEFM	1	1.4615	0.5474	0.684	-0.54745	-2.10557626
HSPB1	3	1.4799	0.5655	0.676	-0.5655	-2.17499882
HNRNPF	2	1.6499	0.7224	0.606	-0.72238	-2.77837917
TAB3	1	1.7427	0.8013	0.574	-0.80132	-3.08201629
AIF1L	2	2.0728	1.0516	0.482	-1.05158	-4.04454200
IQGAP1	2	2.571	1.3623	0.389	-1.36233	-5.23972927
CAPZB	2	3.8102	1.9299	0.262	-1.92987	-7.42256433
TMOD3	7	4.0255	2.0092	0.248	-2.00917	-7.72756918
CAPZA2	4	4.5006	2.1701	0.222	-2.17012	-8.34660518
MYH9	13	6.0183	2.5894	0.166	-2.58936	-9.95906163
ACTN4	14	7.0968	2.8272	0.141	-2.82717	-10.8737255
MYO1B	5	7.7231	2.9492	0.129	-2.94918	-11.3430002
CALM	6	8.3427	3.0605	0.12	-3.06051	-11.7712091
ACTG1	21	13.948	3.802	0.072	-3.80199	-14.6230244